Development of Platform Technologies and Sample Preparation Methods to Improve Diagnosis of the "Big Three" Infectious Diseases of Poverty

By

Westley S. Bauer

Dissertation

Submitted to the Faculty of the

Graduate School of Vanderbilt University

in partial fulfillment of the requirements

for the degree of

DOCTOR OF PHILOSOPHY

in

CHEMISTRY

May 11, 2018

Nashville, Tennessee

Approved:

David W. Wright, Ph.D.

David E. Cliffel, Ph.D.

Timothy P. Hanusa, Ph.D.

G. Kane Jennings, Ph.D.

To those before me who worked tirelessly, sacrificed greatly, and persisted, to allow me to em*bark* on this wonderful journey. In my eyes, this PhD symbolizes more than the academic achievements of a single person; it is a toast to every *leaf* on my family *tree*.

ACKNOWLEDGEMENTS

As I take this opportunity to reflect over my graduate school career, I am proud of my growth as both an independent scientist and as a person. I came to Vanderbilt University seeking a challenge and to test my metal. I found the challenge that I was seeking in a meeting at 9:00 am on a Saturday, in the office of the bioanalytical inorganic chemist, Dr. David Wright. This was unexpected because as a bachelors-level chemist, I surveyed the job market and found a need for PhD-level polymer chemists. A major reason why I came to Vanderbilt was to study under Dr. Eva Harth, a polymer scientist and faculty member at Vanderbilt. However, the Vanderbilt Chemistry department's three-rotation system allowed me to find a research passion that has helped carry me through the highs and lows of graduate school.

That Saturday, I remember walking into the organized chaos that is David's office, for a meeting that I now refer to as the "the graduate student sales pitch." If you are a present or former member of the Wright Lab, you know what I am talking about. There, he laid out the opportunity for me to develop diagnostic technologies at the benchtops in his laboratory and take these innovations to the field for evaluation. This applied science is what steered me away from polymer chemistry and into the global health diagnostic landscape. From that meeting until now, I have crafted what I like to believe is some version of a 5.5 year success story. A success story that could not have been achieved without a tremendous amount of help and support.

First, I would like to thank Dean David Wright for his mentorship, support, and guidance. Thank you for rescuing me from the weeds when I needed it, but also stepping aside to allow me to carve out my own path to becoming an independent

scientist. You challenged me and held my accountable for my science. Additionally, thank you for supporting me in my endeavors outside of the lab as I was awarded the opportunity to conduct research at BASF-SE in Germany as an intern. Under your tutelage, I think we can both agree that I have become an “entrepreneurial” graduate student. It only took you firing me 4 times, kicking 3 chairs, and throwing 1 piece of chalk to motivate me to finally graduate.

To the rest of my committee, Dr. David Cliffel, Dr. Timothy Hanusa, and Dr. G. Kane Jennings – Thank you for your thought provoking discussions and your dedication in attending all of my exams. Even when the Nashville roads were frozen over during a Vanderbilt-issued snow day. Although I wish I was not so stubborn about solving all the research problems I was met with by myself, and sought your guidance more, you have been instrumental in my growth as a scientist.

Next, I would like to thank Wright Lab members past and present. When you are in the graduate school trenches for the number of hours that are required of you to succeed in graduate school, you can grow closer together or farther apart from your lab mates. I am lucky to say that the people that I have shared time with in the Wright lab have become like family to me. To Dr. Chris Gulka and Dr. Steven Randal Jackson – Thank you for showing me how to hold the Wright lab senior graduate student torch and for your sage bits of wisdom like “try not to get emotionally attached to your data.” To Dr. Keersten Ricks and Dr. Kim Fong-League – Thank you for being role models to me. I have nothing but the utmost respect for both of you, your hard work, and your dedication to science. To Dr. Anna Bitting – My baymate. My mom said it all when she apologized to you, on my behalf, the moment that she heard you sat next to me every

day. Thank you for putting up with my shenanigans and for being a sounding board for me when I couldn't think of the appropriate word to write. I am in debt to David's crazy seating chart assignments for giving me the opportunity to sit next to you. To Dr. Alexis Wong and Dr. Lauren Gibson – I consider it an absolute gift that I was able to rub shoulders with both of you starting the day that I arrived at Vanderbilt. In different capacities, you both have become like sisters to me, and for that, I will forever be grateful. It has been a pleasure battling graduate school with you and I cannot wait to see what the future has in store for you both. To Dr. Joseph Conrad (JC) and Dr. Nick Adams – Thank you for taking me under your wings when I joined the lab. I hold your professional advice very dear and am grateful for the friendships that we have developed. To Dr. Christine Markwalter – You have been an inspiration to me throughout my graduate school career. Just when I thought that I could not work any harder, you showed me another level of dedication that I did not know existed. Also, thank you for being my pace horse in writing my dissertation. The "ode" Kelly Richardson – Thank you for being my pipette hand when I did not have one, and really didn't want one. We have developed a dynamic relationship that I think only comes with a high level of mutual respect. I will be forever in your debt for your diligent proofing of my scientific writing. To Megan and Carson – It has been a pleasure being one of your mentors. I have high hopes for both of you and take great comfort in leaving the lab in your very capable hands. To Dr. Mindy Leelawong and Dr. Danielle Kimmel – Thanks for the all of your help that you have given to me. Now that I have addressed all of my friends in the Wright lab, to Andrew Kantor – The single word that comes to my mind when I think of you is, "heroic." Never lose that slow Andrew swag. Thank you for

grounding me and showing me what true toughness and strength really is. If Maze Runner has taught us anything, it is to never stop chasing or running away from things. So continue to do just that.

It means something to be a “Wright lab member” and I will always have a certain affection for those that hold that title. I would also like to thank the honorary member of our lab, Greg our custodian – Thank you for your infectious smile and constant positive attitude. We got to come in to Vanderbilt together and, and now with your retirement, we get to leave together as well. Bad boys for life.

There are many other members of the chemistry department who have influenced my time at Vanderbilt, but a few particularly stand out. Dr. Thomas Struble – Thank you for your friendship. One of the greatest joys of my graduate school experience was going through this battle with you. To Dr. Katie Chong and Dr. Evan “tummy stix” Gizzie – I thought it would be comical to group you two together, so I did. Thank you for wearing echo jeans when you were an adolescent and for your consistent wit, respectively. Also, thank you for your kindness and the friendships that we have fostered over the years. To my collaborators in the Rick Haselton laboratory (Vanderbilt), Jonathan Blackburn laboratory (University of Cape Town, South Africa), and Macha Research Trust (Zambia, Africa) – Thank you for your help and guidance in conducting research over a wide range of disciplines.

Last, but certainly not least, thank you to my family and friends back in MN. Thank you for supporting me on all fronts and allowing me to chase this dream. Without all of you, none of this would have been possible. Thank you for teaching me how to deal with adversity and that nothing in the world can take the place of

persistence. I love you. I came to Vanderbilt as a raw researcher and have been molded and fired into a well-trained independent scientist with the help of all the people listed as well as many, many others.

TABLE OF CONTENTS

Page

LIST OF TABLES

LIST OF FIGURES

CHAPTER I

Introduction

The Infectious Diseases of Poverty

According to the latest published data, infectious diseases were responsible for annual death toll of more than 8.7 million people worldwide.[1] Since antiquity, deaths due to infectious diseases have been inextricably linked to poverty and scarce resources. An estimated 3 billion people—almost 40% of the global population—live on less than 2 USD a day.[1] Today, this group remains at the greatest risk for these illnesses. Just as poverty creates the risk environment necessary for rampant infection, the diseases themselves engender poverty through adverse effects to maternal mortality, child development, and workplace productivity.[2] As a result of this viscous cycle, poverty, through non-genetic heritable principles, has transformed infectious diseases into an "inheritable" condition. The phrase "**i**nfectious **d**iseases of **p**overty" (**IDoP**) is an umbrella term used to describe infectious diseases that are more prevalent among poor and vulnerable populations. IDoP is bifurcated into two distinct disease subsets, the "*big three*" and neglected tropical diseases (NTD). The *big three* IDoP comprise (1) malaria, (2) human immunodeficiency virus-acquired immune deficiency syndrome (HIV-AIDS), and (3) tuberculosis (TB). In 2016 alone, there were an estimated 720,000 malaria deaths, 1.03 million HIV-AIDS deaths, and 1.7 million TB deaths. The majority of victims were children under the age of five. The link between poverty and the IDoP reservoir is illustrated in **Figure 1.1**.[3]

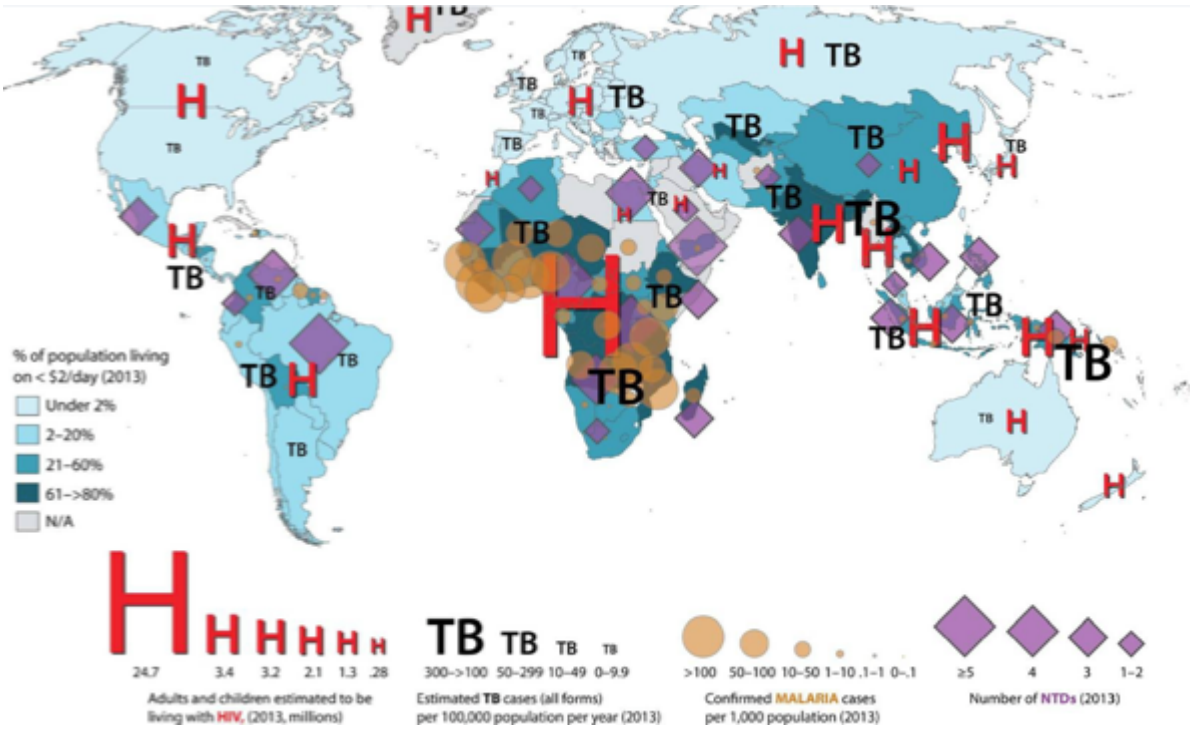

Figure 1.1: The prevalence of the IDoP burden in populations living on less than 2 USD per day.[2]

Disability-adjusted life years (DALYs) reflects the most accurate measure of the devastation these diseases inflict on marginalized populations. DALY can be thought of as one lost year of “healthy” life. Rather than just account for mortality alone, this metric of disease burden encompasses both the years of life lost prematurely as well as the years lost due to disability resulting from health condition or its consequences. Given that children under five are at the most risk, one facet of the IDoP burden that cannot be overlooked is the debilitating impact that the manifested symptoms of these diseases can have on childhood growth and cognitive development. Therefore, patients fortunate enough to survive these chronic bouts of infection may develop impairments that limit vocational opportunities, begetting future poverty. The estimated DALYs lost in 2016 was 56.2 million for malaria, 57.6 million

for HIV-AIDS, and 43.6 million for TB, resulting in a total of approximately 157 million years lost.[4] To put it in more practical terms, this is the equivalent of the number of working years needed to build almost 40 Great Walls of China, or to use a more timely analogy, the amount of time needed to build four concentric walls around the United States.

Brief Epidemiology and Overview of the IDoP's *Big Three*

Malaria, HIV-AIDS, and TB are unified in their disproportionate impact on vulnerable populations. They persist in regions lacking basic healthcare, sanitation, nutrition, shelter, and security. In addition to fundamental development of a society's economy and infrastructure, sustainable public health strategies will require a detailed understanding of each disease's current and historical epidemiology.

Malaria

Malaria is an ancient disease, but our understanding of the malaria parasite begins in 1880, with its discovery in patients by Alphonse Lavern.[5] The disease is caused by infection with a parasitic protozoa belonging to the genus *Plasmodium* that is transmitted exclusively by female *Anopheles* mosquitoes. The five different species of plasmodia all share a very similar five-stage life cycle (**Figure 1.2A**) including stages in both mosquitoes and humans. Out of the five, *Plasmodium falciparum* and *Plasmodium vivax* are the two species that pose the greatest threat. *P. falciparum,* the most pathogenic malaria parasite, is responsible for the most malaria-related deaths. It is the most prevalent species found on the African continent. *P. Vivax* is the dominant malaria parasite in the rest of the world, especially in Southeast Asia and South America.

The malaria infection is an acute febrile illness with symptoms presenting about 10-15 days after an infected mosquito bite. If not treated within 24 hours, symptoms can progress to severe malaria, which can often lead to death. Starting in 2010, a new focus on malaria control and elimination has produced significant results with declining mortality and new infection rates. Unfortunately, this rate of decline has recently stalled and even reversed in some regions.[6] Even though this disease is a completely preventable and curable, malaria continues to be the leading cause of child mortality today. The World Health Organization (WHO) estimates that a child dies from malaria every minute.[6]

HIV-AIDS

Since the first cases were reported in 1981, the HIV epidemic has become one of the world's most serious health and treatment challenges. According to the WHO, there are approximately 36.7 million individuals living with HIV.[7] HIV's hallmark is the target and destruction of CD4 T cells, impairing the body's ability to mount effective immune responses to infections (**Figure 1.2B**). By crippling the body's ability to defend itself, the HIV-infected individual ultimately succumbs to opportunistic infections, AIDS, and death. AIDS status is defined by a <200 CD4 count, or less than 200 CD4 T cells per μL of peripheral blood. The time from acute HIV infection to the development of AIDS ranges from 6 months to 25 years. However, in infants, the disease tends to progress more rapidly.[8] Established modes of transmission include sexual contact, needle injuries, mucous membrane exposure, mother-to-child transmission, and transfusion with contaminated blood products. After almost forty years into the HIV epidemic, considerable advances have been made in prevention

and treatment, but challenges remain regarding access and management of combination antiretroviral therapy (ART). While HIV is not a curable disease, successful lifelong ART management can dramatically increase life expectancy and quality of life.[9]

Tuberculosis

Similar to malaria, TB has also plagued mankind for thousands of years. First identified by the German scientist Robert Koch in 1882, TB is caused by the bacillus

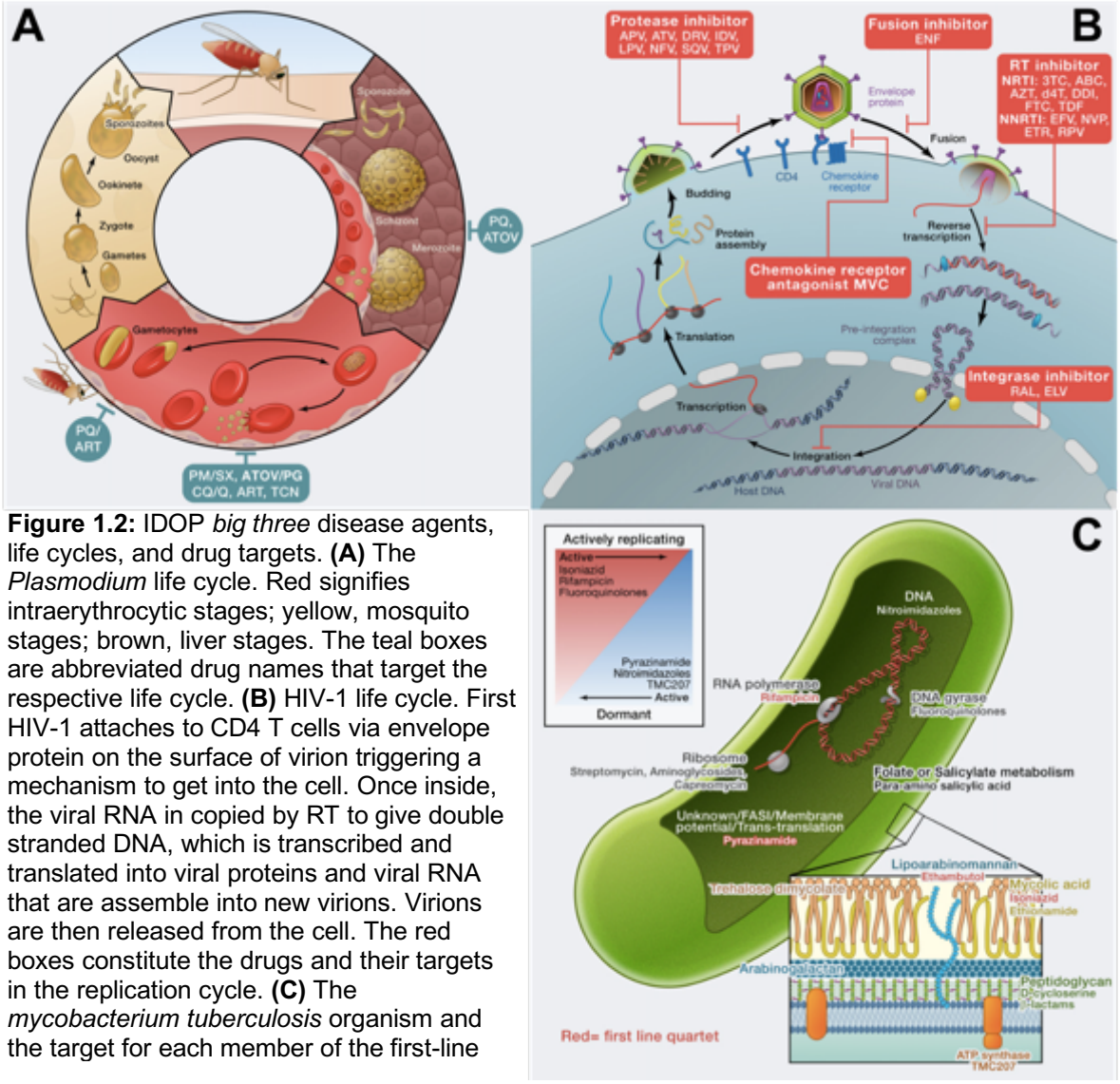

Figure 1.2: IDOP *big three* disease agents, life cycles, and drug targets. **(A)** The *Plasmodium* life cycle. Red signifies intraerythrocytic stages; yellow, mosquito stages; brown, liver stages. The teal boxes are abbreviated drug names that target the respective life cycle. **(B)** HIV-1 life cycle. First HIV-1 attaches to CD4 T cells via envelope protein on the surface of virion triggering a mechanism to get into the cell. Once inside, the viral RNA in copied by RT to give double stranded DNA, which is transcribed and translated into viral proteins and viral RNA that are assemble into new virions. Virions are then released from the cell. The red boxes constitute the drugs and their targets in the replication cycle. **(C)** The *mycobacterium tuberculosis* organism and the target for each member of the first-line

Mycobacterium tuberculosis.[10] To this day, it is still leading cause of death by infectious disease worldwide and the most common cause of death in HIV-infected patients. Almost 12% of the worldwide TB caseload is co-infected with HIV.[4] Although several animal species can be infected by *M. tuberculosis*, human beings remain the principal hosts for the obligate intracellular pathogen.[11] This airborne disease is transmitted when an infected person coughs or sneezes, generating airborne particles called droplet nuclei. When they encounter a TB-susceptible individual, these droplet nuclei travel via the mouth or nasal passages to the lungs. If an active infection develops, the patient will experience severe coughing, fever, and chest pains. However, the yearly probability of developing active symptoms from exposure is very small, culminating in an estimated lifetime risk of around 10%. More than 90% of immunocompetent individuals either eliminate *M. tuberculosis* or contain it in a latent state. Latent-TB is a clinical disorder, where an infected patient's immune system retains sufficient control over replication such that the individual remains free of symptoms. An estimated 2 billion people worldwide have latent TB, which serves as a hidden disease reservoir. The bacilli's slow replication rate and ability to persist in a latent state result in the need for extended drug therapy. A more urgent threat than latent TB is the development of multidrug-resistant TB (MDR-TB), a form resistant to the most important front-line drugs (**Figure 1.2C**).[12] The combination of these factors has made TB an enduring public health risk.

Although caused by vastly different pathogens, the IDoP's *big three* share another common problem beyond their link to poverty—drug resistance.[13] The evolution of resistant variants threatens to make malaria incurable, HIV

uncontrollable, and TB untreatable. TB already prominently displays this effect, and HIV infections require increasingly complex combination therapies. There are numerous reasons why pathogens become drug resistant; however, this phenomenon is largely the result of widespread overuse and misprescription.[13] In fact, up to 50% of all prescribed antibiotics are either not needed or effective as prescribed.[14] In the wake of this problem, the pace of drug development has slowed, leaving only a finite window of time to effectively treat these illnesses with the current class of available medications.[15] The excessive administration of these drugs must be curtailed in order to extend the use life of the most efficacious therapies.

One of the primary ways this challenge can be addressed is through the use of highly specific and sensitive diagnostic tests. Proper utilization of diagnostic tests promotes antibiotic stewardship and affords the best outcome for patients. Appropriate testing allows healthcare providers to identify the infection and prescribe the optimal treatments regimen. As part of a screen-and-treat campaign, front-line diagnostics stand to decrease overall healthcare costs when compared to mass drug administration (MDA).[16] While drug resistance occurs as a consequence of the natural evolutionary process, antibiotic stewardship can significantly slow the development of drug resistance, providing additional time for the innovation of novel treatments.

Challenges to Providing Disease Diagnosis in Low-Resource Settings

William Osler, a founder of modern medicine, once said, “There are three phases to treatment: diagnosis, diagnosis, and diagnosis.”[17] When a diagnosis is made in an accurate and timely manner, the patient receives the best opportunity for

a positive health outcome. A diagnostic test, or diagnostic, is a general term for any test used to diagnose the nature or severity of a particular condition or infection. The information provided by these tests aids in making clinical treatment decisions. A schematic showing the general diagnostic and treatment timeline is provided for reference in **Figure 1.3**.

Diagnosing patients living in rural or resource-poor locations presents a particularly difficult challenge. People living in these settings may have to walk hours just to reach a clinic with the laboratory capacity necessary to support adequate diagnostic testing. If they are unable to travel to these clinics, patients are left to seek treatment at village-level outposts. Adequate testing facilities are limited or nonexistent at these sites. Patients' illnesses are frequently managed syndromically, without the use of diagnostics.[18] As a result, illnesses are frequently misclassified with patients being prescribed drugs that are both ineffective and in limited supply.[19] To mitigate the improper prescription of drugs and to effectively manage the IDoP, there needs to be access to appropriate diagnostic testing in low-resource settings where these diseases thrive.[20]

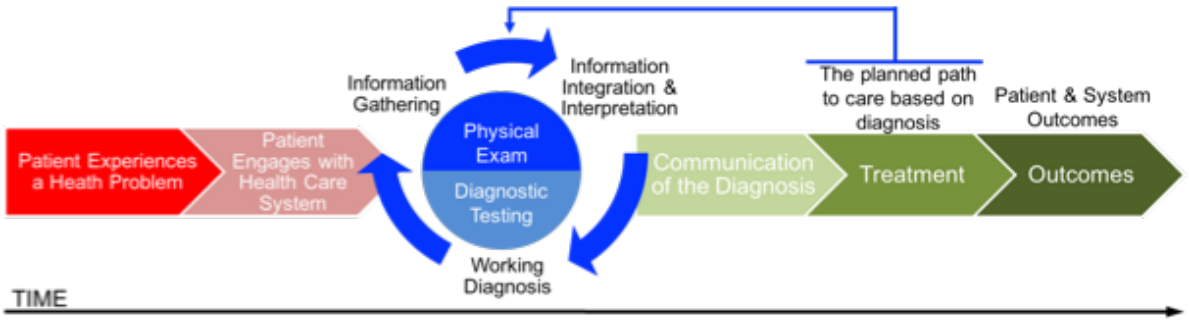

Figure 1.3: Ideal diagnosis and treatment process in resource-poor settings.

In developing countries, the laboratory capacity of healthcare facilities is broken down into three levels. The highest level being **tertiary**, high-capacity reference laboratories with trained personnel, reliable electricity, clean water, and other resources that allow them to conduct and support esoteric testing. **Secondary** facilities are district laboratories and hospitals, where electricity is intermittent and access to clean water may be limited. These facilities are able to provide referral testing and routine diagnostic tests. Finally, **primary** facilities are village-level outposts that have minimal access to electricity and clean water and are only able to provide primary care such as rapid tests, manual serology, and light microscopy.[21]

Currently, low-infrastructure, **primary** health facilities support the majority of the patients affected by the IDoP burden.[22] Surveys conducted by the WHO have found that 72% of the African populace and 42% of the Asian populace are served by minimal or no infrastructure.[23] The lack of quality diagnostic tests at these sites is a major contributor to the infectious disease burden. While many high-quality diagnostic tests and technologies are commercially available, they are neither accessible nor affordable to most patients living in low-resource settings. Gold-standard techniques in infectious disease diagnostics include microscopy, tissue culture, nucleic acid-based tests (NATs), and enzyme-linked immunosorbent assays (ELISAs). Conventional microbial identification methods usually include time-consuming assays that study the organism's morphology and growth in various media conditions.[24] The majority of these methods can only be performed at centralized **tertiary** facilities because they require uninterrupted resources, highly trained staff, and specialized equipment. Consequently, the combination of the distance and cost associated with

seeking medical consultation at any level beyond **primary** leaves large portions of the global population without appropriate diagnostic consultation. In recognition of these healthcare delivery gaps, the WHO and other initiatives such as the Bill and Melinda Gates Foundation have called for the development of point-of-care (PoC) clinical diagnostics able to function in settings with limited infrastructure, minimally trained healthcare personnel, and restricted access to centralized laboratories.[25-28]

The WHO developed the **ASSURED** criteria (**A**ffordable, **S**ensitive, **S**pecific, **U**ser-friendly, **R**apid and robust, **E**quipment-free, and **D**eliverable) for ideal PoC tests in resource-limited settings. With this framework, substantial research efforts have been focused on replacing the standard expensive clinical diagnostic methods with affordable and sensitive rapid diagnostics tests (RDTs). Generally, RDTs employ either lateral flow immunochromatography or flow-through immunoconcentration technology. Of these two, lateral flow immunochromatographic tests, or lateral flow assays (LFAs), have emerged as the leading RDT candidate to fill this PoC diagnostic gap. In addition to being inexpensive, easy-to-use, and portable, they can rapidly indicate the presence of pathogens or pathogen-associate biomarkers in a patient sample. These tests have been adapted to accommodate a variety of samples including blood, serum, urine, saliva, and other exudates. Judged in regard to sensitivity and specificity towards the target biomarker, the performance of LFAs hinge on the quality and abundance of the intended disease biomarker and the nature of its sample matrix.

Briefly, an infectious disease biomarker is a unique biomolecule or biochemical characteristic that can be objectively measured and evaluated as an indicator of the

presence or risk of a disease pathogen. These are typically identified by evaluating the host's or pathogen's biological processes or the host's biological responses to infection, then monitoring these processes during and after treatment. The most common infectious disease biomarker classes are proteins, nucleic acids, small molecules, and carbohydrates.[29] As the ideal PoC diagnostic test would fulfill ASSURED criteria, the ideal infectious disease biomarker would also meet a distinct set of benchmarks. Miller *et al* proposed that the ideal biomarker must follow the SASQUATCH standard: **S**pecific, **A**bundant, **S**table, **Q**uantitatively meaningful, **U**niversal, **A**ccessible in biological fluids, **T**imely, **C**haracterized and well understood, and **H**eterologously expressible.[30] Distilling this acronym down to its core, the efficacy of an infectious disease biomarker lies in its capacity to provide early detection and establish highly specific diagnosis. These qualities expand to include determination of accurate prognosis, appropriate treatment, and disease progression.[31]

LFAs are generally paper membrane-based tests that use immobilized molecular recognition elements (MREs) to screen for the presence of specific biomarkers in patients' peripheral fluids. The test architecture comes in dipstick or cassette formats and can be engineered to detect multiple biomarkers. The targeted biomarker's or biomarkers' presence in a patient sample is often signaled by the development of a colored test line, that can be observed by the unaided eye, within 30 minutes after initiating the test.[32] The principle behind LFAs is simple: a small-volume liquid sample is deposited on the test and flows through various zones on the test using capillary action. This allows the biomarkers present in the sample to interact with a label conjugate and later be arrested at the test line in a "sandwich"

conformation. The rest of the conjugate migrates to the control line where it is directly captured by a secondary affinity agent. As the conjugate is released independently of the biomarker's presence, the control line is evident on every valid test. **Figure 1.4** provides a visual aid for this process and the potential LFA results. The most common LFA example in the United States is a pregnancy test that screens for the beta subunit of the human chorionic gonadotropin (hCG) hormone, which is present in female urine 6-12 days after fertilization.

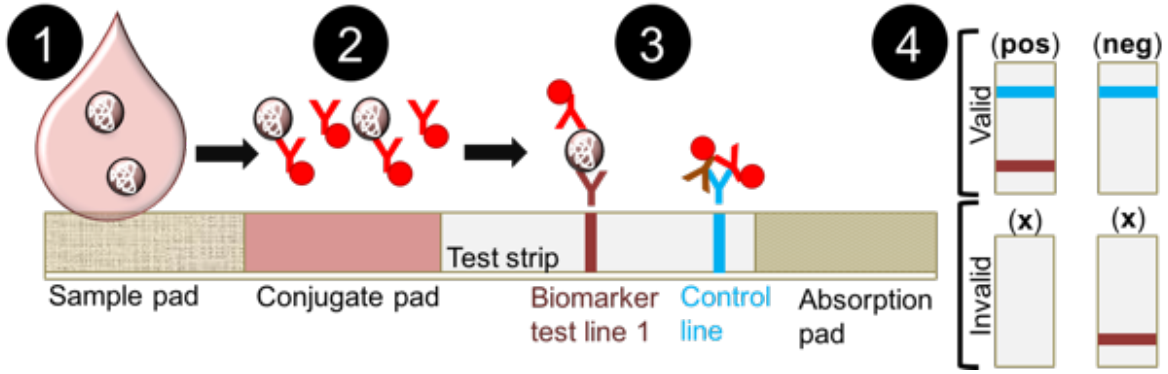

Figure 1.4: Single biomarker LFA configuration, components, and function. (1) A small liquid sample, typically 5 µL, is added to the sample port and the addition of running buffer mobilizes the sample to flow down the test under capillary action. (2) The labeling conjugate interacts with the sample and if the targeted biomarker or biomarkers are present, the gold nanoparticles bind with their respective target and form a "half sandwich." (3) The labeled biomarkers are then separated down the test strip in different zones where they are immobilized by an orthogonal binding element forming a "biomarker sandwich." (4) The possible results for valid and invalid tests.

More importantly, LFAs have already demonstrated significant potential in low-resource settings. Specifically, LFAs for malaria have reached an unparalleled level of technical development, commercialization, and market uptake. Within the field of malaria diagnostics, there are more than 200 commercially available products and in 2013 alone, 319 million malaria LFAs were sold in 48 different countries.[30,33] The success of malaria LFAs has established this technology as more than just a complement to gold standard diagnostics and encouraged the development of LFAs for other infectious diseases, specifically, HIV and TB. However, broader LFA

development and uptake by the medical community has been limited by a number of lingering issues. These range from technical shortcomings to institutional obstacles. Further, it has become apparent that there is a ceiling to the types of measurements that LFAs can make. The LFA technology is more conducive to qualitative testing than detailed quantitative testing. More sophisticated instrumentation is needed for reliable nucleic acid detection and cell counting given the current level of LFA technology.

Strategies to Overcome the Biological and Technical Limitations of LFAs

Although seemingly simple in theory and design, the core technologies behind LFAs are subject to a number of technical and biological vulnerabilities, the most significant being matrix effects, the "hook" effect, specificity issues, and low biomarker insensitivity.[30] These vulnerabilities will be discussed at length in following chapters. Even with these inherent weaknesses, LFAs still currently serve as the best PoC diagnostic modality to extend laboratory testing to rural and low-resource areas. The promise behind LFAs has spurred innovations and advances to overcome these limitations. Examples include signal-amplification strategies, novel detection labels, new test architectures, improved quantification systems, and image analysis equipment.[34-37] However, the development of new LFA diagnostics comes with problems surrounding approval, commercialization, and deployment. While disease may not recognize borders, the individual countries within endemic regions may possess completely different regulatory processes and requirements. Another challenge is community acceptance. The RDT is now a trusted and recognized

diagnostic format in many rural areas. Deviation from the traditional test design is often met with resistance.

As an alternative strategy, front-end sample processing can overcome many LFA limitations without the need to modify the test in any way, therefore, reducing policy and regulatory challenges.[24] This approach was derived from the discovery that part of the platform-wide LFA sensitivity problem was a function of low sample volume tolerance (5-10 µL). Through a process called biomarker or volumetric enrichment, customized affinity magnetic beads are employed to reversibly capture the increased number of target biomarkers available in large sample volumes. Once collected, these biomarkers can be concentrated and eluted into LFA-compatible volumes suitable for addition to the test. Purifying and concentrating target biomarkers from large samples volumes has been found to not only increase sensitivity, but also to mitigate many of the other aforementioned biological and technical problems.[38,39]

Current State of PoC Diagnostics for the IDoP's *Big Three*

As mentioned previously, the first consideration in the development of any PoC diagnostic is biomarker selection. The SASQUATCH criteria indicate how vitally important biomarker selection is to a test's overall success. Upon examining the following biomarker targets associated with the IDoP, it becomes immediately evident how rare biomarkers that fulfill these criteria are.

In the case of malaria, the most frequently used diagnostic biomarker is *P. falciparum* Histidine-Rich Protein II (HRPII).[40] Historically, single biomarker HRPII tests laid the foundation for modern day LFAs. This protein meets some of the

biomarker benchmarks because it is abundant, accessible, stable, and highly specific to *P. falciparum*.[41] However, sole detection of HRPII for malaria diagnosis has proved inadequate. It is only expressed one out of four malaria species. In addition, its absence within a sub-population of *P. falciparum* positive patients in Peru and Brazil indicates a possible mutation, and its persistence in the bloodstream long after parasite clearance fails to differentiate active infections from those successfully treated.[42] To enable the detection of all malaria variations and disease states, HRPII is often detected in combination with a second biomarker, *Plasmodium* lactate dehydrogenase (*p*LDH). These multiplexed LFAs currently serve as the first-choice malaria RDT although they are still unable to detect the disease loads required for effective full elimination campaigns.[43] Improved sensitivity is needed for both single biomarker HRPII LFAs and dual biomarker HRPII/*p*LDH LFAs.[44]

HIV is a more complex disease because it is both incurable and requires continuous monitoring. Six commercially available rapid tests exist for HIV detection that screen for either antibodies against HIV subtypes, the viral capsid p24 protein antigen, or both, in peripheral fluids such as saliva, serum, or whole blood.[45] In a head-to-head comparison performed by the FDA, all tests provided sensitivities >95% and specificities >99%, when compared with conventional ELISAs,[46] validating the use of these tests and biomarkers for use in HIV diagnosis. However, one of the missing PoC diagnostic components in the HIV management landscape is a CD4 T cell enumeration system. The complexity of this type of measurement does not allow for its adaptation to the LFA platform, and the expertise, infrastructure, and cost needed to carry out this analysis using conventional cell counting instrumentation

cannot be directly transferred to low-resource regions. Addressing this shortfall, several groups have developed PoC CD4 cell counting technologies and systems.[47] Although these prototypes hold great promise, no single technology has yet established itself as a viable PoC system.

In many countries, TB diagnosis is still reliant on sputum microscopy, a 100 year-old method with known limitations.[48] This is due, in part, to the lack of sufficiently validated biomarkers to aid the development of improved PoC diagnostics.[49] Of the candidate biomarkers available for TB diagnosis, tests based on the detection of the lipoarabinomannan (LAM) in urine have established themselves as the target of choice for PoC tests. However, urine LAM testing lacks sensitivity for diagnosing TB in HIV-infected patients, and the test itself is unable to distinguish between infection with *M. tuberculosis* and other mycobacterial species.[48] For these reasons, they are only recommended as "rule-in" tests and are not unsuitable as general PoC screening tests.[50] Integrating new specific, high-affinity MREs into these tests could overcome these performance barriers, extending their application.[51]

Scope of This Work

This work seeks to improve the PoC diagnostic landscape for the most pervasive infectious diseases of poverty—malaria, TB, and HIV-AIDS. Through the employment of biomarker enrichment strategies, we aim to improve the performance of the leading commercially available LFAs, as well as develop new technologies to fill voids in the current diagnostic landscape. **Chapters II, III, and IV** report a steady maturation of a sample preparation strategy that employs metal affinity chemistry to concentrate and purify malarial biomarkers. The addition of biomarker-enriched samples to LFAs

surmounted the biological and sensitivity issues that plague malaria LFAs. In **Chapter V**, we evaluate the utility of the microvirin (MVN) lectin to serve as a molecular recognition element for the TB biomarker lipoarabinomannan (LAM). We then employ MVN to develop more sensitive and selective urine-based LAM LFA. In a departure from LFA applications, **Chapter VI** focuses on the development of an open diagnostic platform that automates novel, self-contained assay cassettes for malaria, TB and HIV diagnosis. Specifically, the implementation of this technology equipped with the CD4 cell-enumeration cassette would satisfy a diagnostic gap in HIV disease monitoring. Finally, **Chapter VII** provides an overall summary of this work and a perspective on low-resource diagnostics.

CHAPTER II

Rapid Concentration and Elution of Malarial Antigen Histidine-Rich Protein II Using Solid Phase Zn(II) Resin in a Simple Flow-Through Pipette Tip Format

Reproduced with permission from BIOMICROFLUIDICS (2017) 11, 034115

Introduction

Malaria remains endemic in 97 countries, and the World Health Organization (WHO) estimates that 3.2 billion people are at risk for the disease.[52] Thanks to the coordinated efforts of numerous international health organizations, the goal of elimination is now within reach. Past malaria control efforts demonstrated that achieving this goal would require a long-term commitment to strategic prevention and case monitoring. This level of vigilance prioritizes the need to identify all individuals infected with the parasite, in particular, the asymptomatic carriers that create transmission reservoirs for the disease.[53,54] The deployment of point-of-care (POC) diagnostics that achieve single parasite limits of detection is crucial to pinpointing these cases. Ideally, these tests would combine the robust and straightforward nature of rapid diagnostic tests (RDTs) with the accuracy of gold standard laboratory analysis.[55,56]

When RDTs were first introduced in the early 1980's, they provided a promising resource for POC testing. Unfortunately, these tests remain beleaguered by poor sensitivity and inconsistent quality.[57] Visual interpretation of RDT results is inherently subjective—especially at low parasitemias.[58,59] As part of an effort to mitigate RDT technical limitations and deliver a more conclusive diagnosis, Miller *et al* promoted

integration of the sample preparation process into the RDT workflow.[30] Malarial biomarker purification and enrichment methods have the potential to provide more accurate and objective readings by increasing the test line signal at lower parasitemias, therefore making previously undetectable levels of antigen observable.[38,39,60,61]

The structure of one of the most common malarial biomarkers, *Plasmodium falciparum* histidine-rich protein II (HRPII), lends itself to purification using immobilized metal affinity chromatography (IMAC). Since its inception in 1975, IMAC has become a cornerstone in the field of protein purification because of its ability to capture and purify proteins expressed with high histidine content or labeled with histidine-rich moieties.[62,63] In its most common form, a divalent nickel ion (Ni^{2+}) is immobilized to a chelating ligand anchored to a solid support. The protein's histidine-rich units bind to the free nickel ion through metal chelation chemistry, thereby removing it from its matrix. To elute the isolated protein for use in downstream applications, the IMAC support is exposed to high concentrations of imidazole, histidine's functional side chain, which outcompete the captured proteins for the Ni^{2+} coordination site. Considering that approximately 34% of HRPII's amino acid residues are histidine, the malarial biomarker possesses a natural avidity for divalent metal capture methods. This chromatographic method's utility in capturing HRPII has previously been demonstrated through the use of IMAC magnetic beads charged with Ni^{2+}.[38,39,64]

The current study continues to explore the use of IMAC technology through a practical, inexpensive, and ubiquitous format: the pipette tip. By placing a His-affinity resin bed in the end of a standard plastic pipette tip, the pumping action of the pipette draws the sample back and forth across the IMAC support, capturing HRPII on each

pass. Such an application enables field deployment of the microfluidic flow-through format requiring nothing more than a manual pipette. Incorporation of this platform also makes the required sample preparation and processing both easy and intuitive, necessitating only basic instruction. Most importantly, biomarker capture and elution could be accomplished in minutes. With these qualities at the forefront, we have created and optimized a pipette-based IMAC system specifically designed for HRPII enrichment. Progressing from a complete investigation of HRPII's binding affinity to an analysis of the solid support structure, we eventually established the ideal parameters for the IMAC purification and concentration of HRPII. After the completion of the optimization process, we examined the manufacturability of this system by contracting with a company specializing in custom pipette-based columns. The resulting commercial prototype was then evaluated for its utility in improving both the signal intensity and detection limit of malaria RDTs.

Material and Methods

Recombinant HRPII was graciously provided by PATH (Seattle, WA). D6 *Plasmodium falciparum* malaria stock was cultured in BSL2 facilities at Vanderbilt University. Cube Biotech PureCube Agarose Beads: Ni-NTA, Zn-NTA, Co-NTA, Cu-NTA, Zn-NTA XL, Zn-IDA XL (Monheim, Germany). Cube Biotech PureCube 1-Step Batch Mini columns (Monheim, Germany). Affymetrix USB PrepEase Histidine-Tagged High Yield Purification Resin (Santa Clara, CA, US). Jena Bioscience High Density Zinc Agarose, Low Density Zinc Agarose (Jena, Germany). G-Biosciences Zinc Chelating Resin (Geno Technology, St. Louis, MO). Bio-Rad Chellex-100 Resin (Hercules, CA, US). Clontech TALON Superflow Metal Affinity Resin (Takara Bio Group, Kusatsu,

Shiga, Japan). Bioreclamation IVT CPD Pooled Whole Blood (Hicksville, NY, US). ThermoScientific Nalgene Rapid Flow 0.2 µm filter, Fisher Scientific Certified ACS-Grade Zinc Sulfate crystals, Fisher Scientific Nitric Acid TraceMetal Grade (ThermoFisher, Waltham, MA, US). Certipur Certified Reference Material ICP Multi-Element Standard Solution IV, Sigma-Aldrich Glycerol, Sigma Ethylenediaminetetraacetic acid (Merck KGaA, Darmstadt, Germany). Rainin 250 µL Presterilized Wide Orifice Low Retention tips, Cat # RT-250WSLR (Mettler-Toledo, LLC, Columbus, OH, US). 28 µm stainless steel mesh, Cat # 85385T116 (McMaster-Carr Supply Company, Elmhurst, IL, US). Paracheck® Rapid test for *P. falciparum* malaria Ver. 3 (Orchid Biomedical Systems, Goa, India)

Analysis of divalent metal-HRPII binding kinetics

An Octet RED96 (ForteBio, Ca, USA) was employed to measure the binding kinetics of various divalent metals to HRPII through the use of a technology known as bio-layer interferometry (BLI). Within the parameters of the kinetic assay program, experiments were performed in 96-well plates using eight parallel biosensors manually regenerated with $CoCl_2$, $ZnCl_2$, $NiCl_2$, and $CuCl_2$. The regeneration process involved soaking manufactured nickel-coordinated nitrilotriacetic acid (Ni-NTA) biosensors in a 10 mM glycine pH 2 solution for 30 minutes to remove the factory-supplied nickel then incubating them overnight with the appropriate 10 mM metal ion solution. In order to quantify binding affinity, the freshly charged biosensors were equilibrated in phosphate buffered saline (PBS) for two minutes then incubated for an additional five minutes to incorporate the octet's standard loading step. The tips were then transferred to wells containing fresh PBS for one minute to create a baseline before moving them to sample

wells for a ten minute association step. These wells contained a 1.56 nM to 100 nM titration of recombinant HRPII biomarker diluted in PBS. Once the HRPII binding was complete, the tips were returned to the PBS baseline wells for a five minute dissociation step. This process was repeated for each of the four divalent metals used. In each iteration, one of the eight wells was designated 0 nM to serve as a blank. A comprehensive set of binding parameters was developed using a one-to-one global fit binding model.

Impact of divalent metal selection on HRPII capture

Four different divalent metal ions were screened using identical nitrilotriacetic acid (NTA) ligands and agarose resin bead matrices. In order to test which metal displayed optimal properties for isolating HRPII, 2.5 µL of each variety of IMAC agarose resin was loaded into Cube Biotech PureCube 1-Step Batch Mini spin columns and tested against samples of parasitized blood to measure the amount of time needed for maximum binding. Spin columns were prepared with the given amount of resin and washed with two bed volumes of 18 MΩ deionized (DI) water and one bed volume of equilibration buffer (50 mM phosphate buffer at pH 8.0, 300 mM NaCl, 10 mM imidazole). Each resin was tested in triplicate against identical parasitized lysed whole blood samples. Samples were produced by mixing equal volumes of pooled whole blood with lysis buffer (100 mM phosphate buffer at pH 8.0, 600 mM NaCl, 2% Triton X-100). Lysed samples were first screened through glass wool packed in a syringe and then through a 0.2 µm filter to accommodate the specifications of the spin column. After filtering, the blood/lysis solution was spiked with 200 parasites/µL using lysed D6 *Plasmodium falciparum* malaria parasite. 100 µL of prepared blood samples were

added to each column and mixed on a vortexer (approx. 2000 rpm) for time increments ranging from one to ten minutes to allow time for the HRPII protein to bind to the resin. Immediately following the mixing incubation, the columns were centrifuged at 14,000 x *g* for one minute to clear the supernatant which was then retained for analysis. 100 µL of elution buffer (50 mM phosphate buffer at pH 8.0, 300 mM NaCl, 500 mM imidazole) was added to each tube, and they were incubated again on the vortexer. All samples were eluted over the course of two minutes regardless of their initial binding time. After mixing, the columns were centrifuged again at the same settings, and the eluent retained for analysis. Previous studies utilizing metal affinity bead binding and elution were used to determine initial binding and elution parameters. The concentration of unbound HRPII remaining in the parasitized blood sample and the concentration of HRPII in the eluents were quantified using an HRPII enzyme-linked immunosorbent assay (ELISA).[38] The quantification of HRPII in these two samples informs the percentages of HRPII captured and recovered from the original samples for each of the divalent metals as a function of time.

Divalent metal loading capacity of commercially available solid phases

Inductively coupled plasma optical emission spectrometry (ICP-OES) was used to compare the amounts of metal loaded on equivalent amounts of resin. 50 µL of each resin were added to identical Cube Biotech spin columns. After washing with DI water to remove all stock solutions, each resin was stripped of its coordinated metal ions using three successive chelation washes of 100 mM EDTA solution, pH 8. The resin columns were incubated on a vortexer for five minutes with 200 µL of 100 mM EDTA solution then centrifuged for one minute at 14,000 x *g* to collect the supernatant. 100 µL of each

chelation wash was diluted in 10 mL of 5% trace metal-free nitric acid solution and quantified using a PerkinElmer Optima 7000 DV ICP-OES standardized using Certipur multi-element reference solution. The total amount of metal ions chelated in each wash was calculated and compared.

Standardization based on divalent metal concentration

All resins were standardized based on their number of zinc metal coordination sites. To determine the number of coordination sites, the factory-loaded metal ions were removed from identical volumes of resin, and then the same resin was recharged with Zn^{2+} ions. In a procedure similar to the one used previously to measure the vendor's loading of divalent metals on each resin, equal amounts of the various resins were loaded into the same spin columns. After two initial washes to remove the stock solution, each resin was subjected to five chelation washes. Each wash consisted of a five minute incubation on a vortexer with 300 µL of 100 mM EDTA solution, pH 8, followed by a centrifugation at 16,000 x *g*. All washes were retained for analysis to confirm that all metal ions had been fully stripped. Following the removal of the original metal ions, the resin was washed several times with DI water to ensure the complete removal of EDTA. Once the remaining EDTA had been cleared, each resin column was incubated for five minutes on the vortexer with 300 µL of 100 mM zinc sulfate solution and centrifuged at 16,000 x *g*. This process was repeated two more times for a total of three regeneration incubations. (As Chellex resin does not come with a metal ion preloaded, it was included in the experiment at the beginning of the regeneration wash steps.) After the resins had been recharged, they were washed again with DI water to remove any residual zinc sulfate solution. At this point, the reloaded resins were

stripped again using a chelation process identical to the one used to remove the original metal ions. Upon completion, 100 µL of each chelation wash was diluted in 10 mL of 5% trace metal-free nitric acid solution and analyzed with the same ICP-OES instrument. Final washes were also analyzed to confirm they were completely free of divalent metal ions. Using this data, the resins were standardized by comparing their individual Zn^{2+} loading capacities to the quantity of Zn^{2+} on the manufactured Cube Biotech PureCube Zn-NTA agarose resin and calculating the amount of resin necessary to achieve the same quantity of Zn^{2+} ions.

Solid phase selection

To select the type of resin that would be the most efficient at isolating HRPII, Cube Biotech mini spin columns were each loaded with the volume of resin needed to contain an amount of Zn^{2+} equivalent to that of 5 µL of Cube Biotech PureCube Zn-NTA agarose. Each quantity of resin was stripped and recharged individually using the method previously described. Once each of the resins had been regenerated and washed, a timed binding experiment identical to the procedure employed earlier to examine the binding efficacy of the different metals was conducted to compare the various resins. As the original binding experiment validated the potential for complete capture within one minute, that time point was the only one tested. The two minute elution time remained unchanged. Again, ELISA was utilized to quantify the results. The resins exhibiting the highest binding and elution efficiencies were selected to proceed to the next stage.

Determine optimal packing of prototype flow-through pipette tips

To determine the optimal resin volume and packing level needed to effectively bind and elute HRPII in the IMAC tip format, varying quantities of resin were loaded into stainless steel mesh fritted tips that were constructed in-house for use with manual Eppendorf Research Plus 20-200 µL pipettes. Each tip was made from two Rainin 250 µL Universal-fit Presterilized Wide Orifice Low Retention tips. Using a 3-D printed cutting guide, the end of each tip was cut off approximately 3 mm from the end to provide a wider surface area for fritting. The end was then pressed directly into a small square of 28 µm stainless steel mesh that had been pre-heated on a hot plate until the tip melted into the frit. After the newly-fritted tips had cooled, the excess mesh was trimmed away. The upper frits were made in the same manner except the top of each pipette tip was also cut away so only the last 4 mm attached to the frit remained. Once the modified fritted upper tip was inserted into the top of the fritted bottom tip, each assembled pipette tip contained an approximately 20 µL chamber to hold the resin (**Figure 2.1**)

Both the Jena Low-Density Zn-IDA and the PrepEase High-Yield resins were recharged with Zn^{2+} in 300 µL batches using the procedure detailed earlier, modified to process larger resin lots in 1.5 mL Eppendorf tubes. The two resins that would be used with the manufacturer's original metal ion loading were added to their own 1.5 mL tubes and included in the final wash steps to ensure a similar preparation with the associated resin loss. After removing the final wash, 300 µL of phosphate buffered saline with 0.1% Tween 20 (PBST) was added to each resin to achieve a 50% (v/v) suspension. The resuspended resins were then pipetted into each tip at resin volumes of 2.5, 5, 10, 15,

and 20 µL and prepared in triplicate.

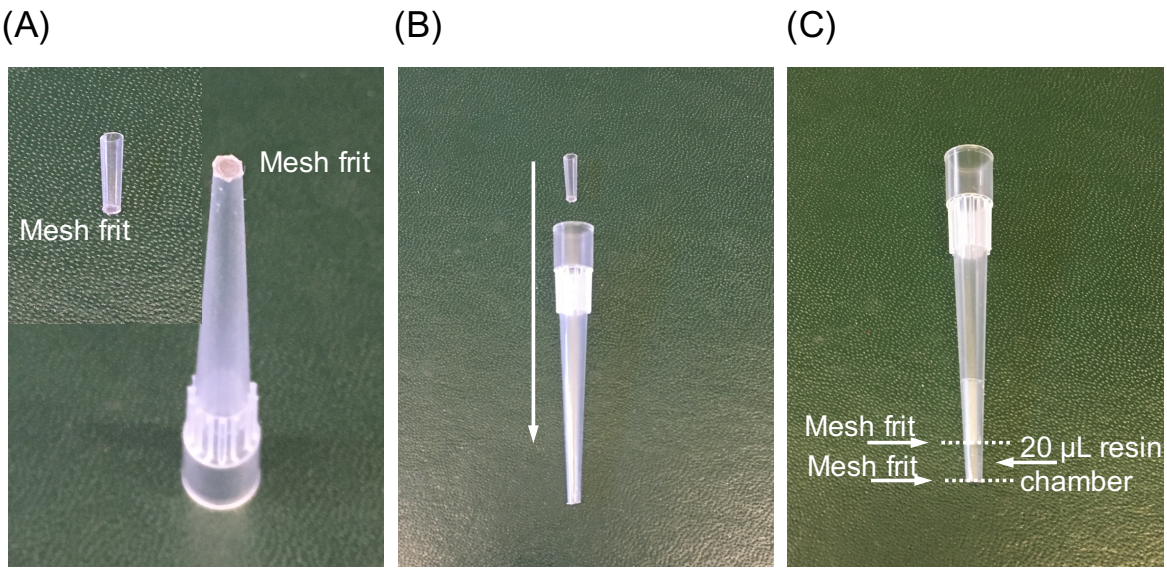

Figure 2.1: Constructing prototype flow-through column. (A) Using a hot plate 28 µm stainless steel mesh was melted onto two modified wide orifice pipette tips. (B) The upper frit was then placed into the top of the bottom-fritted tip and (C) seated at the bottom of the frit generating a 20 µL resin chamber.

Once the IMAC tip was loaded onto the pipette, fluid was steadily taken in and expelled for the allotted duration of each step. First, 100 µL of equilibration buffer was steadily pumped in and out for one minute. Immediately after, the tip was transferred to another tube containing 100 µL of parasitized blood/lysis solution prepared using the same method engaged for both binding experiments with only the 0.2 µm filtration omitted. One minute of binding time was allowed for this step, and, again, the supernatant was retained for testing. After completely expelling the sample solution, the tip was transferred to a third tube containing 20 µL of elution buffer. All samples were eluted by pipetting the buffer up and down for a one minute period. Both the binding supernatants and eluents were quantified using ELISA.

Evaluation of elution processing in prototype flow-through pipette tips

In-house fritted pipette tips were also used to examine the conditions needed to maximize HRPII recovery. First, the volume of the elution reagent was measured against the time of elution processing. As both factors determine the residence time of the reagent, it was deemed appropriate to explore both conditions at once. A single Zn^{2+}-charged resin at a fixed amount (10 µL) was selected for this experiment to establish a baseline for comparison. Each sample was processed in manner similar to the previous experiment. A 2 minute binding step, preceded by a 1 minute equilibration step, ensured complete capture of the biomarker in a 100 µL lysed blood sample at a parasitemia of 200 parasites/µL. Four elution times were tested: 15 seconds, 30 seconds, 1 minute, and 2 minutes. Each time point was processed with six different volumes of elution reagent ranging from 10 µL to 60 µL to determine which combination would provide the most effective elution parameters.

In conjunction with this experiment, Paracheck RDTs were tested for their tolerance to increased sample volume. Samples were constructed by spiking increasing volumes of elution buffer with a fixed amount of parasite culture to determine how the increased volume would alter test line presentation. Each RDT was processed according to the manufacturer's instructions and analyzed using an ESE Quant Lateral Flow Reader (Qiagen, Germany).

Performance validation of commercial 200 µL flow-through columns

Large batches of custom Zn^{2+}-loaded resins were produced using the same method as before, then submitted for manufacture into custom column pipette tips based on the optimized parameters generated in the previous experiments. Photographs of the custom Zn^{2+} flow-through columns were provided for reference

(**Figure 2.2**). Once the tips were acquired, a preliminary test was conducted to ensure that the manufacturer's glycerol-based stabilization fluid would not negatively impact HRPII binding or elution. This was accomplished by filling identical prototype tips containing the equivalent amount of recharged resin with pure glycerol and then processing using established binding and elution times but varying the equilibration time from one to five minutes. The volume of equilibration buffer used was also adjusted to 300 μL to provide adequate dilution of the glycerol. As binding and elution appeared unaffected by the addition of the stabilization liquid, the validation moved forward as planned.

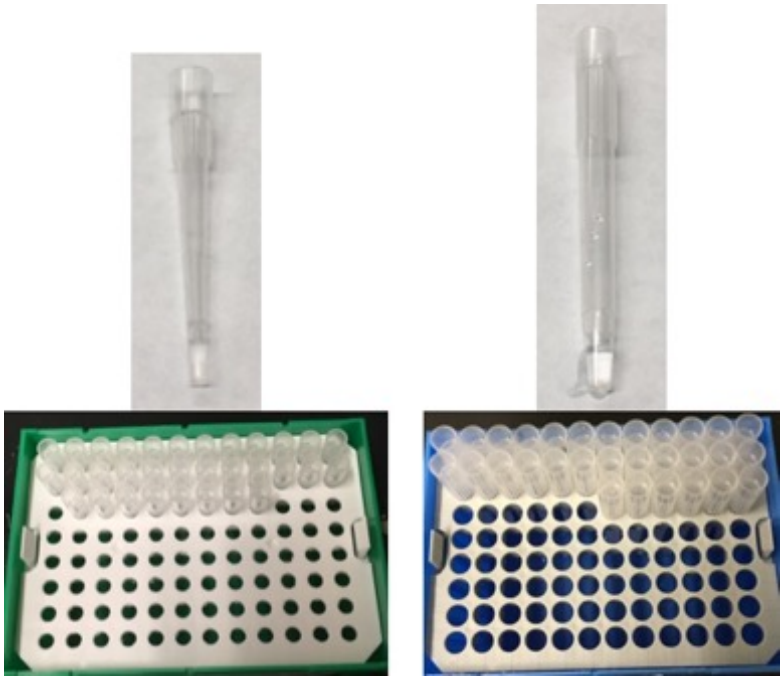

Figure 2.2: Visual of manufactured flow-through columns. The manufactured Zn(II) flow through column (top) and storage vessel (bottom) are shown for the 200 VUP (left) and 1000 VUP (right) columns.

First, the 200 μL tips were evaluated using the previously established processing protocol and three elution buffers containing 600, 700, and 800 mM of imidazole. Equilibration time remained at one minute although the increased equilibration buffer volume was maintained. A full two minute binding time was used for all samples to

ensure complete biomarker collection. The elution step also remained at 30 seconds irrespective of the variations in imidazole concentration. In order to verify recovery, a second elution step was employed to gauge efficiency. Sample preparation procedures were identical to those used in the previous experiment. Each test was performed in triplicate. HRPII content of binding supernatants and final eluents were analyzed using ELISA.

Evaluation of 1 mL commercial flow-through columns

The custom manufactured 1000 μL columns tips were evaluated separately. To accommodate the larger tip dimensions, the elution reagent volume was increased to 30 μL as the original amount failed to adequately cover the resin chamber. Otherwise, the equilibration and elution parameters remained the same. In order to fully gauge the advantages afforded by the increased tip volume, samples of 250, 500, 750, and 1000 μL were tested against binding times of two, three, and four minutes for each of the resins. Triplicate mock samples were prepared using the same methodology as before, but the parasitemia was reduced to a concentration of 50 parasites/μL to prevent potential saturation that could skew the results and to provide a more realistic approximation of test samples from asymptomatic patients. Again, the supernatants and eluents were quantified with HRPII ELISA.

Evaluation of flow-through columns to increase the LoD of commercially available RDTs

Parasitized blood samples processed using the 200 and 1000 μL tips under the optimized parameters were evaluated using Paracheck RDTs. Whole blood samples were spiked with parasite culture equating to 800 pM HRPII and serially diluted two-fold down to 0.79 pM for use with the 200 μL columns. The 1000 μL columns tested a

dilution series ranging from 3.13 pM down to 0 pM. Afterwards, the parasitized whole blood was combined with lysis solution in a 1:1 ratio and filtered through glass wool to remove cellular debris. 200 μL lysed blood volumes were used for the 200 μL columns and 1000 μL for the 1000 μL columns. The complete titration series was performed in triplicate using each column's optimized protocol with the exception of a final adjustment made to the 1000 μL column elution step. Rather than use the tested elution buffer, 700 mM imidazole was spiked into Paracheck's own running buffer, and the two-drop volume (~50 μL) was cycled through the column. The results from pre-processed samples were compared with the results from Paracheck RDTs performed according to the manufacturer's approved protocol using the same blood specimen lots. Each RDT was scanned and quantitated using the ESEQuant Lateral Flow Reader. These readings were used to generate 'Area under the curve' measurements for test line signals in this concentration range for both flow-through column processed samples as well as control samples.

Results

Quantitative binding kinetics and equilibration of divalent metal-HRPII interaction

Ni(II)NTA is commonly used to purify recombinant proteins expressed with six consecutive histidine (hexahis) residues because of its high affinity and selectivity for this tag under relatively mild conditions. The Ni(II)NTA system has been utilized to capture and concentrate HRPII, but to date, no systematic investigation has been conducted into the use of other divalent metals and chelating ligands.[38,39] Although affinity-specificity correlations have been drawn between IMAC metal coordination chemistry and histidine-rich moieties, we have found no reports of quantitative kinetic

data on the interaction between divalent metals and HRPII. Through the employment of BLI, a powerful label-free technique that measures biomolecular interactions in direct binding assays, a comprehensive set of equilibrium and kinetic data for HRPII binding was generated for each of the four divalent metals that commonly participate in IMAC metal coordination chemistry (**Figure 2.3**). The results reflect the general affinity and specificity trends reported for the hexahis-M^{+}-NTA system.[63] To validate the regeneration protocol and ensure that the data obtained was a product of the divalent metal interaction with HRPII rather than a consequence of biosensor manipulation, manufactured Ni(II)NTA biosensors were compared to biosensors that had been stripped and recharged with divalent nickel. No significant difference was observed (**Figure 2.4**).

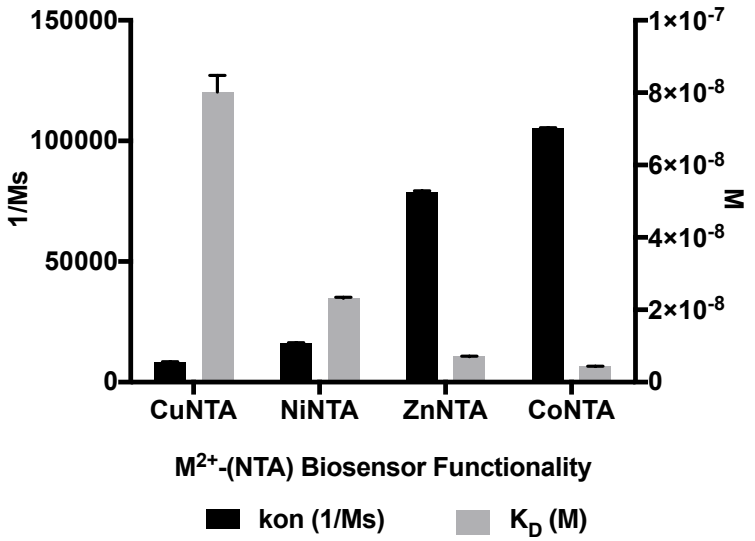

Figure 2.3: Molecular binding characterization of divalent metals with HRPII. Kinetic (black columns) and equilibrium (grey columns) binding data between Cu(II), Ni(II), Zn(II), and Co(II)-NTA data generated employing BLI. We explore how a balance of these characteristics may result in the most desirable outcome.

When selecting a divalent metal to rapidly capture HRPII and elute under mild conditions, kinetic and equilibrium tradeoffs must be considered. A large association

constant (k_{on}) represents the metal that facilitates the fastest capture, while a small equilibration constant (K_D) promotes a tight binding interaction to achieve strong retention. However, the opposite characteristics are desirable when trying to accomplish fast and effective elution. Ideally, a balance between kinetic attributes is the most desirable model to attain reversible capture. According to the BLI results, divalent zinc and cobalt best fit this character. At 7.5×10^4 $M^{-1}s^{-1}$, Zn^{2+} has the second highest k_{on} just below Co^{2+}'s at 1.1×10^5 $M^{-1}s^{-1}$. Divalent Nickel generated a K_{on} of 1.6×10^4 $M^{-1}s^{-1}$ and Cu^{2+} generated the lowest K_{on} value at 8.2×10^3 $M^{-1}s^{-1}$. Divalent zinc and cobalt also exhibited the lowest K_D's at 9.0×10^{-9} M and 5.0×10^{-9} M, respectively. Divalent Nickel displayed a K_D of 2.3×10^{-8} M and Cu^{2+} had the poorest K_D at 8.0×10^{-8} M.

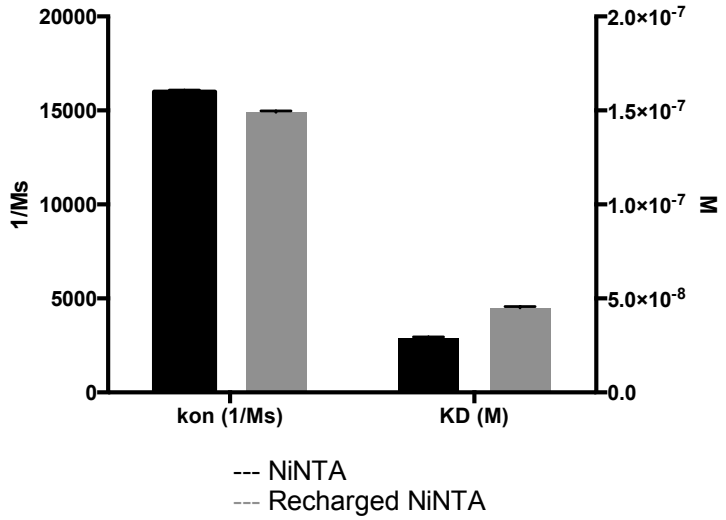

Figure 2.4: Impact of biosensor regeneration on molecular binding characterization. Kinetic binding (left) and equilibrium binding constant (right) data for factory biosensors (black) and biosensors that underwent a divalent metal stripping and Ni^{2+} recharging process.

Divalent metal-HRPII binding utilizing a model agarose solid phase

Cube Biotech resin was selected for use as a model solid phase to explore the active binding kinetics of the same four common coordinating divalent metals with HRPII. To investigate how the different metal species participate in the capture and

elution of HRPII in a complex matrix, the four different metal-loaded versions of this resin were evaluated by their ability to bind and elute HRPII as a function of time from parasitized lysed whole blood samples. In parallel, sister aliquots of the same resins were analyzed for total divalent metal content. This molar quantity signifies the total number of binding sites involved in the capture and elution of HRPII. By generating ratios of HRPII bound and HRPII released to the total amount of divalent metal per sample, performance metrics of nmols HRPII per mole of divalent metal were determined for each activity (**Figure 2.5**).

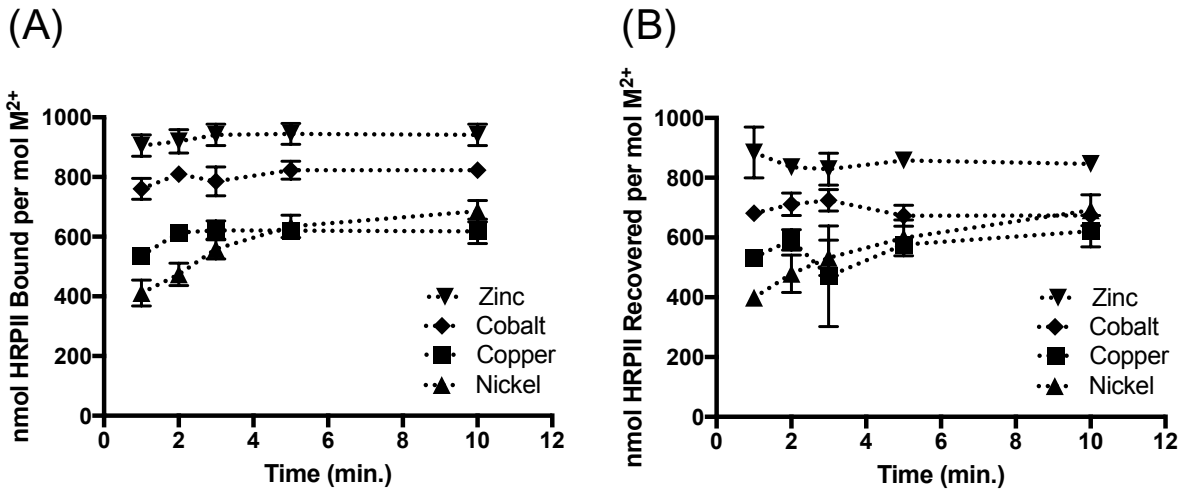

Figure 2.5: Impact of divalent metal selection on HRPII binding and recovery. HRPII binding (A) and recovery (B) performance of each divalent metal based on total HRPII binding per mol of divalent metal anchored to the solid phase. In both capacities Zn^{2+}-loaded resins outperformed the other metals tested. Note: Error bars may be obscured by the data point icon.

These results clearly identify zinc as the optimal divalent metal for HRPII capture and recovery. It presents a key balance of kinetic characteristics, allowing it to quickly bind HRPII yet not so tightly as to inhibit elution. The data also reveals that the most commonly used metal in IMAC chemistry, Ni^{2+}, actually performs quite poorly regarding HRPII capture within a complex matrix. Its poor binding and elution behavior add minutes to the total processing time and lead to incomplete recovery. Substituting zinc

for nickel has the potential to substantially improve the performance of IMAC chemistry in HRPII applications.

Solid phase selection for flow-through device

There are a number of different solid support materials available encompassing a variety of features including: structural material, support monodispersity, functionalization location (surface, internal, mixed), chelate ligand, thermal tolerance, and storage stability. To determine the optimal characteristics needed for the proposed system, eight different commercially available resins representing a variety of these features were selected and screened for HRPII binding and recovery efficiencies. A complete description of all IMAC solid phases tested in this study can be found in **Table 2.1**.

Table 2.1: The physical properties of select IMAC solid phase resins.

Name	Cube Biotech PureCube	Cube Biotech PureCube	Cube Biotech PureCube XL	Cube Biotech PureCube XL	G-Biosciences Zinc Chelating Resin	Jena Biosciences High Density	Jena Biosciences Low Density	Clontech TALON Superflow	Affymetrix USB PrepEase Histidine-tagged High Yield Purification	Bio-Rad Chelex® 100
Ligand	NTA	NTA	NTA	IDA	IDA	IDA	IDA	Tetradentate chelator (patented carboxymethyl aspartate)	IDA	IDA
Metal (Me^{2+})	Zn^{2+}	Ni^{2+}	Zn^{2+}	Zn^{2+}	Zn^{2+}	Zn^{2+}	Zn^{2+}	Co^{2+}	Ni^{2+}	None
Resin	7.5% Cross-linked Agarose	7.5% Cross-linked Agarose	6% Cross-linked Agarose	6% Cross-linked Agarose	6% Cross-linked Agarose	6% Cross-linked Agarose	6% Cross-linked Agarose	Superflow 6 Agarose (6% Highly Cross-linked Agarose)	Macroporous silica	Styrene divinylbenzene copolymers
Diameter (µm)	40	40	400	400	45-165	50-150	50-150	60-160	90	75-150
Manf.. Me2+ Loading	>15 µmol Zn2+/mL	>15 µmol Ni2+/mL (or ~25 µmol/mL)	>25 µmol Zn2+/mL	>30 µmol Zn2+/mL	20-40 μ moles Zn2+/mL resin	20-40 µmol Me2+/ ml resin	5-20 µmol Me2+/ ml resin	≥12 µmol/ml	?	N/A
Orig. Me2+ Loading (µmol/ml resin)	16.135 ± 0.226	20.533 ± 0.180	18.929 ± 0.372	28.518 ± 0.390	21.299 ± 0.826	23.016 ± 0.364	10.584 ± 0.226	15.775 ± 0.418	6.238 ± 0.135	N/A
Zn2+ Loading (µmol/ml resin)	24.503 ± 0.634	26.255 ± 0.741	22.521 ± 0.385	36.339 ± 0.849	22.755 ± 0.754	26.820 ± 0.822	13.248 ± 0.119	27.356 ± 0.696	8.965 ± 0.134	257.951 ± 8.410

While Zn^{2+} was found to be the most desirable divalent metal to employ in an HRPII extraction device, its performance could be enhanced or impeded by the qualities of the solid support. To quantify this effect on the binding and recovery of HRPII, each of the eight IMAC solid phases included in the screen was functionalized with Zn^{2+}. First, a reference metal loading density was determined for each of the candidate resins through the stripping and quantification of the factory-loaded metals (**Figure 2.6A**).

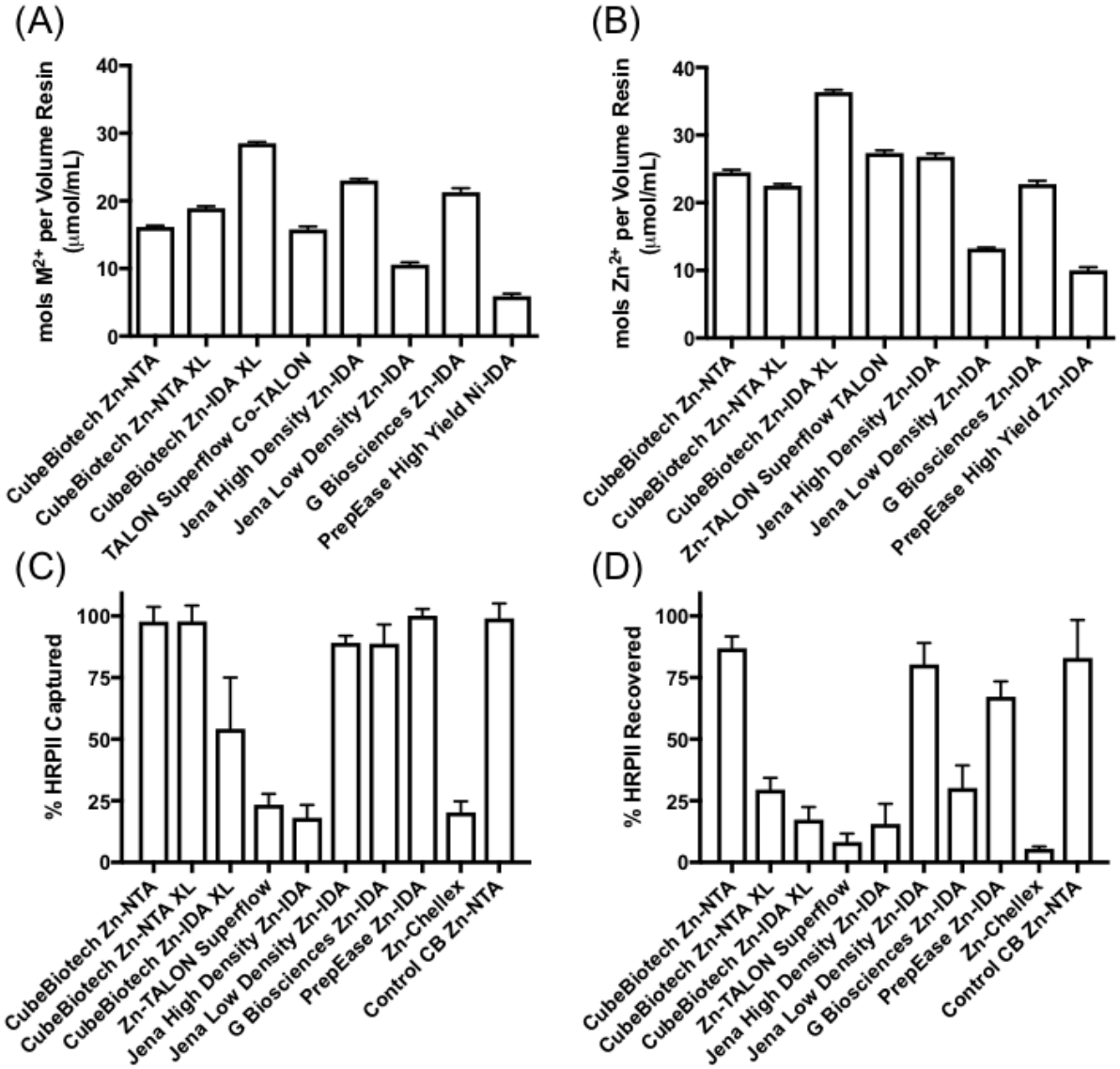

Figure 2.6: IMAC solid phase characterization and performance screen. Factory divalent metal loading density for each resin (A) with their corresponding Zn^{2+} loading densities (B) following the Zn^{2+} metal regeneration protocol provided a basis for normalization to fixed number of Zn^{2+} binding sites. The Zn^{2+}-normalized resins were evaluated using fixed binding and elution times for the capture (C) and recovery (D) of the total molecules of HRPII.

After regeneration with divalent zinc, the resins were stripped again, and the Zn^{2+} loading was quantitated and compared to the original amount. (**Figure 2.6B**). The recharging protocol was optimized to ensure that all divalent metal ions were removed from each solid phase. Even if the commercially available resin was originally functionalized with Zn^{2+}, it underwent regeneration to ensure that all IMAC resins were subject to identical treatments. As a general trend, the loading density of the factory metal was less than that of the regeneration. With the Zn^{2+} loading density determined, a measure based on the number of divalent metal atoms per unit volume of regenerated IMAC resin was produced. This measurement allowed all resins to be standardized with the same total number of Zn^{2+} binding sites. This normalization afforded an independent investigation of solid phase performance in HRPII capture (**Figure 2.6C**) and elution (**Figure 2.6D**).

These data show that although five different types of Zn^{2+}-functionalized resins exhibit capture higher than 90%, only CubeBiotech Zn-NTA, Jena Low Density Zn-IDA, and PrepEase Zn-IDA can efficiently elute more than 80% of the captured HRPII. In general, there was no correlation between the characteristics exhibited by the different solid phases and their subsequent performance in this screen. All three were synthesized with different chelating ligands and varied in terms of size, material, and monodispersity.

The only noticeable trend found in this study was the tendency for resins with lower Zn^{2+} loading densities to exhibit distinctly higher elution. This observation suggests that a higher density of Zn^{2+} may facilitate the rebinding of HRPII to neighboring coordination sites during elution, decreasing the overall elution efficiency.

CubeBiotech Zn-NTA exhibited more moderate Zn^{2+} loading levels yet maintained strong elution behavior. From this difference, it could also be inferred that overall performance is determined by the proximity of coordination sites resulting from the combined effects of loading, ligand, and support. As with the kinetics findings, it appears that balance of characteristics is necessary for optimal results.

Development of a prototype flow-through device with general processing parameters

The three best performing resins, CubeBiotech Zn-NTA, Jena Low Density Zn-IDA, and PrepEase Zn-IDA, were chosen as the preferred resins for flow-through pipette tip column development. To discover optimal design parameters for HRPII capture and elution, in-house fritted column tips were constructed as prototypes. Optimal resin loading was determined by pipetting parasite-spiked, lysed whole blood through a range of packed bed volumes and measuring the amount of HRPII extracted. Fully-packed resin beds appeared to lack the interstitial space necessary for the viscous lysed whole blood solution to pass through, given the pipette's limited vacuum generation. In contrast, loosely packed columns provided more mixing of the solid and mobile phases but lacked the total surface area and residence time needed to completely capture HRPII within the cycle. 10 μL resin beds, or columns half-filled with resin, produced the optimal balance of movement and contact without risk of clogging. HRPII capture efficiencies of 97.7 ± 6.45, 94.7 ± 6.4, and 90.0 ± 5.75% were observed for CubeBiotech Zn-NTA, PrepEase Zn-IDA, and Jena Low Density Zn-IDA, respectively (**Figure 2.7**).

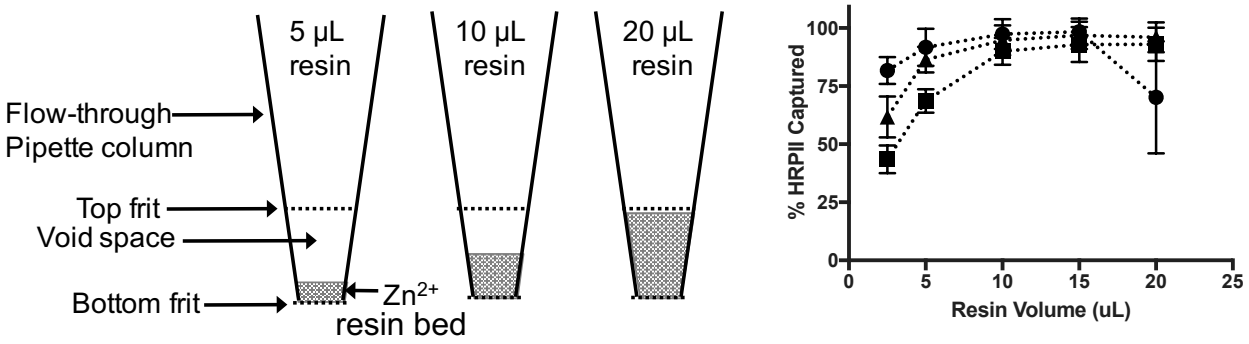

Figure 2.7: Evaluating packed bed resin for HRPII capture performance. As described in the above diagram, various resin volumes were packed into pipette columns constructed in-house. These volumes were tested against Cube Biotech Zn(II)NTA (circles), PrepEase Zn(II)IDA (triangles), and Jena low density Zn(II)IDA (squares) resins to evaluate HRPII capture efficiency in a lysed whole blood matrix.

In order to optimize HRPII elution from a flow-through device, the in-house fritted pipette tips were packed at the optimal 50% level with 10 µL of a single resin (Cube Biotech Zn(II)NTA). To examine the impact of elution reagent volume and processing time on the retrieval of HRPII, this experiment juxtaposed different traverse cycling time points against different elution volumes to discover which combination produced the most effective recovery. A 30 second elution time proved optimal at all reagent volumes tested with the 20 µL volume, providing the highest release at 78.0 ± 19.1 % of the bound protein (**Figure 2.8A**). The recovery decrease associated with increased elution times is likely the result of two primary factors: HRPII rebinding to the solid phase during the longer residence and cycling-induced aeration hindering contact with the elution reagent.

The elution volume of the proposed flow-through system also has implications in the function of the commercial RDTs. As shown in **Figure 2.8B**, a fixed amount of HRPII dissolved in increasing volumes of elution reagent produces a decrease in the test line signal when tests are otherwise performed according to the manufacturer's protocol. This phenomenon is likely the result of drastically reducing HRPII's residence

time in the conjugate pad. Substantially increasing the test volume with a fluid much less viscous than blood increases its mobility in relation to the gold signal reporter, abbreviating the binding window. To avoid this effect, the smallest volume that can efficiently elute the captured HRPII from the flow-through column should be used so as not to lose signal.

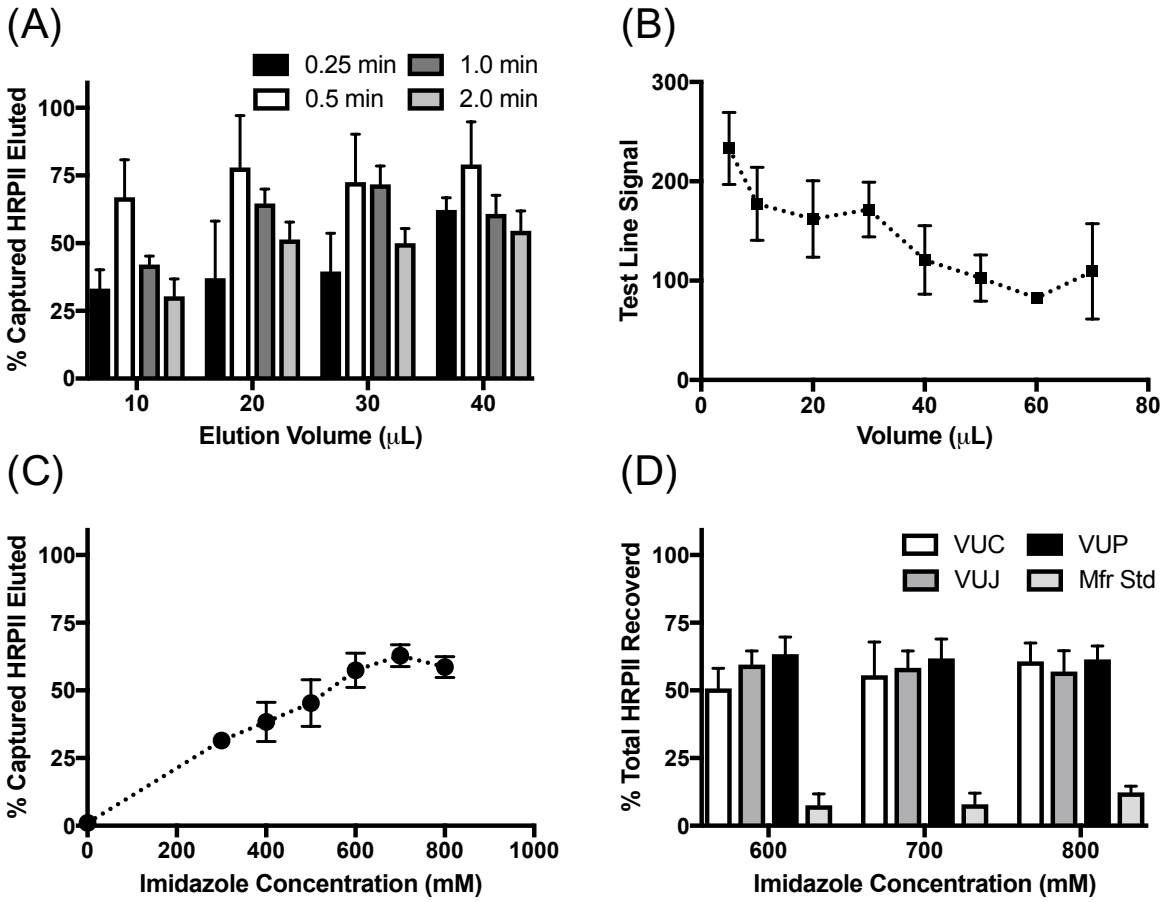

Figure 2.8: Optimizing the elution parameters for Zn^{2+} flow-through columns. (A) Evaluation of the % of captured HRPII eluted from the column as a function of elution volume and pipette cycling time. (B) The effects of increased elution volume on RDT signal. (C) Optimization of imidazole elution concentration for the prototype columns. (D) Final imidazole optimization of the manufactured Zn^{2+} flow-through columns.

The last elution parameter tested was the concentration of the competitive liberating agent, imidazole. The percentage of captured HRPII eluted was monitored as a function of increasing imidazole concentration. By employing the optimal elution

parameters of a 20 μL reagent volume and a 30 second cycling time, a peak concentration range of imidazole was identified between 600 and 800 mM (**Figure 2.8C**).

Evaluation of a manufactured Zn^{2+} flow-through device

Following the initial optimization of the capture and elution of HRPII using a prototype flow-through column, the three prospective Zn^{2+}-regenerated resins identified in the solid phase selection, PrepEase (VUP), Jena Low Density (VUJ), and Cube Biotech (VUC), were prepared and delivered to a commercial manufacturer to be constructed into a flow-through column based on our design parameters. The manufacturer loaded the selected resins into both 200 μL and 1,000 μL pipette tips using their patented method, which also included the addition of a proprietary glycerol-based liquid to each column, aiding in the stabilization of hydrated resin tips at room temperature. The manufacturer's own Ni-IMAC His binding columns were also procured in order to compare the experimental columns to a known commercial standard.

The purpose of this process was to explore the translation of our laboratory-developed sample preparation column into a commercially-manufactured format. Both columns possessed approximately the same size fritted resin chambers and were subsequently packed with the same amount of bed resin (10 μL). The 200 μL manufactured flow-through columns were validated using the processing times and reagent volumes previously determined using the in-house prototype. In addition to the overall device validation, this study also included a more focused evaluation of the elution reagent's imidazole concentration, further assessing the three peak values ranging from 600 to 800 mM. As no significant difference in HRPII elution was

observed, the 700 mM imidazole median concentration was selected for use in the remaining experiments (**Figure 2.8D**).

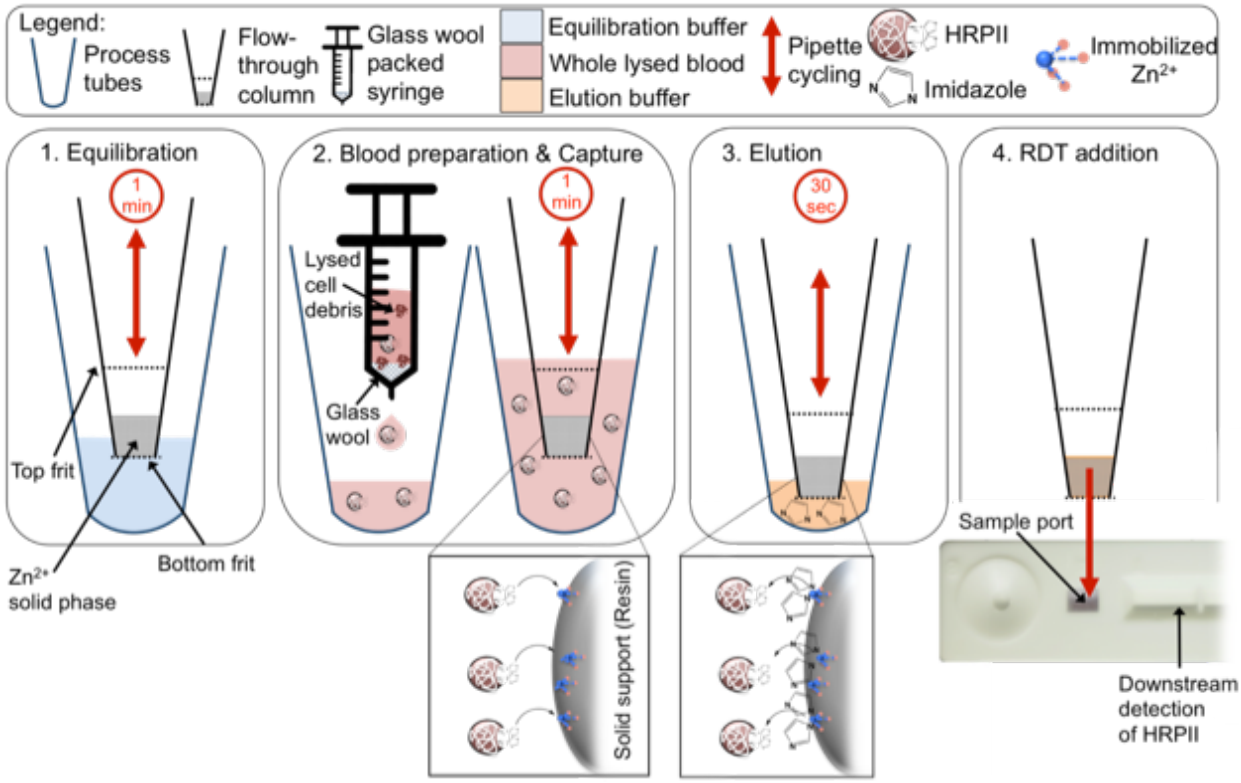

Figure 2.9: Schematic of the operation principle for the flow-through pipette column. (1) First, the pipette column is subjected to an equilibration step where the stabilization formula is expelled from the column and the column is hydrated by pipetting and depressing the pipette in 300 μL of equilibration buffer for 1 minute, or approximately 4 pipette traverse cycles. (2) Following the equilibration step, the column is introduced to a glass wool-filtered whole lysed blood sample where it is once again cycled for 1 min to enable HRPII capture. (3) It then is transferred to a final preparation tube where it cycles 20 μL of 700 mM imidazole elution buffer for 30 sec before (4) all eluent is ejected from the tip directly onto the RDT for downstream detection of HRPII.

Of the three resins validated using 700 mM elution buffer, the VUP candidate yielding 61.8 ± 1.7 % capture of the total HRPII available in the 200 μL whole lysed blood samples was selected to demonstrate the device's capacity to increase the visual intensity of RDT test lines. The decrease in HRPII recovery appears to be the result of a confluence of factors which will be addressed more fully in the Technical Notes section. The completely optimized three minute process is visualized in **Figure 2.9**. The 1000 μL

pipette columns were examined in terms of their capture efficiency in handling increasing sample volumes over extended processing times. The overall capture and elution efficiencies for 1000 μL tips containing VUP were similar, and of the binding times tested, the three minute cycle was deemed sufficient regardless of volume (**Figure 2.10**).

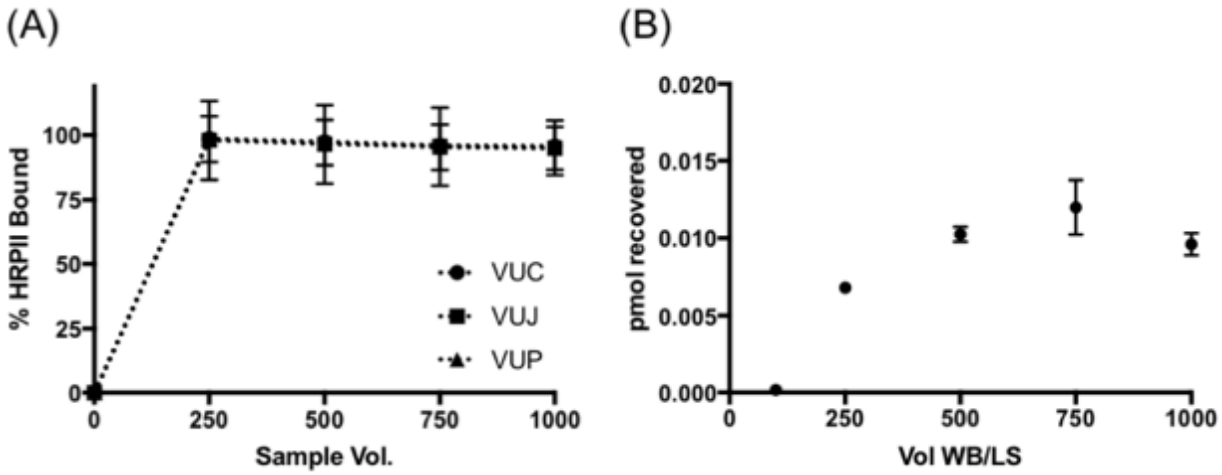

Figure 2.10: Performance of VUP 1 mL flow-through column. (A) As a function of increasing volume, % HRPII bound, or captured, was monitored to ensure a mixing time of 3 min was sufficient to facilitate complete capture. (B) Increasing volumes of a fixed HRPII concentration of lysed whole blood were processed using the VUP-1 mL flow through column and HRPII was quantified in the 20 μL elution volumes using ELISA. Optimization of binding for 1 mL pipette column.

The RDT enhancement step was evaluated using an ESEQuant Lateral Flow Reader. Employment of the RDT reader provided an objective quantification of the test line signal, directly comparing the enriched samples to the 5 μL whole blood control RDTs. The native antigen concentrations used in the parasitized lysed blood samples ranged from of 0.8 pM (46.6 pg/mL) to 800 pM (47.2 ng/mL) HRPII (**Figure 2.11**). The biomarker concentration region between 0 and 50 pM HRPII is often difficult to interpret since faint, poorly-developed test lines can be missed by health workers possessing reduced visual acuity or those operating in reduced lighting conditions.[65] Taking the ratio of 'area under the curve' values of the enhanced samples by that of the control

yields an average signal improvement of 6.8-fold at each of the antigen concentrations within this region. The most pronounced enhancement was observed at 25 pM HRPII with a 12.6-fold augmentation. These results demonstrate that pre-processing with a flow-through column increases RDT test line intensity and enables signal saturation at lower antigen concentrations per sample when compared to controls. This outcome will improve interpretation of test lines and promote more accurate diagnoses by healthcare workers.

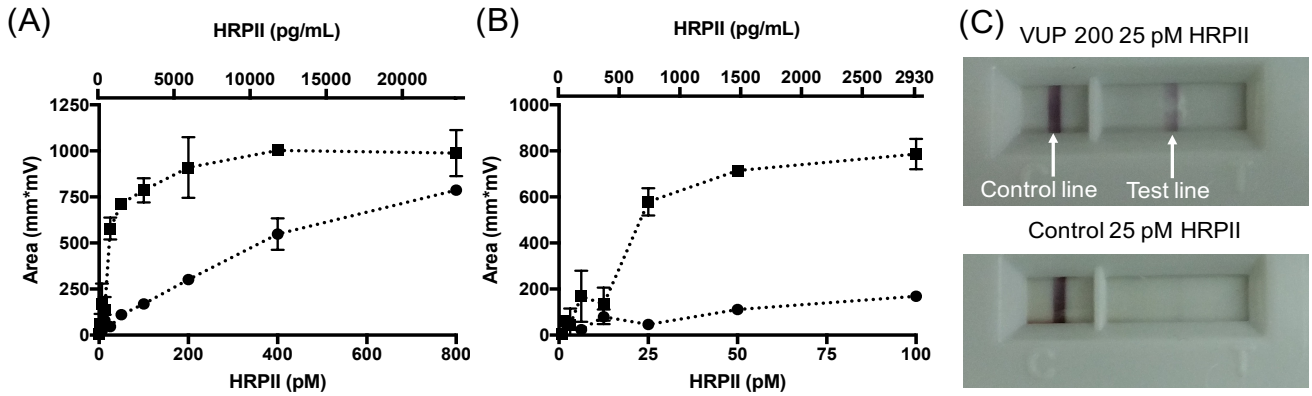

Figure 2.11: Increased LFA signal employing flow-through column process. (A) Reflectance signal measurements from RDTs processed with VUP 200 (squares) flow-through columns and control manufacturer suggested protocol (circles). (B) A detail of the 0-100 pM HRPII concentration regime and (C) representative RDTs for VUP 200 processed (top) and control (bottom) RDTs at 25 pM HRPII. An average enhancement of 6.8-fold was achieved for the 0-50 pM region.

A unique advantage of this preparation strategy lies in its ability to increase an RDT's standard limit of detection. The flow-through format easily adapts to larger pre-processed blood volumes, allowing more biomarker to be captured, concentrated, and delivered to the RDTs. This benefit enables visual detection of extremely low antigen concentrations, which might otherwise go undetected. The approach used to determine detection limit used in this study aligns with the WHO-FIND method for evaluating commercial RDTs.[66] Samples were processed in triplicate, and the lowest antigen concentration that yielded three consecutive positive RDTs was determined to be the

detection limit. The RDT reader was set at signal threshold of 15 mm*mV, where reflectance readings that were less than the threshold would not register a positive reading. This threshold limit was selected because of its correlation to the visual limit of detection as determined by the researchers in this study. The Paracheck-Pf RDT was chosen as an evaluation tool, because it ranks as one of the top performing commercial RDTs.[66] Using this established methodology, the Paracheck RDT achieves a detection limit of 3.13 pM HRPII under the manufacturer's intended protocol.

To explore the utility of the flow-through column as a means to increase detection limits, the RDT's established limit of detection was compared to the enhanced detection limit found using the 1 mL pipette column format (labeled as 1000 VUP) with 500 μL whole blood samples containing 0 - 3.13 pM (185 pg/mL) HRPII (**Figure 2.12**). A 500 μL whole blood sample represents the maximum practical sample volume that can be acquired through finger stick according to the Centers for Disease Control and Prevention.[67] The end result suggests that while this RDT attains a 3.13 pM HRPII limit of detection per the intended protocol, the VUP 1000 flow-through column enhancement decreased this detection limit to 0.78 pM HRPII. In addition, two of three 0.39 pM samples tested yielded positive RDT readings. Although the relationship between HRPII concentration and parasite density is life-stage dependent, the correlation found for the parasite stock culture used in this study suggests that 0.78 pM HRPII is the equivalent of approximately 0.35 parasites/μL.

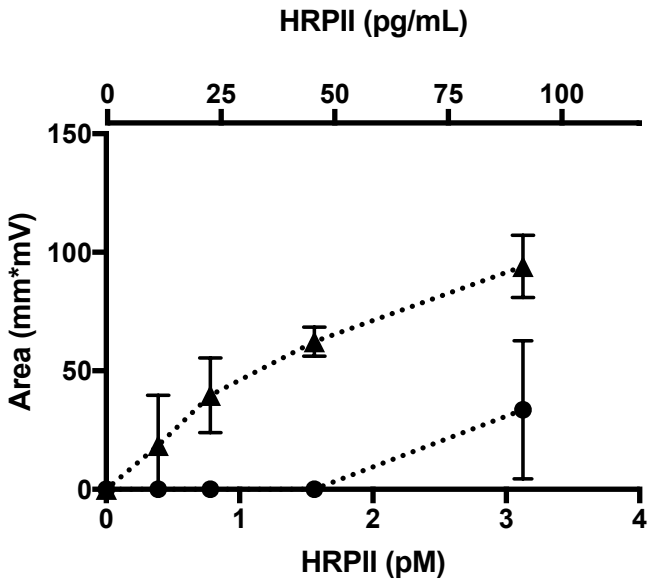

Figure 2.12: Increase in detection limit. Reflectance signal measurements from RDTs processed with VUP 1000 (triangles) flow-through columns and control 5 μL additions according to manufacturer suggested protocol (circles). The detection limit was lowered to 0.78 pM or approximately 0.35 p/μL

Technical Notes

Although the use of a pipette based flow-through column shows great potential as a front-end RDT sample preparation strategy, we identified some technical limitations during its development. First, lysed whole blood tends to clog the porous frit in this format necessitating the use of a glass-wool filtration step to remove the larger cellular debris. While lysing whole blood is necessary to ensure all HRPII biomarker is available for capture, this unintended side effect could be mitigated through an increase in the frit's pore size, allowing the debris to traverse unimpeded. The VUP resin that was ultimately selected in this study possesses an average diameter of ~90 μm, a size that allows for a substantial increase from the 24 μm filter mesh used by the manufacturer.

Another notable issue discovered during the elution step was that the movement of the small volumes of liquid through the solid phase induced bubbling and aeration that diminished HRPII recovery and inhibited effective transfer of eluent to the RDT. Larger volumes of reagent tended to alleviate this issue, but the RDT's failure to

successfully incorporate significant increases in sample volume precluded a complete exploration of this as an option. The culmination of these effects became even more pronounced in the 1 mL tips as adequate contact between the elution buffer and resin became more difficult given the increased interstitial space. Incorporation of the manufacturer's own running buffer into the elution step provided a substantial volume increase partially mitigating this outcome.

Discussion

The World Health Assembly's Global Technical Strategy for Malaria articulates goals of a 90% reduction in malaria infections as well as elimination in 35 new countries.[68] While large gains can be made through simple resource allocation, full elimination requires targeted efforts such as Mass Screen and Treat (MST) programs.[69] Implementation of such initiatives becomes even more challenging when faced with the isolated and rural areas common in malaria-endemic regions. This scarcity of health care facilities and trained personnel has led to an increase in the procurement and use of malaria RDTs, and although more than 80 commercial RDTs are currently available, their low sensitivity and subjective interpretation often hinders the efficacy of these malaria-control programs.[69,70]

The most common mistake made by novice test users is misinterpreting a faint positive or invalid RDT as negative.[71] The intensity of the test line is dependent on antigen levels but varies with matrix factors including blood viscosity and blood volume.[72,73] Matrix-induced anomalies such as incomplete clearing and red background make it more difficult to interpret these tests. These specific anomalies are found in 95% and 85% of products, respectively.[74] Integration of a brief, user-friendly sample

preparation strategy into RDT procedures is the most straightforward solution for removing anomalies associated with the blood matrix and increasing the intensity of test lines at lower HRPII concentrations. However, there are no generally accepted sample preparation strategies for RDTs. Our group has previously developed several magnetic bead-based HRPII extraction approaches that employ metal affinity magnetic beads to capture and escort HRPII to RDTs.[38,39,64]The key advantages of these systems include resistance to micro-channel clogging and direct elution of the magnetic capture beads deposited onto the RDT. This direct deposition of the solid phase onto the RDT promotes more effective HRPII elution and improved limits of detections. However, this system is hampered by longer processing times, more user steps, battery-powered equipment, and higher cost. In contrast, the pipette-based system described in this paper has shorter processing time, needs fewer user steps, requires less equipment, and is less expensive. Although this system does not reach the sensitivity of the magnetic bead-based system, we did achieve a limit of detection suitable for the identification of asymptomatic patients (0.35 parasites/μL) with a method more suited to low resource settings. A recent model generated by Slater *et al* estimates that this threshold will detect greater than 95% of the infectious disease reservoir.[75]

A more practical advantage of the pipette-based flow-through column is its potential for manufacture and commercialization. A commonly unaddressed aspect of POC diagnostic development is cost. This is often a critical barrier that ultimately determines the future of these technologies. While the prototype columns used in this study averaged $2.08 per unit, the economies of scale in conjunction with the growing number of manufacturers offering pipette tip modification will serve to drive down cost.

Unlike other technologies requiring the development of manufacturing platforms, full commercialization of this format could be achieved in the short term through collaboration with an industry partner. The established stability of silica-based resin ensures that this technology will remain field deployable, obviating the need for cold-chain storage and indicating a longer shelf life.[76]

Additional avenues that merit exploration are the use of other materials for the capture of HRPII. Such options include paper monoliths formed with capillary valves or functionalized nitrocellulose.[77,78] These materials can conceivably optimize antigen delivery to RDTs impacting their performance. Another direction we would like to pursue involves the modification of the pipette requirement, either by incorporation of the flow-through column into a disposable unit or through development of a modular component that can produce the cycling vacuum needed to process each tip. All of these technologies present opportunities to further customize this form factor to increase both its efficiency and deployability.

Constructing this processing platform using proven tools and techniques further establishes the robustness of the design concept. Adapting familiar applications to this specific purpose will also serve to overcome the resistance associated with the adoption of new technologies. Together, this combination of factors supports its capacity for commercialization. The possibilities associated with this low-cost, easy-to-use platform are not limited to HRPII; other antigens found in complex matrices could also be purified and enriched for detection by RDT or through other labeled or label-free strategies.

Conclusion

In this study, we established the potential of a flow-through pipette column as a clinical tool to increase the performance of current POC diagnostic technologies. Through extensive characterization and testing, we demonstrated how native HRPII could be concentrated from larger patient samples then released for downstream detection. While this sample pre-processing strategy was used to enhance the sensitivity of a single brand of lateral flow RDTs, we elucidate a method that can easily be adapted to other *Plasmodium falciparum* diagnostics targeting HRPII such as bench-top enzyme-linked immunosorbent assays (ELISA) or other spectroscopic methods where larger elution volumes do not hinder signal output.[22-24] Full development and deployment of this device offers a means for improving on existing diagnostic technologies to further malaria elimination efforts.

Acknowledgements

The authors would like to thank Dr. Kim Fong for culturing D6 *Plasmodium falciparum* used in this work, Austin Hardcastle for prototype production assistance, and M. F. Richards for critical comments concerning the manuscript. We would like to acknowledge Vanderbilt University for support from the Laboratories for Innovations in Global Health Technologies (LIGHT). We acknowledge funding from Intellectual Ventures/Global Good (Bellevue, WA).

CHAPTER III

Magnetically-Enabled Biomarker Extraction and Delivery System: Towards Integrated ASSURED Diagnostic Tools

Reproduced with permission from *Analyst* (2017) May 2; 142(9):1569-1580

Introduction

Intensive control efforts have successfully reduced global malaria prevalence by 30% between 2000-2015.[79,80] Yet, populations in low and middle-income countries (LMICs) still bear a disproportionate burden of malaria disease due to limited diagnostic capacity and treatment availability. The gold standard for diagnosis of malaria parasites is blood smear microscopy, a 100+ year old technique that requires well-trained technicians and instrumentation not readily available in rural areas. These smear techniques are especially challenging for patients with low level disease, where the detection of parasites requires more extensive training than in high level infections. In recent years, the low cost and ease of use of lateral flow immunoassays (LFAs) has precipitated a paradigm shift away from microscopy.[79,81] The widespread use of LFAs has enabled the rapid identification and treatment of patients with high parasite burdens–an important contribution to successful malaria control efforts. However, LFAs lack sensitivity, which prevents the diagnosis of subjects with low levels of parasites who are often asymptomatic carriers of disease.[82-86] The failure of LFAs to identify these disease states leaves individuals untreated, thus maintaining a reservoir for continued transmission.[87-89] As global malaria efforts shift from disease control to disease

elimination, existing LFA performance must be improved to accurately diagnose low levels of parasite at the point of care.

The World Health Organization (WHO) conducted an extensive analysis of commercially available LFAs for malaria diagnosis and concluded that the performance of many commercial malaria LFAs is sub-optimal at levels lower than 200 parasites μL^{-1}.[90] Diagnostic sensitivities in the single-digit parasites μL^{-1} are required to effectively identify the majority of asymptomatic individuals.[75] To address this LFA limitation, several new strategies have been developed that focus on enhancing the test line signal of the LFAs including: enzymatic-based signal enhancement,[91] silver-based enhancement,[92] dual gold nanoparticle detection,[93] architecture-based enhancement,[37] and oligonucleotide-linked gold nanoparticle aggregation.[94] While the development of these new technologies promise potential solutions to this problem, commercialization and deployment of completely new tests will not only be time consuming and expensive, but will also require approvals at the national level and retraining of field healthcare workers. Alternatively, the integration of a biomarker enrichment procedure at the front end of the standard LFA workflow circumvents the need to redesign, remanufacture, and reapprove commercially available LFAs. Although several particle-based biomarker enrichment systems have emerged, most of them suffer from long assay times, need for a cold storage-chain, poor enrichment efficiencies, and most significantly, have not been shown to function in a whole blood matrix.[60,95,96]

Our laboratories have previously developed a sample preparation strategy utilizing magnetic-based metal chelation chemistry to enrich biomarkers from lysed whole blood. In these studies, nickel(II) nitrilotriacetic acid (Ni(II)NTA) magnetic beads

were used to capture and extract histidine-rich protein 2 (HRPII) from lysed whole blood through an extraction cassette prior to LFA deposition.[38,39] Concentrating target biomarker from a large volume sample prior to LFA deposition was found to improve limits of detection, making it possible to measure parasite levels lower than the 200 parasites μL^{-1} WHO standard.

More recently, we reported that magnetic bead deposition onto an LFA within a housing device enabled direct transfer of HRPII onto a selected commercially available LFA.[64] This discovery removed the need for an additional extraction cassette and reduced the user steps needed to complete the procedure. However, the system still suffered from long incubation times, high cost per assay, a cumbersome user interface designed for only one commercial LFA, and the need for laboratory equipment. Here, we report the development of an integrated mBEADS device and workflow that overcomes these failure points to meet the WHO's ASSURED (affordable, sensitive, specific, user-friendly, rapid and robust, equipment-free, and deliverable) criteria for field deployment.[19,97] This report focuses on using the ASSURED criteria as a framework to systematically evaluate all assay components and advance our proof-of-concept technology to a POC system.[45]

We address affordability and rapid biomarker capture by optimizing the capture bead solid phase and chemistry. The optimal capture bead and all assay components are incorporated into a robust, single-use sample preparation tube that when combined with our battery-powered handheld mixer provides a deliverable assay platform. The 3D-printed device is designed to be user-friendly and to interface with five common LFAs that are used in low-resource areas for specific detection of the target biomarker.

Although this system requires some equipment, the battery-powered mixer, mBEADS device, and commercial LFA are compact and can be used on site, which is in line with the equipment-free principle put in place by the WHO.[45] The integrated mBEADS workflow increases the sensitivity of the leading LFAs to be able to detect antigen concentrations in blood associated with single digit parasitemias, while taking less than three minutes to complete, and contributing less than $0.25 to the total assay cost. This sample preparation system is well-aligned with the ASSURED criteria developed by the WHO for POC diagnostics.

Materials and Methods

Sample Preparation

All reagents and buffer components were purchased through Fisher Scientific unless otherwise noted. Pooled whole human blood with a citrate phosphate dextrose anticoagulant was used in each experiment (Bioreclamation IVT, USA, Item: HMWBCPD). *Plasmodium falciparum* parasite (D6 strain) was cultured in our lab as a source of HRPII for all experiments.

Table 3.1: Bead characterization data gathered from manufacturer datasheets and generated by flow cytometry.

Manufacturer	Name of bead chemistry	Magnetic bead size range	Bead composition	Stock bead concentration	Divalent metal loading capacity
Qiagen	Ni-NTA magnetic agarose beads Ni-NTA	20 – 70 µm	Agarose	8 beads/µL	N/A
Cube Biotech	PureCube MagBeads Ni-NTA	25-30 µm	Agarose	203 beads/µL	12 µeqv/mL resin
Clonetech	His60 Ni Magnetic Beads Ni-NTA	20-75 µm	Agarose	2 beads/µL	>20 µmol/g of beads
Bioneer	AccuNanoBeads Magnetic Ni-NTA	400 nm	Agarose	504 beads/µL	N/A

Packed Bead Volume as a Standard for Bead Capture Studies

Stock magnetic beads provided by each manufacturer varied by concentration, size, polydispersity, surface functionalization, and cross-linked solid phase density (**Table 3.1**). This made direct comparisons between the different solid phases challenging. To compare bead performance, bead volumes were standardized by loading 10 µL of homogenously mixed stock beads into a 1 mm diameter 25 µL microdispenser capillary tube (Drummond, USA) that was then closed with tube sealing compound (Mooremedical, USA). Beads were than magnetically compressed to the bottom of the tube using a 1" Neodymium magnet (K&J Magnetics, USA) and tapping the tube against the magnet for 2 min. A caliper was then used to measure the height of the magnetically packed beads inside the capillary tube. This measurement was performed in triplicate for all beads evaluated. Based on the diameter of the tube and the packed magnetic bead height, the packed bead volume was determined and normalized to 5.5 mm^3. Packed bead volume of 5.5 mm^3 corresponds to the following volumes of stock bead solutions: 10 µL of Qiagen, 2.1 µL of Cube Biotech, 5.7 µL of Bioneer, and 9.5 µL of CloneTech beads. See supplemental information for more detail (**Figure 3.1, Table 3.2**).

Bead Capture and Binding Capacity Studies

Four immobilized metal affinity chromatography (IMAC) magnetic beads were screened in these studies: Cube Biotech PureCube Ni(II)NTA MagBeads (Germany), Qiagen Ni(II)NTA Magnetic Agarose Beads (Germany), Bioneer AccuNanoBead Ni(II)NTA (Korea), and CloneTech His60 Ni Magnetic Beads (USA). To evaluate bead performance, whole blood was lysed by mixing 1:1 with lysis buffer (100 mM phosphate

buffer pH 8.0, 600 mM NaCl, 20 mM Imidazole, and 2% Triton X-100 solution). *P. falciparum* D6 parasite culture preparations were spiked into lysed whole blood to achieve concentrations ranging from 65 - 4000 parasites μL^{-1}. The standardized bead volumes were added to 100 µL of lysed whole blood parasite preparations in a 96 well plate (Corning, USA) and allowed to incubate for 10 min on a plate shaker (VWR, USA). After incubation, magnetic beads were separated by a 96-well plate magnet (MagWell, USA), supernatants were collected, and an enzyme-linked immunosorbent assay (ELISA)[23] was performed to measure the residual HRPII not captured by the beads. Bead capture efficiency percentage was calculated based on these HRPII concentrations.

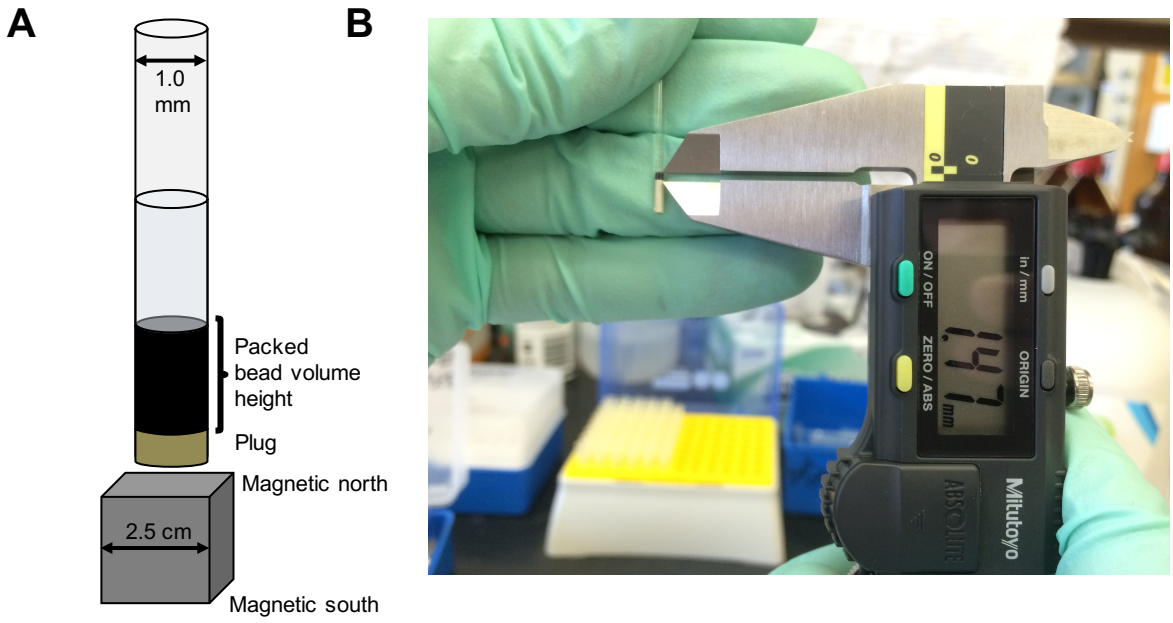

Figure 3.1: The method used to standardize the volume of beads used from each manufacturer for performance comparisons. **A)** 10 µL of homogenized bead solution from the stock bead solution were added to a capillary tube, plugged with cha seal, and magnetically packed using a 1 $inch^3$ Neodymium magnet. **B)** The height of the magnetically packed beads is measured using a caliper.

Table 3.2: Standardization based on magnetically packed bead volume. Data from the magnetically packed bead experiment to determine the magnetically packed volume of beads from separate bead manufactures. The height was then used to determine the standardized volume of stock beads to achieve 5.5 mm^3 magnetically packed volume of beads.

Manufacturer	Volume of stock beads added to capillary tube (µL)	Average packing volume height (mm)	Packed bead volume (mm^3)	Normalized packed volume (mm^3)	Standardized volume of stock bead solution used per assay
Qiagen	10	7.0 ± 0.1	5.5	1	10
Cube Biotech	10	22.6 ± 0.1	26.7	0.21	2.06
Clonetech	10	14.8 ± 0.0	5.8	0.95	9.48
Bioneer	10	24.5 ± 0.1	9.6	0.57	5.71

IMAC Divalent Metal Screening

Agarose beads functionalized with nitrilotriacetic acid (NTA) chelating ligand loaded with one of four divalent metals (Co^{2+}, Ni^{2+}, Zn^{2+}, and Cu^{2+}) were procured from Cube Biotech. Per manufacturer datasheet, the metal ion capacity of these beads is approximately 12 µeqv M^{2+}/mL resin. Binding kinetics were evaluated for each bead type by examining the concentration of HRPII left in sample supernatants as a function of incubation time. Standardized volumes of magnetic beads were added to 100 µL lysed whole blood spiked with *P. falciparum* D6 parasite culture to a final concentration of 200 parasites μL^{-1}. At 1, 2, 5, and 10 min incubation times, beads were separated using a 96-well plate magnet and supernatants were collected. ELISA was used to estimate residual HRPII not captured by the beads.[23]

Single-Use Bead Lyophilization Compatibility and Stability Assessment

Ten different assay compositions (100 µL) were lyophilized in 0.5 mL Flat-Cap PCR Tubes (Fisher Scientific, USA) to assess optimal lyophilization parameters. Trehalose and polyethylene glycol (PEG) 8000 were supplied by Sigma-Aldrich (USA)

and evaluated as potential additives during the lyophilization process to maintain the integrity of the three dimensional agarose network.[98] Samples were frozen at -80 °C, placed in the lypohilizer (Labconco, USA), and dried at -80 °C under vacuum (0.133 mBar). After lyophilization, samples were stored in a plastic bag equipped with silica desiccants. Fifty microliters of hydrating lysis solution (2% triton X-100 in D.I. H_2O) was added to lyophilized samples. Samples were rehydrated and homogenized by mixing for 5 sec on a battery-powered orbital mixer made from a personal massager (Wahl Corporation, prod. no. 4293).[99] Sample preparation tubes were removed from the orbital mixer for the addition of 50 µL of 200 parasites μL^{-1} blood, then returned to the mixer for a 1 min incubation. Samples were then placed on a magnetic rack (Life Technology, USA) to separate the beads from the sample. Each sample supernatant was analyzed by HRPII ELISA to determine capture efficiency.[23] To confirm sample tube stability, this experimental protocol was performed with sample tubes that were housed in a plastic bag containing silicon desiccant packets for 386 days after lyophilization.

Device Design and Development

The mBEADS device utilizes magnetic bead enrichment to deliver concentrated HRPII onto commercially available malaria LFAs to enhance test performance. This was achieved through the use of 1) flexible plastic spacers constructed from zip ties (McMaster-Carr, USA) in the inner rails of the LFA slot to center the alignment of each LFA, 2) a multi-level backstop to position the sample deposition pad of each LFA directly below the sample tube holder, and 3) a soft rubber stopper to enable the sample tube to be depressed for deposition pad contact (**Figure 3.2**). The cantilever-based sample tube holder is a feature that simplifies sample handling analogous to a common

office stapler: it flips open to accommodate loading the sample deposition tube, flips closed for magnetic bead collection, and depresses for bead delivery onto the LFA sample pad. This design also incorporates a lock to secure the sample deposition tube, minimizing sample loss and positioning variability when the top is flipped closed. The final mBEADS device reported here underwent twenty-nine iterations to improve user-centric features, make compatible with 5 commercial RDTs, and optimize bead deposition (**Figure 3.3**). The mBEADS device was fabricated using 3D printing

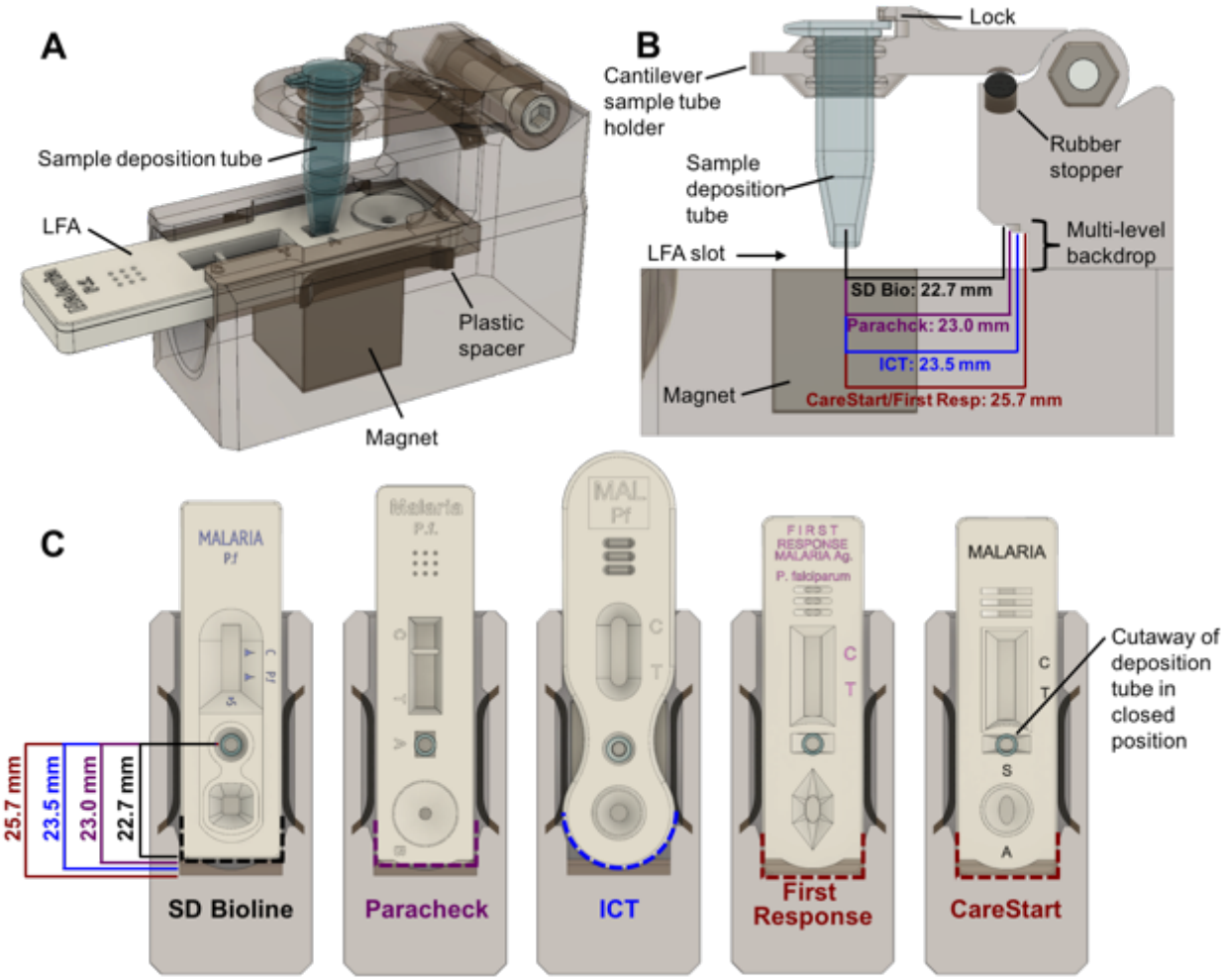

Figure 3.2: 3D device design for automatic LFA alignment and magnetic bead transfer. A) 3D rendering of the mBEADS transfer device shown with Paracheck LFA and sample deposition tube inserted. B) Cross-sectional side view of the bead transfer device depicting the multi-level backstop for aligning each LFA despite the various distances from the end of the LFA to the center of the sample deposition port. C) Cross-sectional top view depicting the variation in depth for each LFA after insertion into the bead transfer device. Dotted lines indicate the backstop position for each LFA.

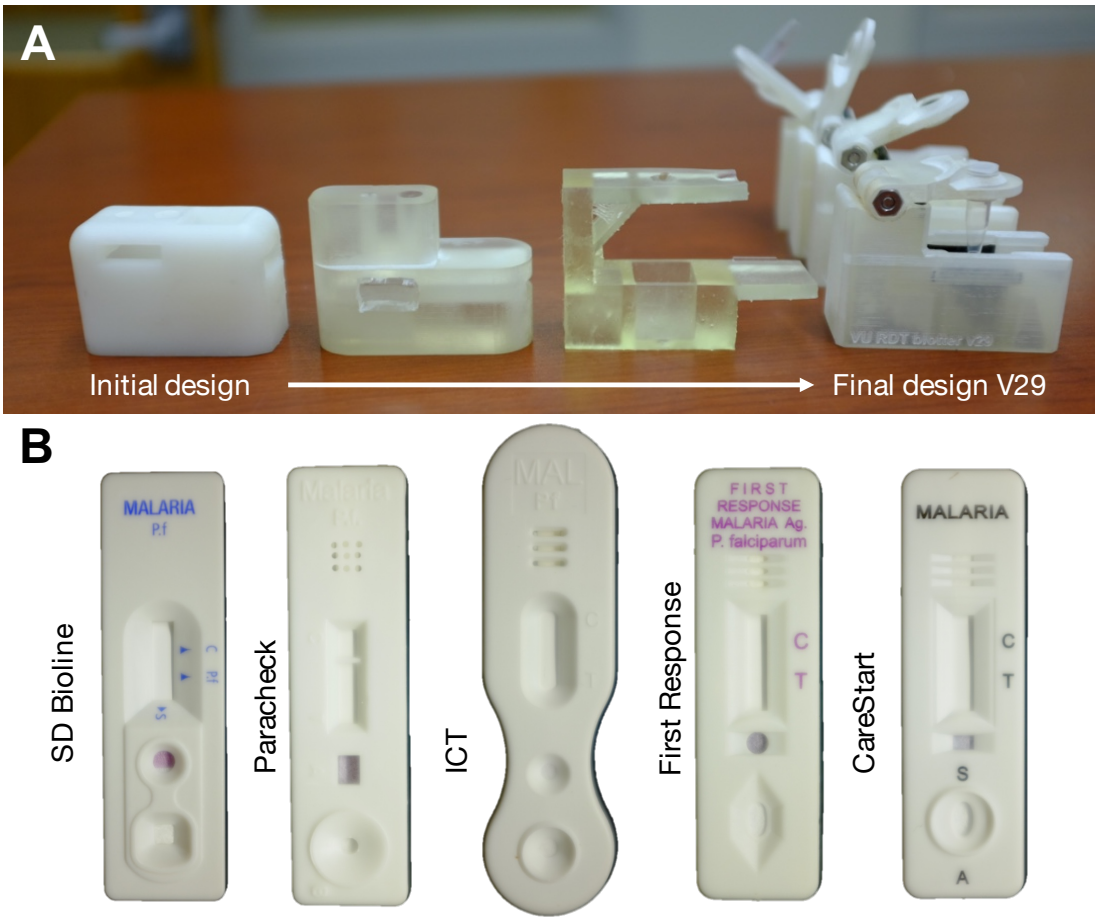

Figure 3.3: The mBEADS device and compatible RDTs. A) A photograph showing multiple iterations of the universal deposition device and B) photographs of the different compatible RDTs depicted in Figure 3.2.

technology allowing for potential modifications to be readily made to accommodate alternate LFAs if desired. Utilizing this 3D technology provides substantial flexibility compared to alternative diagnostic enhancements.[100]

The bead transfer devices were designed using Fusion 360 software (Autodesk). Since manufacturers adopt unique form factors for their tests, mBEADS was engineered to accommodate five commercially available malaria LFAs for *Plasmodium falciparum* HRPII: Paracheck (Orchid Biomedical Systems), SD Bioline (Standard Diagnostics Inc), First Response (Premier Medical Corporation Ltd.), Care Start (AccessBio), and ICT Pf

(ICT International) (Figure 1C). The devices were 3D printed (ProJet 3510 HD *Plus*, 3D Systems, USA) using VisiJet M3 Crystal material (part no. 2184-905).

Magnetically-assisted Bead Gathering Study

To standardize the end-user workflow, the time required for beads to be gathered in the presence of a magnetic field was measured using time-lapse photography. Magnetic beads (5.5 mm^3 µL, Cube Biotech) were added to microcentrifuge tubes with 50, 100, 200, and 300 µL of whole blood lysed with 1:1 v/v, blood/lysis buffer, to a total volume of 100, 200, 400, and 600 µL, respectively. The total lysed blood volumes were vortexed briefly to achieve a homogenous spatial distribution, and then placed in a holder 5 mm above a 1" Neodymium magnet, replicating the magnetic field configuration when the sample deposition tube is placed in the mBEADS device, in its closed position. Additional lighting was used to create a clear distinction between the pixel intensity of the settled beads and that of lysed blood. A video camera (Edgertronic, USA) was set to capture 10 frames per second for 90 s. Images were loaded into custom image-processing software, written in MATLAB v8.5 (MathWorks, USA), and binary image segmentation isolated the clustered beads at the bottom of the tube from the rest of the blood, based on pixel intensity. The combination of lysis buffer and intense illumination resulted in a clear distinction between the beads and lysed blood solution. A connected component algorithm was used to quantify the area (in $pixels^2$) of the settled bead cluster in each frame.

Parasite Titration for Limit of Detection Determination

Enhanced test samples were prepared by hydrating the lyophilized samples with 50 µL of lysis solution as described above. The optimized 1 min mixing time determined

in the incubation studies was used for the lyophilized Zn(II)NTA single-use sample tubes. Samples were prepared with 1, 2, 5, 10, 25, 50, 100, 150, and 200 parasites μL^{-1} for both unenhanced controls and mBEADS enhanced LFAs using each of the following tests: Paracheck, First Response, and ICT Pf. Fifty microliters of blood, spiked at the appropriate parasitemia, was then added to the sample tube and the sample was placed back on the handheld orbital mixer for 1 min. The sample deposition tube, a modified PCR tube, was inserted into the deposition device in the 'open' position. PCR tubes were modified by cutting off the closed end with a razor blade using a standardized custom tool to provide a consistent aperture large enough to facilitate efficient bead transfer upon contact with the LFA conjugate pad (~2 mm diameter). The cap of each PCR tube was sealed with Teflon tape to prevent magnetic bead loss in the crevasses of the lid. After 1 min of mixing, samples were removed via pipette and transferred to the sample deposition tube. The LFA was inserted into the mBEADS device and the device top was flipped to position the sample deposition tube directly over the conjugate pad (aligned with the center of the 1" magnet). The depositions tube's millimeter-diameter tube aperture creates a stable surface tension valve that retained the sample and allowed beads to collect at the meniscus formed at the bottom of the tube during the 1 min bead collection.[101] The developed surface tension valve prevents premature transfer of magnetic beads to the LFA during magnetic bead gathering step. The cantilever-based tube holder was then depressed briefly by the user in order for the bead-filled meniscus to make contact with the conjugate pad, breaking the surface tension valve, and transferring the beads to the LFA. The LFA was removed from the device and running buffer modified with 500 mM imidazole was added to the

LFA running buffer reservoir. For unenhanced controls, 5 µL whole blood samples were pipetted onto the conjugate pad and LFAs were used per manufacturer's instructions.

The HRPII test line signals generated were quantified with an ESEQuant Lateral Flow Reader (Qiagen Inc, USA) between 25 and 30 min after sample deposition. Wicking pads were removed and test strips were inserted into the reader to measure reflectance (test line colorimetric intensity) of the control and test lines for all samples. Test line intensities were analyzed in the ESE Quant LF studio software with a peak area at a fixed baseline using a signal threshold of 30 mV. Experiments were performed in triplicate and reported as average peak area.

Determining the Limit of Detections for LFAs

Each sample, at varying concentrations, was deposited onto an LFA in triplicate, and the mean test line peak areas were calculated to generate one data point for each concentration. For full parasite titration experiments, linear regression was used to develop a statistical model to estimate concentration as a function of signal intensity. The error in the y-intercept and the slope of the regression line were inserted into the following equation to provide the limit of detection (LOD) (**Equation 3.1**). Linear regression and limit of detection calculations were performed for both enhanced and unenhanced LFAs.

$$x_{LOD} = \frac{3(\text{error in y-intercept})}{\text{slope}} \qquad \textbf{(Equation 3.1)}$$

Efficiency of HRPII Deposition by ELISA

HRPII ELISA was used to quantify residual HRPII in specimens after incubation with magnetic HRPII capture beads and subsequent deposition onto the LFA.[38] After deposition of the beads onto the LFA using the mBEADS device, the remaining sample

solution and residual beads were collected in the sample preparation tube via centrifugation. Residual beads were separated using a magnetic rack and supernatants were removed and analyzed using HRPII ELISA. These beads were magnetically separated, washed three times with wash buffer (1X PBS, 0.1% Tween-20), and incubated in elution buffer (50 mM phosphate buffer, 300 nM NaCl, 500 mM imidazole buffer, 0.1% Tween-20) for 5 min. The eluent was then examined by ELISA to quantify the captured HRPII left behind on beads.

Increased Sample Volume Study

To determine the improvement in sensitivity that mBEADS provides with larger sample volumes, additional reagents were prepared at larger total volumes. Lyophilized reagents were scaled appropriately for the desired blood sample volume. The same optimal lyophilization parameters described above were used, except the lyophilization buffer (50 mM phosphate buffer pH 8.0, 300 mM NaCl, 10 mM imidazole, 10% trehalose) mirrored the total sample volume to be added. For example, single-use sample tubes prepared for the 400 µL total sample volumes were lyophilized with 400 µL of lyophilization buffer. All samples were spiked to 1 parasite μL^{-1} for the 50, 100, 200, and 300 µL blood sample volumes used (reported in results as total volumes after the 1:1 lysis method). Mixing times and bead settling times varied: 1 min mixing and 1 min settling time for 100 and 200 µL, and 2 min mixing and 2 min settling time for 400 and 600 µL. Using the mBEADS system, each sample was deposited onto a Paracheck LFA and read, following the suggested 30 min development time, using an ESEQuant Lateral Flow Reader. For control samples, 5 µL whole blood samples were pipetted onto the conjugate pad and developed per manufacturer's instructions. A F-test was

performed on the data series to determine if the variances observed in the data set were significant.

Results

Motivated by the lack of field deployable LFA enhancement technologies, mBEADS was developed to better align a proof-of-concept biomarker enrichment strategy with the WHO's ASSURED criteria. The mBEADS approach has a straightforward workflow composed of a single-use patient sample tube, a transfer pipette, a portable battery-powered mixer,[99] and a user-friendly 3D-printed LFA alignment and bead deposition device that increases the performance of LFAs currently used in the field. Together, these components overcome prohibitive barriers in previous technologies enabling the translation of this sample preparation technique to point of care for countries that are embarking on malaria elimination campaigns.[102] Simply by collecting more whole blood sample from the patient, the proposed system employs rapid magnetic bead assisted capture, concentration, and delivery of target biomarkers to LFAs to achieve the increased diagnostic sensitivity needed to be effective in elimination campaigns.

Magnetic Capture Bead Selection

To make a biomarker enrichment system that is field deployable, improvements in processing time, reagent stability, and assay cost had to be made to our previous approach. The magnetic capture bead, the chemically functional component in this assay, was targeted for system optimization to address these limitations. The system was optimized by exploring the interactions between the capture bead and HRPII. The capture beads used in this study are immobilized metal affinity chromatography (IMAC)

magnetic beads that exploit the affinity of the high number of intrinsic histidines in HRPII towards divalent metals immobilized on a magnetic solid support. This is an ideal capture bead to use in low-resource settings because it is robust, lacks biological capture agents, and provides a gentle elution strategy that is compatible with LFAs. The two functional components of these magnetic beads are the solid phase and the immobilized divalent metal. Previous studies that used IMAC chemistry to isolate HRPII employed 20 µL of Ni(II)NTA Qiagen magnetic beads, calculated to be 11.0 mm^3 of magnetically packed beads, captured approximately 80% of HRPII available in a 100 µL lysed whole blood sample spiked to 200 parasites μL^{-1}. This capture was achieved after a vigorous 10 min mixing step.[64]

Until now, no studies have been performed that investigate how solid phase and choice of immobilized coordinating metal ion impact HRPII capture. To evaluate the impact of magnetic bead solid phase on HRPII capture, four commercially available IMAC solid phases charged with divalent nickel were procured and tested for HRPII capture performance. HRPII capture efficiencies were compared across manufacturers using a standardized magnetic packed bead volume of 5.5 mm^3 with a 10 min mixing step (**Figure 3.4**). Cube Biotech beads provided the most effective solid phase, capturing 80 - 85% of total HRPII available in samples ranging between 65 – 4000 parasites μL^{-1}. Additionally, the Cube Biotech solid phase showed no significant decrease in percentage of HRPII capture across the wide range of parasite densities tested. It was concluded that HRPII binding saturation was not reached and 5.5 mm^3 packed bead volume was a sufficient bead volume to be used in further studies.

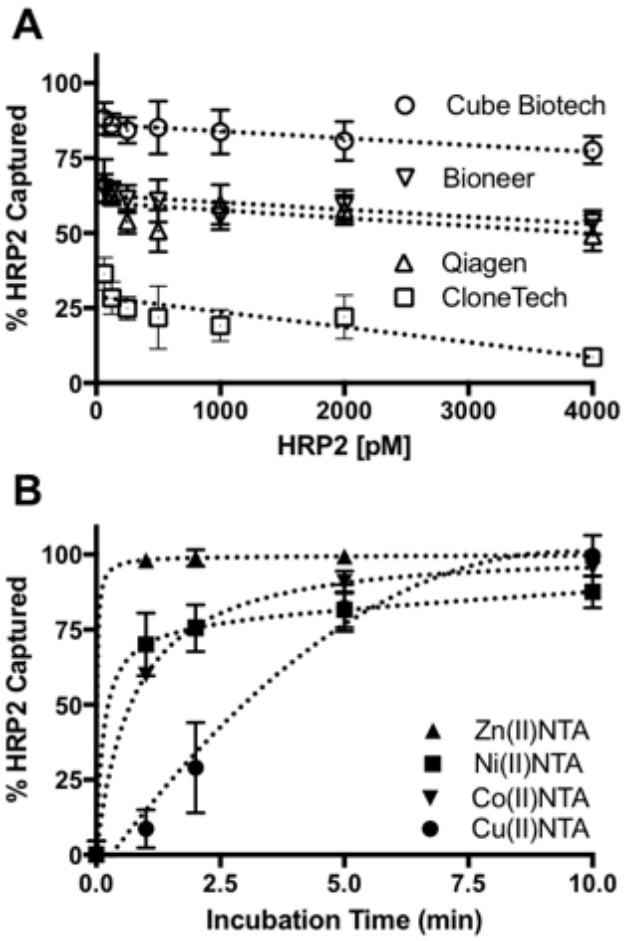

Figure 3.4: Magnetic bead solid phase and divalent metal selection. A) The HRPII capture performance of four different commercially available Ni(II)NTA IMAC solid phases over a range of parasite densities employing a 10 min incubation time. B) Cube Biotech beads equipped with four different divalent metals capture HRPII in 200 parasites μL^{-1} samples as a function of time. Both graphs were fit with nonlinear best-fit trend lines.

Additionally, Cube Biotech beads were the most cost-efficient option, which is examined further in the discussion.

Rapid time to result is crucial in POC assays, and the previous Ni(II)NTA Qiagen bead sample preparation workflow suffered from long mixing times for HRPII capture.[34] Although an improved solid phase for HRPII capture was identified, a 10 min mixing step was not sufficient to capture all the available HRPII. In IMAC chemistry, metals that are strongly fixed to a solid support mediate the interaction between the solid phase and the target. The most common method uses a solid phase equipped with the NTA

ligands to coordinate Ni^{2+} with four valencies (Ni(II)NTA) to fix it in place. The remaining two valencies on Ni^{2+} are then available to coordinate to histidine rich moieties, such as HRPII or the archetypal “His-tag” used in protein purification.[103] However, reports suggest that Zn^{2+} has a uniquely high binding affinity to HRPII compared to other divalent metals.[104,105] To improve binding efficiency and better understand how immobilized divalent metals kinetically interact with HRPII, the relationship between divalent metal species and mixing time was investigated. HRPII capture was evaluated as a function of time using Cube Biotech beads equipped with Ni^{2+}, Zn^{2+}, Co^{2+}, or Cu^{2+} (Figure 2B). Zn(II)NTA, Cu(II)NTA, Co(NTA), and Ni(II)NTA surface functionalization was found to capture 99.7 ± 2.7%, 99.4 ± 6.8%, 95.7 ± 2.1%, and 85.6 ± 5.3% of the available HRPII employing a 10 min mixing step, respectively. However, at shorter mixing times, which are needed for POC diagnostic systems, the surface functionalization was found to have a greater impact. Zn(II)NTA functionalization enabled the capture of 98.2 ± 2.7% of the available HRPII with a short 1 min mixing step, while Cu(II)NTA, Co(NTA), and Ni(II)NTA surface functionalization was found to capture 8.7 ± 6.4%, 59.9 ± 1.9%, and 70.1 ± 10.4 of the available HRPII with a 1 min mixing step, respectively.

Thus, the identification of Cube Biotech, an improved magnetic bead solid phase, and optimal Zn(II)NTA surface functionalization allowed for a 10-fold reduction in mixing time, while also increasing HRPII capture by 20% compared to our previous method.

Development of a Stable Single-Use Sample Tube

A novel single-use patient sample tube containing the necessary biomarker capture components was developed to minimize user steps, increase reagent stability,

and reduce variability in assay performance. Lyophilization of agarose beads, with the addition of excipient lyoprotectants such as sugar and hydrocarbons, has previously been reported to preserve the 3D structure and chromatographic properties of agarose beads.[98] To investigate the impact of the inclusion of all assay components in a single-use sample tube, a lyophilization composition screen was performed. In these experiments several combinations of PEG 8000, trehalose and other stabilizing agents, as well as the mandatory assay reagents including: 5.5 mm^3 Cube Biotech Zn(II)NTA beads, sodium chloride, blocking imidazole, and phosphate buffer pH 8.0 were lyophilized in single-use tubes and evaluated for HRPII capture efficiency after mixing on the battery-powered mixer for 1 min (**Figure 3.5A**). The best performing lyophilization composition consisted of 50 mM phosphate buffer pH 8.0, 300 mM sodium chloride (IMAC Buffer), 10 mM blocking imidazole, and 10% trehalose (Figure 3A.6). Single-use sample tubes prepared with this composition captured ~100% of the HRPII present in a 50 µL whole blood sample (100 µL total sample volume after addition of hydrating lysis solution). Long-term stability of the lyophilized single-use tube was also analyzed. Enclosed in a plastic bag containing desiccating silicon packets at room temperature, these single-use tubes remained stable and maintained the ability to capture 100% of HRPII present in a 50 µL whole blood sample up to 386 days after their preparation (**Figure 3.5B**). No bacterial growth was observed in the hydrating lysis solution during the same timeframe, suggesting that all sample processing reagents have a shelf life of over 1 year at room temperature maintaining the stability requirements of the WHO ASSURED criteria.[28] The development of this single-use

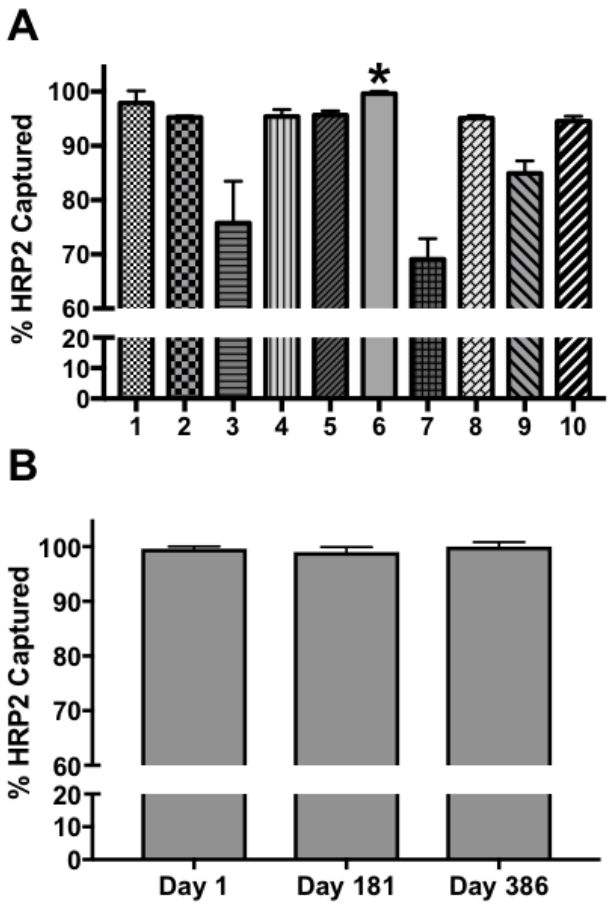

Figure 3.5: Lyophilization composition studies. A) The capture of HRPII by 5.5 mm^3 of Cube Biotech Zn(II)NTA beads in a whole blood sample, after lyophilization in ten different lyophilization compositions: 1) IMAC buffer, 10% PEG 8000 10% trehalose 2) IMAC buffer, 10% trehalose 3) IMAC buffer, 10% PEG 8000 4) IMAC buffer 5) IMAC buffer, 10 mM imidazole, 10% PEG 8000, 10% trehalose 6) IMAC buffer, 10 mM imidazole, 10% trehalose* 7) IMAC buffer, 10 mM imidazole, 10% PEG 8000 8) IMAC buffer, 10 mM imidazole 9) lyophilized beads alone 10) non-lyophilized beads. *Lyophilization composition used in further testing. B) Single-use patient sample tubes were evaluated for HRPII capture efficiency on Day 1, Day 181, and Day 386 after lyophilization.

sample tube and the employment of our battery-powered mixer provides a deliverable high-throughput assay with minimal consumables.

Magnetically-assisted Bead Gathering to Deliver the Greatest Number of Biomarkers to LFAs

The results from this study defined the final steps in the mBEADS workflow using 50 µL whole blood samples (100 µL total sample volume). The final steps in the mBEADS workflow involve operating the user-centric device to align the LFA, use the

on-board magnet to gather the magnetic beads, and deliver them into the LFA sample port employing the cantilever deposition action. Following the rapid 1 min capture of HRPII, all components of the stable single-use tube are transferred to a sample deposition tube on the mBEADS device for a magnetic-assisted gathering step. To promote the best delivery of the magnetic beads onto the LFA, which now harbor all of the HRPII from the sample, it is critical that the greatest volume of beads be gathered at the bottom of the deposition tube. To that end, magnetic-assisted bead gathering time was investigated to provide the minimum time necessary to gather the maximum number of magnetic beads prior to deposition.

Time-lapse photography was used to determine the time necessary for magnetic beads to gather at the bottom of the sample tube. The magnetically gathered bead packet that forms at the bottom of tube, denoted as 2D bead settled cluster area, was monitored and normalized to the final settled cluster area **(Figure 3.6A-B**). For each volume tested, the transient bead collection was highly reproducible (i.e. the settled cluster area increases in a similar manner for each replicate within a given volume). According to a Students *t*-test, there was no statistically significant difference between the time that it took for 90% of the beads to settle for lysed whole blood sample volumes of 100 and 200 µL (4.7 +/- 1.6 s and 4.2 +/- 0.67 s, respectively). However, there was a statistically significant difference in the bead settling time for 400 µL (13.2 +/- 2.9 s) and 600 µL sample volumes (28.6 +/- 5.5 s, $p<0.05$) (**Figure 3.6C**). Consequently, a 1 min bead gathering step was adopted for volumes of 100-200 µL and a conservative 2 min bead gathering time for volumes of 200-600 µL.

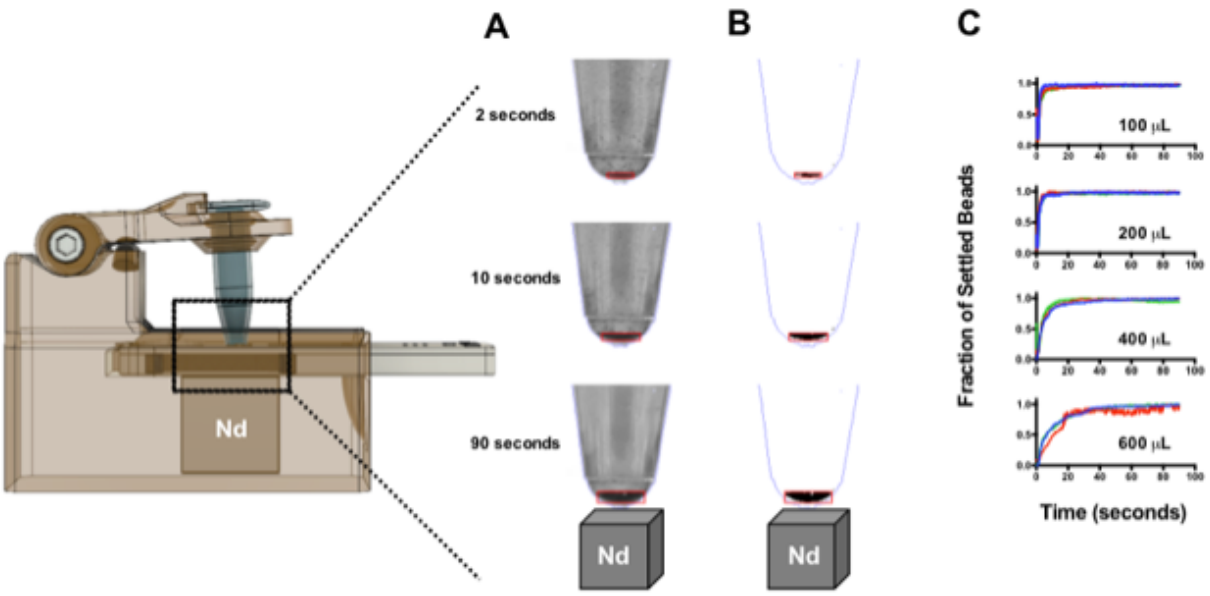

Figure 3.6: Magnetic bead settling time experiments in 100 µL, 200 µL, 400 µL, and 600 µL whole lysed blood samples using time-lapse photography. **A)** The original image, **B)** image converted to a binary to identify only pixels containing clustered magnetic beads, and **C)** bead settled area integrated as a function of time.

mBEADS Biomarker Delivery Efficiency and Enhancement of Leading Commercial LFAs

The most important operation of the mBEADS system is to escort as many possible HRPII biomolecules from a blood sample to a LFA to increase the test line intensity. Therefore, after the components and workflow of mBEADS were defined, biomarker to LFA delivery efficiency was evaluated. An illustration of the full mBEADS process is provided for reference (**Figure 3.7**). By subtracting the residual HRPII left in the sample supernatant (uncaptured HRPII) and on the beads remaining in the sample tube after deposition (captured but not deposited) from the total amount of HRPII in the sample, a biomarker delivery efficiency was determined (**Table 3.3**). The optimized device employing Zn(II)NTA single-use tubes was able to deliver approximately 75% of the total HRPII protein in the sample onto the LFA.

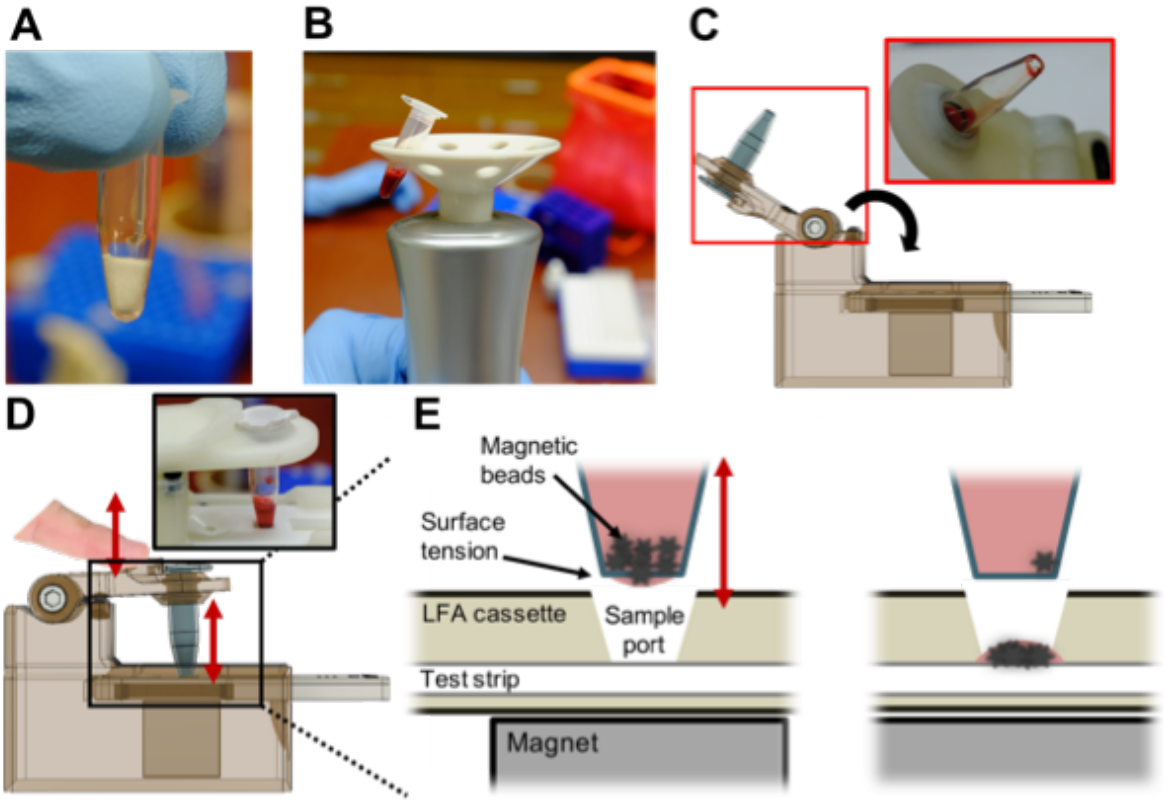

Figure 3.7: The three-minute mBEADS workflow. A) The optimal single-use patient sample tubes are first loaded with hydrating lysis buffer and a whole blood sample and B) positioned onto a portable battery powered mixer for a 1 min mixing cycle. C) The mixed components are then moved by a transfer pipette to a sample deposition tube on board the mBEADS device in the 'open' position, the tube holder is then rotated into the 'closed' position over the LFA sample deposition port for a one-minute bead collection cycle. D) Beads are collected and retained at meniscus of the sample tube by surface tension are delivered to the LFA using the cantilever deposition action, where modified running buffer is added to the LFA test strip to elute HRPII from the beads for downstream detection on the LFA.

Table 3.3: Percent residual HRPII in the sample supernatant and eluted from the beads remaining on beads following the bead deposition step for the Zn-NTA bead type.

	Percent Residual HRPII				
Mixing Time (min)	**0.5**	**1.0**	**2.0**	**5.0**	**10.0**
Zn-NTA Supernatant	3.0 ± 1.0	1.0 ± 1.0	3.0 ± 2.0	1.0 ± 1.0	1.0 ± 1.0
Zn-NTA Bead Elution	22 ± 8	40 ± 20	9 ± 2	33 ± 10	20 ± 5

To determine the increased sensitivity afforded by mBEADS, LOD calculations were performed on data sets composed of standard and mBEADS enhanced LFAs using mock clinical samples over parasite densities ranging from 1 to 200 parasites μL^{-1} for Zn(II)NTA single-use tubes. These studies were performed for each of the following LFA types: Paracheck, ICT Pf, and First Response.

The other two test types that the mBEADs device was designed to incorporate were excluded due to trouble procuring a sufficient number of tests from the manufacturers. Dose-response curves used to calculate the limit of detection for two of the three available malaria LFAs are shown in **Figure 3.8**. The greatest enhancement

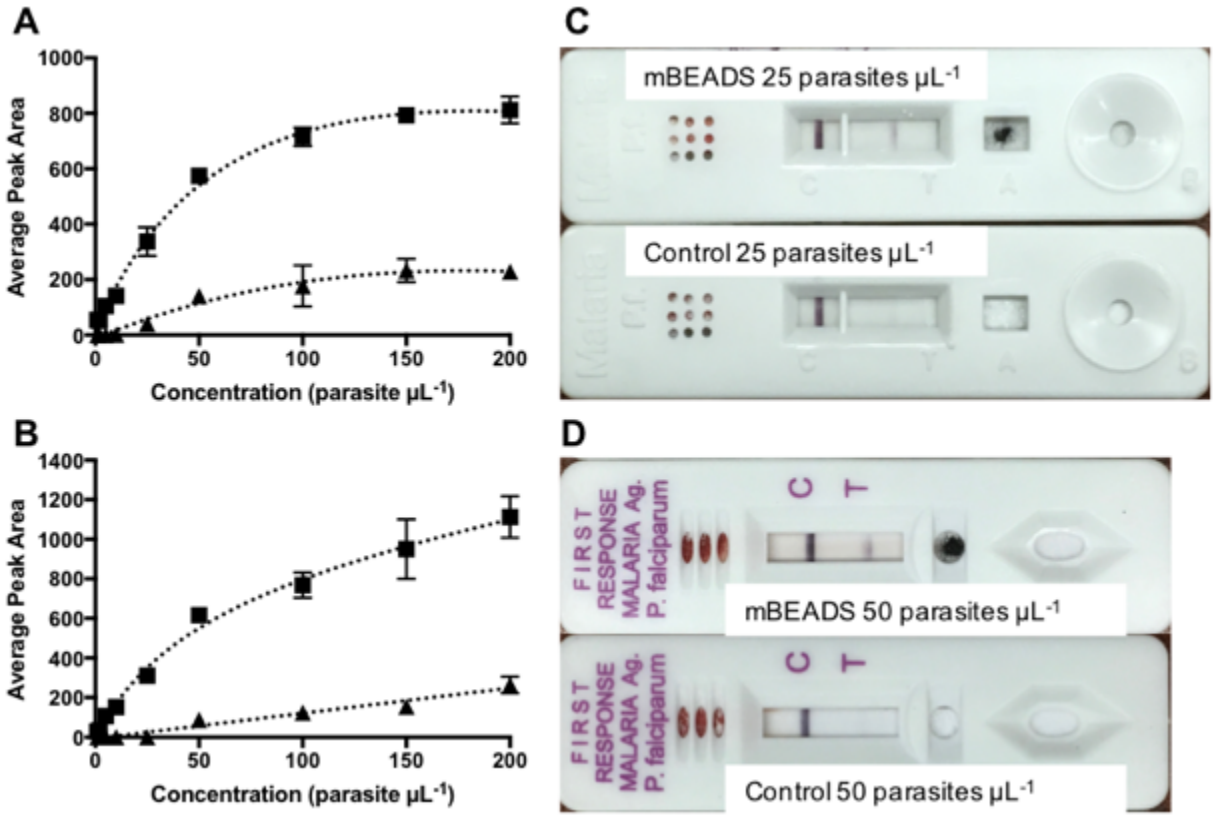

Figure 3.8: mBEADS process enhances malaria LFA tests. A) Paracheck and B) First Response test line signals (T) after employing mBEADS to process 50 µL whole blood samples spiked to parasitemias ranging from 1 - 200 parasites μL^{-1} (squares). Control samples (triangles) were processed in parallel per manufacturer suggested protocol. Both graphs were fit with nonlinear best-fit curves for ease of view. Representative mBEADS processed and control LFAs for (C) Paracheck and (D) First Response tests are also provided.

was observed with First Response tests, where the mBEADS process yielded a LOD at 1.3 ± 0.1 parasites μL^{-1}. **Table 3.4** lists the LODs for each LFA with and without mBEADS enhancement. Detection limits are also reported in the corresponding quantities of HRPII because the mock clinical samples were generated from a high parasite density stock culture.[106]

Table 3.4: Calculated LODs for Paracheck, First Response, and ICT-Pf with and without mBEADS.

LFA Type	LOD of Unenhanced LFAs		LOD of mBEADS Enhanced LFAs	
	[HRPII] (pM)	Parasites μL^{-1}	[HRPII] (pM)	Parasites μL^{-1}
Paracheck	36.0 ± 3.7	21.2 ± 2.2	4.1 ± 0.2	2.4 ± 0.1
First Response	52.0 ± 4.6	30.6 ± 2.7	2.2 ± 0.2	1.3 ± 0.1
ICT Pf	86.7 ± 22.1	51.0 ± 13.0	10.5 ± 0.9	6.2 ± 0.5

The practical whole blood volume that can be readily acquired employing lancets that are supplied in the commercially available LFA kits used in this study is 50 µL. Thus, the experimental protocol to determine the sensitivity of mBEADS LFAs used 50 µL whole blood samples. However, the approach proposed can be easily adapted to incorporate larger patient blood volumes by manipulating the reagent volumes in the single-use sample preparation tubes and incrementally increasing mixing and bead settling times. Using improved lancet technology, finger prick blood collections can acquire up to 300 µL of patient whole blood, further increasing the total amount of HRPII that can be captured and delivered to LFAs. The impact of processing larger whole blood volumes on the HRPII test line development was evaluated employing mBEADS (**Figure 3.9**). Processing larger whole blood volumes increased LFA test-line signal intensity at single parasite densities suggesting that the collection and processing of

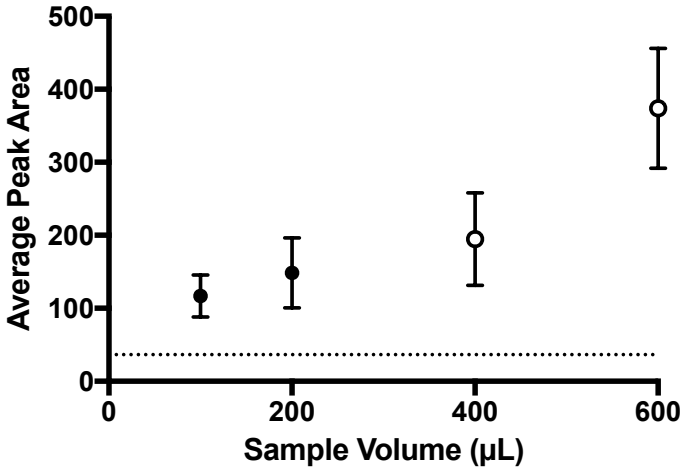

Figure 3.9: Processing larger blood samples volumes further increases LFA signal. Utilizing the mBEADS methodology, LFA signal output was examined as a function of increasing blood sample volume (plotted as total sample volume following the 50:50 whole blood to lysis). Increased volumes of 1 parasite μL^{-1} whole blood samples were processed where 100 and 200 µL sample volumes were mixed for 1 min and bead settling time was set to 1 min (closed circles) and 400 µL and 600 µL total sample volumes (open circles) were conservatively mixed for 2 min and bead settling time was set to 2 min. A F-test concluded that no significant difference exists between the variances observed on the graph.

whole blood volumes larger than the 50 µL used in this study could lead to an even more thorough detection of the asymptomatic infectious reservoir.

Discussion

Intensive control efforts have significantly reduced malaria disease burden, and many regions are undergoing a crucial shift from malaria control to malaria elimination.[81,107,108] High sensitivity detection at the point of care is an essential diagnostic component as malaria elimination campaigns scale up globally. One of the greatest challenges facing elimination campaigns is the effective identification of individuals with asymptomatic disease who may serve as a parasite reservoir.[53,109] Using the WHO's ASSURED criteria as a framework, we have developed a biomarker enrichment approach that integrates simple, user-centric sample preparation with commercially available LFAs to generate very high sensitivity measurements of

Plasmodium falciparum HRPII. Using mathematical models, Slater *et al.* showed that diagnostic sensitivity of 200 parasites μL^{-1} at the point of care allows for the detection of only 55% of the infected population.[75] In this study, some of the leading *Pf* malaria LFAs were selected to be integrated with mBEADS. The LODs for these LFAs range from 21-50 parasites μL^{-1}. The improvement in the detection limit of LFAs to single-digit parasitemia increases the detection of the infectious reservoir to 95%.[75] Thus, the greatest advantage of the integration of mBEADS with existing LFA technology is achieving the single parasite density detection limits that will be necessary for malaria elimination campaigns without the need to remanufacture commercial tests. Additionally, while some current lab-based assays such as PCR or ELISA can approach this level of sensitivity, unlike LFAs, they cannot be deployed at scale or in low resource settings where elimination campaigns will operate.[110]

The progression from our proof-of-concept technology to this field-deployable mBEADS platform was guided by selection criteria that sought to improve commercially available LFA sensitivity without adding a cumbersome process, burdensome cost, or lengthy time requirements. We believe that by further refinement we can reduce this two-tubed system to a one-tubed system to further reduce user step. Additional cost per assay is rarely addressed in the development of LFA enhancement strategies but is one of the greatest prohibitive barriers to their translation and acceptance in low and middle-income countries. The most expensive component of particle based enhancement systems is often the biomarker capture bead. In our previous work, the chosen bead system was ~$2.20 per assay.[64] To better visualize the relationship between HRPII capture and bead cost, percent HRPII capture efficiencies at 200 parasites μL^{-1} were

plotted against the bead cost per assay for each bead manufacturer (**Figure 3.10**). The most desirable beads are those that are inexpensive beads and most effectively capture HRPII, which are found in the top left portion of the graph. The Cube Biotech Zn(II)NTA magnetic beads selected for mBEADS were not only the most effective HRPII capture magnetic bead, capturing ~100% of HRPII with a 1 min mixing step, but also the least expensive at $0.09 per assay. The total additional cost of employing the complete mBEADS process is $0.25 per LFA, permitting the mBEADS device has a lifetime of 500 uses.

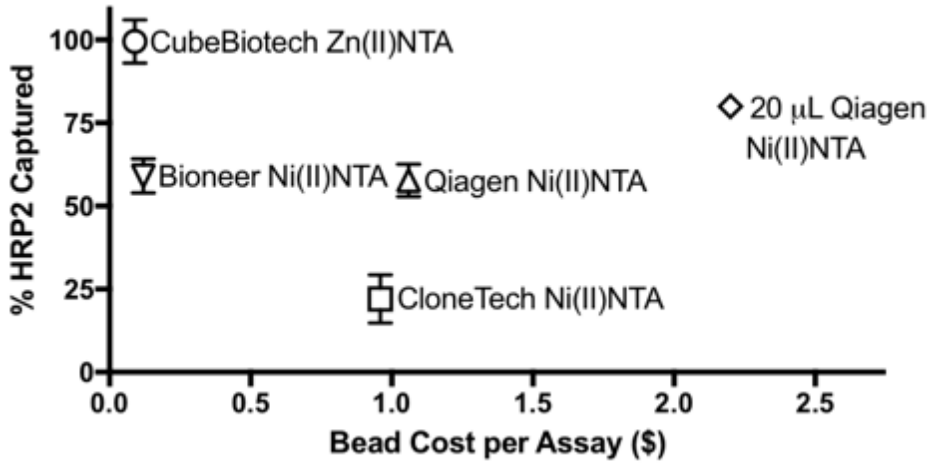

Figure 3.10: HRPII capture efficiency plotted against the cost of 5.5 mm^3 magnetically packed volumes of IMAC beads manufactured. A 1 min mixing cycle was used for Cube Biotech Zn(II)NTA and 10 min mixing cycles were used for the other three IMAC beads.

Moreover, of the particle-based sample preparation systems reported in the literature, this is the only one that has been demonstrated to function in whole blood, purifying HRPII from components of blood that may interfere with LFAs.[60,95,96] The magnetic bead deposition was tailored to have minimal sample carryover volume, resulting in improved test clearance. Furthermore, it likely prevents the transfer of LFA interferents, such as autoantibodies associated with human rheumatoid factor, and

human anti-mouse antibodies that induce false positive test results.[111] The deposition of a small number of beads also provides a theoretical maximum HRPII binding and delivery capacity that would provide tolerance against the hook effect phenomenon known to give false negative results.[112] To this end, the general performance and robustness of widely-deployed LFAs is increased by employing mBEADS.

Conclusion

Malaria eradication has become a promising and realistic target due to global initiatives to diagnose infection, treat positive cases, and decrease transmission rates. However, current POC diagnostics are not sensitive enough to detect low parasite densities present in some asymptomatic patients. For malaria elimination campaigns to be effective, POC diagnostics must be able to detect the single digit parasitemias that are associated with this asymptomatic patient reservoir.[75] Instead of dealing with the challenges of developing, implementing, and gaining governmental approval of a new next-generation rapid diagnostic tests to achieve this, we propose the enhancement of current, widely used technologies using the integrated mBEADS system. The ASSURED-criteria aligned mBEADS system enhances the preeminent deployable LFAs to achieve the diagnostic sensitivity needed for elimination campaigns to finally eradicate malaria.

Acknowledgements

This work was financially supported in part by the National Institutes of Health, Fogarty International Center Grant #D43 TW009348. This work was also supported by the Bill and Melinda Gates Foundation: OPP1123092 Magnetically-enabled Biomarker and Extraction Device, mBEADS. The authors would like to thank Dr. Kim Fong for

culturing D6 *Plasmodium falciparum* used in this work and M. F. Richards for critical comments concerning the manuscript.

CHAPTER IV

Metal Affinity-Enabled Capture and Release Antibody Reagents Generate a Multiplex Biomarker Enrichment System that Improves Detection Limits of Rapid Diagnostic Tests

Reproduced with permission from *Anal. Chem.* 89, 19, 10216-10223

Introduction

The economic and infrastructural realities of the infectious disease demographic render many classic diagnostic technologies ineffective at the point of need.[23,113] The advent of immunochromatographic rapid diagnostic tests (RDTs) based on lateral flow overcomes many of the issues associated with these technologies by providing a tool that is easy to use, inexpensive, quickly processed, and can be manufactured and distributed in large quantities. Today, RDTs represent a core diagnostic modality for the identification of many infectious diseases ranging from HIV and sexually transmitted diseases to influenza, tuberculosis, and malaria.[30,114-119]

Although the lateral flow RDT platform appears ideal for point-of-care (POC) diagnostic tests, it suffers from several technological shortcomings. As reviewed by Miller *et al*, these limitations include low sensitivity, use of suboptimal recognition agents, and subjective interpretation.[30] Of these constraints, improving RDT sensitivity has been a major focus for improvement. Previous tactics include the enhancement of test band signal output through use of different material detection probes, the addition of bioconjugates such as enzymatic signaling molecules, the application of a dual-particle

detection strategy, or the modification of test architecture.[93,120-122] Although these methods show promise, they require redesigning and remanufacturing current RDTs as well as retraining healthcare personnel.

Front-end biomarker enrichment techniques address the poor sensitivity issue using an alternate strategy that is primarily aimed at overcoming the small volume restriction imposed by RDTs.[60,123] Biomarker enrichment functions by isolating, purifying, and concentrating the increased copies of biomarkers available in larger RDT-incompatible sample volumes into an appropriate volume that can be added to these tests. This strategy improves test sensitivity while bypassing the need to redesign and remanufacture commercial tests. Purifying target biomarkers from matrix-specific interferents also minimizes test anomalies such as poor sample clearance, which leads to improved interpretation of test results. Further, biomarker enrichment processes are able to interface with emerging RDT test band enhancement technologies as they are developed.

Our group has developed a magnetically-enabled biomarker extraction and delivery system (mBEADS) as a front-end biomarker enrichment strategy.[124] This system functions via the use of metal affinity magnetic beads to capture, concentrate, and deliver enriched *Plasmodium falciparum* Histidine Rich Protein-II (HRPII) to single-antigen lateral flow malaria RDTs to improve their visual limits of detection.[39,125] However, the sole detection of HRPII does not provide the adequate diagnostic information needed to make the best-informed malaria treatment decisions in many regions. HRPII is only found in one of the five species of malaria known to infect humans and remains in host circulation for up to one month after parasite clearance

confounding the ability to distinguish resolved and active infection.[126] Additionally, the growing prevalence of populations that display deletions in the HRPII gene reduce the efficacy of sole HRPII-based diagnostic tests.[127-129]

For those reasons, multi-antigen malaria lateral flow RDTs are ideal. Detecting the biomarker combination of HRPII and *Plasmodium* lactate dehydrogenase (*p*LDH) allows for the identification of all malarial species, informs the semi-speciation of infection needed to prescribe the proper treatment,[130] and more precisely monitors treatment efficacy.[131-133] This is because *p*LDH is found in all malaria infections, making it an ideal positive indicator of malaria infection, and HRPII provides information on the speciation of infection. However, a report on the current state of HRPII/pan-*p*LDH dual-antigen malaria RDTs by Gatton *et al*. highlighted the poor sensitivity of these tests. Particularly, these combination tests frequently return only a positive HRPII band and a negative pan-*p*LDH band at low parasite densities, due to the insensitivity of the *p*LDH test bands.[134] Since pan-*p*LDH should always be positive during active infection, healthcare workers would be unable to interpret a positive HRPII signal as being caused by persistent antigenamia or active infection.

In this study, we develop a multiplex biomarker enrichment system to address the need for increased sensitivity of HRPII/pan-*p*LDH RDTs. Specifically, we focus on increasing the sensitivity of the limiting *p*LDH test band, while also enhancing the HRPII test band, to achieve dual positive HRPII/pan-*p*LDH band readings at very low *Plasmodium falciparum* parasitemias. The metal affinity-based biomarker enrichment system used in previous work was limited to only biomarkers that have high affinity towards immobilized metals, such as HRPII. In contrast, *Plasmodium* lactate

dehydrogenase is not histidine rich and cannot be enriched employing this method. To enable the capture of histidine-poor biomarkers, like *p*LDH, we extend the specificity of immunocapture to the metal affinity system by conjugating histidine-rich peptides, a metal affinity handle, to antibodies. This modification allows an antibody to be reversibly loaded onto metal affinity solid phases while also being susceptible to gentle, competitive elution. By virtue of their operation, we refer to these modified antibodies as 'Capture and Release' (CaR) antibody reagents. Equipping metal affinity magnetic beads with pan-*p*LDH CaR antibody reagents generates a multiplex bead that captures both *p*LDH and HRPII—*p*LDH through immunospecific capture and HRPII through M^{2+}-histidine coordination. Following capture, both biomarkers can be magnetically enriched and released to be responsive to detection in a dual-antigen malaria RDT.

Materials and Methods

Materials

All Fluorenylmethyloxycarbonyl (FMOC)-protected amino acids, resins, peptide activators, and biotin were purchased from Advanced Chemtech and Aapptec. FMOC-Amido-dPolyethlyene $glycol_6$-acid (PEG_6) was purchased from Quanta Biodesign (OH, USA). Commercially available monoclonal antibodies were procured from Fitzgerald and Vista Diagnostics. All Octet RED96 biosensors were purchased from FortéBio (CA, USA). Sulfosuccinimidyl 4-(N-maleimidomethyl)-cyclohexane-1-carboxylate (sulfo-SMCC, No-Weigh™ Format) heterobifunctional crosslinker, 0.5 mL Zeba™ 7k MWCO spin desalting columns, MagnaRack™ magnetic separation rack, metal affinity Dynabeads® His-Tag Isolation and Pulldown magnetic beads, EZ-Link™ plus activated peroxidase kit, and Pierce™ Biotin Quantitation kit were purchased from ThermoFisher

Scientific (MA, USA). Recombinant *Plasmodium falciparum* and *Plasmodium vivax* *p*LDH (rcPfLDH and rcPvLDH) were procured for CTK Biotech (CA, USA). ICT dual malaria RDTs were purchased from ICT diagnostics (Cape Town, South Africa). Whole pooled blood was obtained from bioreclamationIVT (TN, USA). pLDH ELISA kits were acquired from apDia (Belgium) and TMBone solution was purchased by Promega (WI, USA). Malaria strain *P. falciparum* D6, cultured in Vanderbilt University's BSL2 facilities and characterized by a trained microscopist (299,000 p/μL), was utilized to prepare mock clinical blood samples. Deionized water was used with a resistivity of 18 MΩcm. All other reagents, buffers, and solvents were used without further modifications from either Sigma-Aldrich or Fisher Scientific.

Instrumentation

Absorbance measurements were collected on a BioTek Synergy H4 plate reader (VT, USA). The His_6 Peptide was synthesized on a Peptide Machines Discovery-4 synthesizer (CA, USA). Peptides were purified with reverse phase high-powered liquid chromatography (HPLC) using a Waters Prep LC 4000 Preparative Chromatography System (MA, USA) containing a Waters 2487 dual wavelength detector. Matrix-assisted laser desorption/ionization (MALDI) mass spectrometry analysis was performed with an Applied Biosystems Voyager STR-4211 (MA, USA) instrument using a reflectron time-of-flight (TOF) mass analyzer. Real-time bio-layer interferometry (BLI) binding assays were performed with a ForteBio Octet RED96 bio-layer interferometer (CA, USA). Bead size and concentration was determined using Countess® II automated cell counter procured from ThermoFisher Scientific (MA, USA). RDTs were read on a ESEQuant lateral flow reader procured from Qiagen (Germany).

Solid-Phase Peptide Synthesis of C-Peg$_6$-H-H-H-H-H-H-Peg$_6$-Biotin (His$_6$-Biotin)

A cysteine rink amide resin was first loaded into a fritted peptide synthesis vessel. The resin was then swelled in dimethylformamide (DMF) as preparation for FMOC group removal through a 20 min treatment with 20% piperidine (v/v) in DMF. Afterwards, 3x molar excess (compared to the resin substitution) of FMOC-protected PEG_6 was coupled onto the resin overnight using 3x molar excess of hydroxybenzotriazole (HOBT) and 1,3-diisopropylcarbodiimide (DIC) activators. Following the overnight reaction, the resin was washed with DMF and methanol. For coupling procedures, 6x molar excess FMOC-amino acids were dissolved in a 6-dram vial containing 4 mL DMF, 6X molar excess HOBT, and 6x molar excess DIC. Coupling and deprotection reactions were performed on a plate shaker to agitate the resin, 60 min for coupling and 20 min for deprotection. Following the six sequential histidine additions, FMOC-protected PEG_6 was coupled onto the histidine-peptide overnight using the same conditions shown above. Finally, the peptide chain with PEG_6 spacer was biotinylated for one hour using 6x molar excess biotin, 6x molar excess HOBT, and 6x molar excess DIC.

Solid-Phase Peptide Synthesis of C-PEG$_6$-H-H-H-H-H-H-Ac (His$_6$)

Outside the peptide synthesizer, a cysteine rink amide resin was first swelled in DMF and subsequently deprotected with 20% piperidine in DMF for 20 min. Afterwards, 3x excess of the FMOC-protected PEG_6 was coupled onto the resin overnight using 3x molar excess HOBT, 3x molar excess (2-(1H-benzotriazol-1-yl)-1,1,3,3-tetramethyluronium hexafluorophosphate) (HBTU), and 6x molar excess diisopropylethylamine (DIEA). After washing the resin with DMF and methanol, the resin

was added to the peptide synthesizer to attach the histidine chain. For coupling procedures, FMOC-amino acids (0.4 M) dissolved in HBTU/DMF (0.2 M) were reacted with HBTU/DMF (0.4 M) and 40% v/v DIEA/DMF. Coupling reactions were performed for 60 min, while deprotection reactions were performed for 20 min. Finally, the peptide was acetylated for one hour using a 1:1:2 ratio of acetic anhydride:DIEA:DMF.

Peptide cleavage, purification, and characterization

After washing, the resin was incubated with 5 mL of 90:5:3:2 volume ratio of trifluoracetic acid:thioanisole:1,2-ethanedithiol:anisole for two hours while gently shaking to cleave the peptides that were then precipitated into cold diethyl ether and centrifuged (4°C, 1500 *g*, 5 min) four times to remove the ether and soluble organics. Next, the crude peptides were dissolved in 10 mL 1:1 water:acetonitrile and lyophilized. Afterwards, the peptides were further purified using reverse phase chromatography. The peptides were dissolved in 3 mL 1:1 water:acetonitrile and injected into a HPLC with a reverse-phase C18 column. Each dual wavelength-visualized HPLC product was collected in a separate purified fraction, lyophilized, and analyzed using MALDI-TOF (**Figure 4.1**). Micrograms of each peptide were dissolved in 1:1 water:acetonitritile, and 0.5 µL samples of the resulting solutions were spotted onto a MALDI plate. Immediately afterwards, 0.5 µL α-Cyano-4-hydroxycinnamic acid (CHCA, 20 mg/mL) matrix solution was mixed with the deposited peptide. Following the MALDI examination of each fraction, all pure fractions were combined, and stock solutions of 6 mM His_6-Biotin and 3 mM His_6 peptides were prepared and stored at -40ºC.

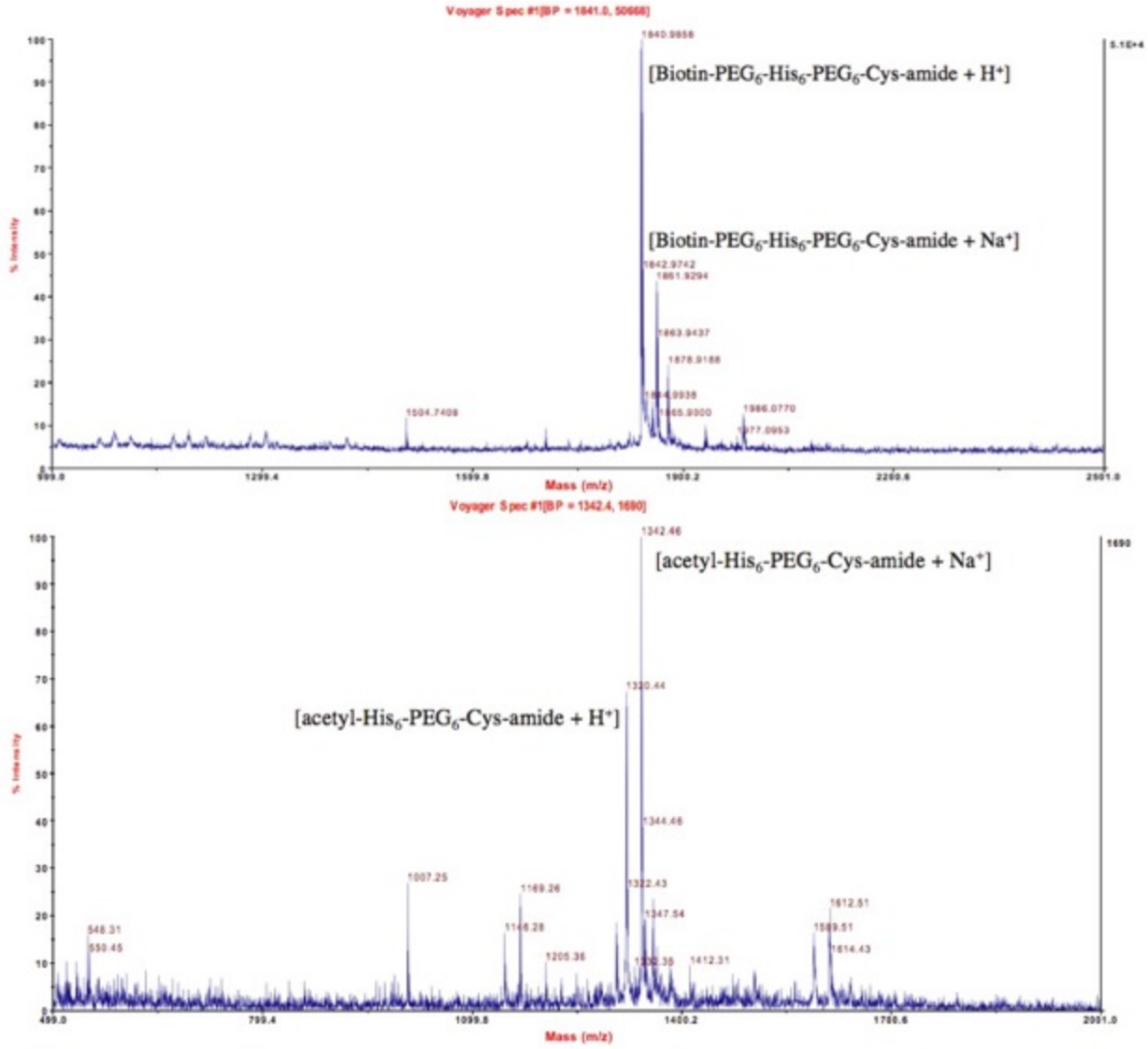

Figure 4.1: MALDI-MS spectrum of His_6-Biotin peptide (top) and His_6 peptide (bottom).

Conjugation strategy

All mAbs used in this study are commercially available pan-specific anti-*p*LDH mouse monoclonal (mAb) IgG antibodies. Each one was diluted from its respective stock concentration to 1 mg/mL in phosphate buffered saline (PBS) before activating for 30 min at room temperature with sulfosuccinimidyl 4-(N-maleimidomethyl) cyclohexane-1-carboxylate (sulfo-SMCC). The activated mAbs were then separated from excess sulfo-SMCC reagent using a 7k molecular weight cut-off (MWCO) Zeba desalting column.

Following this purification step, synthesized His_6 or His_6-Biotin peptides were introduced to the activated mAbs at a 20x molar equivalence with respect to mAb concentration. Following another 30-min incubation step at room temperature, the mAb conjugate was purified from excess peptide using the same desalting columns. Process control mAbs were prepared in the same manner except that no activating sulfo-SMCC was added. The initial mAb, conjugated mAb reagent, and process control concentrations were measured by micro-volume analysis using a BioTek Take3 plate.

Characterization of CaR mAb reagents

A model anti-*p*LDH antibody (clone 19g7) was first functionalized with sulfo-SMCC at molar equivalents of 5x, 10x, 20x, 40x 60x, and 80x using the above conjugation protocol without alteration. A commercially available Pierce™ biotin quantitation kit was employed to determine the number of peptides per mAb. No modifications were made to the manufacturer's suggested microplate procedure for the quantitation of moles of biotin per mole of IgG protein. This assay was also performed for each mAb bioconjugate process control. The calculation of moles of biotin per mole IgG led to the implementation of two correction factors: one based on the positive control and one based on its respective process controlled mAb. An Octet RED96, equipped with seven parallel ready-to-use Ni-NTA biosensors, was used to survey the impact that degrees of conjugation had on CaR mAb-*p*LDH binding. First, the Ni-NTA biosensor was introduced to a solution of 0.025% Tween 20 in phosphate buffered saline (PBST) for a 300 s equilibration step. Immediately after, the biosensors were moved to new wells for a loading step. Each well contained 3 μg/mL of mAbs functionalized with the previously indicated series of sulfo-SMCC molar equivalents.

Once loaded, a baseline was established by transferring the biosensors to wells containing PBST for another 60 s before being moved to new wells for an association step using 25 nM rc*Pf*LDH. The binding phase shift maximum was collected at the end of 400 s. In addition, the same sulfo-SMCC conjugation conditions for each CaR mAb reagent was used to functionalize the respective antibodies with His_6 peptides, rather than a His_6-Biotin, to ensure that the terminal biotin did not interact with biosensor during the kinetic experiments. No significant difference was observed in the kinetic and equilibrium binding data between the two analogs.

Employing Biolayer Interferometry (BLI) as an affinity screening tool to optimize pan anti-pLDH CaR mAb reagents

Nine pan-specific anti-*p*LDH mAbs were conjugated with the model antibody optimized conditions of 40x molar excess sulfo-SMCC and 20x molar excess His_6-Biotin peptide to generate *p*LDH CaR mAb reagents. Following the conjugation, each CaR mAb reagent was subjected to several kinetic experiments on the Octet RED96 to screen for apparent binding affinities to rc*Pf*LDH and rc*Pv*LDH. Eight parallel ready-to-use Ni-NTA biosensors were first equilibrated in PBST for 300 s before being loaded with 3 μg/mL of a sole *p*LDH CaR mAb reagent. The loaded biosensors were then introduced to wells containing PBST for 60 s to create a baseline, then transferred to sample wells containing either rc*Pf*LDH or rc*Pv*LDH serial diluted two-fold starting at 100 nM in addition to a 0 nM reference well. The biosensors remained in the sample wells for a 400 s association step before being returned to the baseline wells for a 900 s dissociation step. Using the Octet's analytical software, a global 1:1 fit model was selected to derive the kinetic (k_{on}, k_{off}) and equilibrium binding (K_D) data. Further

individual optimization of six selected CaR mAb reagents yielded apparent binding affinities for optimized CaR mAb reagents.

Conjugation optimization of selected CaR mAb agents

All capture and release reagents that were found to bind both rc*Pf*LDH and rc*Pv*LDH, as well as anti-*p*LDH mAb clone 14c2, were selected to undergo complete conjugation optimization based on the results identifying the most favorable range of conjugation levels. 30 μL at 1 mg/mL of each of the six selected capture and release agents were conjugated using 10x, 20x, 30x, and 40x molar excess sulfo-SMCC along with 20x molar excess His_6-Biotin peptide. The antibodies conjugated at each condition were then evaluated for the ability to bind rc*Pf*LDH. Kinetic experiments employing Ni-NTA biosensors (see previous experimental outline above) were performed to generate equilibrium constants, which were used as metric to determine optimal conjugation for each of the different capture and release agents. In addition, the optimal sulfo-SMCC conjugation conditions for each CaR mAb reagent was used to functionalize the respective antibodies with a His_6 peptide. Kinetic binding experiments were then performed on the biotin-less CaR mAb reagents.

Methodology for calculating theoretical loading density

The theoretical CaR mAb bead coverage was calculated using an estimated CaR mAb docking area of 33.4 nm^2.[135] Docking area is the amount of space an immobilized mAb loaded on a bead will occupy. Given that each IgG possesses an approximate molecular weight of 150 kDa, this value can be used in conjunction with the mAb concentration and docking area per mAb to generate a total estimated docking area. The diameter of the magnetic His-Tag Isolation and Pulldown Dynabeads microparticles

was measured to be 1.1 μm using a Countess II Automated cell counter. Combining this information with the 1.325×10^7 beads/μL stock concentration resulted in a total bead surface area. Dividing the total CaR mAb docking area by the total bead surface area then multiplied by 100 yielded the theoretical bead coverage percentage.

Impact of CaR mAb reagent bead loading density on pLDH capture

Optimized capture and release reagents were loaded onto 4 μL of stock metal affinity magnetic Dynabeads (~10,600 beads) at different loading densities to evaluate capture proficiency, or percent capture of native *Pf*LDH from a lysed whole blood sample matrix. To create bead-loading concentrations ranging from unloaded to saturated, CaR mAb reagent concentrations associated with 0 to 100% theoretical monolayer coverage were calculated at 5.72 μM, 1.43 μM, 378 pM, 89.2 pM, 22.3 pM, and 5.58 pM CaR mAb reagent per L of beads (**Figure 4.2**).

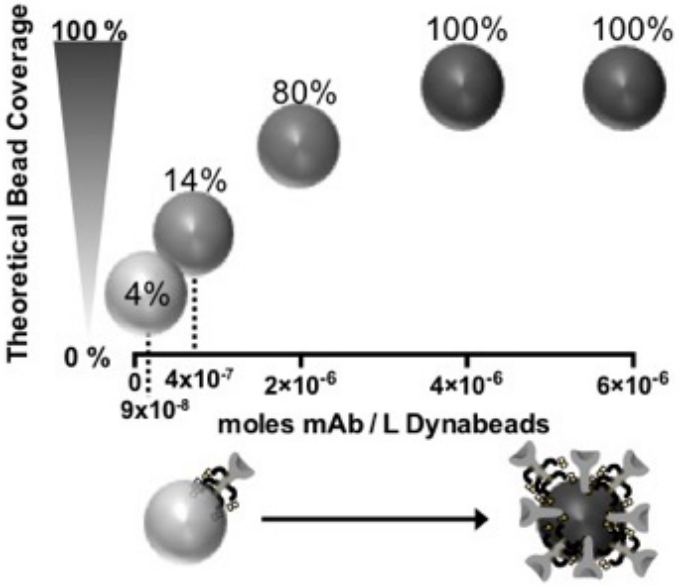

Figure 4.2: Antibodies per magnetic bead correlated to theoretical bead loading density. An illustration to visualize the correlation between moles CaR mAb/L Dyna-beads and theoretical bead coverage.

This experiment was performed by adding the predetermined volume of magnetic beads to a 1.5 mL microcentrifuge tube and washing two times with 1 mL PBST (0.025% Tween 20 in phosphate buffered saline). Washing was performed by magnetically separating the beads, removing the supernatant, and resuspending in PBST. Following the washes, beads were resuspended in the same volume of PBST retrieved from the stock bead slurry to maintain the same bead concentration. To achieve the desired bead coverage, concentrated CaR mAb reagents were added to each bead suspension to produce the appropriate calculated concentration. Once prepared, the microcentrifuge tubes were mixed on a rotisserie for a 10 min bead loading step. To complete the preparation of the CaR multiplex beads, loaded beads were washed twice with 1 mL PBST after incubation to remove excess or loosely bound CaR mAb reagents and resuspended in the same volume of PBST retrieved from the original stock bead slurry to maintain bead concentration.

Samples were created by diluting stock *Plasmodium falciparum* D6 culture into whole blood to a parasitemia of 200 p/μL. Two hundred microliters of 200 p/μL whole blood was added to a 1.5 mL microcentrifuge followed by the addition of 200 μL of lysis buffer (100 mM phosphate buffer pH 8.0, 600 mM NaCl, 0.025% Tween 20, 2% Triton 100) and 4 μL of CaR multiplex beads suspension. Each mixture was then vortexed gently for 10 min before magnetically separating the capture beads. The supernatant was collected and examined for uncaptured *p*LDH using a commercially available *p*LDH ELISA kit. Each coverage variation was tested in triplicate. Following this quantitation, an average % *p*LDH uncaptured and subsequent % *p*LDH captured was determined when compared to the processed positive controls.

Multiplex capture bead evaluation

The optimal loading density of 8.92×10^{-8} mols 19g7-His_6-Biotin/L Dynabeads was applied to create multiplex beads to evaluate the simultaneous capture of both HRPII and *p*LDH. 200 p/μL spiked whole blood samples with beads were prepared and processed in a method identical to the one used to determine *p*LDH capture efficiency. Following a 10 min bead mixing step, beads were magnetically separated and the supernatant was tested with a HRPII ELISA[136] and an ApDIA *p*LDH ELISA kit to measure residual HRPII and *p*LDH. Quantitation of the unbound biomarkers was used to determine the biomarker capture efficiency of this system. Optimized multiplex beads were evaluated alongside bare, metal affinity Dynabead controls. Bare metal affinity Dynabead controls were prepared the same as CaR mAb beads without the addition of CaR mAbs during the incubation step.

Release chemistry optimization

Elution of the captured antigens was measured after exposing the multiplex capture beads harboring consistent antigen concentrations to 10 μL of elution buffer (50 mM phosphate buffer pH 8, 300 mM NaCl, and 0.025% Tween 20) containing different concentrations of imidazole. Buffer with increasing concentrations of imidazole were evaluated in regard to the *p*LDH remaining on-bead and the amount of HRPII recovered in the eluent following the elution cycle. Each biomarker was quantitated using an on-bead *p*LDH ELISA and an HRPII plate ELISA, respectively.

The elution conditions for the CaR mAb-*p*LDH immunocomplexes was optimized using a known *p*LDH ELISA pair. An anti-*p*LDH CaR mAb reagent (Clone 10PO9DS) was modified using 40x molar excess sulfo-SMCC and 20x His_6-Biotin peptide.

Multiplex beads were prepared by incubating beads with 5.71×10^{-6} mols CaR mAb reagent 10PO9DS per L Dynabeads, saturating CaR mAb levels, and the rest of the CaR mAb bead preparation was followed without alteration. Whole blood samples parasitized at 2,000 p/μL were processed according to the established method. After the beads were magnetically separated and the supernatant removed, they were washed with 200 μL PBST, magnetically separated again, and the wash solution was removed. Samples were then resuspended for two min in 10 μL of elution buffer containing imidazole concentrations ranging from 0 mM (control) to 1 M imidazole. For the quantitation of *p*LDH following the elution, the beads were washed with 200 μL of PBST then resuspended in 100 μL of 5 μg/mL anti-*p*LDH (clone 10PO9F) horseradish peroxidase conjugate (prepared using EZ-Link plus activated peroxidase kit) in a 5% bovine serum albumin (BSA) PBST solution. The beads were incubated with the conjugate for 20 min while vortexing gently. The now labeled *p*LDH remaining on bead was magnetically separated and washed 3x with 200 μL PBST. The last wash and bead slurry was transferred to a transparent 96-well plate (Corning, USA) and following the removal of the third wash, 100 μL of TMB_{one} solution was added to each well, covered with tin foil, placed on a plate shaker (VWR, USA) and mixed for 10 min. After 10 min development step, 100 μL of 2 M H_2SO_4 was added to each well to quench the reaction and the plate was read at 450 nm using a plate reader with path length corrected. The percent biomarker released was determined by comparing the amount of *p*LDH remaining on the bead to the initial amount of *p*LDH in the sample.

A similar experiment was performed to optimize the release of HRPII from the CaR multiplex bead. In this variation, beads were prepared using the optimized

conjugation criteria then subjected to the same samples and processing used to evaluate *p*LDH elution. Once the HRPII had been eluted into an identical set of imidazole buffers, the beads were then magnetically separated, and all 10 μL of elution buffer was then transferred to a 96-well holding plate. Ninety microliters of 0.1% BSA PBST was added to each well. The theoretical enriched concentration of 4,000 p/μL was diluted to 100 p/μL for analysis in an HRPII plate ELISA run according to literature precedent.[136]

CaR mAb reagent RDT compatibility screening

Immunocomplexes were formed by incubating each identified pan anti-*p*LDH CaR reagent with native *p*LDH from culture. Stock parasite culture was diluted to 2,963 p/μL, which correlated to ~4,000 pM native *p*LDH protein. The culture dilution was aliquoted at 50 μL, and CaR agents were spiked in at 400 nM to achieve a 100x molar excess, or 100:1 ratio, when compared to *p*LDH. The samples were then gently mixed for 30 min on a plate shaker before spotting 5 μL of each onto a separate ICT Dual RDT and running according to the manufacturer's suggested protocol. In addition to complexed samples, *p*LDH controls without CaR mAbs were also prepared. Twenty minutes after sample addition the lateral flow assay strip was quantified using an ESEQuant Lateral Flow Reader.

Multiplex capture and release reagents to increase the sensitivity of RDTs

Multiplex beads were prepared according to the optimized specifications. Samples were prepared by spiking 200 μL mock clinical samples to parasitemias ranging from 1 – 200 p/μL. In triplicates, multiplex capture and release experiments were carried out using the previously determined capture method and eluted in 10 μL

600 mM imidazole elution buffer. After completion, the 10 μL eluent was spotted onto a dual antigen-malaria ICT RDT, and the test was run according to manufacturer suggested protocol. Unenhanced samples were run in parallel to the experimental samples using the manufacturer's recommended 5 μL whole blood sample additions. All tests were allowed 30 min to develop, removed from their cassettes, and read on an ESEQuant Lateral Flow Reader. The threshold for positive readings was set to 15 mm*mV. This threshold was selected to provide an objective reading that correlates to the visual limit of detection for the RDT as determined by the researcher. The RDT limit of detection (LOD) were determined by the lowest parasitemia to register three consecutive HRPII/*p*LDH dual positive readings. Samples were prepared and assayed with smaller parasitemia step sizes around the perceived LOD to obtain a more accurate LOD.

Results and Discussion

Conjugation optimization

The conjugation of the mAb to a histidine-rich peptide is the critical step that enables a mAb to be reversibly loaded onto a metal affinity magnetic bead to generate the multiplex biomarker capture system (**Figure 4.3A**). In essence, immobilized CaR antibody reagents act as vehicles to capture, purify, and concentrate histidine-poor biomarkers. Equipping metal affinity magnetic beads with *p*LDH CaR mAb reagents provides an orthogonal capture strategy to simultaneously capture, enrich, and release *p*LDH and HRPII onto a RDT for downstream detection (**Figure 4.3B-E)**.

Compromising the function of an antibody is the key risk associated with the conjugation of exogenous peptides. Antibody affinity can be ablated or lost through

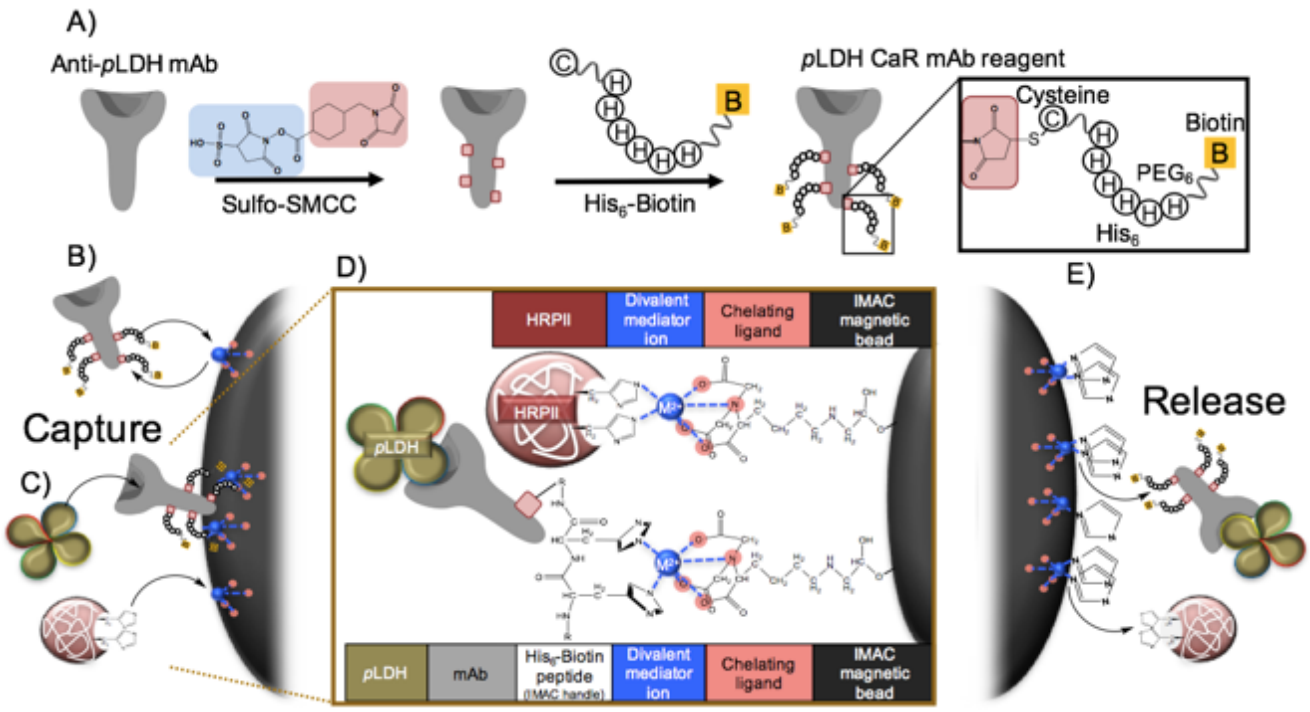

Figure 4.3: Conjugation strategy and operation principle for the *p*LDH and HRPII biomarker enrichment strategy. A) An anti-*p*LDH mAb is conjugated to a sulfhydryl containing His_6-Biotin peptide using bifunctional crosslinking reagent (sulfo-SMCC) to become a *p*LDH CaR mAb reagent. B) CaR mAb reagents can then be reversibly loaded onto an immobilized metal affinity chromatography (IMAC) magnetic Dynabead to C) generate a multiplexed bead that captures *p*LDH and HRPII. D) A more detailed illustration of the components involved in multiplex capture of *p*LDH and HRPII. E) Following the capture of both biomarkers, the biomarkers are magnetically enriched, and released using a high imidazole salt elution buffer for downstream detection.

functionalization of essential primary amines in or near the antigen-binding fragment (Fab). Modifying these critical lysine residues can lead immobilized antibodies to adopt inactive conformations. However, a high degree of histidine-rich peptide coupling is preferred because it promotes high avidity of the CaR mAb reagent to the metal affinity magnetic bead. A two-part conjugation optimization was used to promote the highest degree of peptide coupling while maintaining the antibody's maximum level of antigen recognition (**Figure 4.4A-B**).

Based on optimized results, nine commercially available pan-*p*LDH mAbs were conjugated and evaluated as potential CaR mAb reagents. Of the nine synthesized CaR mAb reagents, five proved to be pan-specific CaR mAb reagents by binding the *p*LDH

isoforms that represent the two most prevalent malaria species, *Plasmodium falciparum* and *Plasmodium vivax*.[137] The five observed pan-specific anti-*p*LDH clones (19g7, 10-P09CS, 1246, 12g1, and 1201) were selected to undergo a second, full conjugation optimization. Clone 14c2 was also selected as a candidate based on the hypothesis that the epitope for this mAb clone was found outside of the recombinant model *p*LDH proteins used in this study. This optimization study revealed that not all IgG mAbs were effected similarly by the conjugation strategy and demonstrated the importance of optimizing each antibody independently.

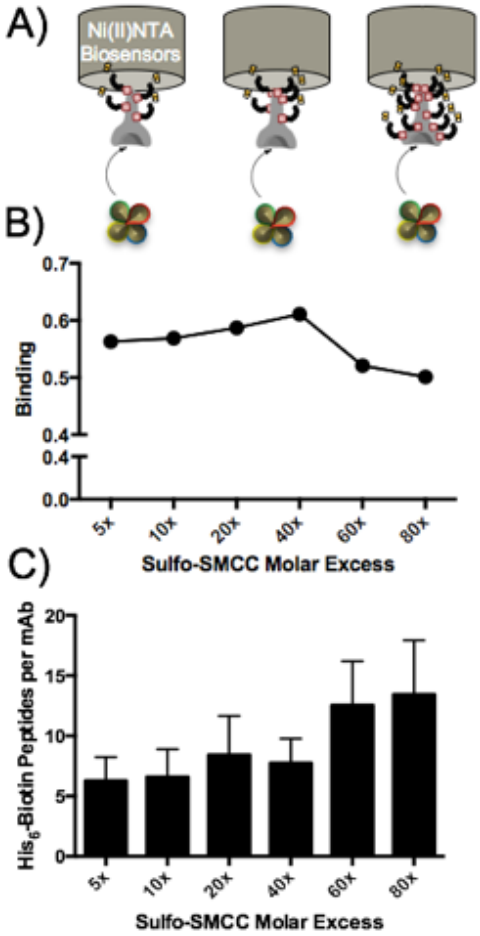

Figure 4.4: Impact of coupling strategy on antigen recognition. A model antibody, clone 19g7, was used to determine optimal conjugation conditions for the mouse IgGs employed in this study. A) An illustration of the experiment on Ni-NTA biosensors used to determine the B) impact of degree of mAb conjugation on CaR mAb reagent binding to rcPfLDH. C) Number of His6-Biotin peptides per mAb following the conjugation protocol as a function of molar equivalents of sulfo-SMCC.

Table 4.1: Quantitative binding data between anti-*p*LDH CaR mAb reagents and two *p*LDH isoforms: rcP*f*LDH and rcP*v*LDH. No observed binding is represented as NB. The different antibodies are distinguished by their commercial IgG clonality label. The number of peptides per CaR mAb is also provided.

His_6-Biotin modified anti-*p*LDH mAbs		**Recombinant *Pf*LDH**			**Recombinant *Pv*LDH**		
IgG clone	His_6-Biotin peptides per mAb	k_{on} (1/Ms)	k_{off} (1/min)	K_D (M)	k_{on} (1/Ms)	k_{off} (1/min)	K_D (M)
10PO9CS	4.9 ± 1.1	4.07E+04	3.13E-5	7.70E-10	1.87E+04	5.61E-6	3.00E-10
15f10	6.6 ± 1.1	2.02E+04	6.04E-4	2.99E-08	NB	NB	NB
14c2	5.1 ± 1.6	NB	NB	NB	NB	NB	NB
19g7	5.7 ± 1.4	1.07E+05	<1.00E-7	<1.00E-12	9.17E+04	3.28E-5	3.58E-10
12g1	5.2 ± 2.3	2.53E+04	1.30E-4	5.15E-09	4.24E+04	8.73E-5	2.06E-09
6c9	5.4 ± 1.9	2.74E+04	2.93E-4	1.07E-08	NB	NB	NB
1201	3.4 ± 1.7	3.51E+04	2.29E-4	6.53E-09	5.50E+02	4.42E-4	8.04E-07
1246	5.6 ± 0.9	2.58E+04	<1.00E-7	<1.00E-12	1.46E+03	1.52E-4	1.04E-07
10PO9F (PfLDH mAb)	5.1 ± 1.0	7.18E+03	2.03E-4	2.83E-08	NB	NB	NB

Following the two-part conjugation optimization study, each CaR mAb reagent was characterized for the number of peptides per antibody and a full list of kinetic binding parameters for both rc*Pf*LDH and rc*Pv*LDH was generated (**Table 4.1**). The terminal biotin synthesized as part of the His_6-Biotin peptide was used to quantitate the number of conjugated peptides per antibody. Of the CaR mAb antibodies surveyed, clone 19g7 displayed ideal binding characteristics (high k_{on}, low K_D) and proved to be compatible with the internal reagents of the selected RDT (**Figure 4.5**). However, a reduced signal was observed by *p*LDH when immunocomplexed with the CaR mAb 19g7.

Optimized pLDH CaR mAb reagent on-bead binding evaluation

The on-bead capture performance of the six conjugation-optimized CaR mAb reagents was investigated by functionalizing the metal affinity magnetic beads with different CaR mAb loading densities and subjecting them to native *p*LDH capture experiments in lysed whole blood. Optimal magnetic bead loading involves several

considerations. First, free divalent metal binding sites must be available to capture histidine-rich biomolecules, specifically the second target biomarker HRPII. If an excess of metal binding sites is not available, additional non-target histidine-rich biomolecules can compete for binding sites, which could decrease the system efficiency. Second, increasing antibody surface coverage on a particle surface has been shown to induce steric hindrance and mAb crowding, which often leads to antibodies loading in inactive conformations.[138] Lastly, the less CaR mAb reagent used the more economic feasible the approach.

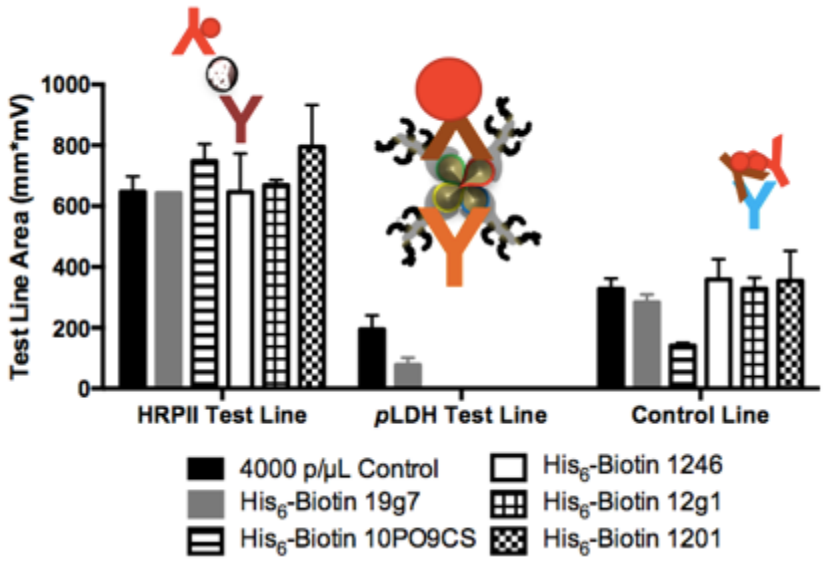

Figure 4.5: RDT compatibility study. Reflectance signal on the RDT HRPII, *p*LDH, and control test bands employing the capture and release strategy.

Multiplex capture beads were loaded with varying quantities of CaR mAb reagents and then evaluated for their ability to capture native *p*LDH in a parasitized lysed whole blood matrix. Theoretical bead coverage calculations were used to ensure that a full range of loading densities was explored**.** As a general trend, *p*LDH capture efficiency increased along with CaR mAb reagent loading density (**Figure 4.6A**). CaR mAb reagent clone 19g7, which exhibited ideal affinity parameters to *p*LDH per BLI

experiments, captured more antigen with less antibody coverage. This finding confirmed the validity of the BLI instrument with Ni-NTA biosensors as a suitable platform to screen and optimize antibody reagents for assay development. Since no pan-*p*LDH mAb necessarily has the same binding affinity to *p*LDH, it is important to fully characterize reagents before use in diagnostic systems.[30]

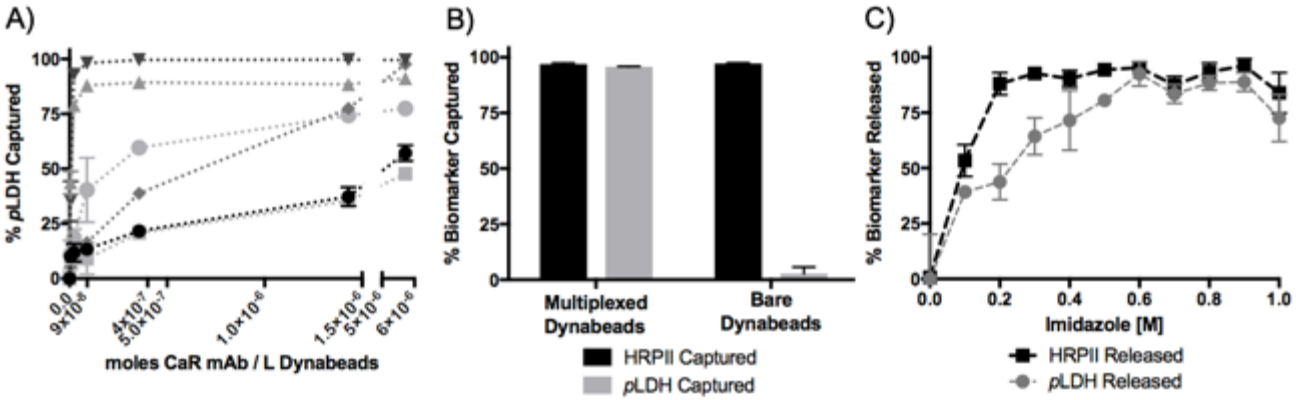

Figure 4.6. On-bead binding studies in parasite-spiked lysed whole blood. A) The impact of increased CaR mAb reagent loading on percent *p*LDH capture (pan anti-*p*LDH CaR mAb reagent clones: 19g7 (inverted triangles), 10-P09CS (triangles), 1246 (grey circles), 12g1 (diamonds), 1201 (black circles), 14c2 (squares). B) The *p*LDH and HRPII capture efficiencies of multiplex beads equipped with 9×10^{-8} mols CaR mAb 19g7 / L Dynabeads and unloaded bare metal affinity beads. C) The impact of increasing the concentration of imidazole on the percent biomarker released from bead surface.

Multiplex bead capture and release optimization

With a RDT-compatible, high affinity *p*LDH CaR mAb reagent identified, the multiplex capture of native HRPII and *p*LDH was evaluated. Multiplex beads composed of unoccupied metal binding sites and loaded CaR mAb reagent 19g7 were mixed in a lysed parasitized whole blood sample, magnetically separated, and the supernatant was analyzed for uncaptured *p*LDH and HRPII. The multiplexed Dynabeads captured 97 ± 0.5% of available HRPII and 96 ± 0.3% of *p*LDH. Metal affinity magnetic Dynabeads without CaR mAb reagents captured an equivalent amount of HRPII but only 2.7 ± 2.9%

of the available pLDH (**Figure 4.6B**), therefore, validating the selective and compatible orthogonal binding of CaR mAb reagents.

One major advantage to the immobilized metal affinity chromatography system is the mild elution reagent used to recover metal-coordinated biomolecules. The multiplexed elution chemistry was investigated as a function of increasing concentrations of the common elution agent, imidazole. Imidazole is the side chain of histidine and competitively elutes HRPII and immunocoplexed *p*LDH from the bead surface at high concentrations. Nearly all the HRPII was eluted from the beads with the addition of 300 mM imidazole but 600 mM imidazole was needed to release the maximum amount of *p*LDH-CaR mAb immunocomplexes. At an optimal 600 mM imidazole, 92.5 $\pm$ 5.6% and 95.3 $\pm$ 2.0% of captured *p*LDH and HRPII, respectively, are released from the beads (**Figure 4.6C**).

Multi-biomarker capture and release to enhance a dual-antigen malaria RDT

The goal of this study was to develop a multiplex biomarker enrichment system, by combining the specificity of immunocapture with the utility of magnetically-enabled metal affinity separation, to enhance a dual-antigen malaria RDT. Employing beads equipped with an optimal 4% loading density of CaR mAb reagent 19g7, the multiplex biomarker enrichment process was performed on 200 μL mock clinical samples (**Figure 4.7A1-5**).

Enriched samples were compared to unprocessed controls at parasite densities ranging from 0-200 p/μL. This is a particularly important range for dual-antigen malaria RDTs because it represents the parasite densities commonly undetected or mistaken as false-negatives by healthcare workers.[139] Specifically, the *p*LDH test band is unreliable

at detecting malaria infections with parasite densities lower than 100 p/μL, rendering them insufficient for detection of all disease carriers.[102]

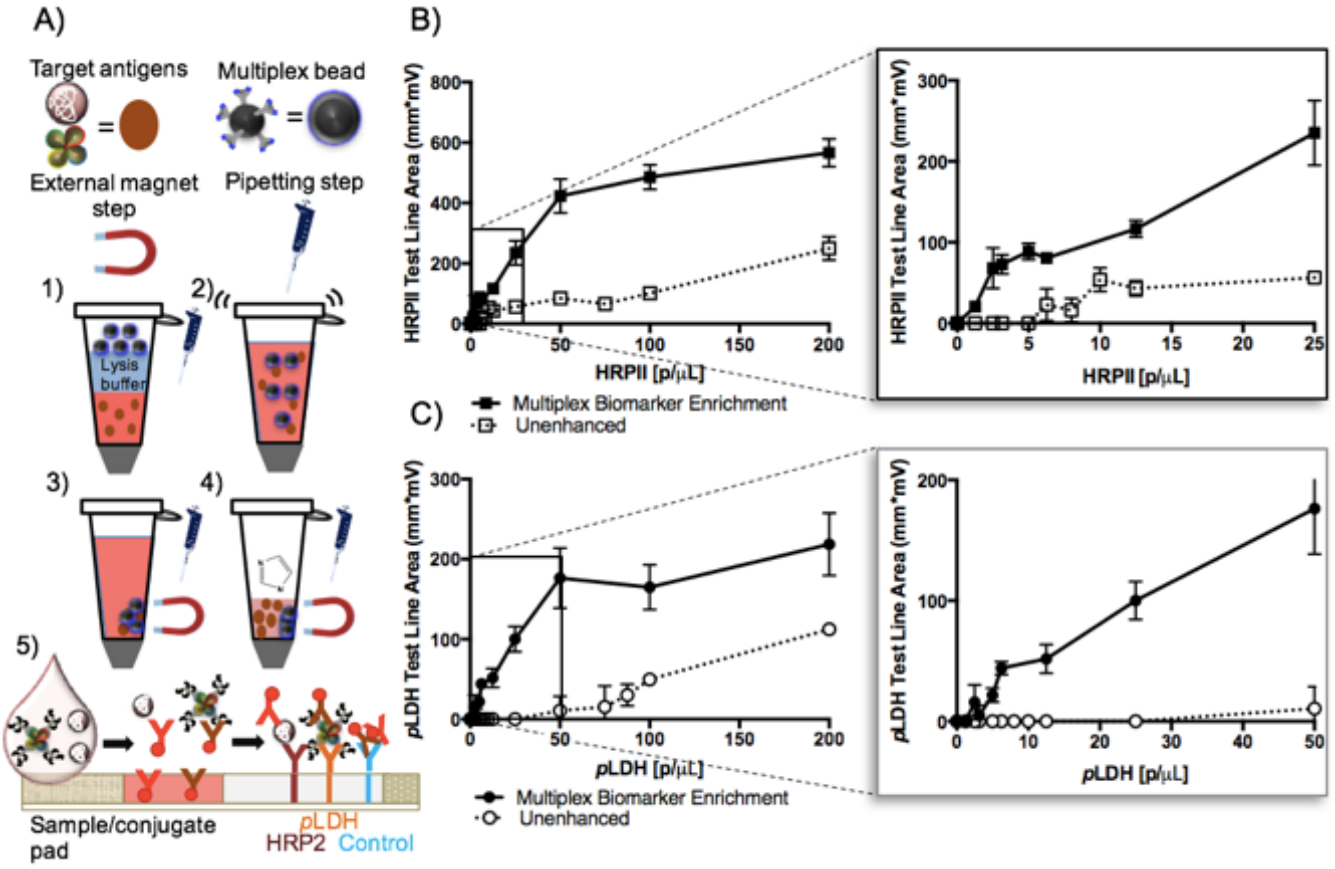

Figure 4.7: Multiplex biomarker enrichment strategy to enhance a dual-antigen malaria RDT. A) The multiplex biomarker enrichment process: 1) 200 μL of lysis buffer and multiplex magnetic beads are added to 200 μL of mock clinical sample spiked to parasite densities ranging from 0-200 p/μL, 2) the sample is mixed for 10 min, 3) beads are magnetically separated, supernatant is removed, 4) 10 μL of 600 mM imidazole elution solution is added and mixed, beads are magnetically separated from the eluent, and 5) the eluent is spot onto the RDT for downstream detection. Using a LFA reader, the developed test bands for B) HRPII and C) *p*LDH are reported for each parasite densities to determine the LOD for the multiplex capture and release strategy as well as unenhanced control samples. A representative control RDT and an RDT processed with the multiplex biomarker enrichment system at 25p/μL are provided for reference (**Figure 4.8**).

Even when both bands are positive, the pan-*p*LDH band often remains faint even at densities as high as 2,000 p/μL. This disparity in antigen test band performance is a result of a combination of factors. First, the internal antibodies employed for each respective antigen's tests line and gold conjugate possess different binding avidities.[134]

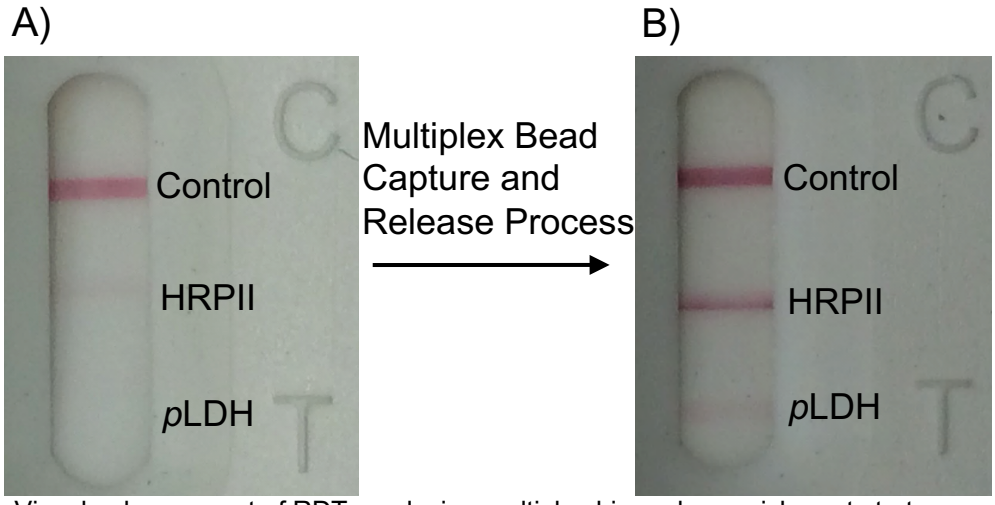

Figure 4.8: Visual enhancement of RDT employing multiplex biomarker enrichment strategy on ICT Dual malaria RDTs. A) A photograph taken 30 min after an RDT was run with 5 µL of 25 p/µL per manufacturer suggested protocol. B) A photograph taken 30 min after an RDT was run after processing 200 µL of 25 p/µL per the multiplex bead capture and release protocol.

Second, there is a difference in clinical *p*LDH and HRPII antigen abundances depending on the life-stage of the parasite and persistence of infection. HRPII has been shown to circulate at concentrations significantly higher than *p*LDH.[140]

Following the multiplexed capture and release process, an increased test band signal intensity is observed for both biomarkers. This is a result of the increased concentrations of HRPII and *p*LDH delivered to the RDT (**Figure 4.7B-C**). Increasing test bands signal leads to increased visual LODs. In this study, the test LOD was determined as the lowest parasitemia that generated three consecutive optically positive HRPII and pan-*p*LDH test bands when read on an RDT reader. This result informs the correct diagnosis by the test. Employing an optical reader to determine LODs eliminates the subjective interpretation of faint test bands characteristic of the lowest detectible antigen concentrations. Additionally, it eliminates background noise associated with variations in test strip texture and clearance. This method of LOD determination follows the WHO-FIND RDT evaluation program to test commercial malaria RDT

performance.[66] Implementation of this sample preparation strategy improved the dual positive test band sensitivity from 87.5 p/μL (117 pM *p*LDH, 31.0 pM HPRII) to 5.00 p/μL (6.70 pM *p*LDH, 1.80 pM HRPII), resulting in a 17.5-fold improvement in test visual LOD. The HRPII test band returned a positive test band for all positive samples processed. The lowest parasitemia processed was 1.25 p/μL (6.70 pM *p*LDH, 0.450 pM HRPII), which returned only a positive HRPII band. Consequently 1.25 p/μL was below the test detection limits of the test as it informs an incorrect test diagnosis. It is hypothesized that the HRPII test band will be positive at much lower parasite densities but this was not investigated.

Implementing this biomarker enrichment strategy increases the sensitivity of a dual-antigen malaria RDT to detect HRPII and *p*LDH biomarker associated with low levels of infection. To frame the RDT LOD within the ongoing detection needs of elimination campaigns, Slater *et al.* generated a model to estimate the relationship between diagnostic sensitivity and onward infection. Using current multi-antigen RDT technology, this model predicts that the detection of biomarker concentrations associated with 100 p/μL enables the discovery of approximately 65% of the disease reservoir.[141] However, the proposed biomarker enrichment strategy lowers the RDT detection limits to biomarker concentrations associated with single digit parasite densities. This would achieve 95% detection of the infectious disease reservoir.[141] Furthermore, multiplex analysis of HRPII and *p*LDH allows the identification of the malaria species as *P. falciparum* or non-*P. falciparum* to inform an appropriate treatment course and better monitors the efficacy of treatment.

Beyond improving the detection limits of both target biomarkers, the proposed enrichment technique addresses other technical vulnerabilities inherent to the core RDT technology. Purifying biomarkers from confounding blood agents mitigates test anomalies such as sample clearance issues, and removes matrix components that lead to non-specific signal.[30] Although this system is not field deployable in its current state, it highlights the "proof-of-concept" applications for CaR mAb functionalized magnetic beads to improve the performance of multi-antigen RDTs. Our previous work has laid the foundation for translating magnetic bead-based sample preparation technologies, like the one presented, to the point of care.[124]

Conclusion

Motivated by the advantages of the metal affinity-based biomarker enrichment system, we developed an agnostic method to transform antibodies into metal affinity-compatible CaR reagents. This method harnesses the advantages of both immunoaffinity and immobilized metal affinity chromatographic techniques. The unification of these two technologies generates a multiplex biomarker enrichment method that translates to a multitude of disease biomarkers through the simple, yet versatile, process of conjugating our immobilized metal affinity chromatography-compatible handle to an assay-compatible molecular recognition element of interest. In this study, the employment of a anti-*p*LDH CaR mAb reagent afforded the orthogonal capture and enrichment of *p*LDH and HRPII. The addition of enriched samples to a HRPII/pan-*p*LDH RDT improved both test band signals to the visual LOD needed for malaria elimination campaigns to make informed diagnostic decisions.

Although other strategies exist to couple antibodies to magnetic beads, these strategies often involve covalent attachment. Liberating biomarkers from beads surfaces, therefore, necessitates harsher elution conditions. These conditions can impact the integrity and structure of the biomarker, leaving the biomarker inactive for downstream detection. The proposed enrichment platform adopts a more specific and gentle elution mechanism allowing biomarkers to be responsive to downstream detection.

The His_6-peptide conjugation technique can be applied to any antibody or other amine-containing capture agents. Two or more CaR reagents targeting different biomarkers could be loaded onto metal affinity magnetic beads, either together or on their own separate beads to customize this strategy to other disease targets. However, as the number of different targets increase, the number of beads in the system must be optimized to ensure that the efficiency of the system is not compromised. This strategy is also expected to have utility in serological diagnostic assays. In this alternative format, antigens would be functionalized with His_6 peptides, then loaded onto a bead surface for antigen-specific antibody capture, purification, and detection. In any format, new CaR reagents must undergo compatibility studies to ensure that they suitably interface with the desired detection strategy. To that end, this study not only serves as an enrichment strategy to improve the detection limit of dual-antigen malaria RDTs, but also as a platform with wide applicability to other label or label free detection assays.

Acknowledgement

The authors would like to thank Kim Fong for her expertise in parasite culturing and microscopy, David Gasperino (IVL) for thoughtful discussions, and M. F. Richards

and K. A. Richardson for their critical comments concerning the manuscript. We would like to acknowledge Vanderbilt University for support from the Laboratories for Innovations in Global Health Technologies (LIGHT). We acknowledge funding from Intellectual Ventures/Global Good (Bellevue, WA).

CHAPTER V

The Utility of Microvirin to Increase the Specificity and Sensitivity of Lipoarabinomannan-Based TB Diagnostics

Introduction

Despite being a treatable disease, tuberculosis (TB) has resurged as the world's leading infectious disease killer. Yet, with early diagnosis and appropriate treatment, most deaths from TB can be prevented.[48] The global burden of TB stands at about 9 million and in 2016, there was an estimated 1.7 million TB deaths globally.[142] One of the factors in this high mortality is that the causative agent, *Mycobacterium tuberculosis* (*M. tb*), is the most common opportunistic infection in HIV-positive patients. Further, the proportion of HIV-positive TB patients reported to have died during treatment was about 3 times higher compared to non-HIV patients. Reasons for comparatively poor outcomes for HIV-positive TB patients include late detection and delay in starting antiretroviral therapy (ART) or TB treatment. In fact, the world fails to detect 38% of the estimated new cases of TB per year.[143,144] Conventional TB diagnosis rely on technologies that are insensitive and nonspecific such as 100-year-old sputum smear microscopy and chest radiography. Moreover, the diagnostic accuracy of these techniques is further impaired in patients with HIV coinfection.[145]

Globally, the use of rapid diagnostic tests is increasing and many countries are phasing out the use of smear microscopy and chest radiography. In response to the high TB mortality in HIV-positive patients (estimated to be 40%), the WHO approved the Alere Determine TB LAM Ag lateral flow assay (LFA) as a point-of-care (POC) "rule-in"

test for people with HIV or with very low CD4 counts (<100 CD4 T cells/mm^3).[146] Lipoarabinomannan (LAM) is a principle glycolipid present on mycobacterial cell walls and is shed from metabolically active or degenerating bacterial cells. The rapid adoption of biomarker-based LAM testing in HIV endemic areas is expected to help ensure early diagnosis and overcome challenges with diagnosing TB in people with low CD4 counts.[147]

LAM has also been the target of several other immunological tests including enzyme linked immunosorbent assays (ELISA) in both plate and dipstick formats.[148-150] In any format, the WHO has only approved urine-based LAM testing to "rule-in" potential patients. This is due largely to their variable performance, measured by their sensitivity and specificity. Results from clinical studies and a meta-analysis present sensitivities between 13%-93%, where increased sensitivity was correlated to the severity of patient immune suppression as the concentration of LAM in urine was found to depend on the patient's immunocompetence. It is suspected that the LAM concentration presented in the urine of non-HIV TB patients was out of the range of current tests.[151,152] Similarly, although most studies have reported high positive predictive values, there remains unexplained variability from individual studies reporting specificities ranging from 79%-100%.[153] While poor specificity may reflect the shortcomings from individual assays, it is also possible that false-positive results are due to cross reactivity with non-tuberculous mycobacteria (NTM).[148,154,155]

The LAM antigen has three structural domains: (1) a phosphatidylinositol linker, (2) a polysaccharide backbone, and (3) a capping motif, where the linker and backbone are conserved in all mycobacterium and the capping motif varies.[156] There are three

classifications of LAM that based on variations in their capping motif. The mannose-capped variant of LAM (ManLAM) is unique to the surface envelope of slow-growing, pathogenic mycobacteria such as *M. tb* making it an attractive target for new capture and detection agents.[157] In this study, we have expressed microvirin (MVN), an α-(1,2)-mannose-specific lectin, and demonstrate its wide utility in ManLAM TB diagnostics. By pairing this reagent with high affinity anti-LAM monoclonal antibodies we developed highly sensitive and specific diagnostics.

Materials and Methods

Expression and purification of MVN

E. coli DH5α competent bacteria were transformed with the MVN-pET15b plasmid in Tris-EDTA pH 8.0 buffer by heat shock. The transformed bacteria were plated onto ampicillin LB Agar plates. Colonies were selected from the plates and incubated overnight in LB medium with 100 μg/mL ampicillin. Then, the plasmid was extracted from the bacterial culture using the ZymoResearch Plasmid Miniprep Kit and the concentration of the plasmid was determined using Nanodrop spectrometry. *E. coli* BL21 pLysS competent bacteria were transformed with the MVN-pET15b plasmid (190 ng plasmid per 100 μL bacteria) by heat shock. The plasmid-transformed bacteria were plated onto ampicillin LB Agar plates. Colonies were selected from the plates and incubated in LB medium with 100 μg/mL ampicillin as a starter colony. 5 mL of the starter colony was incubated with 400 mL Terrific Broth until the OD_{600} was approximately 0.6. Then, expression of MVN was initiated by the addition of IPTG at a concentration of 1 mM. Following an additional 3-hour incubation, the cultures were pelleted and re-suspended in BPer Bacterial protein extraction reagent (Thermo

Scientific: Cat. No. 78248) with benzonase nuclease (0.1 mg/mL final concentration) (Sigma: Cat. No. E1014-5KU) and lysozyme (0.75 μL per 1 g bacterial pellet) (Fluka: Cat. No. 62971). Following a 30-minute incubation, the insoluble proteins were pelleted and the supernatant was transferred to a clean tube. The protein concentration of the supernatant was determined by BCA assay. SDS PAGE and Anti-His_6 Western Blot were performed on the protein lysate to confirm the presence of MVN. MVN was purified using Ni-NTA His-Bind Resin (Merck Millipore: Cat. No. 70666) and dialysis.

Bioconjugation

MVN was conjugated to biotin at its stock concentration of 0.613 mg/mL with a 20x molar equivalence of EZ-Link NHS-PEG4-Biotin (Thermo Scientific: Cat. No. 21329) in DI water. Following a 30-minute incubation step at room temperature, the MVN-biotin conjugate was purified from excess biotin reagent using a 7k MWCO Zeba desalting column (Thermo Scientific: Cat. No. 89883). The concentration of the resulting MVN-biotin conjugate was determined by micro-volume analysis using a BioTek Take3 plate on a BioTek Synergy H4 plate reader (VT, USA) with the lysozyme setting. Anti-LAM antibodies Ab25 and Ab170 were procured from The Foundation for Innovative New Diagnostics (FIND). FIND Ab25 and FIND Ab170 were conjugated to biotin with a 20x molar equivalence of NHS-biotin in DI water. Following a 30-minute incubation step at room temperature, the antibody-biotin conjugate was purified from excess biotin reagent using a 7k MWCO Zeba desalting column. The concentration of the resulting antibody-biotin conjugate was determined by micro-volume analysis using a BioTek Take3 plate and the IgG setting.

FIND Ab25 was conjugated to horseradish peroxidase using EZ-Link Plus Activated Peroxidase (Thermo Scientific: Cat. No. 31489). The single-use tube was dissolved in DI H_2O and added to the antibody, followed by sodium cyanoborohydride. The reaction was incubated of 1 hour at room temperature. Quenching buffer was added and allowed to react for 15 minutes. The resulting antibody-conjugate was transferred to an Amicon Ultra-0.5 mL Centrifugal Filter Ultracel - 100K spin filter (Millipore Sigma: Cat. No. UFC510024) and centrifuged for 10 minutes at 14,000 g. The spin filter was washed twice with PBS then flipped upside-down in a new tube and centrifuged for 2 minutes at 1,000 g. The concentration of the antibody-conjugate was determined by microvolume analysis using a BioTek Take3 plate and the IgG setting.

Kinetic characterization of molecular recognition elements by bio-layer interferometry

Anti-LAM antibodies CS35 and CS40 were procured from the American Type Culture Collection (ATCC). MVN and Ab25 and Ab170 were conjugated to biotin using the aforementioned strategy. Following the conjugation, each molecular recognition element was subjected to a kinetic experiment on the ForteBio Octet RED96 (CA, USA) to determine binding affinity to H37Rv ManLAM.[158] Dip and Read Streptavidin biosensors (ForteBio: Cat. No. 18-5021) were used for the kinetic experiments with biotinylated MVN, Ab25, and Ab170 and Dip and Read Anti-Mouse Fc capture biosensors (ForteBio: Cat. No. 18-5090) were used for the kinetic experiments with CS35 and CS40. The biosensors were first introduced to a biosensor buffer (0.1% BSA (Fisher: BioReagents: Cat. No. BP9706100), 0.020% tween 20 PBS (Fisher BioReagnets: Cat. No: BP337100) for a 300 second equilibration step, followed by a loading step where the biosensors were transferred to wells containing MVN-biotin

(0.125 μg/mL) or biotinylated antibody (0.5 μg/mL) for 400 seconds. The loaded biosensors were moved to wells containing biosensor buffer for a 60 second baseline step and then transferred to sample wells containing a two-fold serially diluted range of H37Rv ManLAM with a buffer reference well for a 400 second association step. The two-fold serial dilution began at an initial concentration of ManLAM such that the starting concentration of ManLAM was at least 10x higher than the expected K_D and the lowest concentration was 2x lower than the expected K_D.[159] Lastly, the biosensors were moved back to the wells that they were baselined in for a 900 second dissociation step. The same procedure was used Dip and Read Ni-NTA biosensors (ForteBio: Cat. No. 18-5103) to determine the binding affinity of MVN-His6, except the biosensor buffer was 0.020% tween 20 PBS and MVN was loaded onto the biosensor at 4 μg/mL. Inside the software, a global 1:1 fit model was selected to derive the kinetic (k_{on}, k_{off}) and equilibrium (K_D) data.

Stability test of MVN by bio-layer interferometry

MVN was conjugated to biotin using the aforementioned strategy and stored at 4°C. Repeated kinetic experiments at set time points were performed to determine binding affinity over time as a representation of stability. The kinetic experiments were performed in the same manner as before.

Binding pair evaluation by bio-layer interferometry

MVN was conjugated to biotin using the aforementioned strategy. The binding pair evaluation was run on the Octet RED96, equipped with 7 parallel ready-to-use streptavidin biosensors. The biosensors were first introduced to a streptavidin biosensor buffer (0.1% BSA, 0.020% tween 20 PBS) for a 300 second equilibration step, followed

by a loading step where the biosensors were transferred to wells containing 0.125 μg/mL MVN-biotin conjugate for 400 seconds. The loaded biosensors were moved to wells containing streptavidin biosensor buffer for a 60 second baseline step and then transferred to sample wells containing either 10 nM H37Rv ManLAM or a buffer reference well for a 400 second association step. The biosensors were moved back to the baseline wells for a 120 second baseline step and then transferred to wells containing 25 nM non-conjugated Ab25, 25 nM non-conjugated Ab170, 25 nM non-conjugated MVN, or a buffer reference well for another 400 second association step. Lastly, the biosensors were moved back to the wells that they were baselined in for a 900 second dissociation step. Inside the software, a global 1:1 fit model was selected to derive the kinetic (k_{on}, k_{off}) and equilibrium (K_D) data.

Development and Assembly of Urine-based ManLAM LFA

The AD1520 Aspirate/Dispense Platform (BioDot, Irvine, CA) was used to deposit antibody and MVN solution onto membranes. The deposited antibodies, MVN, and MVN complexes adsorb to the nitrocellulose surface at the location of their deposition and do not flow down the membrane when a sample is added. Since the test line and control lines are spatially separated, there is no cross-reaction between the capture agents. 1 mg/mL goat anti-mouse antibody (Life Technologies Cat. No. 31160) in PBST was used to print the control line. MVN and streptavidin-complexed MVN, pre-formed by incubating biotinylated MVN and streptavidin (4:1 molar ratio) on a rotisserie for 30 min without purification,[160] were printed at several different test line concentrations. 0.971 mg/mL streptavidin-complexed MVN was printed for the tests evaluated in this paper. FF120HP nitrocellulose (Whatman Cat. No. 10547001) and

Fusion5 (GE Healthcare Cat. No. 8151-9915) membranes were used to construct lateral flow assays. The control line and Strep-MVN test line were deposited as described above and the membrane was dried at 40 °C. Next, membranes were blocked with 100 mL of either 1X Denhardt's Solution (Invitrogen Cat. No. 1692489) or Pierce Protein-Free T20 blocking buffer (ThermoFisher Cat. No. 37573)—Pierce Protein-Free T20 blocking buffer was found to be the optimal blocking buffer for this test. Following the blocking step, membranes were dried at 40 °C for 14 hrs. A CF7 wicking pad (Whatman Cat. No 8117-2250) was then attached to the backing card with the wicking pad overlapping the membrane. A CM4000 membrane cutter (Biodot) was then used to cut assembled LFAs perpendicular to test and control lines into 5 mm wide tests. LFAs were stored in foil pouches with desiccant until use. Prior to use the backing card was cut to remove the portion of the test dedicated for a conjugate pad and the tests were run as "half-strips." Prior to running half-strip LFAs, a paperclip was used to ensure contact between the overlapping wicking pad and the nitrocellulose strip. Tests were run by spiking 5 µL of OD 10 AuNP into 100 µL of urine and allowing test to run for 25 min. Test and control lines were quantified with an ESEQuant Lateral Flow Reader (Qiagen) between 25 and 30 min after sample deposition. Test line intensities were analyzed in the ESE Quant LF studio software with a peak area at a fixed baseline using a signal threshold. Experiments were performed in triplicates and reported as average peak area.

Gold Conjugate Preparation for Employment on LFA

Gold nanoparticles (AuNPs) 40 nm in diameter (BBI solution Cat. No. GC40) at an optical density (OD) of 1.04 were used to create gold-antibody conjugates for

detection on LFAs. OD measurements were measured at 535 nm on an Agilent 8453 G1103A spectrometer (Agilent Technologies). The pH of the 1.04 OD gold colloid solution was increased to 8.0 using 100 mM potassium carbonate solution. Five microliters of Anti-LAM Ab-25 or Ab-170, provided at a concentration of 1 mg/mL by FIND, was then added to this gold colloid solution to made a 0.010 mg/mL gold-protein solution, vortexed for 10 s, and incubated on a rotisserie for 15 min. Blocking buffer (50 mM borate buffer with 10% (w/v) BSA) was added at a volume 10% of the initial gold solution and the solution was returned to the rotisserie for 30 min. After incubation the gold solution was centrifuged for 30 min at 5000 rcf, the supernatant was removed and the remaining conjugate pellet was diluted to an OD of ~10 with storage buffer (50 mM borate buffer with 1% (w/v) BSA and stored at 4 °C. Conjugates were never stored for more than 2 months.

Results and Discussion

New approaches of TB control and care are needed. Provided that accurate diagnosis is the cornerstone of TB control, non-sputum based diagnostics serve as the most practical tests to enable well-timed diagnosis and appropriate treatment. Timely treatment is needed to reduce the unacceptably high number of deaths due to this otherwise curable disease.[161] Conventional TB diagnostic tests, including recently WHO approved GeneXpert MTB/RIF tests, all require biohazardous *M. tb*-positive sputum samples. Yet, is difficult for many active TB patients to produce sputum samples, including those co-infected with HIV, diabetes patients, and children.[49,162,163] Alternatively, urine analysis obviates the biohazards associated with sputum handling and can be easily collected from all patients.[50] LAM is an advantageous biomarker to

detect in urine because it is heat stable and does not readily degrade over time.[150] The sensitivity and specificity shortcomings associated with current urine-based LAM tests are the consequence of several mechanisms, including the characteristics of the test-capture reagents, patient selection during test assessment, condition of the urine sample, and the variable concentration of excreted LAM that has been reported to vary between 1 ng/mL and several hundred ng/mL depending on the manifestations of co-infected disease.[151,164] Of these, the selection of the test-capture reagents is the only factor that is diagnostic test dependent and can be improved.

Current LAM detection tests employ either polyclonal or monoclonal antibodies. Polyclonal antibodies are more likely to recognize multiple antigenic epitopes on LAM compared to monoclonal antibodies but risk batch-to-batch variation, influence cross reactivity, and are not sustainable for mass production of quality LFAs. Though Monoclonal antibodies (mAb) target a single epitope, the majority of mAbs generated against LAM target the mycobacterial-conserved portion of the antigen. Pathogenic mycobacteria species express ManLAM while non-pathogenic mycobacterium express either phosphoinositol capped LAM (PILAM), in the case of *M. smegmatis*, or LAM that is devoid of either phosphoinositol or mannose caps (AraLAM), in the case of *M. chelonae*. The first antibody produced that exclusively targets the unique α-(1,2)-mannose linkages exhibited on ManLAM capping motif was reported by Chan *et al*, but its diagnostic utility has yet to be fully investigated.[165]

The discovery of MVN, a highly specific α-(1,2)-mannose binding lectin, was reported in 2006 by Kehr *et al*.[166] Since then, it has been investigated for anti-HIV-1 activity and as a neutralizing agent for hepatitis C virus infections.[167-170] To evaluate the

feasibility of MVN to selectively capture ManLAM for use in next generation TB diagnostics, MVN was subjected to kinetic and affinity binding bio-layer interferometry experiments on the Octet platform with procurable LAM variants (**Table 5.1**). Commercially available LAM antibodies procured from the BEI repository and FIND were also evaluated employing the same design of experiments. When comparing the quantitative binding data between MVN and available anti-LAM antibodies, MVN exhibited the second highest binding affinity and displayed improved specificity as it did not bind to PILAM. No appreciable binding was found for either of the anti-LAM polyclonal antibody matrixes and this was thought to be a caused by the higher concentration of nonspecific antibodies within the matrix being immobilized on the biosensor that skewed the global binding data. This gives more evidence to why polyclonal antibodies are not ideal for employment in quality controlled diagnostics.

Table 5.1: Kinetic binding analysis of LAM recognition elements to different LAM variants.

	Binding affinity (K_D) to Antigens			
	H37Rv *M. tb* ManLAM	*M. leprae* ManLAM	*M. smegmatis* PILAM	*M. chelonae* AraLAM
MVN	0.453 nM	0.386 nM	**N.B.**	X
MVN-Biotin	0.567 nM	X	X	X
Ab-25	1.32 nM	0.967 nM	0.817 nM	X
Ab-170	0.636 nM	0.118 nM	< 1.0 pM	X
CS-35 mAb	< 1.0 pM	< 1.0 pM	X	X
CS-40 mAb	8.74 nM	X	113 nM	X
Anti-LAM polyclonal (Rabbit)	N.B.	N.B.	N.B.	X
Anti-LAM polyclonal (Guinea pig)	N.B.	N.B.	N.B.	X

X—Binding kinetics study have not yet been performed
N.B.—No binding observed

Improved test selectivity is of primary importance for infection control because treatment regiments differ between certain mycobacterium species.[157] The selective

capture of ManLAM affords the ability to discriminate between pathogenic and non-pathogenic mycobacteria, which the current TB LAM LFA is incapable of doing. However, in addition to *M. tb*, there are several other pathogenic mycobacterial species that express ManLAM, such as *M. leprae*, which are captured with MVN. Fortunately, most ManLAM-presenting pathogenic bacteria either cause symptomatic TB, which typically affects the lungs, or cutaneous infection. TB-causing pathogenic species, such as *M. bovis*, have the same or very similar treatment strategies for *M. tb* infection. Mycobacterium that cause cutaneous infections, such as *M. leprae*, induce illness that can be differentiated from *M. tb* empirically(symptomatically) based on signature skin sores or lesions. Therefore, screening tests such as LFAs do not need to further differentiate to provide proper treatment.[171]

After confirming the high affinity and specificity of MVN to ManLAM, the greater utility of this capture reagent was explored. MVN has several advantageous biophysical properties; it was expressed with a N-terminal hexahistidine affinity tag and has a single intrinsic lysine residue, akin to a site selectable site, which lends itself to facile bioconjugation techniques including biotinylation for immobilization to any streptavidin coated substrate or to streptavidin anchor protein to load onto nitrocellulose.[172] A PyMOL rendering of the MVN crystal structure shows the location of the lysine residue and N-terminal hexahistidine tag in proximity to the α-(1,2)-mannose binding site (**Figure 5.1A**). A practical advantage to using MVN is that like mAb production, MVN can be expressed in vectors at a large scale and is resistant to batch-to-batch variation.[173] Stability is an important parameter to the utility of protein-based capture reagents. To examine the stability of native MVN and biotin conjugated MVN, kinetic

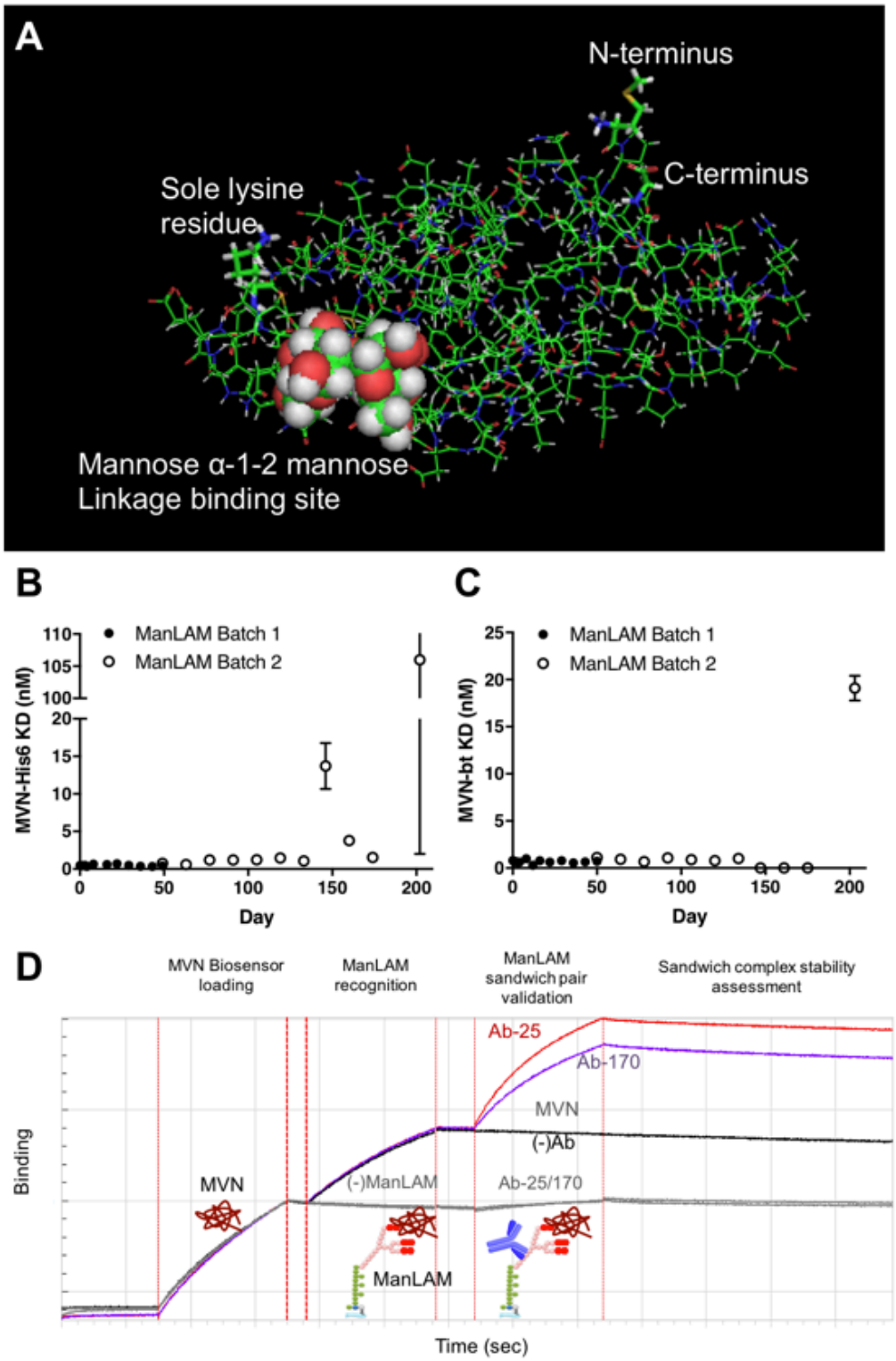

Figure 5.1. MVN crystal structure, stability studies, and binding pair assessment. **A)** PyMOL rendering of the resolved crystal structure for MVN with the major components labeled. **B)** MVN stability study where kinetic binding experiments of native MVN and **C)** biotinylated MVN to ManLAM were performed for 200+ days. **D)** Orthogonal binding pair assessment for MVN.

binding experiments were conducted over 200+ days. MVN remained stable at 4° C for approximately 175 days. After 200 days, a significant increase in affinity constant was observed, which is an indication of degradation **(Figure 5.1B and C**).

In traditional "sandwich" style in vitro diagnostics, orthogonal binding pairs are employed to capture and detect biomarkers of interest. Pairing MVN with an orthogonal, high-affinity LAM capture element is therefore needed to detect ManLAM in LFAs and ELISAs. Due to nonspecific binding observed between the CS-35 mAb and MVN, as well as supply issues, the potential orthogonal binding element were Ab-25, Ab-170, and MVN. The nonspecific binding to CS-35 was minimized but not eliminated employing PNGase F amidase to remove N-linked oligosaccharides from the antibody surface (data not shown). Both Ab-25 and Ab-170 were selected as candidate orthogonal mAbs because they provided stable binding complexes when "sandwiched" with MVN (**Figure 5.1D**). MVN did not form a self-binding pair even though ManLAM was suspected to have several mannose caps per antigen.[156]

The identification of several orthogonal high-affinity binding mAbs initiated the development of a urine-based LFA. It is only necessary for one of the two capture reagents in the orthogonal binding pair to be specific toward the α-(1,2)-mannose moiety for discrimination between pathogenic and nonpathogenic LAM variants. Due to the ubiquitous use of antibodies in particle-based detection conjugates, Ab-25 and Ab-170 were selected for the detection conjugate and MVN was selected as the test line capture agent. However, due to its small size (14.3 kDa), MVN was adsorbed to the test through nitrocellulose-binding streptavidin anchor proteins.[78] The optimal membrane

and blocking solution were identified to be FF120HP nitrocellulose and protein-free T20 blocking buffer, respectively. Although further optimization needs to be performed to determine the optimal MVN-streptavidin test line concentration, AuNP conjugate, and test concentration of AuNP, proof-of-concept LFA experiments were performed to establish MVN as a viable test line capture reagent in the first reported TB ManLAM LFA (**Figure 5.2A**).

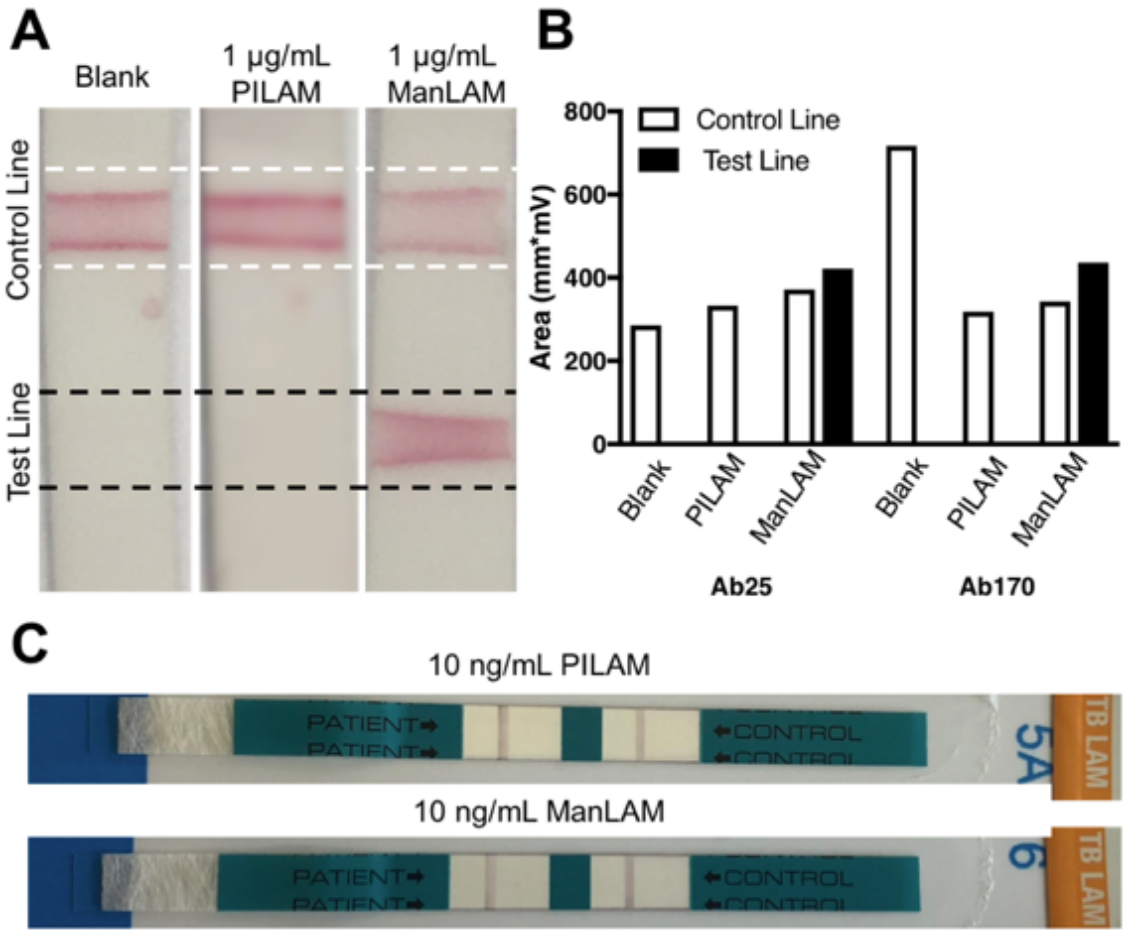

Figure 5.2. The employment of MVN to develop novel TB ManLAM LFA. **A)** Half-strip TB ManLAM LFA experiment that were challenged with blank urine and urine spiked with PILAM and ManLAM. **B)** The quantitative values from half-strip LFAs employing an LFA reader. **C)** The only current commercially available TB LAM LFA challenged with PILAM and ManLAM.

The results mirrored those observed in kinetic binding experiments as MVN employed on the test line was able to discriminate ManLAM from PILAM in urine. Both Ab-25 and Ab-170 AuNPs were viable conjugates to be employed on the TB ManLAM LFA but further experiments must be performed to identify the optimal conjugate and concentration to achieve the most sensitive LFA results (**Figure 5.2B**). Initial testing shows great promise for the development of a urine-based TB diagnostic that overcomes the selectivity issues that plague the Alere TB LAM Ag tests (**Figure 5.2C**).

Conclusion

We believe that we have only scratched the surface of the potential that MVN has as a capture reagent in developing new and improving existing urine-based TB ManLAM diagnostics. The demonstration of MVN as a ManLAM-selective capture agent is the foundational component to developing a highly sensitivity ManLAM TB LFA. Following further optimization studies, the resulting ManLAM LFA is expected to be more selective and sensitive than the sole commercially available Alere TB LAM LFA.

MVN can be employed as a capture element in a variety of other ways as well. The intrinsic hexahistidine affinity tag lends itself to the sample preparation method previously reported in our lab.[174] By reversibly immobilizing MVN on the surface of metal affinity magnetic beads, MVN is able to capture ManLAM and be released under mild conditions as a MVN-ManLAM complex. The addition of these MVN-functionalized beads to large-volume urine samples allows for the capture and magnetic enrichment of ManLAM, as well as the ability to elute exceptionally high numbers of MVN-ManLAM complexes into the 60 µL sample volume for Alere TB LAM LFAs. Additionally, the 3-antibody steric problem observed with the capture, release, and detection of a

biomarker on a commercial LFA employing 150 kDa antibodies will hopefully be mitigated due to sterically favorable 14.3 kDa size of MVN.[174] Front-end sample preparation using MVN functionalized magnetic beads not only has the opportunity to deliver increased copies of ManLAM to the test, which increases the sample sensitivity of the LFA, but will also act to preselect ManLAM in urine. Consequently, the only LAM variant that will be delivered to tests after sample preparation will be ManLAM alleviating the cross-reactivity issues that plague the current Alere TB LAM LFA.

Given that the normal bladder capacity in adults range from 300 - 400 mL, an easily acquirable sample volume from any patient, including children, would be 10 mL.[175] If MVN functionalized magnetic beads could capture and deliver 80% of the available ManLAM in the 10 mL urine sample to the test, then a theoretical enhancement of 133 would be achieved. Increasing the sensitivity of Alere TB LFA tests 133-fold may allow detection of all patients, even those that have high immunocompetence. This sensitivity increase could revolutionize the TB diagnostic space and enable this LFA to become more than just a “rule-in” test—It could become the keystone for future TB control strategies.

Lastly, MVN can be employed in more traditional diagnostic methods including plate and bead-based ELISA strategies. Its single intrinsic lysine residue enables site directed amine conjugation to a plethora of different substrates and detection molecules. The nucleophilic amine group can be used to directly conjugate to a substrate or can be biotinylated for immobilization to any streptavidin coated substrate including magnetic beads to act as a capture agent. It can also be conjugated to

enzymes, fluorophores, quantum dots, or other signal generating materials to serve as a detection element.

Acknowledgement

I would like to acknowledge and share the credit of these initial findings with Megan van der Horst. Megan executed many of the BLI experiments outlined in this chapter and will be co-authoring a manuscript with me on this topic with the expected submission date in the summer of 2018. I would also like to acknowledge our collaborators on this project; Dr. Jonathan Blackburn and Dr. Leshern Karamchand. Dr. Karamchand initially expressed the MVN lectin and his expertise in biochemistry has been instrumental for this project.

CHAPTER VI

Demonstration of a Semi-Automated, Menu-based Diagnostic Instrument Appropriate for Low-Resource Settings

Credit for the findings described in this section must be shared. Dr. Keersten Ricks and Anna Bitting, who developed and optimized of the protein-based and nucleic-acid based assay cassettes, respectively. Instrument design and prototyping was accomplished by our collaborators in Dr. Fredrick Haselton's Laboratory. I am the primary author for the manuscript detailing these findings, which is currently being prepared for submission.

Introduction

The accurate and timely diagnosis of infectious diseases is key to accessing proper interventions and improving clinical outcomes in resource-poor settings.[176] However, primary health centers and clinics in resource-limited settings lack the necessary diagnostic technologies for healthcare workers to make informed treatment decisions during clinical visits. Diagnostics are imperative to the healthcare process as they inform the appropriate treatment and guide the safe and rationale use of medicines.[25] Currently, most primary care and municipal clinics are able to provide basic diagnostic tests like manual serology, microscopy, and rapid diagnostic tests (RDTs).[177] However, this diagnostic capacity is not adequate for diagnosing and managing most diseases. As a result, it is estimated that only 45% of those who need specific testing in low-resource settings, such as sub-Saharan Africa, receive it.[20] A

major cause of this inadequacy is that the diagnostic landscape today is populated with systems that have not been designed to function in resource-constrained settings.

The need to develop simple, low-cost diagnostics has been accompanied by a paradigm shift from control of diseases in centralized healthcare facilities to prevention and early treatment in primary health facilities.[178,179] This shift demands low-resource diagnostic systems with sophisticated sets of diagnostic capabilities.[180,181] However, the emergence of new diagnostic systems for resource-poor settings has been hindered by the perception, and often the reality, of a low return on investment and the challenges regarding implementation in less-developed healthcare systems.[182] To overcome this obstacle, the Bill & Melinda Gates Foundation developed a list of essential diagnostics and target product profiles (TPP) as a Grand Challenge in Global Health Initiative. Our team of researchers and engineers developed a diagnostic system as part of this Grand Challenge aimed at meeting the needs of end users in level 1 health centers.[22,183]

Herein, we describe the design and development of an open diagnostic platform consisting of a portable, automated instrument and a menu of interchangeable assay cassettes. Instrument development was performed in conjunction with proof-of-concept assay cassettes for protein detection, cell counting, as well as isothermal- and polymerase chain reaction-based (PCR) nucleic acid amplification testing (NAAT). We recently described the development of a simple, yet robust, multiphase fluidic assay platform used to concentrate disease biomarkers from complex biological matrixes (**Figure 6.1A**).[38,101,184] This platform coordinates magnetic bead-based biomarker capture with sequential solution processing inside of a length of tubing separated by immiscible fluid separators called surface tension valves (STVs), all without the need for

expensive valve and pump configurations. Further, this self-contained assay format has shown utility as an automated sample preparation system.[185,186] Herein, we build upon these technological principles in the development of a prototype “one-touch” instrument that automates sample processing and detection for a variety of diagnostic and prognostic biomarkers. This instrument consists of several integral device components including: a universal rotary mounting cartridge (i.e. a cartridge to mount self-contained assay cassettes); a motion control system and fixed magnet to manipulate the transit of magnetic beads through various processing solutions; a compact thermal control system for nucleic acid amplification; and an optical detector (**Figure 6.1B**).

A combination of magnetic bead-based biomarker concentration, target labeling, and signal amplification were utilized to develop five disposable assay cassettes (**Figure 6.1C**). Each assay cassette was developed to contain minimal sample preparation steps and optimized to achieve the greatest extraction efficiencies. Of these, an index of four disposable assay cassettes were selected to interface with the final integrated prototype one-touch instrument to demonstrate the flexibility of this platform. The protein detection and cell-counting assay cassettes employ antibody functionalized magnetic beads to capture a malarial protein biomarker and CD4 T cells, respectively. Both of these assays employ an enzyme conjugate for exclusive target biomarker labeling and subsequent signal production for quantitative optical detection. Alternatively, silica-functionalized magnetic beads were employed to extract, process, and release DNA for amplification in a nucleic acid detection chamber.

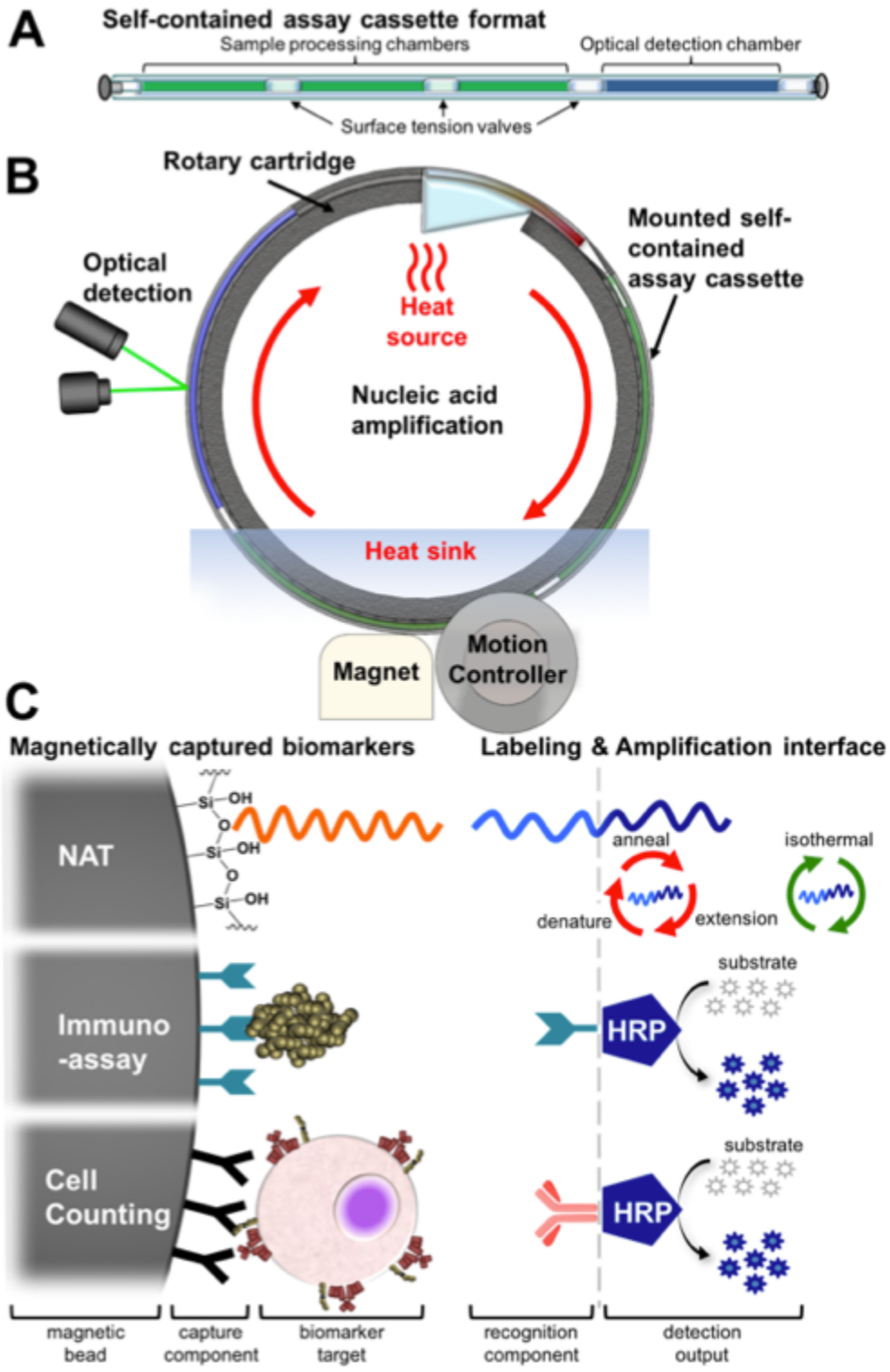

Figure 6.1: Foundational technologies for the one-touch system. **A)** Visual depiction of the self-contained assay cassette format and the **B)** rotary instrument design with the components needed for cassette automation. **C)** The bead surface functionalization and signal amplification interface employed in the featured assay cassettes.

Until now, no device has been developed that enables extraction and detection of multiple biomarker classes. The advent of this platform has the ability to extend the diagnostic modalities of enzyme-linked immunosorbent assay (ELISA) and NAAT to low-resource settings. Point-of-care access to this device would eliminate the need to transport samples to high capacity laboratories, reduce the errors associated with arduous sample processing and detection, and allows test results to be available at the patient's bedside.

Materials and Methods

Device Components

The Arduino UNO Rev3 programmable controller was purchased from Arduino (Cat# A000066). The stepper motor drive controller (Cat# STR4), stepper motor (Cat# HT23-401), and power supply (Cat# PS150A24) were purchased from Applied Motion Products. Cubic magnets were purchased from SuperMagnetMan (Cat# Cyl0360 N40). The Qiagen ESELog USB Multichannel Fluorescence reader (Cat# 9002069) was purchased from Qiagen. The Peltier heating element (Cat# VT-31-1.0-1.3) was purchased from TE Technology. The TDK Lambda Z+Power Supply (Cat# Z36-6-U) was purchased from TDK Lambda. The Omega TC, K-type small gauge 0.05" thermocouple (Cat# 5TC-TT-K-36-36) was purchased from Omega. The components were assembled using aluminum components made in-house by the Vanderbilt machine shop. The plastic cartridges were designed and printed in-house using SolidWorks software and a NovaCopy ProJet HD 3000 Plus 3D printer. A Compact CCD spectrometer (Cat# CCS100) and T-Cube LED Driver (Cat# LEDD1B) was

purchased from THORLABS. Plastic fluorescent standard slides (Cat# BZA44677) were purchased from Axon Instruments.

Integrated One-Touch Device Setup

The components installed on the integrated one-touch prototype included a cartridge wheel, stepper motor, magnet harnessed in a spring-loaded mount, thermal control system, and an optical detector configuration that allowed for both fluorescence and "calculated absorbance" readings. Diagrams showing hardware connection and the software schematic is provided for reference (**Figure 6.2**). All assays were interfaced with the integrated instrument, which operated all of its code on a Microsoft Surface. The Surface connects over Ethernet/TCPIP to the National Instruments Compact RIO-9076 (cRIO). The cRIO has two C-series modules an NI-9402 for digital I/O to run the motor controller and an NI-9211 for reading the thermocouples. The cRIO has an FPGA that was used to create the signals to drive the STR4 stepper motor controller from Applied Motion. The Peltier was powered by a TDK-Lambda Z36-6-U power supply capable of 216 W but only about 18 W of power was necessary. The system communicates over the USB to the power supply. The system communicated over the USB to the power supply.

Hardware Connectivity and Instrument Operation

After turning on the Microsoft Surface, the hardware mounted on the breadboard platform was turned on; switch is in the back next to the power cord. This would turn on the TDK-Lambda power supply. Three cables connect the Surface dock to the instrument, one purple network cable, and two USB cables**.** These were connected to the STR4 motor controller and motor and were confirmed to be connected and properly

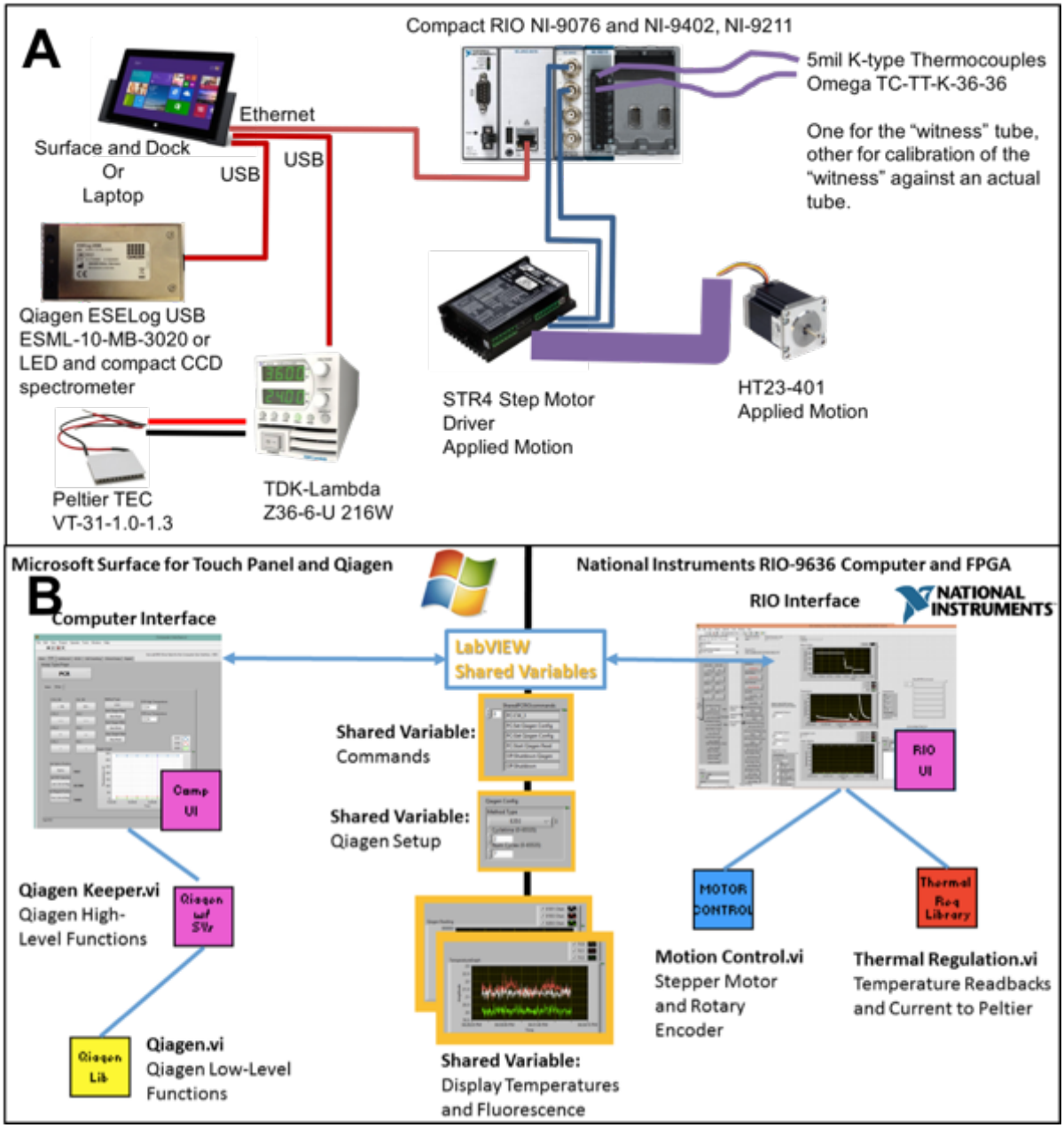

Figure 6.2: Diagrams of the one-touch hardware and software connections. **A)** A detailed connectivity map showing each of the hardware components used in the development of the one-touch instrument. **B)** The high-level software components are shown in the figure with those running on the Surface on the left and with Computer Interface shown at the top. On the right are shown software elements that run on the RIO computer with RIO Interface the main control program. Items along the middle bar are the LabVIEW Shared Variables that enable communication and data sharing between the two computers.

functioning by toggling the switch on the right, under the platform. A pair of 1/8” diameter copper tubing sleeves 5/8” long, one for the cassette and one for the witness tube, were soldered together to form a block that makes thermal contact with the Peltier for heating. The thermocouple for the witness tube was plugged into the instrument, and threaded through the cap so that it was submerged halfway in the chamber.

Hardware Alignment and Tube Mounting for Absorbance-based Cassettes

Use the motor switch to turn off the motor to allow mounting the tube onto the cartridge. The fluorescent chip affixed to the cartridge was considered the zero point for absorbance-based cassettes, as all of the chamber lengths were measured from this point. The number of chambers needed and chamber size were predetermined based on specific assay needs. Assay tubes were placed onto the cartridge with the detection chamber aligned with the red colored fluorescent chip recessed into the channel of the cartridge assembly (**Figure 6.3A**). Following the mounting of the assay cassette, the motor and controller were turned back on with the switch below the platform. The rest of the tubing was fit onto the cartridge by ensuring the tubing was secured in the cartridge grooves. The last alignment step was to ensure that the magnet was touching the assay tube on the cartridge and that the spring force seems appropriate to maintain contact during rotation.

Hardware Alignment and Tube Mounting for Fluorescent-based Cassettes

First the motor switch was used to turn off the motor to allow mounting the tube onto the cartridge. To maintain proper alignment for the NAAT fluorescent-based cassettes, detection chambers were threaded into the copper sleeve going upward (**Figure 6.3B**). It was vital that the liquid in the final chamber was visible through the

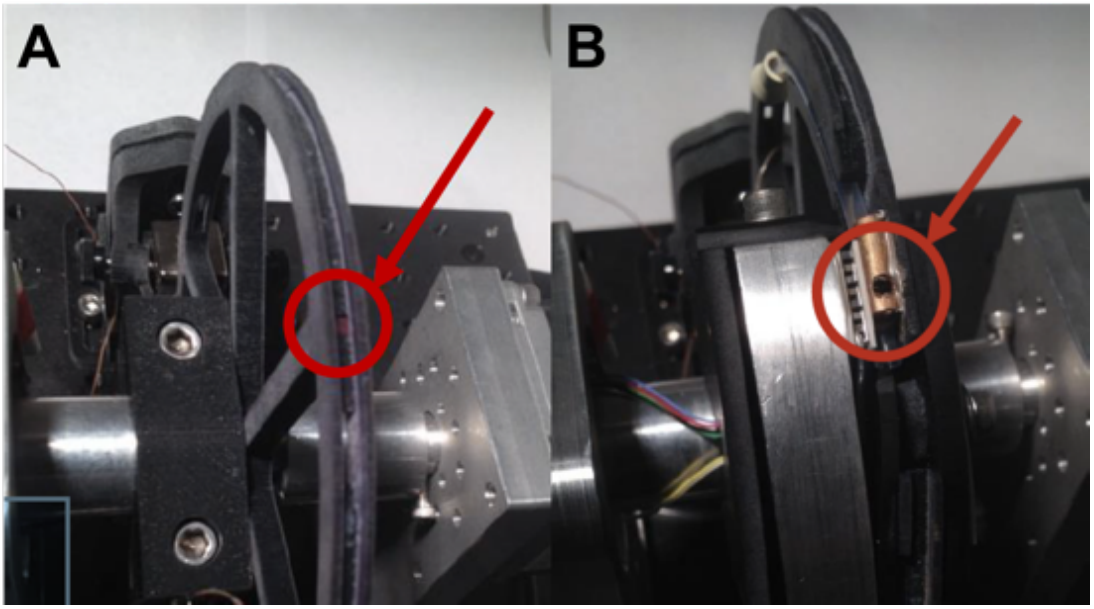

Figure 6.3: Detection chamber mounting positions. A) Fluorescent chip shown at center of red circle where absorbance detection-based cassette's detection chambers were aligned with during cassette mounting. B) At a different section of the cartridge wheel, a copper sleeve with around widow for external optical detection of the amplification/detection chamber was inserted within to provided uniform heating/cooling for fluorescent NAT-based cassettes.

hole. The remainder of the respective assay tube was fit onto the cartridge rim. To ensure alignment of the Qiagen fluorometer and the hole, an extra software button named "Blink Qiagen" was incorporated so that the incident light could be matched up with the hole. The Qiagen optical detector employed in this breadboard prototype had the following two channels: (1) 470nm emission / 520nm detection, and (2) 565 nm emission / 625 nm detection. If not aligned, a thumb screw allowed the user to adjust the Qiagen mount to move it left to right. The motor and controller was then turned back on and the on-board magnet was confirmed to be touching the assay cassette and cartridge with the spring force appropriate to maintain contact during rotation.

Software Operation: In the program folder, the LabVIEW Project view was selected to open the software. In the "MotionControl" folder, within the Project view, the appropriate cassette program was selected by double clicking the appropriate program

(ProteinQuantitation, CellCount, or the appropriate NAAT). A separate program was developed to meet the needs of each proof-of-concept assay cassette. On the Motor Setup tab, a “Blink Qiagen” button was provided to ensure that the final detection chamber for each assay cassette was aligned with the Qiagen detector. To enable a flexible software interface and ability to translate future assays to cassette form, tabs within each program were installed. The absorbance-based assays (protein quantitation and cell counting cassette programs) were provided with tabs to enter “Chamber Positions” and “Mixing times” to be customized for each chamber size and incubation time. Similarly, the tab provided for NAAT assay cassette motor control was “Extraction Cycle Count.” For the assays tested, these values were saved in their respective program and when opened to the “Run Page” tab, “One Touch Go” was selected to initiate. A reference reading was initially measured at the detection chamber followed by the assay being processed according to the predetermined optimal values, ending in a final sample optical measurement.

Data Analysis

For the NAAT tests, the direct fluorescence measurement was plotted vs time on the Microsoft Surface. The fluorescent readings for the PCR-based cassette and LAMP-based cassette were measured while at the optimal PCR cassette annealing temp and at every min for LAMP-based cassettes, respectively. The average measurement corresponding to cycles 3-10 was used to calculate a baseline, the baseline was subtracted from each cycle’s fluorescence, and the time needed for the normalized data to reach the predetermined assay-specific fluorescence threshold was observed as the amplification time and an answer was returned. The instrument also calculated the

absorbance measurements for the protein quantitation and cell counting programs employing the fluorescent detector using **equation 6.1**. The results of these experiments were listed as “calculated absorbance.” This could then be compared to a previously determined linear regression to return a positive reading or further, quantitative information for the selected biomarker.

$$\text{Absorbance} = -\text{LOG}_{10}(\text{Sample fluorescence/reference fluorescence}) \qquad (\textbf{Equation 6.1})$$

Assay Cassette Development

Protein Quantitation: HRPII On-Bead ELISA Cassette

Materials: Ni(II)NTA Magnetic Agarose Beads (Cat# 36111) were purchased from Qiagen Inc. MyOne™ Streptavidin T1 magnetic particles (Cat# 65601) were purchased from Life technologies. Pooled whole blood collected in CPD (Cat# HMWBCPD) was purchased from Bioreclamation LLC. Anti-*pf*HRPII antibodies (IgG) for streptavidin particle surface modification as well as the detection antibody for the on-bead ELISA (Cat# ab9206 and ab30384, respectively) were purchased from Abcam Inc. 3,3’,5,5’-tetramethylbenzidine (TMB) One solution (Cat# G7431) was purchased from Promega Corporation. Micro Spin Desalting Columns (Cat# 89882) were purchased from Fisher Scientific. MagWell 96-well plate magnet (Cat# 57624) was purchased from EdgeBio. All other reagents were purchased from Sigma Aldrich Inc. or Fisher Scientific Inc.

Parasitized Whole Blood Sample Preparation

Whole blood collected in CPD was mixed 1:1 (v:v) with 2x lysis buffer (100 mM sodium phosphate, 2% Triton X-100, 0.01% Tween 20) and allowed to lyse until the blood because translucent. The lysed blood was filtered through a glass wool-packed

plastic syringe. Blood was lysed freshly for each experiment. *Plasmodium falciparum* stock (37,475 parasites/μL) was cultured in our laboratory and was added to the appropriate volumes of filtered, lysed blood to achieve the desired parasite concentration per the desired experiment. Generally, 50 parasite/μL was positive and 0 parasites/μL whole lysed blood samples were used in the optimization of the HRPII protein quantitation cassette as positive and negative samples, respectively.

On-Bead HRPII ELISA Reagent Selection and Optimization Within a Plate

On-Bead ELISAs (OBEs) were performed in a plane, 96-well polystyrene plates. Ten microliters of magnetic beads, Ni(II)NTA or Ab functionalized streptavidin, were added to 100 μL of sample along with detection Ab at a given concentration. After the specified mixing time on a plate shaker, the plate was placed on the MagWell 96-well plate magnet to pull the beads to the edge of the well. The beads were washed with buffer three times (Phosphate buffer saline, 5% BSA, 0.02% tween 20). The MagWell plate magnet was used in between each solution removal to ensure minimal loss of beads. Before removing the final wash, all samples were transferred to fresh wells before adding 100 μL detection substrate, TMB. After incubating the beads with TMB, the plate was placed on a plate magnet, the colorimetric product was transferred to a new plate, and the plate was read on a Synergy H4 hybrid plate reader at 650 nm (or 450 nm if the reaction was quenched with H_2SO_4). This general protocol was used for the optimization of all the assay buffers, reagent concentrations, and other parameters before being adapted to the self-contained assay format.

On-Bead HRPII ELISA ELISA Cassette Construction and General Protocol

The all-in-one OBE experiments were performed inside of a self-contained assay cassette. Generally, 10 µL of the functionalized streptavidin beads were added to a 100 µL of parasitized whole blood sample with the detection Ab-Horseradish peroxidase (HRPx) conjugate. Following the addition of the reagents, the entire sample was loaded into a preconstructed assay cassette and mounted on the instrument where the detection chamber was aligned with the reflective or fluorescent backing. The cassette tube was constructed using a 3D printed template guide. Please see **Figure 6.5A** for a schematic of the assay cassette. The process chambers were loaded by a 22 gauge 6" long deflected point septum penetration needle and multiflex pipette tip. The cassette was loaded by first sealing the sample loading end of the tubing with Chā-Seal, a clay sealing compound. By closing one end, the long needle or pipette tip could be inserted inside the tubing and the processing chambers could be loaded with an inside out approach as the fluid would travel towards the open end. This inside out approach prevented contamination between chambers and aided in stabilizing the processing chambers during preparation. First, the TMB detection chamber was loaded into the downstream end of the tubing, the entire tube was completely sealed, and the clay plug at the sample addition end of the tube was cut out using a razor. Two sequential wash solutions were then loaded with the long septum needle and followed by the addition of the sample with a multflex pipette tip. The assay cassette was sealed once again, mounted onto the instrument, and the protein-detection program was selected for the assay to run hands free. There was no need to quench reaction because solid phase containing the detection enzyme is removed from the tube following an incubation cycle.

Therefore, the spectrometer collected the colorimetric change in the detection chamber at 650 nm.

Cell Counting: CD4 Enumeration Assay Cassette Development

Materials: Dynabeads® CD4 Positive Isolation Kit (Cat# 11331D), MagnaRack Magnetic Separation Rack (Cat# CS15000), CountBright™ absolute counting beads (Cat# C36950), and the flow analysis antibodies CD14-PerCP (MHCD1413), CD4-FITC (MHCD0401), CD45-PerCP (MHCD4531), CD8-APC (MHCD0805) were procured from Life Technologies™/Thermofisher Scientific (Grand Island, NY). The flow analysis antibody CD3-PE (clone OKT3) was purchased from Biolegend (San Diego, CA). Chromogenic detection antibody: anti-human CD3 (clone OKT3) conjugated to horseradish peroxidase (Cat# LS-C260009-200) was purchased from LSBio (Seattle, WA). Fluorinated ethylene propylene (FEP) tubing (Semi-Clear Red, .093" ID, 1/8" OD, .016" Wall - Part # 9369T19) was procured from McMaster Carr Supply Co (Atlanta, GA).TransFix was obtained from Cytomark, a division of caltag medsystems (Sheffield, UK). Trucount Tubes (Cat# 340334), Tritest™ CD3/CD4/CD45 (Cat# 342444), Falcon™ 5 mL polystyrene flow cytometry tubes, and FACS Lysing Solution (Cat# 349202) were purchased from BD (Franklin Lakes, New Jersey). PE reference standard calibration beads (Cat# 828) was procured from Bangs Laboratories (Fishers, Indiana).

Sample Acquisition and Preparation

Whole blood samples were acquired from health donors or de-identified clinical HIV+ patients. For healthy donors, the Vanderbilt clinical research center collected 10 mL of intravenous whole blood from consenting donors under proper IRB approval (VUIRB#130684). Blood was collected in purple cap vaccutubes and used within 8 hrs

of collection. When these samples are used in a study they will be denoted as “whole blood samples.” Thirty de-identified clinical patient samples previously collected in purple capped vaccutubes were acquired as remnants from requisitioned routine CD4 testing conducted at Vanderbilt Medical Center under proper IRB approval. All specimens were acquired within 8 hrs of Vanderbilt clinical flow cytometry center conducting a clinical CD4 count.

Quantitative Flow Cytometry to Determine Donor CD3 Antigen Density

Whole blood samples were collected and a FACS lyse, no wash protocol was performed with on whole blood samples to generate healthy PBMC donor samples. Cell populations were labeled with 1.5 µL of CD4-FITC, CD3-PE (OKT3) and CD8-APC in the dark at room temperature for 30 min. A stopping gate was provided to collect 10,000 CD3+CD4+ cells. Following the collection of this subset of cells, FlowJo data processing software was used to determine the geometric mean fluorescent intensity (gMFI) of the target cell subset. Experiments were conducted on a 3-laser BD LSRII. PE Calibration beads were used to standardize the flow cytometer before each experiment and generate a relationship between mean fluorescent intensity (MFI) and CD3 antigen density exhibited on CD4 T cells. Following the standardization of the instrument, before each sample analysis, a homogenous suspension was achieved by vortexing gently for 10 sec.

Cassette Extraction Force Simulation—Fixed vs. Unfixed Cells

Certain additional forces exist in our cassette-based isolation compared to the conventional microcentrifuge-based isolation used by the CD4 Positive Isolation Kit. To evaluate how native CD4 T cells and fixed CD4 T cells respond to the isolation

cassettes' inherent forces, the comprehensive force of a full cassette-based isolation was broken down into three fundamental forces: 1) compression force, 2) surface tension valve force, and 3) shear force. Each of these forces were simulated as to best isolate each individual force and the cellular response to these forces were evaluated employing a quantitative flow cytometry approach. Surrogate whole blood samples were prepared according to the procedure described above. CD4 magnetic beads were added to sister 100 µL samples and following a gentle 10 min mixing step on a rotisserie, native captured CD4(+) cells were set aside and 15 µL of transfix fixation agent (recommended transfix volume per unit sample volume) was added to the 'fixed' captured CD4(+) cells. All sample were inverted 5 times, regardless of fixative addition, and allowed to incubate for 5 min at room temperature. Both native and fixed cell samples were then subjected to force simulations in triplicate. The compression force was simulated by magnetically compressing the magnetic bead-captured cell complexes into a pellet using a Neodymium magnet (1" X 1") for 10 min, the total perceived compression time in the assay cassette. The surface tension force was simulated by fanning out the capture beads into a monolayer inside the extraction tube, holding them in place by the magnet, and gently pushing 4 subsequent 100 µL wash chambers over the beads that were separated by 1 cm wide STV. The self-contained assay shear forces were simulated by first loading an extraction tube full of washing solution and magnetically moving the captured cells over a distance of ~19.5 cm, the total length of CD4 enumeration assay cassettes. The samples were then analyzed employing the quantitative flow cytometry approach similar to the one described above.

Construction of CD4 T-Cell Enumeration Assay Cassette

A volumetric single-platform approach was employed in the construction of the cassette to generate a cell count. Each cell extraction cassette was constructed using 20 cm piece of FEP tubing. Before sample loading, the extraction tubing was pre-loaded with the processing fluid chambers. Please see **Figure 6.6A** for a schematic of the assay cassette. The successive processing chambers were separated by air gaps that we call surface tension valves. The process chambers were loaded by a 22 gauge 6" long deflected point septum penetration needle and multiflex pipette tip in the same manner as the protein detection cassette. Please see protein assay cassette construction above for details. The detection chamber (100 µL of 0.025% Tween 20 TMBone solution) was first loaded at the opposite end of the tubing with a long multiflex pipette tip. The tube was sealed following the addition of the detection chamber. The Chā-Seal plug was then cut out of the sample side of the tube and then the septum penetration needle was used to load the rest of the chambers in this order: wash chamber, wash chamber, CD3-HRPx labeling chamber. The ~100 µL wash chambers comprised Dalbeccos Phosphate Buffer Saline (DPBS) with 4% Fetal bovine serum (FBS), 0.025% Tween20, and 2 mM EDTA. The labeling chamber contained this same composition with the addition of an optimal 3 µg/mL anti-CD3-HRPx antibody. After all processing solutions were loaded, the cassette was ready for sample loading.

Clinical Utility of the Automated CD4 Enumeration Assay and Statistical Analysis

All thirty de-identified clinical samples were collected from the Vanderbilt clinical cytometry center and transferred to be handled in BSLII facilities at Vanderbilt University in accordance with correct BSLII safety practices. Samples were collected as part of clinical validations of the One-touch automated CD4 enumeration cassette with venous

blood collected in EDTA-coated tubes. The researcher was blinded for this study. Test results and demographic data from each patient were collected by a third party and entered into the Vanderbilt StarBright database. At a rate of 5 specimens per day, a total of 30 specimens were processed. From each specimen, 300 µL of whole blood was transferred into a micro centrifuge tube that was prepared with 20 µL of magnetic beads and 45 µL of Transfix. This sample was placed on a rotisserie for a 5 min mixing step, magnetic beads were separated employing a magnetic stand and the beads were resuspended in 100 µL of wash buffer in preparation to be loaded into a preconstructed CD4 enumeration assay cassette. The cassette was then mounted on the one-touch instrument containing a polished aluminum cartridge containing three assay channels. Triplicates were performed for each of the samples on the instrument to evaluate intra-assay variability on the automated system. Only once all samples were processed, the medical resource numbers were correlated to the CD4 count generated by the clinical flow cytometry core. Results were expressed as mean and standard deviation from each set of technical replicates (n=3). Graphpad Prism 5.0b was used to perform statistical analysis. A receiver operator curve was also prepared with a 500 cells/µL threshold.

NAAT Cassettes: Malaria PCR and TB Isothermal Cassette Development

Malaria PCR Assay Cassette Development

Materials: Primers, probes, and malaria reference standard templates were purchased from Integrated DNA Technologies. SuperScript III RT/Platinum TAQ mix (Cat# 11732-088) and Dynabeads MyOne Silane magnetic beads (Cat# 37002D) were purchased from Life Technologies. Quanta PerfectA 2x mastermix was purchased from VWR

(Quanta Biosciences, Cat# 84010). EvaGreen™ was purchased from Biotium (Cat# 31000) Dye Filtration swabs (Cat# 5001.02) were purchased from Salimetrics Inc. Fluorinated ethylene propylene (FEP) tubing was purchased from McMaster Carr (Cat# 2129T11 and # 9369T46). Hemato-Seal tube sealing compound (Cat# 02-678) was purchased from Fisher Scientific. All other materials and reagents were purchased from Sigma Aldrich or Fisher Scientific. EvaGreen™ Dye fluorescence (Cat# 31000) was purchased from Biotium (CA, USA).

Malaria Sample Composition and PCR Assay Run

Plasmodium falciparum (malaria parasite) infected sample panels were prepared and provided by PATH for final instrument evaluation. *Plasmodium falciparum* D6 parasite cultured in our laboratory was used for assay cassette optimization. The *Plasmodium falciparum* 18S rRNA gene extracted from the PATH panel samples was quantified by qPCR according to protocols adapted from PATH.[187] Primers, probe, and amplified gene sequence are provided in **Table 6.1**. DNA from malaria parasite was amplified via qPCR using Quanta PerfectA 2x mastermix in 25 µL reaction volumes. Final primer concentration was 400 nM for each primer and the final EvaGreen concentration was 800 nM. For quantification, each reaction was performed in parallel with a standard curve prepared by serially diluting synthetic DNA amplicons in TE buffer. The sequence of the amplified gene was purchased from Integrated DNA Technologies (IDT). Ten-fold dilutions for the standard curve were prepared from 10^7 copies/µL to 10 copies/µL. No template controls were also performed with no DNA added. Thermal cycling was performed using the Roche LightCycler 96, and cycle threshold (Ct) values were calculated using the provided software.

Table 6.1: Primer and probe sequences for PCR of extracted *P. falciparum* DNA. The probe is only used for off-line PCR after manual on roller-based device extraction, as the in-tube PCR uses EvaGreen dye for detection.

Forward Primer	5' – ACA TGG CTA TGA CGG GTA ACG – 3'
Reverse Primer	5' – TGC CTT CCT TAG ATG TGG TAG CTA – 3'
Probe	5' – FAM-TCA GGC TCC CTC TCC GGA ATC GA-BHQ1 – 3'
Biomarker Template	5' – ACA TGG CTA TGA CGG GTA ACG GGG AAT TAG AGT TCG ATT CCG GAG AGG GAG CCT GAG AAA TAG CTA CCA CAT CTA AGG AAG GCA – 3'

PCR Cassette Tube Construction and Sample Preparation

The PCR cassettes were prepared in a 43 cm length of 2.36 mm i.d. FEP tubing. PCR cassettes were loaded by pipetting the following solutions: 50 µL of PCR reaction mixture (**Table 6.2**), 300 µL 70% ethanol, and 300 µL PCR chaotropic wash buffer (80% ethanol, 640 mM guanidine thiocyanate, 1.6 mM Tris pH 8.0, 160 µM EDTA, 0.08% Triton X-100). Please see **Figure 6.10A** for a schematic of each of the NAAT assay cassettes. Processing solutions were loaded in reverse order so that the processing solutions did not come in contact with the mineral oil or PCR reaction mixture. First the ethanol solution was loaded into the upstream end of the tubing, then the chaotropic wash buffer was pipetted into the tube moving the ethanol solution down the tube. Each solution was separated from the next by a ~6 mm air valve.

Table 6.2: Components of the in-tube PCR reaction and their concentrations.

Component	**Volume per 50 µL reaction**	**Final Concentration**
5X KAPA2G Buffer	10 µL	1X
MgCl2 (25 mM)	3 µL	1.5 mM
dNTP mix (10 mM each)	1 µL	200 µM
Forward primer (10 µM)	2 µL	400 nM
Reverse primer (10 µM)	2 µL	400 nM
KAPA2G polymerase (5 units/µL)	0.5 µL	2.5 units/reaction
EvaGreen (20 mM)	2 µL	800 µM
PCR grade water	29.5 µL	-

For sample preparation, 100 µL sample of malaria parasite-infected human blood culture (5% hematocrit) or pooled whole blood spiked with synthetic DNA was combined

with 300 µL lysis buffer (4 M guanidine thiocyanate, 10 mM Tris HCl pH 8.0, 1 mM EDTA, 0.5% Triton X-100) and incubated at room temperature for 10 minutes to lyse red blood cells. The lysed samples were then filtered using one-fourth of a Salimetrics swab (Cat# 5001.02), and the sample was expressed from the swab by using a 5-mL plastic syringe. After the addition of 100 µL of 100% isopropanol and 7.8 x 10^8 silica-coated magnetic beads (25 µL suspension) to the filtered sample, it was incubated for 3 minutes at room temperature. Following nucleic acid adsorption, the tube contents were pipetted into the end of the preloaded tubing proceeded by the addition of 20 µL of mineral oil and 50 µL of PCR solution to the downstream end of the tube without an air valve between. The loading end (upstream) was then sealed with clay sealing compound and the opposite side with a polystyrene screw.

Malaria PCR Cassette Parameters and Thermocycling

By monitoring the temperature of the witness tube, the temperature of the fluid in the assay tube was estimated for temperature feedback and control purposes without having to directly access the fluid in the assay tube. The motor drove the axle, moving magnetic beads through the array of solutions within the tubing, depositing the beads in the PCR solution and pulling them back out after a short elution time. Once the extraction portion of the assay was complete, the instrument began PCR thermocycling. The Peltier device heated the solutions until the witness tube registered 95 °C, and then switched off and allowed the witness tube and assay tube to cool down to 56 °C, when it began heating again. This was repeated for 45 cycles, or the operator could stop the reaction early. At the end of each cycle, when the witness tube temperature read 56 °C,

the Qiagen fluorescence detector read the EvaGreen fluorescence, enabling detection of nucleic acid.

Isothermal LAMP TB Assay Cassette Development

Materials: Semi-clear Blue 0.093"ID, 1/8" OD, 0.016" Wall FEP Tubing (Cat# 9369T24) was purchased from McMaster-Carr. All other reagents were purchased from Sigma Aldrich or Fisher Scientific. LAMP primers were designed using PrimerExplorer v4. All primer sequences were procured from IDT. Optigene Master Mix, containing GspM2.0 polymerase, was purchased from OptiGene (United Kingdom). SYTO-9 was replaced by 0.1 μM SYTO-82 (Life Technologies, NY)

Surrogate TB Sample preparation

In a 2 mL microcentrifuge tube, 500 μL chemically inactivated TB-infected synthetic sputum sample was combined with 500 μL TB lysis/binding buffer (4 M GuSCN, 25 mM sodium citrate, 4.9% Triton X-100, 0.2% sodium dodecyl sulfate, pH 7.0) and 6.0 x 10^8 silica-coated magnetic beads (20 μL suspension). Samples were vortexed for 10 minutes on a Fisher Vortex Genie 2 set to speed 4 to lyse the bacterial cells and capture released nucleic acids.

Preparation of Sample and Cassette Construction

The pre-loaded processing solutions tube must be loaded in reverse order so that the ethanol solution is pushed down the length of the tube but never comes into contact with the mineral oil or isothermal reagents. It was essential that the ethanol (Chamber 4), which inhibits nucleic acid amplification, did not come into contact with the oil or the isothermal reagents. In order to push the solutions down the length of the tube both ends of the tube must be unplugged. First, a 70-cm length of 2.36 mm I.D. FEP

tubing was prepared. Into the upstream end of the tubing, 300 µL 70% ethanol was then pipetted into the tube (precipitate/rinse chamber 2). Leaving an air valve approximately 6mm in length, 100 µL 80% ethanol, 5 mM potassium phosphate, pH 8.0 (precipitation chamber 1) was then pipetted into the upstream end of the tubing. Again, leaving an air valve approximately 6mm in length, 300 µL LAMP chaotropic wash (4 M guanidine hydrochloride, 25 mM sodium citrate, pH 7.0) was then pipetted into the upstream end of the tubing.

Following the 10-min mixing cycle needed for TB DNA biomarker IS6110 adsorption, the magnetic beads and sample contents were pipetted into the upstream end of the preloaded tubing (note that the tube is still uncapped at both ends to allow for the solutions to move). To the downstream end of the tubing, 20µL of PCR grade mineral oil was loaded following the air valve adjacent to the ethanol chamber. The final chamber composed of 50µL of previously prepared isothermal amplification LAMP solution (30uL Optigene Master Mix (GspM2.0), 25µL Syto-82 (2mM), 1µL each primer (**Table 6.3**)) was then pipette into the downstream end of the tubing so that the LAMP amplification solution was in direct contact with the oil and there was no air in between the two solutions. The downstream end was then sealed first using a # 4-40 polypropylene (or polystyrene) screw wrapped with Teflon tape that came into contact with the isothermal amplification solution. Finally, the upstream end of the tubing was sealed using clay sealant.

Table 6.3: Primers for isothermal LAMP amplification of the IS6110 sequence of TB

TB – LAMP	F3	TGATCCGGCCACAGCC
	B3	TCGTGGAAGCGACCCG
	FIP	GCTACCCACAGCCGGTTAGGTGTCCCGCCGATCTCGT
	BIP	TCACCTATGTGTCGACCTGGGCGCCCAGGATCCTGCGA
	Probe	FAM-TCGCCTACGTGGCCTTT-MGBQ
	Temp/Cycles	65°C / 41 cycles

Results and Discussion

While there are a few reports describing instruments that perform sample processing or analysis, little work has been done to combine sample processing and analysis in one simple instrument.[188,189] The diagnostic landscape is crowded with expensive instruments that rely heavily on user-processing.[180] Our approach to developing a high performance diagnostic system at a low cost per assay was to develop an instrument designed to interfaced with multiple interchangeable, disposable assay cassettes. Decoupling the autonomous one-touch instrument function from individual assay cassettes allowed for the cassette waste to be retained within a disposable unit. More importantly, it enabled integration of more sophisticated device components, such as an optical detector, as reusing components for every assay spreads out the capital cost over the lifetime of the instrument. Our open one-touch platform automates both sample processing and detection for a variety of biomarker classes with the press of a single button. This strategy, along with most of the reported automated systems, employs magnetic beads to capture targets and move them from one solution to another for processing and analysis.[190,191] Magnetic beads are commercially available with diverse surface chemistry making then an ideal solid support for extending the assay menu.

Modular Instrument Components:

To enable the parallel development and optimization of prototype instruments and different self-contained assay cassettes, several breadboard instruments were built with the subsystems needed for each assay type. However, all breadboard instruments consisted of a set of common integral components: an axel-driven motion control

system, an assay cartridge wheel, a fixed magnet, an on-board optical detector, and a computer to drive the motion and optical detection programs (**Figure 6.4**). A thermal control system was installed on NAAT instruments to enable thermal cycling and temperature control. This system consisted of heating/cooling element that made thermal contact with a copper sleeve, which interfaced with both the NAAT detection chamber and a "witness tube." The witness tube was a small length of tubing with the necessary solutions to mimic the detection chamber. By monitoring the temperature of a thermocouple within the witness tube, the temperature of the fluid in the assay tube could be estimated and controlled without having to directly access the fluid in the assay tube. Automated thermal control was adjusted based on target and primer sequence specifications.

The central component to the one-touch instrument was the cartridge wheel. It provided the channels for universal cassette mounting and secure individual assay cassettes in place during processing. The movement of the cartridge was controlled by an axel-driven stepper motor. This motor provided clockwise and counterclockwise motions at various speeds, which were tailored to meet the needs of each assay. The magnet was encased in a spring-loaded plastic holder to maintain constant pressure between the magnet and the assay cassette mounted on the cartridge. The motion-controlled cartridge and fixed magnet worked in concert to process each assay

cassette. A limitation to magnetic bead-based sample processing exists in their tendency to aggregate in complex matrixes when continually subjected to a magnetic field. Therefore, the axle driven one-touch instrument was designed to attain a rotational movement adjacent to a fixed magnet so that magnetic beads could be moved in and out of the magnetic field when desired. To offer flexibility during assay cassette development, two different bead movement programs were developed.

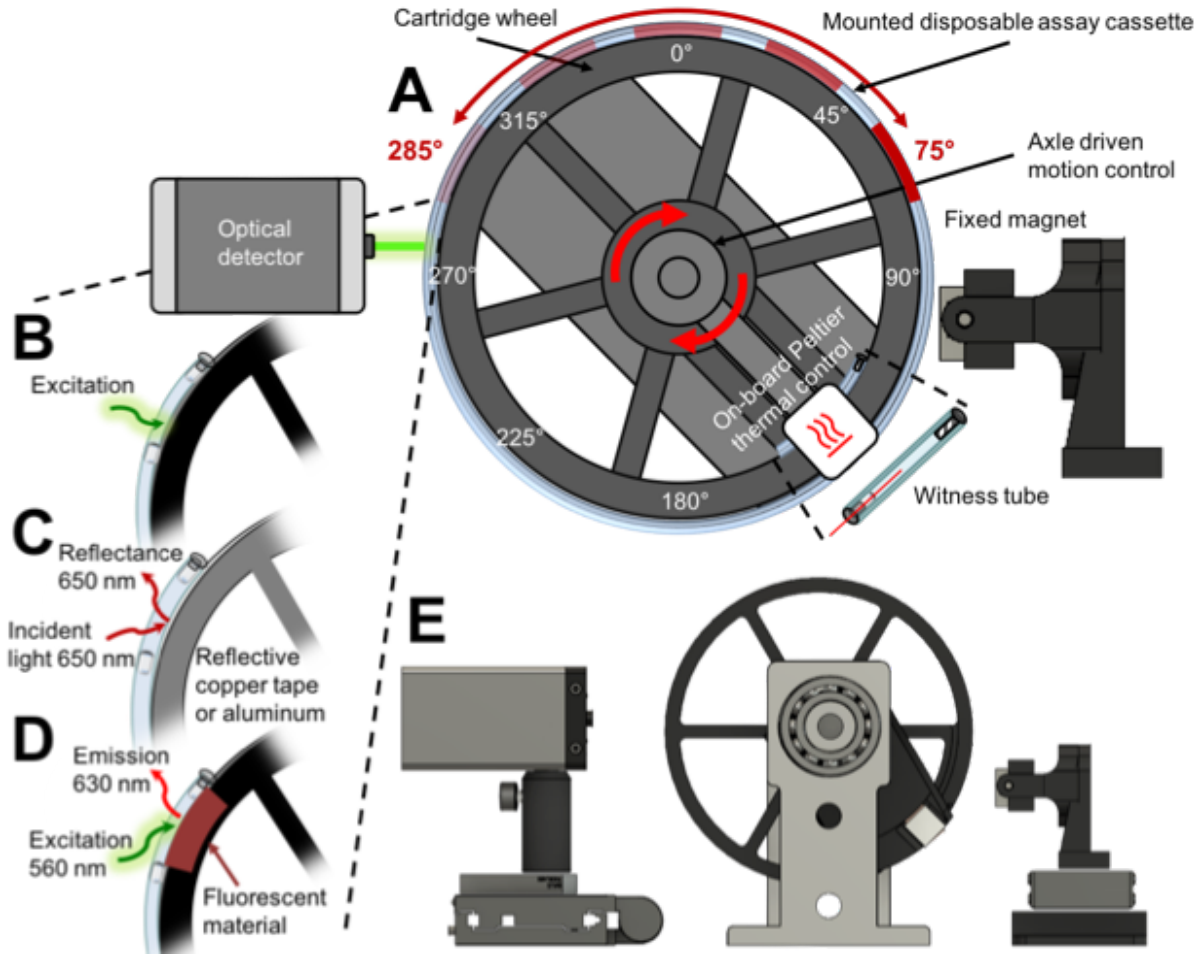

Figure 6.4: Device subcomponents highlighting the different optical detection strategies. **A)** A visual representation of the "windshield wiper" mixing motion where a processing chamber, represented in red, is moved back and forth between the 285° and 75° cartridge positions. **B)** Traditional fluorometer where an optical detector excites at a narrow band wavelength and measures fluorescence. **C)** A reflectance absorbance geometry where an incident light reflected from lustrous cartridge backing back to a separate detector. **D)** Hybrid optical detection scheme that allows a fluorometer to also generate a "calculated absorbance" measurement. **E)** A schematic showing the general instrument configuration.

One of the movement mechanisms was programmed so that the motor performed three fast cartridge revolutions minus 5º with respect to its initial position. Then it would slowly advance 10º per extraction cycle resulting in a net 5º advancement per extraction cycle. Rapid revolutions overcame the magnetic force of the fixed magnet leaving all magnetic beads in the processing chamber while slow movements collected the magnetic beads and advance them. The second mixing program developed emulated a “windshield wiper” like mixing motion. This program offered the ability to mix for a set time within a chamber. Once magnetically escorted into a processing chamber, the cartridge would quickly rotate the central portion of the chamber past the fixed magnet and to the 285º cartridge wheel position retaining the beads within the chamber (**Figure 6.4A**). The wiping mixing motion presumed by then rotating slowly back and forth between the 75º and 285º positions with a 3s pause in between each wipe. This pause allowed for the particles to fall to the opposite end of the chamber in a motion closely mimicking rotisserie-style mixing. Following the customized mixing time, the cartridge wheel would circle back around to the fixed magnet to slowly traverse beads through the STV to the next processing chamber. Once completing the programmed cycle in the final reaction chamber, the assay cartridge was rotated to move the beads out of the final chamber. To demonstrate both of these programmed motions, the NAAT assay cassettes adopted the net 5º advancement motion and the absorbance-based cassettes adopted the “windshield wiper” motion.

The initial and final programmed movements for all assays positioned the assay cassette’s detection chamber in alignment with the on-board detector for reference and final external optical measurement, respectively. Several different optical detection

methods were surveyed during the development of the device. Conventional fluorescence detection was implemented on the breadboard instrument for NAAT cassettes to be able to detect amplified DNA with an intercalating dye (**Figure 6.4B**). Absorbance detection was used for detection of colorimetric substrate responses in protein detection, and cell counting assays. A broad-spectrum LED and spectrometer were mounted in a geometry so that the angled incident light would radiate from the LED through the transparent cassette tubing and detection chamber solution to a lustrous material backing on the cartridge, where it would then be reflected back to the spectrometer (**Figure 6.4C**). Copper and polished aluminum were examined as potential reflective backings.

A third optical detection strategy was investigated as a way to converge these two optical detection strategies, allowing a single fluorometer to capture both optical signals (**Figure 6.4D**). Opposed to traditional transmittance-absorbance readings, a plastic fluorescence standard stationed inside the cartridge channel can be excited to emit wavelength paired with the absorbance band of the fluid substrate in the detection chamber. Positioning the cassette's detection chamber adjacent to the fluorescent standard affords the ability of using the fluorescent detector's narrow band excitation wavelength to excite the fluorescent standard and measure the emitted photons transmitted from the standard through the detection chamber. The intensity of the emitted photons was measured by the detector and when comparing the final measurement to the reference measurement, a calculated absorbance measurement could be acquired (**Equation 6.1**). The general instrument geometry for this combined absorbance and fluorescent detection method is depicted in **Figure 6.4E**.

All movement, heating, and optical detector operation was coordinated in programs within MatLAB and controlled employing a portable computer. Each individual assay cassette had its own specific multi-level program on the command panel. After selecting the appropriate program, the assay was initiated by pressing the “one-touch-go” button on the digital user interface. To enable multiple cassettes to be processed in unison, a multi-channel cartridge wheel and motorized optical stage were also evaluated. This additional feature afforded the ability of a single detector to travel back and forth between assay cassettes mounted within different cartridge channels.

Assay Cassette Development

The lack of high impact diagnostic assays that can be performed at low-infrastructure sites, which serve the majority of the global population, has been a critical factor in the continued devastation of infectious disease.[22] Specifically, there is an urgent need to make protein detection, cell counting, and NAAT assays accessible.[183] However, in their current form, these tests cannot be sustainably performed outside of well-equipped laboratories. The availability of this menu of assays is crucial to implementing successful global health initiatives because it allows healthcare workers to evaluate patients’ organ function, detect the presence of disease biomarkers, monitor disease progression, identify drug resistant pathogens, and surveil emerging infectious threats.[179] To demonstrate the flexibility of the assay cassette platform, we developed five different cassettes that encompass the aforementioned index of assays. Although each individual assay cassette requires a specific set of processing solutions, five general magnetically bead-assisted steps exists in each assay cassette: (1) biomarker capture, (2) wash, (3) label, (4) signal amplification, and (5) detection. The sequential

solution processing of the self-contained assay format lends itself to the translation of most traditional 96-well plate assays. With minor adjustments, established 96-well plate style assays can be adapted to generate magnetic bead enabled tube-based cassettes. Moreover, the optically transparent tube allows the signal generated in the detection chamber (fluorescent or colorimetric) to be measured externally without the need to transfer the chamber contents. A typical assay cassette contains 4-6 preloaded processing chambers with each chamber consisting of approximately 100 µL of solution prepared in a sterile environment.

This section outlines the development and optimization of four proof-of-concept assay cassettes including a *Plasmodium falciparum* Histidine-Rich Protein II (HRPII) protein detection cassette, a CD4 T-cell enumeration assay for cell counting, and two NAAT assays: a PCR-based malaria assay and an isothermal-based LAMP TB assay. Although the premise of this platform was to eliminate as many user steps as possible, there was still a need to perform 3-5 simple sample preparation steps per disposable cassette. Sample preparation steps consisted of reagent addition to primary samples, large volume mixing followed by magnetic bead collection, filtration and sample loading. Following these off-line steps, the sealed cassettes could be mounted on the one-touch instrument in the proper position and initiated on the user interface. The automation of sample processing and detection not only alleviates laborious assay steps but also was expected to increase the reproducibility of each assay.[192]

Protein Detection Assay Cassette—Plasmodium falciparum Histidine-Rich Protein II

Protein antigens are some of the most commonly evaluated biomarkers for pathogen detection, evaluating disease progression, and monitoring responses to

treatment. The most common type of method for detecting proteins in a complex biological sample is through ELISA. As part of the menu of assays needed in low-resource settings, we designed an on-bead ELISA assay cassette aimed at detecting HRPII. HRPII is a protein that is produced and secreted during the entire lifecycle of the *Plasmodium falciparum* malaria parasite, the most prevalent and deadly malaria species in sub-Saharan Africa.[40] It is often used as a diagnostic and prognostic marker for *falciparum* malaria and was therefore selected to serve as a model protein in the development of a proof-of-concept antibody-based protein detection cassette. This strategy could be adapted to different proteins or other classes of biomarkers that have established antibody pairs used in ELISA.

This assay cassette was based on a sandwich ELISA format (**Figure 6.5A**), where a capture antibody immobilized on the magnetic solid support binds the HRPII, and an enzyme-conjugated detection antibody binds completing the on-bead HRPII "sandwich." In high infrastructure health facilities, ELISAs are recognized as the gold standard laboratory technique for quantitative and qualitative protein detection. However, in their conventional plate-based form, they can require 5-8 hrs and many user steps to complete.[193] In contrast to the traditional microplate ELISA methods, magnetic bead-based assays are advantageous because they overcome mass transport limitations, by providing active mixing within the sample, reducing assay time.[35,194] Therefore, the adaption of a traditional ELISA to an automated magnetic bead-based cassette alleviates both the lengthy time requirement and the user steps necessary for signal detection.

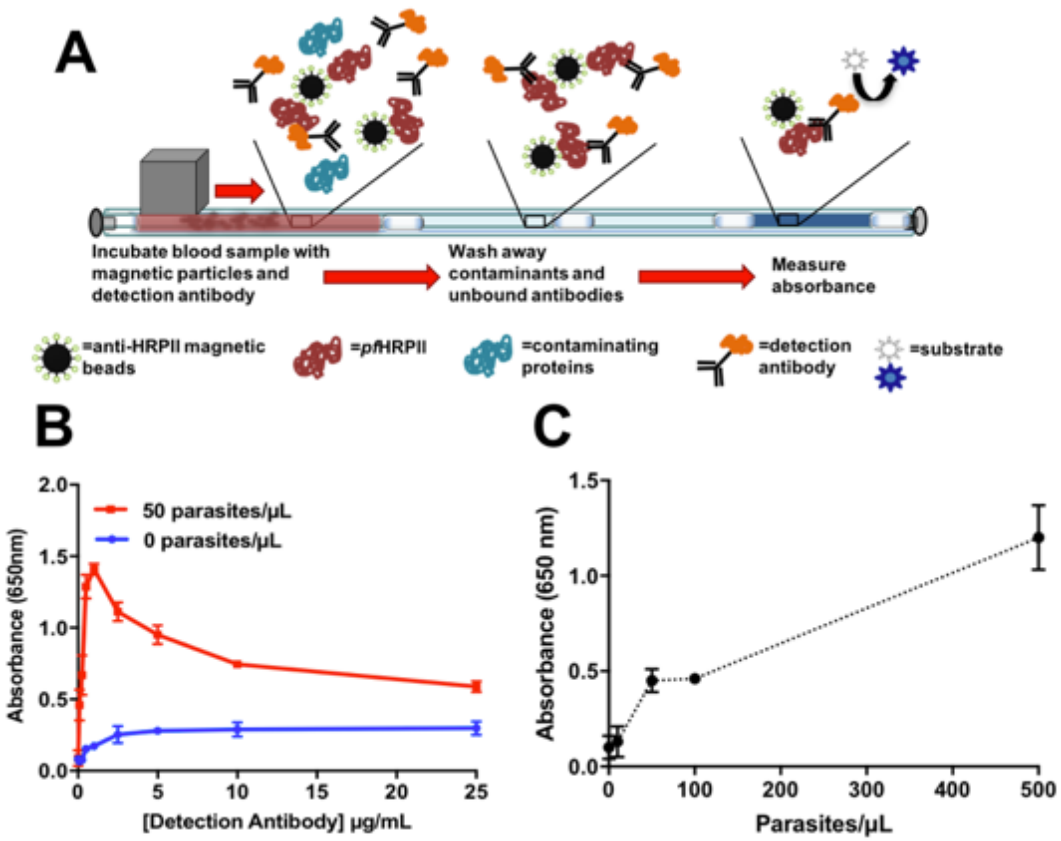

Figure 6.5: Protein detection cassette optimization. **A)** The HRPII cassette operation scheme. **B)** The all-in-one reagent optimization where number of beads was fixed while detection antibody was increased. **C)** A dose-response curve for the automated HRPII detection cassette.

In the development of the protein detection cassette, the critical assay features were magnetic bead type and the concentration of detection antibody in the all-in-one reaction chamber. Previously, we have reported the ability to extract and purify HRPII from complex matrixes employing Ni(II)NTA magnetic beads.[38,39,195] This was our initial bead selection for the HRPII assay, but due to high observed background signal and long incubation times needed for >90% capture, antibody-functionalized streptavidin magnetic beads were used instead. This platform presented another clear advantage in being able to adapt this capture strategy to other targets simply by altering the biotinylated antibody during bead functionalization. After 1 min, ~100% of the HRPII

from the sample was captured employing the anti-HRPII magnetic bead compared to 30 min needed for the Ni(II)NTA particles (data not shown).

The concentration of the anti-HRPII detection antibody, the volume of beads added, and the incubation time were investigated outside of the cassette in an attempt to optimize background signal. In a 50 parasite/μL sample, maximum signal was achieved at 1 μg/mL detection antibody (**Figure 6.5B**). Beyond this concentration, a reduction in signal was observed and is hypothesized to be a result of the hook effect, when HRPII molecules become saturated by detection antibody and are unable to bind the bead surface.[196] Upon varying the volume of functionalized magnetic beads with the optimal 1 μg/mL detection antibody, signal began to saturate at 10 μL of beads. Given these results, 1 μg/mL detection antibody and 10 μL beads were selected as optimal parameters for the HRPII protein detection cassette. It was also determined that a 10-min sample and detection chamber incubation time was ideal in signal to noise comparisons (data not shown). All of these parameters were entered into the command panel for a one-touch device delegated for protein detection. Using the protein detection program, which employed the “windshield wiper” mixing motion described above, a preliminary experiment was performed with samples spiked with parasite and a HRPII dose-response was observed (**Figure 6.5C**). A concentration-dependent response within a clinically relevant antigen range was observed. This assay cassette design is expected to have utility in detecting other protein biomarkers as well as other biomarker classes, such as carbohydrates. All that is required is an established orthogonal molecular recognition element pair and re-optimization of assay parameters.

Cell Counting Assay Cassette—CD4 T-Cell Enumeration

An absorbance-based CD4 T-cell enumeration cassette was developed to serve as a proof-of-concept cell counting assay cassette. Measurement of CD4 T cells is crucial in the case management of Human Immunodeficiency Virus (HIV), particularly in determining the eligibility for, and treatment response to, antiretroviral therapy (ART). The HIV epidemic has become one of the world's most serious health and treatment challenges, and the World Health Organization (WHO) estimates that a majority of the 36.7 million individuals infected with HIV live in low-resource regions.[197] HIV targets and destroys CD4 T cells, impairing the subsequent development of effective immune responses. In an untreated course of HIV infection, the number of CD4 T cells decline and eventually the immune system's regenerative capacity is overwhelmed, breaks down, and opportunistic diseases overrun. Upon effective treatment with ART, however, the concentration of CD4 T cells per microliter of peripheral blood (CD4 count) rebounds and is preserved.[198] Therefore, CD4 count is used as a proxy to monitor immune system health, disease progression, and efficacy of ART. Additionally, new WHO guidelines advise initiating ART treatment at CD4 count of <500.[199] In order to be successful, ART management relies on frequent and consistent assessment of CD4 count. A number of technologies are available for CD4 enumeration ranging in complexity, operating equipment, and overall cost.[47]

The need for reliable low-resource CD4 T-cell counting led to the development of the CD4 T cell enumeration cassette (**Figure 6.6A**). The cassette assay functions by employing anti-CD4 magnetic beads to capture cells expressing CD4 proteins from peripheral blood samples. Inside the cassette, the magnetic beads then carry captured

CD4+ cells into a labeling chamber consisting of an anti-CD3 detection antibody. This orthogonal labeling strategy extorts the unique CD4+CD3+ expression profile on CD4 T cells and removes the need to deplete confounding CD4+ monocytes, decreasing time to result.[200,201] To validate that CD3 protein was a suitable marker for assay signal production, the differences in CD3 expression density on patient samples were analyzed. On the CD4 T cells of six patients, a 10.5% coefficient of variance (%CV) was observed via quantitative flow cytometry (**Figure 6.7**). This variance is thought to be caused by physiological differences in CD4 T cells between donors.[202]

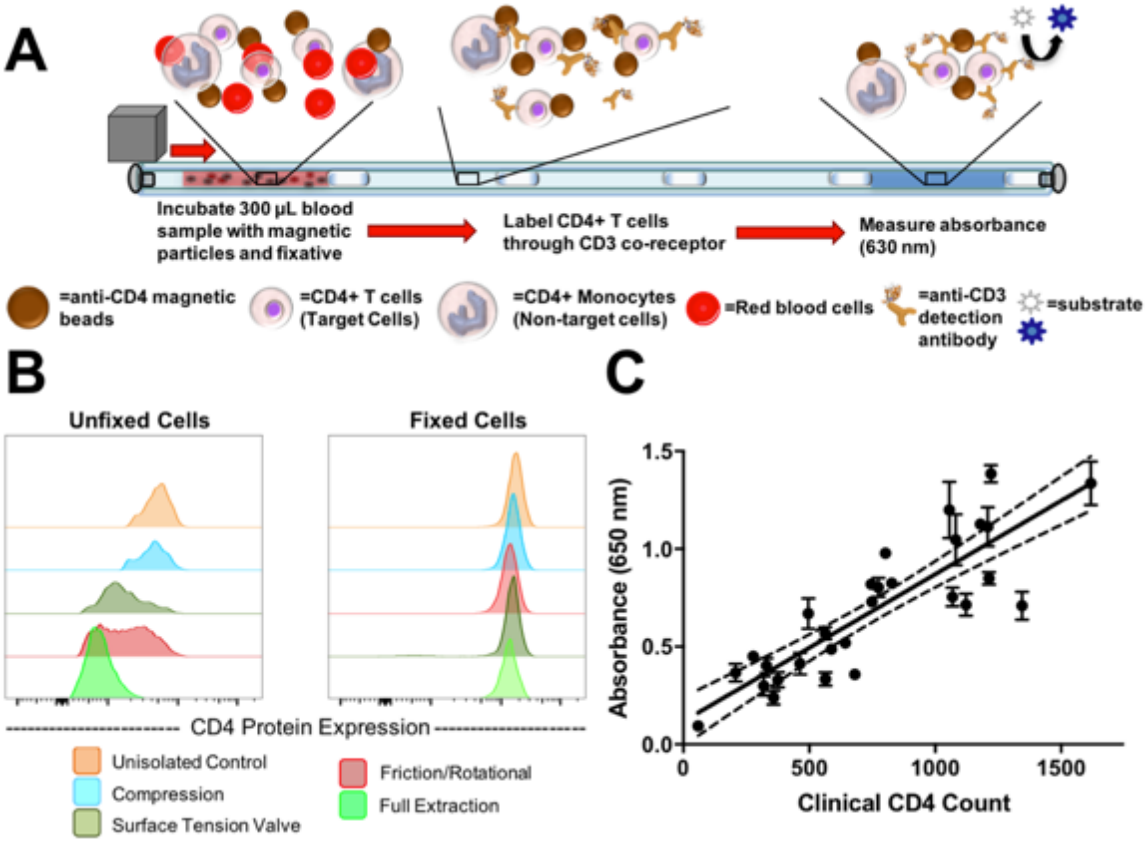

Figure 6.6: Design and optimization of the CD4 cell enumeration cassette. **A)** The CD4 T-cell enumeration scheme. **B)** Histogram plots of the CD4 protein expression on CD4+CD3+ unfixed (left) and fixed (right) cell subsets following extraction force simulations. **C)** Correlation graph comparing clinical CD4 count measurements to the average absorbance values (n=3) generated from 30 HIV+ patients on the one-touch instrument.

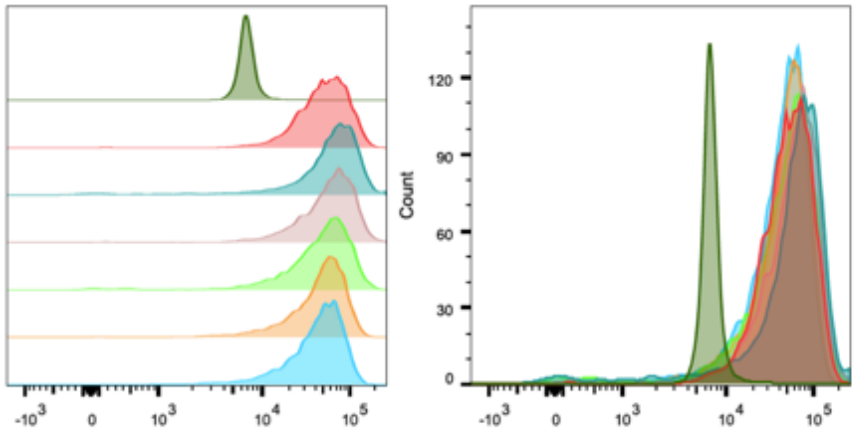

Flow Cytometry Sample	Geometric Mean Flu.
Bead Reference	7400
CD4+CD3+ Donor 1	48544
CD4+CD3+ Donor 2	47017
CD4+CD3+ Donor 3	53195
CD4+CD3+ Donor 4	40477
CD4+CD3+ Donor 5	42607
CD4+CD3+ Donor 6	39775

Average

45,269 ± 5,231

Figure 6.7: CD3 antigen density on CD4+ T cells from 6 different healthy donors. A fluorescent standard (reference bead) was employed to calibrate the flow cytometer before each sample collection (dark green). The left graph shows offset histograms and the right graph shows complete overlay of CD3 density on CD4+ T cells of different donors. The table below is a compilation of the geometric mean fluorescence for each donor after 5,000 CD4+CD3+ events were collected.

The critical assay features found in adapting whole cell magnetic bead-based extraction and enumeration into a self-contained cassette were the need for cell fixation and the employment of biocompatible FEP tubing. This is the first report that successfully combines cell fixation and magnetic-bead based extraction of CD4 T cells. If a fixative is not used in the tube-based assay, the bead-cell mass aggregates after traversing through the first chamber, impairing downstream detection. A force simulation was performed to evaluate how the different forces intrinsic to the extraction cassette impact the CD4 expression of the target cells (**Figure 6.6B**). The reduced CD4 expression observed on the target cells following a full extraction is potentially due to a combination of mechanical forces and a dynamic cellular response leading to down regulation of CD4 proteins. The employment of a fixative mitigates these phenomena,

conserving target surface marker expression, and providing a robust cell specimen for processing and enumerating. Several fixation strategies were explored but Transfix was found to be the optimal fixative (data not shown). The optimized CD4 extraction and enumeration cassette resulted in a purity of 70.0%, compared to 39.1% for conventional based separation, and 93.4 ± 2.8% capture of the CD4+CD3+ target cells (**Figure 6.8A-C**).

To evaluate the performance of the semi-quantitative CD4 enumeration assay cassette, HIV+ clinical specimens were employed. The automation of the CD4 enumeration cassette was performed on a breadboard instrument containing a cartridge wheel machined from aluminum containing three assay cassette channels for mounting and processing assays in triplicate. Additionally, a movable optical stage was also incorporated to enable a single detector to travel between each assay during initial and final optical measurements. All other common one-touch modular components remained the same. A picture of this iteration of the one-touch instrument is provided for reference (**Figure 6.8D**). Clinical HIV+ specimens were analyzed on this one-touch instrument using the CD4 enumeration cassette. The results of the 30 samples analyzed showed a good linear correlation (**Figure 6.6C)**. As a measure of precision, intra-assay variability was evaluated on the triplicate reading of each specimen, resulting in an average coefficient of variation of 8.2%. Additionally, employing the WHO 2013 threshold guideline for ART initiation of 500 cells/μL, a receiver operator curve (ROC) was composed.[203] This dichotomous threshold yields excellent accuracy in discriminating between those patients below and above the 500 cells/μL cutoff determined by an area under the curve of measurement of 0.93 (**Figure 6.9**).

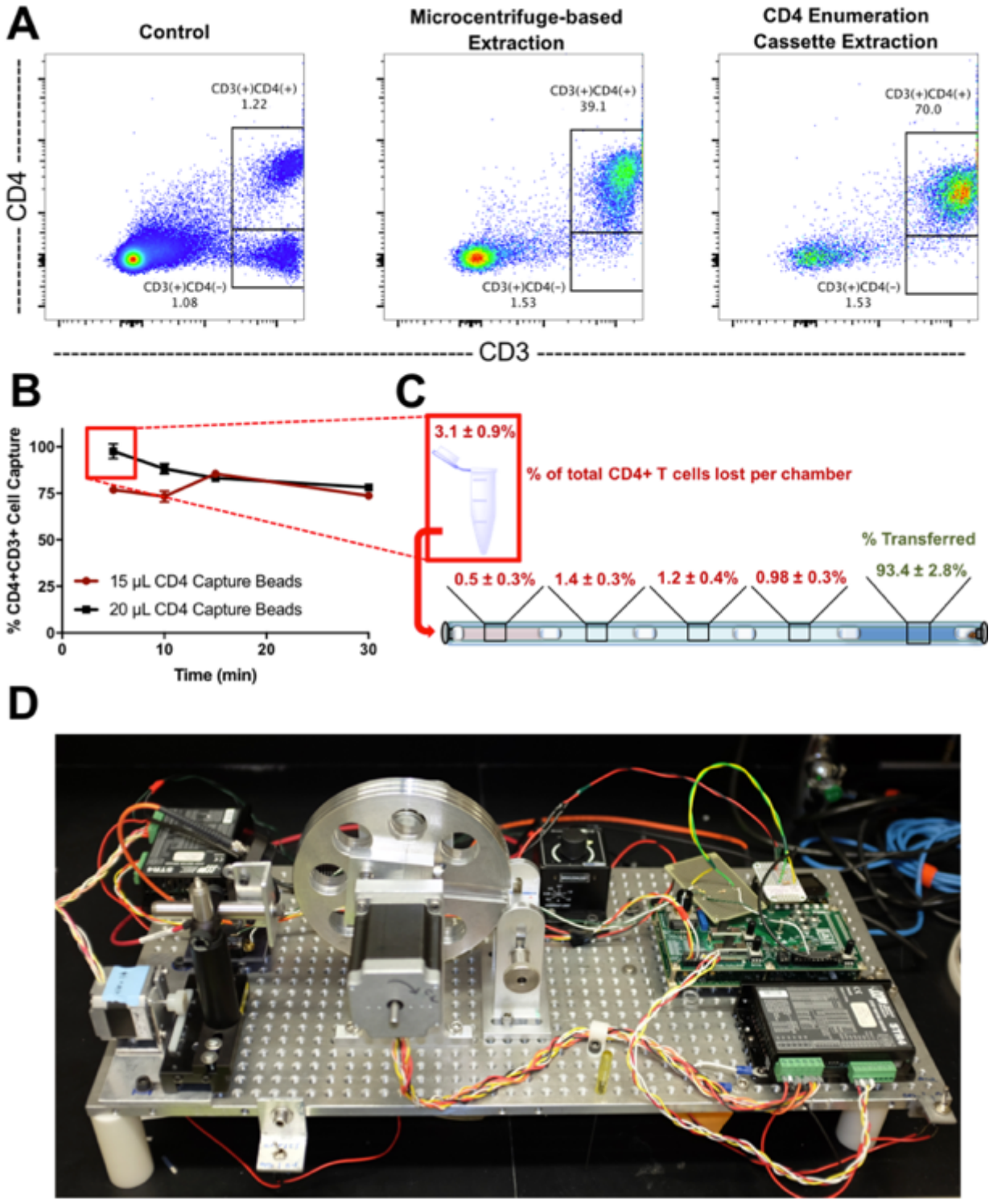

Figure 6.8: CD4 T cell enumeration cassette performance data. A) Pseudo color dot plots with CD4 protein expression on the y-axis and CD3 Protein expression on the x-axis where the target cell population and the sample purity is provided in the top right quadrant. B) Bead volume optimization experiment and C) the transfer efficiency of CD4+CD3+ target cells into the detection chamber employing an indirect cell counting method. D) A visual representation of the one-touch instrument used to optimize and validate the CD4+ T cell enumeration cassette.

Misclassified samples tended to be downward misclassifications leading to ART prescription earlier than necessary, which is preferred over under-treatment.[1] These results indicate that this assay cassette has utility in generating semi-quantitative CD4 counts for HIV-management programs.

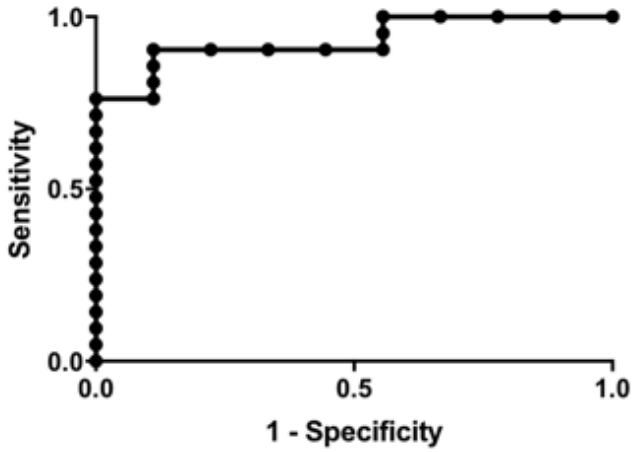

Figure 6.9: CD4 T cell enumeration cassette receiver operator curve. Employing the WHO recommended 500 CD4+ T cell/μL dichotomous cutoff for the initiation of ART treatment, 30 patient samples with clinical CD4 count attached were analyzed on the one-touch instrument.

Nucleic Acid Testing Cassettes—Malaria Polymerase Chain Reaction (PCR) and TB Loop Mediated Isothermal Amplification (LAMP) Cassettes

Because of its specificity and versatility, DNA is commonly used as a biomarker for the detection of human pathogens. NAATs can be used to identify pathogens as well as investigate drug resistant genes. DNA is also a practical biomarker because it is relatively stable at room temperature, provided that processing solutions are not contaminated with DNase. However, DNA sequences are often present at much lower concentrations than other biomarkers in patient samples, so a target amplification step

is often needed before the DNA biomarker can be detected. To date, the most reliable DNA amplification method is PCR, which requires expensive equipment and reagents as well as extensively-trained technicians to perform. These requirements are the largest barriers to the ubiquitous use of DNA as a biomarker in low-resource settings. Newer NAAT technologies such as LAMP, an isothermal amplification technique, have gained considerable attention for use in resource-poor settings.[204,205] To evaluate the utility of both of these NAAT forms on the one-touch platform, a PCR-based malaria cassette was developed and an already optimized LAMP-based TB cassette was employed to detect malaria and TB specific DNA sequences, respectively.[186]

Silica-based extraction techniques are frequently used to capture and purify all nucleic acids in a sample. Both self-contained NAAT cassettes were designed to transport silica-functionalized magnetic beads through a series of processing solutions into a thermally controlled detection chamber, where target DNA would be released and amplified (**Figure 6.10A**). Our laboratory has previously used magnetic beads to isolate nucleic acids from sample matrices such as urine, synthetic sputum, blood, and nasal swabs.[184-186,206] Therefore, the main optimization for this assay cassette concerned the in-line PCR reaction.

The critical assay factors identified for in-line PCR thermocycling were the prevention of PCR reaction mixture evaporation within the tubing and to ensure no air bubbles were introduced to the PCR chamber. The DNA extraction portion of the cassette separates chambers with STVs, or short volumes of air, but applying heat to the PCR chamber caused the reaction mixture to evaporate and then condense in the air valve nearest to the chamber. Additionally, air bubbles introduced to the PCR

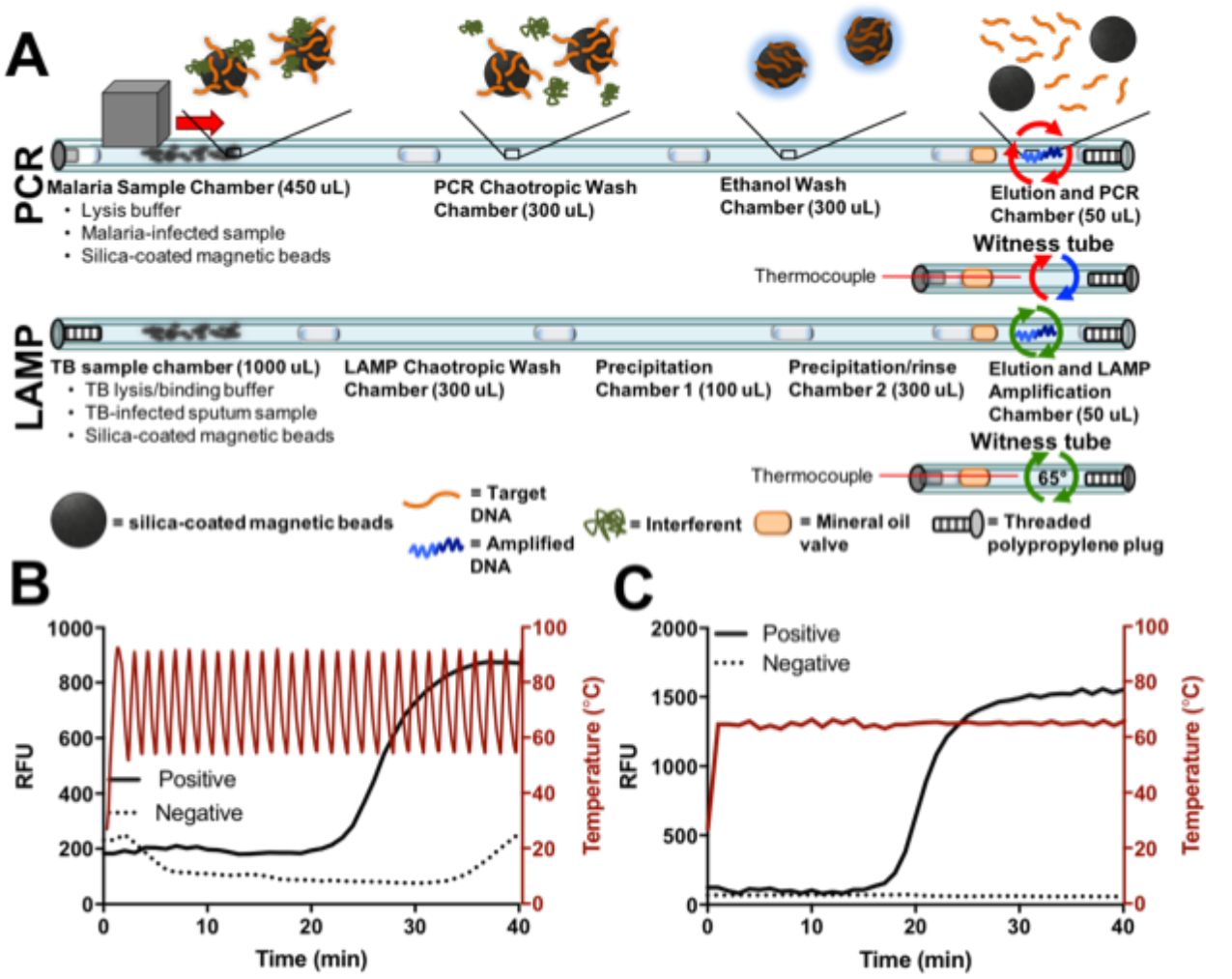

Figure 6.10: Design and operation of thermally regulated NAAT cassettes. **A)** The PCR-based and LAMP-based cassette schemes. **B)** Whole blood samples spiked with (positive) and without (negative) malarial DNA that were processed independently with the PCR-based malaria cassette. Included is the temperature readings within the witness tube during thermocycling. **C)** Synthetic sputum samples processed spiked with and without TB DNA. Included is the temperature readings within the witness tube during isothermal heating at 65º C.

chamber expanded when heated, which intermittently interfered with the PCR reaction and optics. To avoid these problems, the PCR reaction mixture was separated from the air valve by mineral oil, and the end of the tubing was sealed with a polypropylene screw directly behind the PCR chamber. Great care was also taken to eliminate air bubbles when pipetting the PCR mixture into the tubing.

The PCR chamber reaction temperature was monitored employing a “witness tube,” or short piece of tubing containing PCR mixture and mineral oil mounted beside

the assay tubing on the instrument. This tube allowed for temperature monitoring without needing to directly access the detection chamber of the cassette. By design, thermocycling would proceed by heating until the witness tube reached 95ºC, then passive cooling was used to bring the reaction temperature down to 56ºC. Modern PCR instruments hold these reaction temperatures for a set amount of time, typically 30 to 60 seconds, but in an effort to decrease assay time, a KAPA2G fast polymerase was used to reduce cycling hold times to 1 s. The average time to result for this assay was 85 min, including benchtop preparation. By comparison, a typical column-based DNA extraction requires roughly 30 min, and the same PCR assay in a LightCycler 96 required roughly 30 min to set up and 108 min to run, for a total time to result of 168 min. This is roughly twice the time it takes to achieve the same result with our one-touch device. The critical assay conditions for the LAMP-based cassette were previously determined.[186]

Each of the NAAT cassettes was demonstrated on the one-touch instrument using positive and negative surrogate patient samples (**Figure 6.10B-C**). In each case, fluorescent responses were observed for positive sample sets while negative sample sets did not provide a measurable fluorescent output within the optimized isothermal and thermocycling time thresholds. The temperature recorded within the witness tube was also plotted to show the precision that the on-board thermal control system provides when executing each NAAT cassette.

Integration

Dedication to simplicity and cost strongly influenced the final design of the integrated prototype instrument. TPP-driven tradeoffs governed instrument ease-of-use

specifications and assay parameters such as time-to-result, and cost. Before integration, assay cassettes were optimized on dedicated breadboard instruments. The development of a widely integrated one-touch instrument allowed for a single instrument to autonomously run all assay cassettes. The integrated prototype instrument featured a touchscreen display, which provides the user with a simple graphical interface for cassette selection and viewing test results. When the user selected the desired cassette, only the necessary instrument components would be activated. The graphical interface displayed the incoming data and ran simple analytics (Fourier transformations; first derivatives) to generate test results. The software could also save the collected results to a text file, which could be uploaded to the cloud, or emailed to a third party for off-site analysis. An image of the final prototype instrument is presented in **Figure 6.11A**.

Within a controlled laboratory setting, a performance evaluation was conducted as part of a feasibility assessment aimed at determining the detection limits for the menu of four disposable cassettes. As part of the Bill and Melinda Gates's Grand Challenge initiative, the Program for Appropriate Technology in Health (PATH) developed standardized sets of patient surrogate samples for malaria and TB. These panels were used as the validation specimens for both of the NAAT cassettes as well as the HRPII protein detection cassette. However, there was no standardized CD4 T-cell panel so internal surrogate samples were produced. Each assay cassette was run independently, requiring both manual sample preparation and one-touch automation (**Figure 6.11B**). The total time-to-result for protein detection, cell counting, PCR-based NAAT, and LAMP-based NAAT cassettes was 34 min, 36 min, 85 min, and 65 min,

respectively. The performance evaluation for each cassette included a wide range of target biomarker concentrations. The protein detection cassette detected the malaria biomarker, HRPII, with a calculated limit of detection of 1.2 parasites/μL (**Figure 6.11C**). The cell counting assay provided a limit of detection of 111 CD4 T cells/μL with a concentration dependent response up to 1,500 CD4 T cells/μL (**Figure 6.11D**). The PCR-based NAAT detected a medium malarial DNA PATH sample (1% parasitemia) within 54 min of instrument processing time (**Figure 6.11E**). The LAMP-based NAAT cassette differentiated a negative control from a low PATH sample with 45 min of instrument processing time (**Figure 6.11F**).

All design, prototyping, and assessment was accomplished in a high-capacity laboratory with trained personnel. The next step in development is field studies that will be performed to validate the performance characteristics in the intended settings of use. Field studies will establish the route for product introduction and user-driven design modifications. The one-touch system provides a platform for delivering a more sophisticated set of diagnostic capabilities to primary health centers, while also providing an apparatus geared for use by minimally trained operators.

An instrument must be inexpensive and simple to maintain to be sustainable in a low-resource field setting, so we have designed this one-touch device with cost in mind. We have maximized the extent to which expensive sub-systems, like the optical and thermal control systems, are shared between the assays. As configured, the system cost is about $15,000. The material cost of the disposable assay cassettes, based on low volume estimates, is approximately: $5 per protein assay, $5.13 per cell enumeration assay, $4.14 per isothermal assay, and $4.90 per PCR assay.

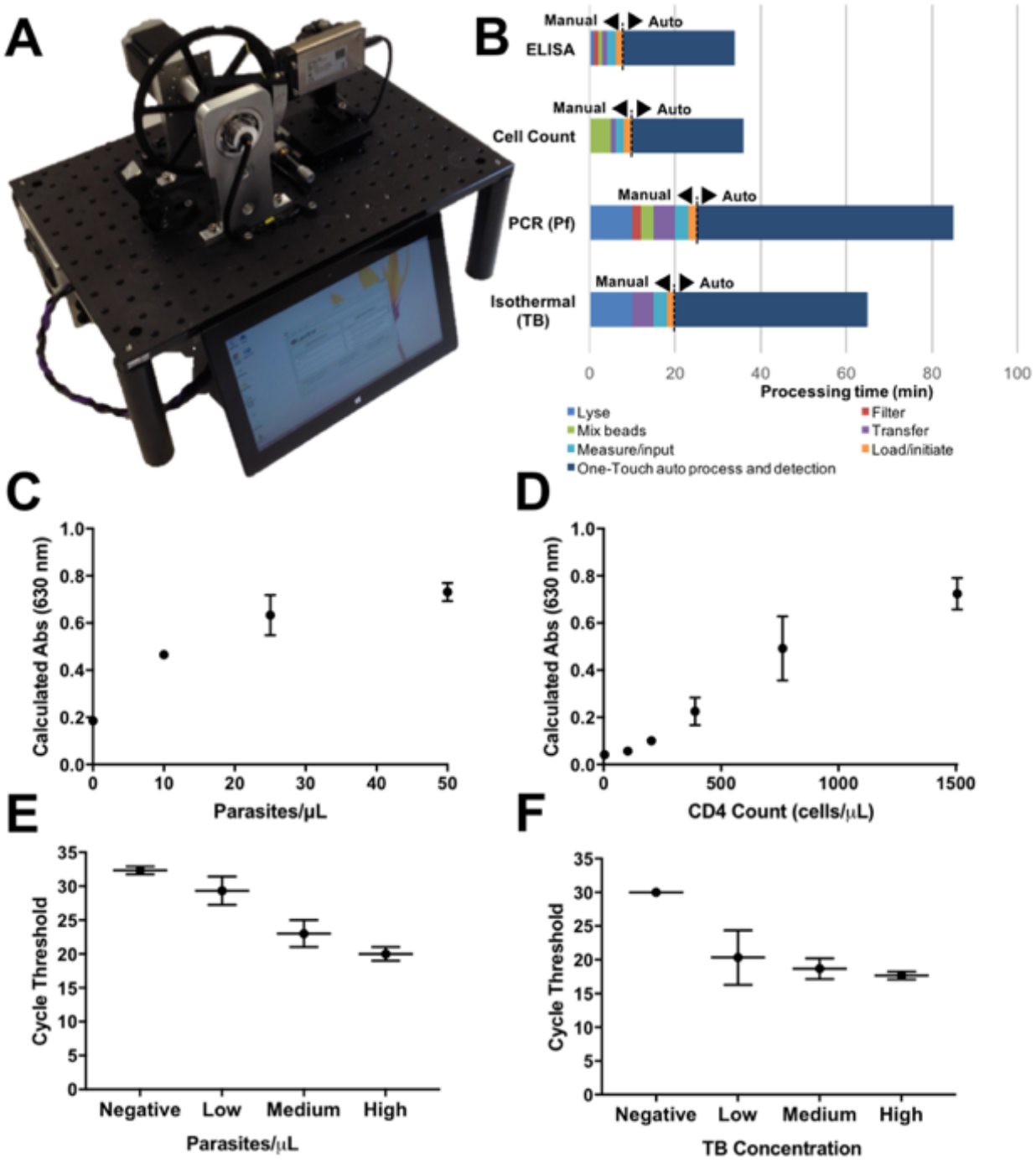

Figure 6.11: Cassette assay performance assessment of the integrated one-touch system. A) Visual depiction of the integrated one-touch device. B) Time requirements for each assay cassette. Dose response curves provided for C) parasite spiked whole blood samples and D) peripheral blood primary samples employing the HRPII protein detection and CD4 T-cell enumeration cassettes, respectively. Negative, low, medium, and high DNA panel sample provided by path for malaria and TB that were analyzed by the malaria E) PCR-based and F) TB LAMP-based NAAT cassettes, respectively.

However, each of the instrument components and assay cassettes were designed for being manufactured at scale. With increased volume, each of these cost estimates is expected to decrease substantially.

In its current form, several limitations to the one-touch platform exist. Several of the assay cassettes contain reagents that require preservation within a cold chain, like enzymes and detection substrates. We are in the process of converting theses chambers into dry reagents that can be rehydrated upon the use of blister packs on-site. This would also alleviate any STV instability issues during shipping or due to day-to-day heat fluctuations. The current prototype is also reliant on a direct power source but is being modified to contain an on-board battery. Lastly, we are developing a system of quality control measures that include positive and negative assay control cassettes. The future operators of this device will require some level of training to perform basic sample preparation and to run the one-touch instrument, but the user interface was designed to be as simple as possible. With further improvements and a training plan, a universal diagnostic system such as this could revolutionize how diagnostics are performed at level 1 healthcare facilities.

Conclusion

Timely medical diagnostics are crucial for successful treatment, management, and control of infectious diseases. But access to high-impact diagnostic tests is often limited in low-resource areas. To meet this need, we designed a “one-touch” instrument designed to interface with interchangeable self-contained assay cassettes that were developed to detect several biomarker classes. Proof-of-concept diagnostic assay cassettes were generated for protein detection, cell counting, and NAAT to deliver a

strong menu of assays to primary healthcare facilities. On the open one-touch platform, each assay cassette can be analyzed interchangeably by selecting the program on the graphical user interface, without the need to alter the one-touch instrument in any way. The instrument is able to return results that inform diagnosis and treatment decisions with the press of a single button. The completion of a feasibility assessment study demonstrated the successful analysis of all cassettes. The one-touch system was constructed with technologies that are simple and lend themselves to mass production, providing a diagnostic platform that is now ready for field studies.

Acknowledgements

The authors would like to thank the Bill and Melinda Gates foundation for their financial support under the Gates Grand Challenge funding mechanism, PATH for suppling panels of samples to validate the NAAT cassettes, Bruce Greig (MT(ASCP), CCy) and Jill Albright from the Vanderbilt Medical Center Hematopathology Laboratory for suppling the de-identified HIV+ clinical specimens, VICTR funding for reagents needed to optimized the CD4 T-cell enumeration cassette (VR14113), The project was supported by CTSA award No. **VR14113 (**P.I. Westley Bauer**)** from the National Center for Advancing Translational Sciences. Its contents are solely the responsibility of the authors and do not necessarily represent the official views of the National Center for Advancing Translational Sciences or the National Institutes of Health

CHAPTER VII

Perspective

Summary and Future Outlook

Most diagnostic laboratory testing throughout the world occurs in centralized reference laboratories. However, the majority of the global population does not have access to these tertiary healthcare facilities. Point-of-care (PoC) testing is the most promising avenue to deliver diagnostics to at-risk populations. PoC testing typically refers to the performance of a diagnostic test outside of a traditional diagnostic laboratory—typically near the site of a patient or in a primary healthcare facility. Over the past few decades, the PoC diagnostic field has been driven by the feverish demand for technologies to detect the infectious diseases of poverty (IDoP). This demand has resulted in two major approaches to PoC test development: 1) instrument-free diagnostics and 2) open diagnostic systems that can execute sophisticated assays on a single, common platform. These dichotomous approaches provide diagnostic testing for different use-case scenarios, as instrument-free diagnostics are fit for primary healthcare facilities, while the more complex systems require more resources and are thus targeted for facilities beyond primary levels. This dissertation encompasses work on the enhancement of equipment-free diagnostics as well as in the development of a novel high-performance open diagnostic platform.

Specifically, my work employed these approaches to improve diagnosis of the "*big three*" IDoP—malaria, HIV-AIDS, and tuberculosis (TB). First, the developed

sample preparation tools improved the sensitivity of malaria tests to enable commercial tests to detect an estimated 95% of the infectious reservoir. Second, a next-generation urine-based TB lateral flow assay (LFA) was developed using microvirin (MVN) on the LFA test line to differentiate between variants of the lipoarabinomannan (LAM) biomarker. The discrimination between the LAM variants improved test specificity compared to the commercially available TB LAM ag LFA. Finally, in collaboration with biomedical engineers, we developed a high-performance, “open” diagnostic system and a menu of assays, which has the potential to deliver complex diagnostic tests to secondary healthcare facilities.

I would be remiss if I did not emphasize the importance of magnetic beads in my dissertation work and their future potential. The use of magnetic beads as a solid support to capture a biomarker within complex matrices has several advantages, including faster assay kinetics and the reduction of matrix effects due to facile separation and washing steps. Using magnetic beads, biomarkers can be specifically isolated, purified, and concentrated by simple magnetic actuation. For these reasons, magnetic beads are amendable to low-resource settings and can practically replace the need for classical centrifugation or chromatographic separation techniques. Yet, their most valuable feature is that their surface functionality can be easily tailored to capture almost any biomarker. The successful application of magnetic particles in this work, as well as in other emerging technologies, demonstrates the promise of this technology. However, improvements, particularly with regard to the number of user steps, are still needed to fully align these technologies with the ASSURED criteria to make them truly applicable at the point of care.

The rational development of PoC diagnostic tools and systems must begin with a thorough understanding of the user requirements in the intended setting. Given the wide range of laboratory infrastructure in the 3 levels of healthcare facilities, it is unlikely that a single technology will serve as the silver bullet. Thus, it is critically important to develop both equipment-free and open-system platforms in parallel. In collaboration with the Macha research trust (Zambia, Africa), our research team has traveled to Zambia to field-test technologies developed in our laboratory. Field deployment is critical for identifying technological weaknesses and developing user-centric design principles that impact how end-users perceive new technologies. A cyclic optimization and design process was instituted so that we could return to our high-infrastructure laboratory at Vanderbilt, make augmentations, and deploy back to the field. Although technological weaknesses can be identified and addressed in the laboratory rather quickly, functioning parameters such as “too many steps” are more nuanced and difficult to assess. The general trend conveyed to the PoC diagnostic field is that with every additional assay step, there becomes a greater chance that the end user will incorrectly perform the assay. Through our iterative optimization and design process, we concluded that the mBEADS sample preparation process described within had too many user steps.

Leveraging the chemistries developed and used for multiplex biomarker enrichment in **Chapters II-IV**, we generated an alternative design concept that combined these elements into a single equipment-free device coined, “the origami RDT.” The origami RDT employed the same principles at the mBEADS system but reduced the user steps needed to three (**Figure 7.1**). This was accomplished by

removing multiple pipetting steps, the need for magnetic beads, and active mixing. As part of the Bill and Melinda Gates Grand Challenges Initiatives, we submitted a proposal based on the origami RDT and were awarded $100,000 to investigate the feasibility of this device design. Initial findings show promise for this type of design and work to make this technology a reality is ongoing.

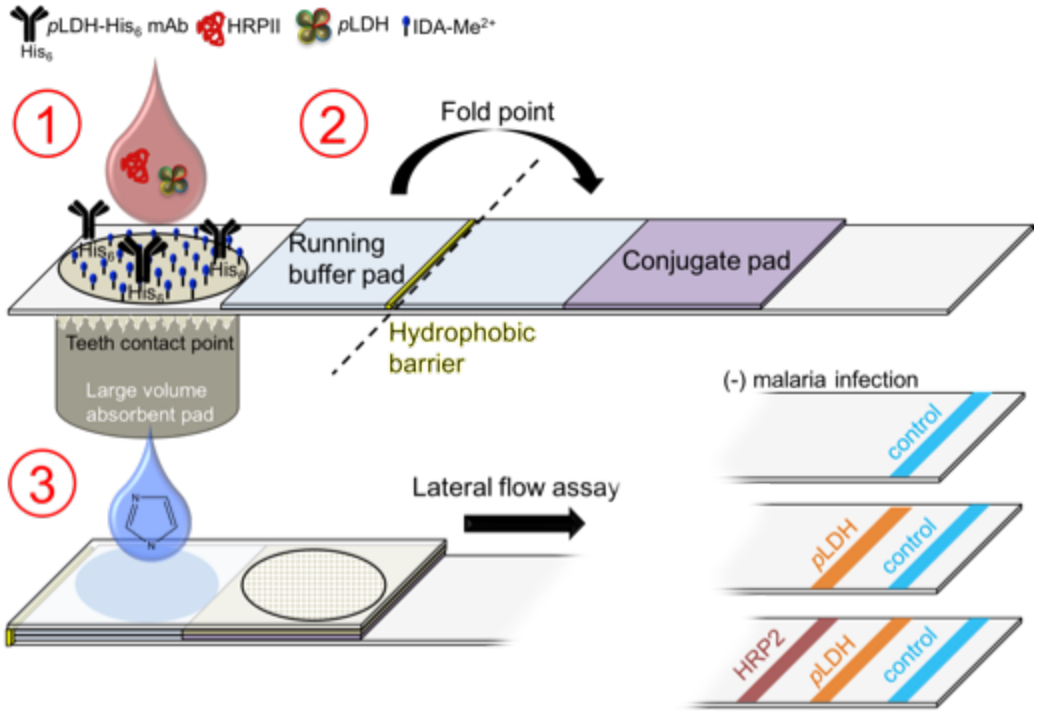

Figure 7.1: The design concept for the origami RDT. 1) First, large volumes are passed through an affinity bed tailored to biomarkers of interest employing vertical flow. 2) Next, the RDT is folded to detach from the vertical flow portion and interface with the lateral flow portion of the assay. 3) Last, imidazole-containing running buffer would be added to release target biomarkers from the affinity bed for downstream detection on the lateral flow assay.

This relationship underlines the import roles that academic groups and nonprofit organization have in the development of low-resource diagnostic technologies. The fundamental technologies behind most low-resource diagnostics were developed and spun out of academic laboratories that were initially funded by non-profit organizations like the Bill and Melinda foundation. This pipeline is a departure from conventional in-vitro assay development, where products are targeted for use in high-capacity

laboratories to maximize profits. Industrial companies do not frequently enter the low-resource diagnostic space due to the rational fear of minimal return on investment. Therefore, it is incumbent upon academic institutions and global health-focused nonprofit organizations to develop fundamental tools and technologies to “de-risk” entrance into this space.

Only with continued and constant research efforts will we be able to develop the PoC technologies needed to disrupt the vicious cycle of infectious disease and poverty. Government-funded programs provide another type of funding mechanism that enables academic institutions to perform research in this space. In the United States, the National Institute of Health (NIH) is one of the primary medical research supporters. These types of research initiatives are essential to serve our humanitarian duty and also to protect the health and safety of Americans. Diseases know no borders, and PoC diagnostics are critical to detecting and managing forthcoming pandemics at their point of origin so that their impact can be minimized.

Of the *big three* IDoP, the fight against malaria has provided a model for disease elimination campaigns. Malaria is one of the biggest public health successes of the 21st century as the number of deaths due to malaria has declined by almost 50% between 2000 and 2015. With the support of global health initiatives, tools and treatments have be developed that prevent and cure malaria; but in recent years, global investments have plateaued and progress has stalled. If we can build and maintain an unwavering commitment to combat infectious diseases, fights against malaria are ones that we can win.

As a person that was born into a fortunate position (opportunistic demographic within an affluent country), I believe that it is my duty to help those that are less fortunate—a duty that I have tried to fulfill throughout my graduate career. During the last 5.5 years, I have developed new methods and systems that improve the diagnosis of diseases that are pervasive in impoverished populations. The stories in this dissertation are the distillation of research that is considered to have "worked." However, countless hours were spent generating ideas and carrying out experiments that ultimately "failed." These disappointing results will never be printed in a manuscript but have guided projects and made me the persistent scientist that I am today. Cheers to all my failed experiments.

APPENDIX A

Illustrations of Future Concepts and Designs

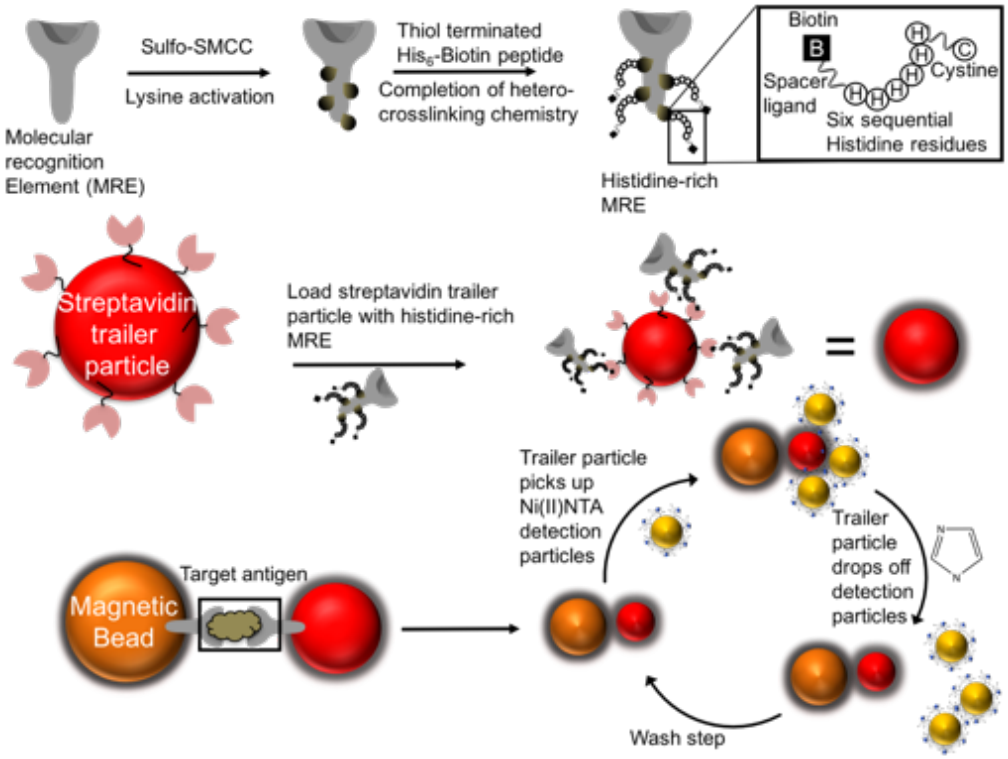

Cyclic linear capture and release amplification strategy.

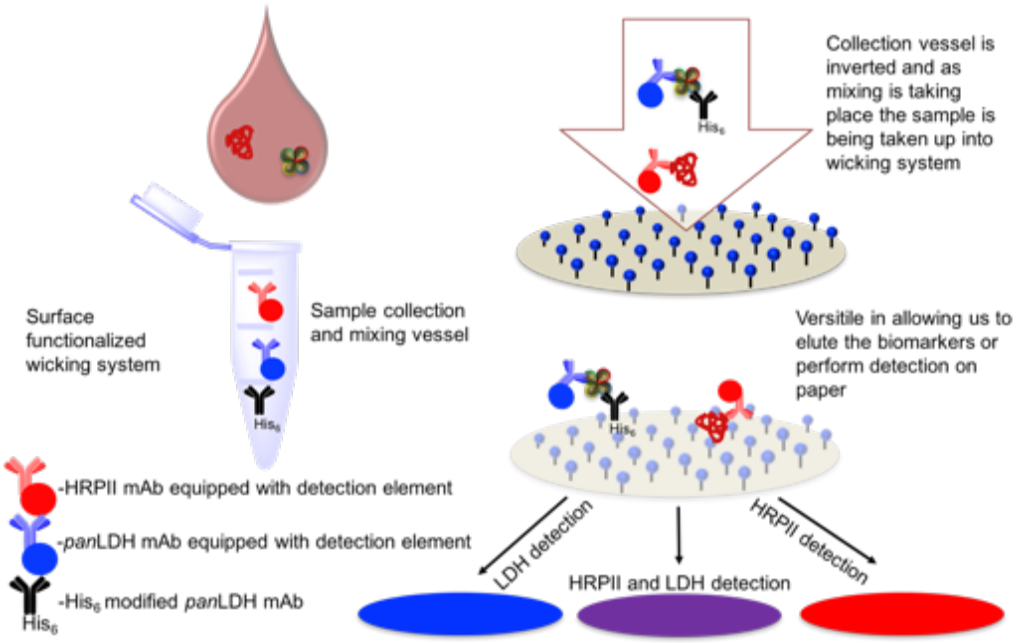

Multiplex flow through device concept with visual readout.

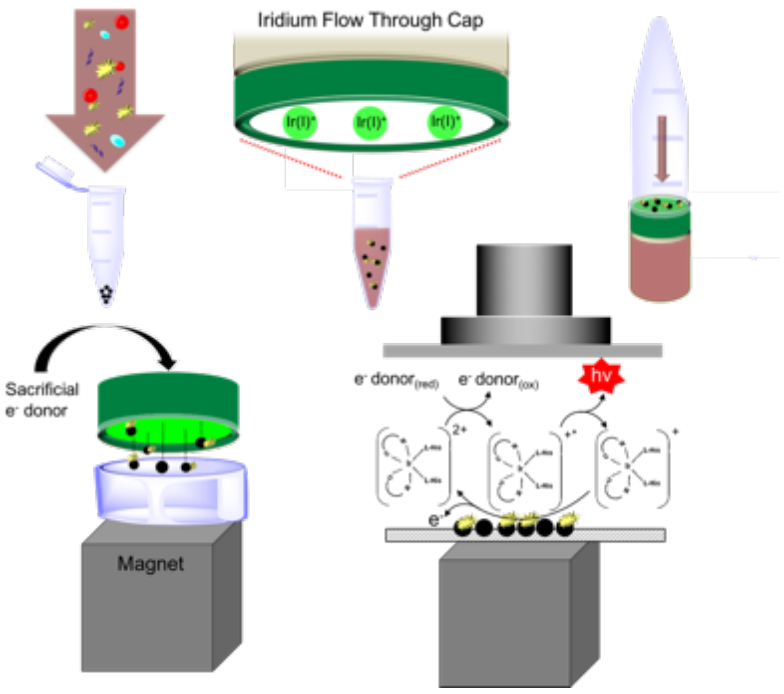

Rapid capture, concentration, and detection of HRPII from blood employing an Iridium flow through cap and electrochemiciluminescence (ECL).

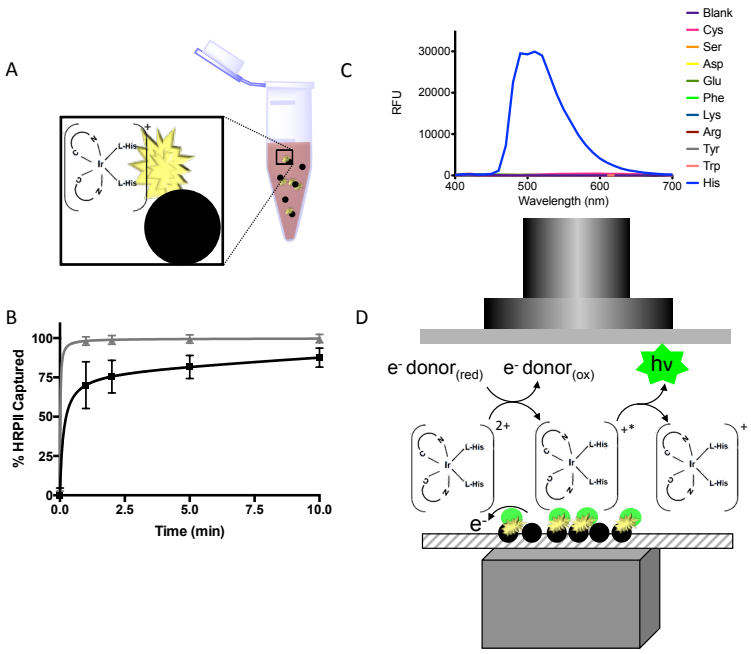

Feasibility of HRPII-Ir-ECL detection strategy (A) HRP2 captured by Zn(II)NTA magnetic bead and labeled with Ir1. (B) Time course and capture yield of Zn(II)NTA magnetic beads vs. traditional Ni(II) NTA beads. (C) Spectra for **Ir(1)** reacted with various amino acids highlighting the specificity for histidine. (**D**) ECL cell for the detection of HRPII.

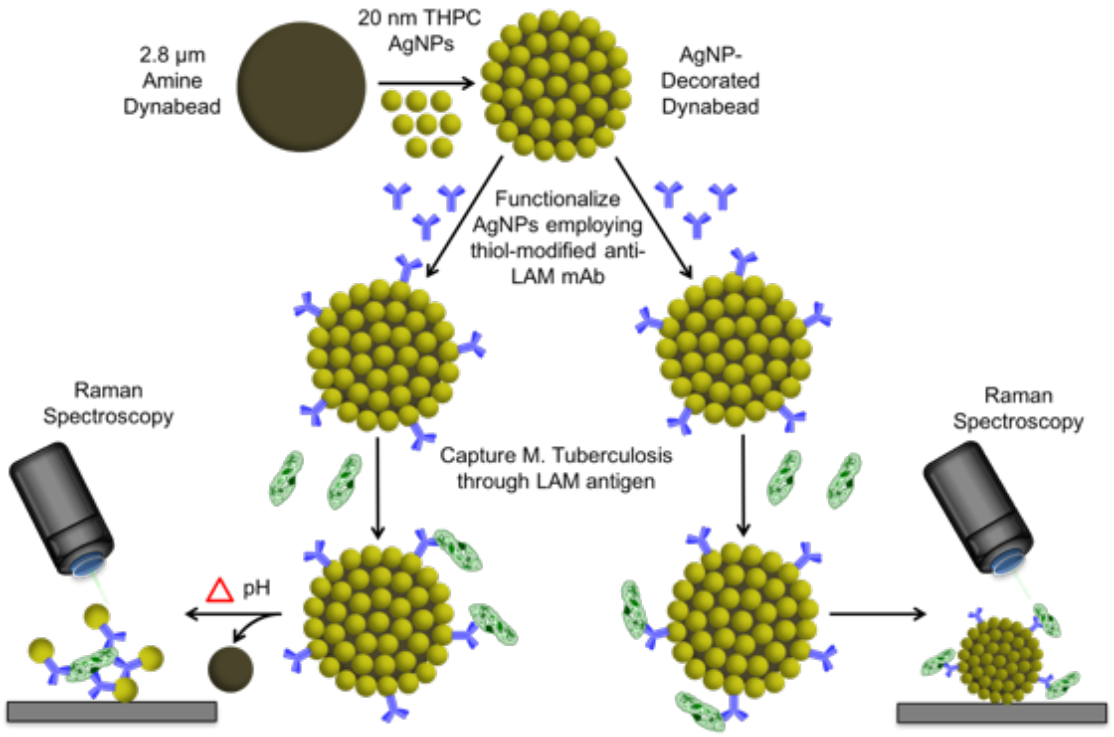

Capture and release of M. tuberculosis for TB detection employing gold plated Dynabeads and surface enhanced raman spectroscopy (SERS).

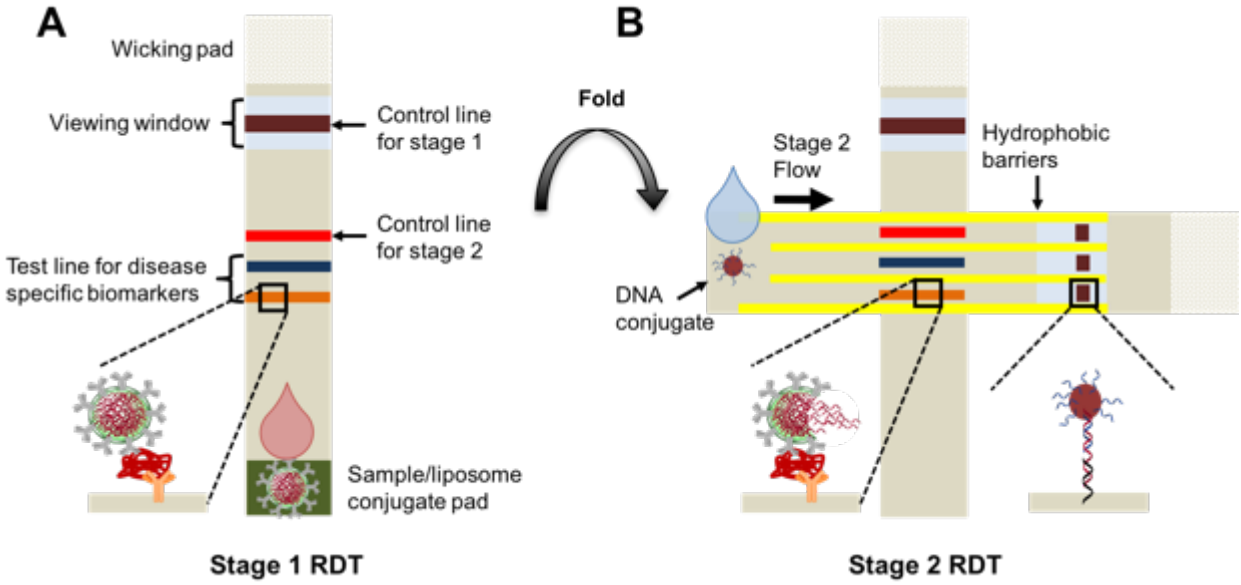

Using DNA-encapsulating liposomes conjugates for signal amplification of multiplexed lateral flow assays. **A)** First traditional lateral flow concentrates the liposome at the test line. **B)** After the development of the test line, you fold a secondary paper over the test to provide hydrophobic for a secondary flow. The second running buffer lyses open the DNA packed liposome releasing it down the secondary strip for enhanced signal development.

REFERENCES

1. *Global report for research on infectious diseases of poverty* 2012.
2. Hansen C, Paintsil E. Infectious Diseases of Poverty in Children A Tale of Two Worlds. *Pediatr Clin N Am.* 2016;63(1):37-+.
3. Life, death, and disability in 2016. *Lancet.* 2017;390(10100):1083-1083.
4. Evaluation IfHMa. GBD Compare. In: LANCET, ed2016.
5. Cox FEG. History of the discovery of the malaria parasites and their vectors. *Parasite Vector.* 2010;3.
6. WHO. *World Malaria Report.* 2017.
7. Shah M, Hanrahan C, Wang ZY, et al. Lateral flow urine lipoarabinomannan assay for detecting active tuberculosis in HIV-positive adults. *Cochrane Db Syst Rev.* 2016(5).
8. Newell ML, Coovadia H, Cortina-Borja M, et al. Mortality of infected and uninfected infants born to HIV-infected mothers in Africa: a pooled analysis. *Lancet.* 2004;364(9441):1236-1243.
9. Deeks SG, Lewin SR, Havlir DV. The end of AIDS: HIV infection as a chronic disease. *Lancet.* 2013;382(9903):1525-1533.
10. Lawn SD, Zumla AI. Tuberculosis. *Lancet.* 2011;378(9785):57-72.
11. Fogel N. Tuberculosis: A disease without boundaries. *Tuberculosis.* 2015;95(5):527-531.
12. Gandhi NR, Nunn P, Dheda K, et al. Multidrug-resistant and extensively drug-resistant tuberculosis: a threat to global control of tuberculosis. *Lancet.* 2010;375(9728):1830-1843.
13. Goldberg DE, Siliciano RF, Jacobs WR. Outwitting Evolution: Fighting Drug Resistance in the Treatment of TB, Malaria and HIV. *Cell.* 2012;148(6):1271-1283.
14. CDC. Antibiotic / Antimicrobial Resistance. 2018; https://www.cdc.gov/drugresistance/about.html.
15. Panda S, Swaminathan S, Hyder KA, et al. Drug resistance in malaria, tuberculosis, and HIV in South East Asia: biology, programme, and policy considerations. *Bmj-Brit Med J.* 2017;358:67-70.
16. WHO. *Mass drug administration, mass screening and treatment and focal screening and treatment for malaria.* 2015.
17. Osler W. *Principles and practice of medicine.* New York: D. Appleton; 1892.
18. Mabey D, Vos T. Syndromic approaches to disease management. *Lancet.* 1997;349:26-28.
19. Peeling RW, Mabey D. Point-of-care tests for diagnosing infections in the developing world. *Clin Microbiol Infec.* 2010;16(8):1062-1069.
20. Pai NP, Vadnais C, Denkinger C, Engel N, Pai M. Point-of-Care Testing for Infectious Diseases: Diversity, Complexity, and Barriers in Low- And Middle-Income Countries. *Plos Med.* 2012;9(9).
21. Thayer RM. Point of Care Testing (POCT): The Time is Now. 2014.
22. Mills A. Health Care Systems in Low- and Middle-Income Countries. *New Engl J Med.* 2014;370(6):552-557.

23. Girosi F, Olmsted SS, Keeler E, et al. Developing and interpreting models to improve diagnostics in developing countries. *Nature.* 2006;444 Suppl 1:3-8.
24. Carinelli S, Marti M, Alegret S, Pividori MI. Biomarker detection of global infectious diseases based on magnetic particles. *New Biotechnol.* 2015;32(5):521-532.
25. Urdea M, Penny LA, Olmsted SS, et al. Requirements for high impact diagnostics in the developing world. *Nature.* 2006;444 Suppl 1:73-79.
26. Kessel M. Diagnostics as the first line of defense in global health security. *Nat Biotechnol.* 2014;32(6):513-514.
27. Drain PK, Hyle EP, Noubary F, et al. Diagnostic point-of-care tests in resource-limited settings. *Lancet Infect Dis.* 2014;14(3):239-249.
28. Kafkova J. Rapid diagnostic point of care tests in resource limited settings. *Int J Infect Dis.* 2016;45:56-57.
29. Yang IS, Ryu CS, Cho KJ, et al. IDBD: Infectious disease biomarker database. *Nucleic Acids Res.* 2008;36:D455-D460.
30. Miller E, Sikes HD. Addressing Barriers to the Development and Adoption of Rapid Diagnostic Tests in Global Health. *Nanobiomedicine (Rij).* 2015;2.
31. Baker M. In biomarkers we trust? *Nat Biotechnol.* 2005;23(3):297-304.
32. Koczula KM, Gallotta A. Lateral flow assays. *Essays Biochem.* 2016;60(1):111-120.
33. Jacobs J, Barbe B, Gillet P, et al. Harmonization of malaria rapid diagnostic tests: best practices in labelling including instructions for use. *Malaria J.* 2014;13.
34. Goryacheva IY, Lenain P, De Saeger S. Nanosized labels for rapid immunotests. *Trac-Trend Anal Chem.* 2013;46:30-43.
35. Scherr TF, Gupta S, Wright DW, Haselton FR. An embedded barcode for "connected" malaria rapid diagnostic tests. *Lab Chip.* 2017;17(7):1314-1322.
36. Ge XX, Asiri AM, Du D, Wen W, Wang SF, Lin YH. Nanomaterial-enhanced paper-based biosensors. *Trac-Trend Anal Chem.* 2014;58:31-39.
37. Parolo C, Medina-Sanchez M, de la Escosura-Muniz A, Merkoci A. Simple paper architecture modifications lead to enhanced sensitivity in nanoparticle based lateral flow immunoassays. *Lab Chip.* 2013;13(3):386-390.
38. Davis KM, Swartz JD, Haselton FR, Wright DW. Low-Resource Method for Extracting the Malarial Biomarker Histidine-Rich Protein II To Enhance Diagnostic Test Performance. *Anal Chem.* 2012;84(14):6136-6142.
39. Davis KM, Gibson LE, Haselton FR, Wright DW. Simple sample processing enhances malaria rapid diagnostic test performance. *Analyst.* 2014;139(12):3026-3031.
40. Jain P, Chakma B, Patra S, Goswami P. Potential Biomarkers and Their Applications for Rapid and Reliable Detection of Malaria. *Biomed Res Int.* 2014.
41. Mouatcho JC, Goldring JPD. Malaria rapid diagnostic tests: challenges and prospects. *J Med Microbiol.* 2013;62:1491-1505.
42. Maltha J, Gamboa D, Bendezu J, et al. Rapid Diagnostic Tests for Malaria Diagnosis in the Peruvian Amazon: Impact of pfHRPII Gene Deletions and Cross-Reactions. *Plos One.* 2012;7(8).
43. WHO F, CDC. *Malaria rapid diagnostic test performance. Results of WHO product testing of malaria RDTs: round 7 (2015-2016).* 2017.

44. Ahmed R, Levy EI, Maratina SS, et al. Performance of four HRP-2/pLDH combination rapid diagnostic tests and field microscopy as screening tests for malaria in pregnancy in Indonesia: a cross-sectional study. *Malaria J.* 2015;14.
45. Wu G, Zaman MH. Low-cost tools for diagnosing and monitoring HIV infection in low-resource settings. *B World Health Organ.* 2012;90(12):914-920.
46. Delaney KP, Branson BM, Uniyal A, et al. Evaluation of the Performance Characteristics of 6 Rapid HIV Antibody Tests. *Clin Infect Dis.* 2011;52(2):257-263.
47. Glynn MT, Kinahan DJ, Ducree J. CD4 counting technologies for HIV therapy monitoring in resource-poor settings - state-of-the-art and emerging microtechnologies. *Lab Chip.* 2013;13(14):2731-2748.
48. Pai M, Nicol MP, Boehme CC. Tuberculosis Diagnostics: State of the Art and Future Directions. *Microbiol Spectr.* 2016;4(5).
49. Walzl G, Ronacher K, Hanekom W, Scriba TJ, Zumla A. Immunological biomarkers of tuberculosis. *Nat Rev Immunol.* 2011;11(5):343-354.
50. Sarkar P, Biswas D, Sindhwani G, Rawat J, Kotwal A, Kakati B. Application of lipoarabinomannan antigen in tuberculosis diagnostics: current evidence. *Postgrad Med J.* 2014;90(1061):155-163.
51. Hamasur B, Bruchfeld J, van Helden P, Kallenius G, Svenson S. A Sensitive Urinary Lipoarabinomannan Test for Tuberculosis. *Plos One.* 2015;10(4).
52. WHO. *Malaria rapid diagnostic test performance: results of WHO product testing of malaria RDTs: (2014-2015).* 2015.
53. Wu L, van den Hoogen LL, Slater H, et al. Comparison of diagnostics for the detection of asymptomatic Plasmodium falciparum infections to inform control and elimination strategies. *Nature.* 2015;528(7580):S86-S93.
54. McMorrow ML, Aidoo M, Kachur SP. Malaria rapid diagnostic tests in elimination settings-can they find the last parasite? *Clin Microbiol Infec.* 2011;17(11):1624-1631.
55. Yager P, Domingo GJ, Gerdes J. Point-of-Care Diagnostics for Global Health. *Annual Review of Biomedical Engineering.* 2008;10(1):107-144.
56. Luppa PB, Muller C, Schlichtiger A, Schlebusch H. Point-of-care testing (POCT): Current techniques and future perspectives. *Trac-Trend Anal Chem.* 2011;30(6):887-898.
57. Sharma S, Zapatero-Rodriguez J, Estrela P, O'Kennedy R. Point-of-Care Diagnostics in Low Resource Settings: Present Status and Future Role of Microfluidics. *Biosensors-Basel.* 2015;5(3):577-601.
58. Mukadi P, Gillet P, Barbe B, et al. SMS photograph-based external quality assessment of reading and interpretation of malaria rapid diagnostic tests in the Democratic Republic of the Congo. *Malaria J.* 2015;14.
59. Scherr TF, Gupta S, Wright DW, Haselton FR. Mobile phone imaging and cloud-based analysis for standardized malaria detection and reporting. *Sci Rep-Uk.* 2016;6.
60. Nash MA, Waitumbi JN, Hoffman AS, Yager P, Stayton PS. Multiplexed Enrichment and Detection of Malarial Biomarkers Using a Stimuli-Responsive Iron Oxide and Gold Nanoparticle Reagent System. *Acs Nano.* 2012;6(8):6776-6785.

61. Posthuma-Trumpie GA, Korf J, van Amerongen A. Lateral flow (immuno) assay: its strengths, weaknesses, opportunities and threats. A literature survey. *Anal Bioanal Chem.* 2009;393(2):569-582.
62. Porath J, Carlsson J, Olsson I, Belfrage G. METAL CHELATE AFFINITY CHROMATOGRAPHY, A NEW APPROACH TO PROTEIN FRACTIONATION. *Nature.* 1975;258(5536):598-599.
63. Block H, Maertens B, Spriestersbach A, et al. Immobilized-Metal Affinity Chromatography (Imac): A Review. *Method Enzymol.* 2009;463:439-473.
64. Ricks KM, Adams NM, Scherr TF, Haselton FR, Wright DW. Direct transfer of HRPII-magnetic bead complexes to malaria rapid diagnostic tests significantly improves test sensitivity. *Malaria J.* 2016;15.
65. Gatton ML, Rees-Channer RR, Glenn J, et al. Pan-Plasmodium band sensitivity for Plasmodium falciparum detection in combination malaria rapid diagnostic tests and implications for clinical management. *Malaria J.* 2015;14.
66. Programme-FIND WGM. Malaria Rapid Diagnostic Test Performance-Results of WHO product testing of malaria RDTs: round 6 (2014–2015). In:2015.
67. Prevention CfDCa. Steps for Collecting Finger Stick Capillary Blood Using a Microtainer. https://www.cdc.gov/labstandards/pdf/vitaleqa/Poster_CapillaryBlood.pdf.
68. Organization WH. *Global Technical Strategy for Malaria 2016–2030.* United Kingdom2016.
69. Tiono AB, Ouedraogo A, Diarra A, et al. Lessons learned from the use of HRP-2 based rapid diagnostic test in community-wide screening and treatment of asymptomatic carriers of Plasmodium falciparum in Burkina Faso. *Malaria J.* 2014;13.
70. WHO. LIST OF KNOWN COMMERCIALLY-AVAILABLE ANTIGEN-DETECTING MALARIA RDTS
Information for national public health services and UN Agencies wishing to procure RDTs. http://www.wpro.who.int/malaria/internet/resources.ashx/RDT/docs/MD_table34%2B(1)_totallistofISO131485criteria.pdf.
71. Harvey SA, Jennings L, Chinyama M, Masaninga F, Mulholland K, Bell DR. Improving community health worker use of malaria rapid diagnostic tests in Zambia: package instructions, job aid and job aid-plus-training. *Malaria J.* 2008;7.
72. Peeling RW, Smith PG, Bossuyt PMM. A guide for diagnostic evaluations. *Nat Rev Microbiol.* 2010:S2-S6.
73. Organization WH. *Malaria Rapid Diagnosis, Making it Work, Informal Consultation on Field Trials and Quality Assurance on Malaria Rapid Diagnostic Tests.* WHO Regional Office for the Western Pacific Manila, 20032003.
74. Organization WH. *Malaria Rapid Diagnostic Test Performance Summary results of WHO product testing of malaria RDTs: rounds 1-6 (2008–2015).* 2015.
75. Slater HC, Ross A, Ouedraogo AL, et al. Assessing the impact of next-generation rapid diagnostic tests on Plasmodium falciparum malaria elimination strategies. *Nature.* 2015;528(7580):S94-S101.
76. R. Stock CBFR. *Chromatographic Methods.* Springer; 2013.

77. Floris P, Connolly D, White B, Morrin A. Development and characterisation of switchable polyaniline-functionalised flow-through capillary monoliths. *Rsc Adv.* 2014;4(83):43934-43941.
78. Holstein CA, Chevalier A, Bennett S, et al. Immobilizing affinity proteins to nitrocellulose: a toolbox for paper-based assay developers. *Anal Bioanal Chem.* 2016;408(5):1335-1346.
79. Organization WH. *World malaria report 2014.* WHO/HTM/GM;2014.
80. Bhatt S, Weiss DJ, Cameron E, et al. The effect of malaria control on Plasmodium falciparum in Africa between 2000 and 2015. *Nature.* 2015;526(7572):207-+.
81. Bell D, Peeling RW. Evaluation of rapid diagnostic tests: malaria. *Nat Rev Microbiol.* 2006:S34-S40.
82. Lindblade KA, Steinhardt L, Samuels A, Kachur SP, Slutsker L. The silent threat: asymptomatic parasitemia and malaria transmission. *Expert Rev Anti-Infe.* 2013;11(6):623-639.
83. Lin JT, Saunders DL, Meshnick SR. The role of submicroscopic parasitemia in malaria transmission: what is the evidence? *Trends Parasitol.* 2014;30(4):183-190.
84. Bousema T, Okell L, Felger I, Drakeley C. Asymptomatic malaria infections: detectability, transmissibility and public health relevance. *Nat Rev Microbiol.* 2014;12(12):833-840.
85. Perkins MD, Bell DR. Working without a blindfold: the critical role of diagnostics in malaria control. *Malaria J.* 2008;7.
86. Wongsrichanalai C, Barcus MJ, Muth S, Sutamihardja A, Wernsdorfer WH. A review of malaria diagnostic tools: Microscopy and rapid diagnostic test (RDT). *American Journal of Tropical Medicine and Hygiene.* 2007;77(6):119-127.
87. Steenkeste N, Rogers WO, Okell L, et al. Sub-microscopic malaria cases and mixed malaria infection in a remote area of high malaria endemicity in Rattanakiri province, Cambodia: implication for malaria elimination. *Malaria J.* 2010;9.
88. Stresman GH, Kamanga A, Moono P, et al. A method of active case detection to target reservoirs of asymptomatic malaria and gametocyte carriers in a rural area in Southern Province, Zambia. *Malaria J.* 2010;9.
89. Okell LC, Bousema T, Griffin JT, Ouedraogo AL, Ghani AC, Drakeley CJ. Factors determining the occurrence of submicroscopic malaria infections and their relevance for control. *Nat Commun.* 2012;3.
90. Organization WH. *Malaria rapid diagnostics test performance: results of WHO product testing of malaria RDTs: Round 5 (2013).* 2014.
91. He YQ, Zhang SQ, Zhang XB, et al. Ultrasensitive nucleic acid biosensor based on enzyme-gold nanoparticle dual label and lateral flow strip biosensor. *Biosens Bioelectron.* 2011;26(5):2018-2024.
92. Rohrman BA, Leautaud V, Molyneux E, Richards-Kortum RR. A Lateral Flow Assay for Quantitative Detection of Amplified HIV-1 RNA. *Plos One.* 2012;7(9).
93. Choi DH, Lee SK, Oh YK, et al. A dual gold nanoparticle conjugate-based lateral flow assay (LFA) method for the analysis of troponin I. *Biosens Bioelectron.* 2010;25(8):1999-2002.

94. Hu J, Wang L, Li F, et al. Oligonucleotide-linked gold nanoparticle aggregates for enhanced sensitivity in lateral flow assays. *Lab Chip.* 2013;13(22):4352-4357.
95. Yoshimatsu K, Lesel BK, Yonamine Y, Beierle JM, Hoshino Y, Shea KJ. Temperature-Responsive "Catch and Release" of Proteins by using Multifunctional Polymer-Based Nanoparticles. *Angew Chem Int Edit.* 2012;51(10):2405-2408.
96. Pereira DY, Chiu RYT, Zhang SCL, Wu BM, Kamei DT. Single-step, paper-based concentration and detection of a malaria biomarker. *Anal Chim Acta.* 2015;882:83-89.
97. Mabey D, Peeling RW, Ustianowski A, Perkins MD. Diagnostics for the developing world. *Nat Rev Microbiol.* 2004;2(3):231-240.
98. Meng QQ, Wang JX, Ma GH, Su ZG. Lyophilization of CNBr-activated agarose beads with lactose and PEG. *Process Biochem.* 2009;44(5):562-571.
99. Scherr TF, Ryskoski HB, Sivakumar A, et al. A handheld orbital mixer for processing viscous samples in low resource settings. *Anal Methods-Uk.* 2016;8(40):7347-7353.
100. Gross BC, Erkal JL, Lockwood SY, Chen CP, Spence DM. Evaluation of 3D Printing and Its Potential Impact on Biotechnology and the Chemical Sciences. *Anal Chem.* 2014;86(7):3240-3253.
101. Adams NM, Creecy AE, Majors CE, et al. Design criteria for developing low-resource magnetic bead assays using surface tension valves. *Biomicrofluidics.* 2013;7(1).
102. Britton S, Cheng Q, McCarthy JS. Novel molecular diagnostic tools for malaria elimination: a review of options from the point of view of high-throughput and applicability in resource limited settings. *Malaria Journal.* 2016;15.
103. Bornhorst JA, Falke JJ. Purification of proteins using polyhistidine affinity tags. *Applications of Chimeric Genes and Hybrid Proteins, Pt A.* 2000;326:245-254.
104. Evers TH, Appelhof MAM, Meijer EW, Merkx M. His-tags as Zn(II) binding motifs in a protein-based fluorescent sensor. *Protein Eng Des Sel.* 2008;21(8):529-536.
105. Panton LJ, Mcphie P, Maloy WL, Wellems TE, Taylor DW, Howard RJ. Purification and Partial Characterization of an Unusual Protein of Plasmodium-Falciparum - Histidine-Rich Protein-Ii. *Molecular and biochemical parasitology.* 1989;35(2):149-160.
106. Desakorn V, Dondorp AM, Silamut K, et al. Stage-dependent production and release of histidine-rich protein 2 by Plasmodium falciparum. *T Roy Soc Trop Med H.* 2005;99(7):517-524.
107. Bell DR, Wilson DW, Martin LB. False-positive results of a Plasmodium falciparum histidine-rich protein 2-detecting malaria rapid diagnostic test due to high sensitivity in a community with fluctuating low parasite density. *American Journal of Tropical Medicine and Hygiene.* 2005;73(1):199-203.
108. Alonso PL, Ballou R, Brown G, et al. A Research Agenda for Malaria Eradication: Vaccines. *Plos Med.* 2011;8(1).
109. Lo E, Zhou GF, Oo W, Afrane Y, Githeko A, Yan GY. Low Parasitemia in Submicroscopic Infections Significantly Impacts Malaria Diagnostic Sensitivity in the Highlands of Western Kenya. *Plos One.* 2015;10(3).

110. Alemayehu S, Feghali KC, Cowden J, Komisar J, Ockenhouse CF, Kamau E. Comparative evaluation of published real-time PCR assays for the detection of malaria following MIQE guidelines. *Malaria J.* 2013;12.
111. Lee JH, Jang JW, Cho CH, et al. False-Positive Results for Rapid Diagnostic Tests for Malaria in Patients with Rheumatoid Factor. *J Clin Microbiol.* 2014;52(10):3784-3787.
112. Luchavez J, Baker J, Alcantara S, et al. Laboratory demonstration of a prozone-like effect in HRPII-detecting malaria rapid diagnostic tests: implications for clinical management. *Malaria J.* 2011;10.
113. St John A, Price CP. Existing and Emerging Technologies for Point-of-Care Testing. *Clin Biochem Rev.* 2014;35(3):155-167.
114. De Cock KM, Bunnell R, Mermin J. Unfinished business - Expanding HIV testing in developing countries. *New Engl J Med.* 2006;354(5):440-442.
115. Greer L, Wendel GD. Rapid Diagnostic Methods in Sexually Transmitted Infections. *Infect Dis Clin N Am.* 2008;22(4):601-+.
116. Herring AJ, Ballard RC, Pope V, et al. A multi-centre evaluation of nine rapid, point-of-care syphilis tests using archived sera. *Sex Transm Infect.* 2006;82:V7-V12.
117. Bronzan RN, Mwesigwa-Kayongo DC, Narkunas D, et al. Onsite rapid antenatal syphilis screening with an immunochromatographic Strip improves case detection and trip treatment in rural south African clinics. *Sex Transm Dis.* 2007;34(7):S55-S60.
118. Gomez S, Prieto C, Vera C, J RO, Folgueira L. Evaluation of a new rapid diagnostic test for the detection of influenza and RSV. *Enferm Infecc Microbiol Clin.* 2016;34(5):298-302.
119. Manabe YC, Nonyane BAS, Nakiyingi L, et al. Point-of-Care Lateral Flow Assays for Tuberculosis and Cryptococcal Antigenuria Predict Death in HIV Infected Adults in Uganda. *Plos One.* 2014;9(7).
120. Linares EM, Kubota LT, Michaelis J, Thalhammer S. Enhancement of the detection limit for lateral flow immunoassays: Evaluation and comparison of bioconjugates. *J Immunol Methods.* 2012;375(1-2):264-270.
121. Zhang C, Zhang Y, Wang S. Development of multianalyte flow-through and lateral-flow assays using gold particles and horseradish peroxidase as tracers for the rapid determination of carbaryl and endosulfan in agricultural products. *J Agr Food Chem.* 2006;54(7):2502-2507.
122. Fu E, Liang T, Spicar-Mihalic P, Houghtaling J, Ramachandran S, Yager P. Two-Dimensional Paper Network Format That Enables Simple Multistep Assays for Use in Low-Resource Settings in the Context of Malaria Antigen Detection. *Anal Chem.* 2012;84(10):4574-4579.
123. Sabatte G, Feitsma H, Evers TH, Prins MW. Protein biomarker enrichment by biomarker antibody complex elution for immunoassay biosensing. *Biosens Bioelectron.* 2011;29(1):18-22.
124. Bauer WS, Kimmel DW, Adams NM, et al. Magnetically-enabled biomarker extraction and delivery system: towards integrated ASSURED diagnostic tools. *Analyst.* 2017.

125. Ricks KM, Adams NM, Scherr TF, Haselton FR, Wright DW. Direct transfer of HRPII-magnetic bead complexes to malaria rapid diagnostic tests significantly improves test sensitivity. *Malar J.* 2016;15(1):399.
126. Iqbal J, Siddique A, Jameel M, Hira PR. Persistent histidine-rich protein 2, parasite lactate dehydrogenase, and panmalarial antigen reactivity after clearance of Plasmodium falciparum monoinfection. *J Clin Microbiol.* 2004;42(9):4237-4241.
127. Gamboa D, Ho MF, Bendezu J, et al. A Large Proportion of P. falciparum Isolates in the Amazon Region of Peru Lack pfHRPII and pfhrp3: Implications for Malaria Rapid Diagnostic Tests. *Plos One.* 2010;5(1).
128. Koita OA, Doumbo OK, Ouattara A, et al. False-negative rapid diagnostic tests for malaria and deletion of the histidine-rich repeat region of the HRPII gene. *Am J Trop Med Hyg.* 2012;86(2):194-198.
129. Bharti PK, Chandel HS, Ahmad A, Krishna S, Udhayakumar V, Singh N. Prevalence of pfHRPII and/or pfhrp3 Gene Deletion in Plasmodium falciparum Population in Eight Highly Endemic States in India. *Plos One.* 2016;11(8).
130. Reyburn H. New WHO guidelines for the treatment of malaria. *Brit Med J.* 2010;340.
131. Fu Q, Schoenhoff' FS, Savage WJ, Zhang PB, Van Eyk JE. Multiplex assays for biomarker research and clinical application: Translational science coming of age. *Proteom Clin Appl.* 2010;4(3):271-284.
132. Aydin-Schmidt B, Mubi M, Morris U, et al. Usefulness of Plasmodium falciparum-specific rapid diagnostic tests for assessment of parasite clearance and detection of recurrent infections after artemisinin-based combination therapy. *Malar J.* 2013;12:349.
133. Piper R, Lebras J, Wentworth L, et al. Immunocapture diagnostic assays for malaria using Plasmodium lactate dehydrogenase (pLDH). *American Journal of Tropical Medicine and Hygiene.* 1999;60(1):109-118.
134. Gatton ML, Rees-Channer RR, Glenn J, et al. Pan-Plasmodium band sensitivity for Plasmodium falciparum detection in combination malaria rapid diagnostic tests and implications for clinical management. *Malar J.* 2015;14:115.
135. Cytodiagnostics. Gold, Silver, and Gold NanoUrchin Conjugate Technical Information. In.
136. Davis KM, Swartz JD, Haselton FR, Wright DW. Low-resource method for extracting the malarial biomarker histidine-rich protein II to enhance diagnostic test performance. *Anal Chem.* 2012;84(14):6136-6142.
137. Piper RC, Buchanan I, Choi YH, Makler MT. Opportunities for improving pLDH-based malaria diagnostic tests. *Malaria J.* 2011;10.
138. Saha B, Evers TH, Prins MWJ. How Antibody Surface Coverage on Nanoparticles Determines the Activity and Kinetics of Antigen Capturing for Biosensing. *Anal Chem.* 2014;86(16):8158-8166.
139. Jang JW, Cho CH, Han ET, An SS, Lim CS. pLDH level of clinically isolated Plasmodium vivax and detection limit of pLDH based malaria rapid diagnostic test. *Malar J.* 2013;12:181.

140. Martin SK, Rajasekariah GH, Awinda G, Waitumbi J, Kifude C. Unified parasite lactate dehydrogenase and histidine-rich protein ELISA for quantification of Plasmodium falciparum. *Am J Trop Med Hyg.* 2009;80(4):516-522.
141. Slater HC, Ross A, Ouedraogo AL, et al. Assessing the impact of next-generation rapid diagnostic tests on Plasmodium falciparum malaria elimination strategies. *Nature.* 2015;528(7580):S94-101.
142. WHO. *Global Tuberculosis Report.* 2017.
143. WHO. *Global Tuberculosis Report.* Geneva2015.
144. Steingart KR, Ng V, Henry M, et al. Sputum processing methods to improve the sensitivity of smear microscopy for tuberculosis: a systematic review. *Lancet Infect Dis.* 2006;6(10):664-674.
145. Reid MJA, Shah NS. Approaches to tuberculosis screening and diagnosis in people with HIV in resource-limited settings. *Lancet Infect Dis.* 2009;9(3):173-184.
146. Dheda K, Barry CE, Maartens G. Tuberculosis. *Lancet.* 2016;387(10024):1211-1226.
147. TAG. *Pipeline Report* 2017.
148. Dheda K, Davids V, Lenders L, et al. Clinical Utility of a Commercial LAM-ELISA Assay for TB Diagnosis in HIV-Infected Patients Using Urine and Sputum Samples. *Plos One.* 2010;5(3).
149. Sarkar S, Tang XLL, Das D, Spencer JS, Lowary TL, Suresh MR. A Bispecific Antibody Based Assay Shows Potential for Detecting Tuberculosis in Resource Constrained Laboratory Settings. *Plos One.* 2012;7(2).
150. Lawn SD. Point-of-care detection of lipoarabinomannan (LAM) in urine for diagnosis of HIV-associated tuberculosis: a state of the art review. *Bmc Infect Dis.* 2012;12.
151. Lawn SD, Edwards DJ, Kranzer K, Vogt M, Bekker LG, Wood R. Urine lipoarabinomannan assay for tuberculosis screening before antiretroviral therapy diagnostic yield and association with immune reconstitution disease. *Aids.* 2009;23(14):1875-1880.
152. Kerkhoff AD, Wood R, Vogt M, Lawn SD. Prognostic Value of a Quantitative Analysis of Lipoarabinomannan in Urine from Patients with HIV-Associated Tuberculosis. *Plos One.* 2014;9(7).
153. Minion J, Leung E, Talbot E, Dheda K, Pai M, Menzies D. Diagnosing tuberculosis with urine lipoarabinomannan: systematic review and meta-analysis. *Eur Respir J.* 2011;38(6):1398-1405.
154. Boehme C, Molokova E, Minja F, et al. Detection of mycobacterial lipoarabinomannan with an antigen-capture ELISA in unprocessed urine of Tanzanian patients with suspected tuberculosis. *T Roy Soc Trop Med H.* 2005;99(12):893-900.
155. Johnson MM, Odell JA. Nontuberculous mycobacterial pulmonary infections. *J Thorac Dis.* 2014;6(3):210-220.
156. Mishra AK, Driessen NN, Appelmelk BJ, Besra GS. Lipoarabinomannan and related glycoconjugates: structure, biogenesis and role in Mycobacterium tuberculosis physiology and host-pathogen interaction. *Fems Microbiol Rev.* 2011;35(6):1126-1157.

157. Ryu YJ, Koh WJ, Daley CL. Diagnosis and Treatment of Nontuberculous Mycobacterial Lung Disease: Clinicians' Perspectives. *Tuberc Respir Dis.* 2016;79(2):74-84.
158. Kamat V, Rafique A. Designing binding kinetic assay on the bio-layer interferometry (BLI) biosensor to characterize antibody-antigen interactions. *Analytical Biochemistry.* 2017;536:16-31.
159. Myszyka DG. Improving biosensor analysis. *J Mol Recognit.* 1999;12(5):279-284.
160. Jauset-Rubio M, Svobodova M, Mairal T, et al. Ultrasensitive, rapid and inexpensive detection of DNA using paper based lateral flow assay. *Sci Rep-Uk.* 2016;6.
161. Goletti D, Petruccioli E, Joosten SA, Ottenhoff THM. Tuberculosis biomarkers: from diagnosis to protection. *Infect Dis Rep.* 2016;8(2):24-32.
162. Jacobs R, Maasdorp E, Malherbe S, et al. Diagnostic Potential of Novel Salivary Host Biomarkers as Candidates for the Immunological Diagnosis of Tuberculosis Disease and Monitoring of Tuberculosis Treatment Response. *Plos One.* 2016;11(8).
163. Bacakoglu F, Basoglu OK, Cok G, Sayiner A, Ates M. Pulmonary tuberculosis in patients with diabetes mellitus. *Respiration.* 2001;68(6):595-600.
164. Conesa-Botella A, Loembe MM, Manabe YC, et al. Urinary Lipoarabinomannan as Predictor for the Tuberculosis Immune Reconstitution Inflammatory Syndrome. *Jaids-J Acq Imm Def.* 2011;58(5):463-468.
165. Chan CE, Gotze S, Seah GT, et al. The diagnostic targeting of a carbohydrate virulence factor from M.Tuberculosis. *Sci Rep-Uk.* 2015;5.
166. Kehr JC, Zilliges Y, Springer A, et al. A mannan binding lectin is involved in cell-cell attachment in a toxic strain of Microcystis aeruginosa. *Mol Microbiol.* 2006;59(3):893-906.
167. de Souza RC, Muniz GD, Siqueira AS, et al. Investigating the effects of point mutations on the affinity between the cyanobacterial lectin microvirin and high mannose-type glycans present on the HIV envelope glycoprotein. *J Mol Model.* 2016;22(11).
168. Huskens D, Ferir G, Vermeire K, et al. Microvirin, a Novel alpha(1,2)-Mannose-specific Lectin Isolated from Microcystis aeruginosa, Has Anti-HIV-1 Activity Comparable with That of Cyanovirin-N but a Much Higher Safety Profile. *J Biol Chem.* 2010;285(32):24845-24854.
169. Min YQ, Duan XC, Zhou YD, et al. Effects of microvirin monomers and oligomers on hepatitis C virus. *Bioscience Rep.* 2017;37.
170. Shahzad-ul-Hussan S, Gustchina E, Ghirlando R, Clore GM, Bewley CA. Solution Structure of the Monovalent Lectin Microvirin in Complex with Man alpha(1-2)Man Provides a Basis for Anti-HIV Activity with Low Toxicity. *J Biol Chem.* 2011;286(23):20788-20796.
171. CDC. *Mycobacterium bovis (Bovine Tuberculosis) in Humans.* Division of Tuberculosis Elimination;2011.
172. Koniev O, Wagner A. Developments and recent advancements in the field of endogenous amino acid selective bond forming reactions for bioconjugation (vol 44, pg 5495, 2015). *Chem Soc Rev.* 2015;44(15):5743-5743.

173. Lipman NS, Jackson LR, Trudel LJ, Weis-Garcia F. Monoclonal versus polyclonal antibodies: Distinguishing characteristics, applications, and information resources. *Ilar J.* 2005;46(3):258-268.
174. Bauer WS, Gulka CP, Silva-Baucage L, Adams NM, Haselton FR, Wright DW. Metal Affinity-Enabled Capture and Release Antibody Reagents Generate a Multiplex Biomarker Enrichment System that Improves Detection Limits of Rapid Diagnostic Tests. *Anal Chem.* 2017;89(19):10216-10223.
175. Lukacz ES, Sampselle C, Gray M, et al. A healthy bladder: a consensus statement. *Int J Clin Pract.* 2011;65(10):1026-1036.
176. Caliendo AM, Gilbert DN, Ginocchio CC, et al. Better Tests, Better Care: Improved Diagnostics for Infectious Diseases. *Clin Infect Dis.* 2013;57:S139-S170.
177. Balsam J, Ossandon M, Bruck HA, Lubensky I, Rasooly A. Low-cost technologies for medical diagnostics in low-resource settings. *Expert Opin Med Diagn.* 2013;7(3):243-255.
178. Nations U. The Millenium Development Goals Report. 2015.
179. Ghani AC, Burgess DH, Reynolds A, Rousseau C. Expanding the role of diagnostic and prognostic tools for infectious diseases in resource-poor settings INTRODUCTION. *Nature.* 2015;528(7580):S50-S52.
180. Yager P, Edwards T, Fu E, et al. Microfluidic diagnostic technologies for global public health. *Nature.* 2006;442(7101):412-418.
181. Verbarg J, Plath WD, Shriver-Lake LC, et al. Catch and Release: Integrated System for Multiplexed Detection of Bacteria. *Anal Chem.* 2013;85(10):4944-4950.
182. Weigl BH, Boyle DS, de los Santos T, Peck RB, Steele MS. Simplicity of use: a critical feature for widespread adoption of diagnostic technologies in low-resource settings. *Expert Rev Med Devic.* 2009;6(5):461-464.
183. Schroeder LF, Guarner J, Elbireer A, Castle PE, Amukele TK. Time for a Model List of Essential Diagnostics. *New Engl J Med.* 2016;374(26):2511-2514.
184. Bordelon H, Adams NM, Klemm AS, et al. Development of a Low-Resource RNA Extraction Cassette Based on Surface Tension Valves. *Acs Appl Mater Inter.* 2011;3(6):2161-2168.
185. Bitting AL, Bordelon H, Baglia ML, et al. Automated Device for Asynchronous Extraction of RNA, DNA, or Protein Biomarkers from Surrogate Patient Samples. *Jala-J Lab Autom.* 2016;21(6):732-742.
186. Creecy A, Russ PK, Solinas F, Wright DW, Haselton FR. Tuberculosis Biomarker Extraction and Isothermal Amplification in an Integrated Diagnostic Device. *Plos One.* 2015;10(7).
187. Gama BE, Silva-Pires FDS, Lopes MNR, et al. Real-time PCR versus conventional PCR for malaria parasite detection in low-grade parasitemia. *Experimental Parasitology.* 2007;116(4):427-432.
188. Tighe PJ, Ryder RR, Todd I, Fairclough LC. ELISA in the multiplex era: Potentials and pitfalls. *Proteom Clin Appl.* 2015;9(3-4):406-422.
189. Kim S, De Jonghe J, Kulesa AB, et al. High-throughput automated microfluidic sample preparation for accurate microbial genomics. *Nat Commun.* 2017;8.

190. Kwon Y, Hara CA, Knize MG, et al. Magnetic Bead Based Immunoassay for Autonomous Detection of Toxins. *Anal Chem.* 2008;80(22):8416-8423.
191. Beyor N, Yi LN, Seo TS, Mathies RA. Integrated Capture, Concentration, Polymerase Chain Reaction, and Capillary Electrophoretic Analysis of Pathogens on a Chip. *Anal Chem.* 2009;81(9):3523-3528.
192. Li M. Laboratory automation: letting scientists focus on science. *Bioanalysis.* 2015;7(14):1699-1701.
193. Markwalter CF, Ricks KM, Bitting AL, Mudenda L, Wright DW. Simultaneous capture and sequential detection of two malarial biomarkers on magnetic microparticles. *Talanta.* 2016;161:443-449.
194. Chou J, Wong J, Christodoulides N, Floriano PN, Sanchez X, McDevitt J. Porous Bead-Based Diagnostic Platforms: Bridging the Gaps in Healthcare. *Sensors-Basel.* 2012;12(11):15467-15499.
195. Bauer WS, Kimmel DW, Adams NM, et al. Magnetically-enabled biomarker extraction and delivery system: towards integrated ASSURED diagnostic tools. *Analyst.* 2017;142(9):1569-1580.
196. Sturgeon CM, Viljoen A. Analytical error and interference in immunoassay: minimizing risk. *Ann Clin Biochem.* 2011;48:418-432.
197. WHO. *Global Health Observatory data.* 2016.
198. Hammer SM. Antiretroviral Treatment as Prevention. *New England Journal of Medicine.* 2011;365(6):561-562.
199. WHO. *WHO issues new HIV recommendations calling for earlier treatment.* 2013.
200. Lyamuya EF, Kagoma C, Mbena EC, et al. Evaluation of the FACScount, TRAx CD4 and Dynabeads methods for CD4 lymphocyte determination. *J Immunol Methods.* 1996;195(1-2):103-112.
201. Howard AL, Pezzi HM, Beebe DJ, Berry SM. Exclusion-Based Capture and Enumeration of CD4(+) T Cells from Whole Blood for Low-Resource Settings. *Jala-J Lab Autom.* 2014;19(3):313-321.
202. Peeling RW, Sollis KA, Glover S, et al. CD4 Enumeration Technologies: A Systematic Review of Test Performance for Determining Eligibility for Antiretroviral Therapy. *Plos One.* 2015;10(3).
203. Vitoria M, Vella S, Ford N. Scaling up antiretroviral therapy in resource-limited settings: adapting guidance to meet the challenges. *Curr Opin HIV AIDS.* 2013;8(1):12-18.
204. Notomi T, Okayama H, Masubuchi H, et al. Loop-mediated isothermal amplification of DNA. *Nucleic Acids Res.* 2000;28(12).
205. Seok Y, Joung HA, Byun JY, et al. A Paper-Based Device for Performing Loop-Mediated Isothermal Amplification with Real-Time Simultaneous Detection of Multiple DNA Targets. *Theranostics.* 2017;7(8):2220-2230.
206. Bordelon H, Russ PK, Wright DW, Haselton FR. A Magnetic Bead-Based Method for Concentrating DNA from Human Urine for Downstream Detection. *Plos One.* 2013;8(7).

WESTLEY S. BAUER, Ph.D.

LinkedIn: www.linkedin.com/in/westley-bauer
Email: Westley.s.bauer@gmail.com

16062 Rhinestone St NW
Ramsey, MN 55303
Mobile: +1(612) 865-5938

PROFILE

Bioanalytical chemist seeking to apply scientific acumen, diverse technical expertise, and strong problem-solving & communication skills as a senior scientist.

- Industrial laboratory experience:
  - Interned at BASF-SE (Germany) to develop a method to analyze the volatility of herbicide formulations.
  - 3 years at 3M as a technical aid supporting the Building & Commercial Service Division.
  - Proven ability to contribute expertise and provide creative solutions to execute leadership directives.
- Managed 5 different research projects as a graduate student resulting in 5 co-authored peer-reviewed manuscripts while 3 others that are under review or being prepared for submission.
- Extensive experience in sample preparation and in-vitro assay development where I cultivated in-depth knowledge of biomarker separation and quantitation from complex matrixes.
- 4 years serving in student leadership positions at Vanderbilt University.

EDUCATION

PhD (Bioanalytical Chemistry), 2018 — Vanderbilt University (TN)

Bachelor of Science, Chemistry, 2012 — University of St. Thomas (MN)

RESEARCH EXPERIENCE

Research Assistant—Vanderbilt University, Department of Chemistry 06/12-present

Mentorship: Dr. David Wright, Dr. David Cliffel, Dr. Timothy Hanusa, Dr. G. Kayne Jennings, Dr. Fredrick Haselton

Dissertation Focus:

Developing new and integrating existing diagnostic tools to build platform technologies that meet global health needs

Research Projects:

- Developing and characterizing new *Mycobacterium tuberculosis* (M.TB) molecular binding reagents for next generation M.TB diagnostics. ***1 publication in preparation***
- Traveled to rural Zambia and conducted a field trial for a rapid malaria diagnostics enhancement technology: magnetically-assisted biomarker extraction and delivery system (mBEADS). ***1 publication in preparation***
- Developed, automated, and clinically validated a novel, low resource CD4+ T cell enumeration platform. ***1 publication in preparation***
- Developed and evaluated the utility of a metal affinity-enabled multiplex biomarker enrichment strategy to improve limits of detection for multi-antigen rapid diagnostic tests. ***1 related publication under review***
- Designed, fabricated, and validated the components of an integrated malaria diagnostic system (mBEADS) for low-resource settings. ***1 related publication***
- Constructed, validated, and explored the commercial utility of a flow-through sample preparation tool that increases the performance of malaria rapid diagnostic tests. ***1 related publication***
- Co-authored a review that applied mass transfer theory to clinical biomarker capture. ***1 related publication***
- Employed an Iridium probe for the detection of histidine rich protein II. ***1 related publication***
- Synthesized functionalized polycarbonates employing a Tin(II) trifluoromethanesulfonate catalyst under practical conditions. ***1 related publication***

Intern—BASF-SE (Germany), Plant Application and Delivery Optimization Technology 05/17-present

Project Goal: One of the major sources of environmental pollution by herbicides is through atmospheric transport. The goal of my project is to develop and validate an analytical method that evaluates the volatility of herbicide formulations.

Research Project Accomplishments:

- Engineered a simple system that simulates atmospheric conditions and chromatographically isolates volatiles.
- Evaluated the volatility of different herbicide formulations employing the novel system and liquid chromatography-mass spectrometry (LC-MS).

Laboratory Technician—3M, Building and Commercial Service Division 10/09-09/12

- Investigated and reconciled consumer product issues employing analytical laboratory techniques.
- Developed and standardized test methods for product comparison.
- Managed and completed a competitive product profile while maintaining industry standard laboratory records.

Undergraduate Research Assistant—University of St. Thomas, Dept. of Chemistry 01/10-06/12

Research Assistant, Prevette Laboratory

Project Goal: Polycations are often used as non-viral gene delivery agents due to their ability to electrostatically bind DNA. However, the positive charge of polycation results in aggregation in vivo leading to poor delivery efficiency.

Research Project Accomplishments:

- Synthesized and purified a library of poly ethylene glycol (PEG) functionalized polyethylenimine (PEI) polymers with different conjugation ratios (PEI:PEG) to serve as 'shielded' non-viral delivery vehicles.
- Characterized polymers by nuclear magnetic spectroscopy (NMR) and size exclusion chromatography (SEC). Performed DNA binding studies employing isothermal titration calorimetry (ITC), gel electrophoresis, and fluorescence spectroscopy.

Research Assistant, Ippoliti Laboratory

Project Goal: A fundamental project aimed at understanding the temperature-dependent coalescence of small molecules employing dynamic temperature NMR.

Research Project Accomplishments:

- Employed diverse organic chemistry techniques to synthesize and purify quaternary ammonium compounds.
- Performed dynamic NMR temperature studies on 1,1,4,4-tetramethylpiperazine to evaluate coalescent properties.

Research Assistant—University of St. Thomas/Valspar Corporation Collaborative Project 02/11-06/12

Project Goal: Latex paints are a stable dispersion of polymers in an aqueous medium. As a quality control measure, we developed an algorithm that distinguishes and quantitates individual polymers in latex paint formulations employing thermal analysis techniques.

Research Project Accomplishments:

- We developed an algorithm that predicts the polymer composition of a latex paint using the glass transition temperatures (T_g) generated by thermal gravimetric analysis techniques.

TEACHING EXPERIENCE & MENTORING

Vanderbilt University, Mentor to Peruvian Research Fellows, Nashville, TN 02/14-present

- Serve as a research mentor for a 3-month training course to facilitate active learning and technology transfer.

Vanderbilt University, Organic Chemistry Lab Instructor, Nashville, TN 2 Sections; 08/12-06/13

- Conducted informative lectures on experimental design and background.
- Developed, graded, and punctually returned weekly lab reports.
- Held open office hours to foster an active and learning environment.

University of St. Thomas, ESL tutor-mentor, Minneapolis, MN 12/06-10/10

- Tutored ESL students in math and science at an intercity school for 3 hours per week.

SERVICE & LEADERSHIP ACTIVITIES

Treasurer—Vanderbilt University, Graduate Student Council	05/15-05/17
Program developer—Vanderbilt University, Materials Outreach for Rural Education (MRS-MORE)—	08/13-08/15
Treasurer—Vanderbilt University (VICB), Chemical Biology Association of Students	05/14-05/15
Vice President—Vanderbilt University (VICB), Chemical Biology Association of Students	05/13-05/14
Active Member—University of St. Thomas, Chemistry Club, St. Paul MN	02/07-05/11

HONORS, SCHOLARSHIPS

DAAD RISE Professional Scholarship—Funded international summer internship	2017
Best Poster—Vanderbilt Institute of Chemical Biology Student Research Symposium	2016
Rising Young Investigator Award—Gordon Research Conference, Bioanalytical Sensors	2016
Best Poster—Gordon Research Conference, Bioanalytical Sensors	2016
Graduated with Honors (cum laude), **Dean's List** (7 semesters)—University of St. Thomas	2006-2012
Member—National Society of Collegiate Scholars	2006-2012

FUNDED GRANT WRITING

Contributed to an investigator-initiated NIH (NANO) RO1 Grant 2017

- Grant Proposal: *A 100-fold more sensitive TB diagnostic based on magnetic concentration and "coffee-ring" formation*, PIs: Wright, Haselton, Blackburn (UCT), Scored in 4th percentile—projected to be funded **($1.25 million**)

Co-authored a Gates Foundation Grand Challenge Exploration Grant 2016

- Grant Proposal: *Large Volume Origami RDT*, PI: David W. Wright, Funded **($100,000**)

Graduate Student Association Travel Grant (2x $500), Vanderbilt University 2016

Vanderbilt Institute of Clinical and Translational Research (VICTR) grant to pursue novel research as a primary investigator ($2,000) 2015-2016

ASSOCIATIONS & MEMBERSHIPS

Graduate Student Council	2014-present
Chemical Biology Association of Students	2013-present
American Chemical Society	2010-present
Life Science Tennessee	2013-present

POSTERS & CONFERENCE PRESENTATIONS

1. **Bauer, W. S.**, Bitting A., Gibson L.: *Global Perspectives Gained from Field Studies Conducted in Rural Zambia*, Vanderbilt Chemistry Student Speaking Series (2017) – ***Oral Presentation**
2. **Bauer, W. S.**, Wright, D.: *Multiplex Magnetically-Enabled Biomarker Enrichment System to Enhance Rapid Diagnostic Tests*, Vanderbilt Institute of Chemical Biology student symposium (2016) – ***Best Poster**
3. **Bauer, W. S.,** Gulka C.,[1] Adams N., Haselton, F., Wright, D.: *Multiplex Biomarker Enrichment Strategy for the Enhancement of Rapid Diagnostic Tests*, Vanderbilt Institute of Nanotechnology Science and Engineering student summer seminar series (2016) – ***Invited Oral Presentation**
4. **Bauer, W. S.**, Gulka C.,[1] Adams N., Haselton, F., Wright, D.: *Multiplex Biomarker Capture-and-Release Reagents for the Enhancement of Malaria Rapid Diagnostic Tests*, Bioanalytical Sensors Gordon Research Conference (2016) – ***Invited Oral Presentation: Rising Young Investigator Award**
5. **Bauer, W. S.**, Gulka C.,[1] Adams N., Haselton, F., Wright, D.: *Biomarker Capture-and-Release Reagents for the Enhancement of Malaria Rapid Diagnostic Tests*, Bioanalytical Sensors Gordon Research Conference (2016) – ***Best Poster**
6. **Bauer, W. S.**, Scherr, T.; Conrad, J.; Haselton, F.; Wright, D.: *Development and Automation of a Self-Contained CD4*

Enumeration Strategy to Inform HIV Infection and Reduce Mother-to-Child Transmission, Southeastern Pediatric Research Innovation Conference (2016) – Poster presentation

7. **Bauer, W. S.**, Conrad, J; Haselton, F.; Wright, D.: *Development of a robust self-contained CD4 cell isolation and enumeration approach,* Southeastern Regional Meeting (2014) – Poster presentation
8. **Bauer, W. S.**, Conrad, J; Haselton, F.; Wright, D.: *Development of a robust self-contained CD4 cell isolation and enumeration approach,* Southeastern Regional Meeting (2014) – Poster presentation
9. **Bauer, W. S.**, Chamberlain, K.; Prevette, L.E.: *The Effect of Polyethylene Glycol Conjugation on the Binding Affinity of DNA with Polyethylenimine,* University of Minnesota MRSEC Summer Research Expo (2011) – Poster presentation
10. **Bauer, W. S.** *Biochemical Suitability of Crop Residues for Cellulosic Ethanol: Disincentives to Nitrogen Fertilization in Corn Agriculture,* Senior Seminar (2011) – Oral presentation at student seminar series for the University of St. Thomas chemistry department.

PUBLICATIONS

1. **Bauer, W. S.**; Van der Horst, M.; Karamchand, L.; Blackburn J.; Wright, D. W. The Utility of the Lectin Microvirin to Increase Specificity of Lipoarabinomannan-Based Tuberculosis Diagnostics. **80% completed**, Expected submission: Summer 2018—*ACS Infectious Disease*
2. **Bauer, W.S.**; Scherr, T.; Conrad J. A, Davis, K. M.; Haselton F. R.; Wright, D. W. Menu-Based Diagnostic Instrument Appropriate for Low-Resource Settings. In preparation. Expected submission: Spring 2018, **Preparing for submission—*PLOS ONE***
3. **Bauer, W. S.**; Gulka C. P.; Silva L.; Markwalter C. J.; Adams N. M.; Wright D. W.; Metal Affinity-Enabled Capture and Release Antibody Reagents Generate a Multiplex Biomarker Enrichment System that Improves Detection Limits for a Rapid Diagnostic Test. *Anal. Chem*. 89, 10216-10223 (**2017**)
4. **Bauer, W. S.**; Richardson, K. A.; Adams, N. M.; Ricks, K. M.; Gasperino, D. J.; Ghionea, S. J.; Rosen, M.; Nichols, K. P.; Weigl, B. H.; Haselton, F. R.; Wright, D. W., Rapid concentration and elution of malarial antigen histidine-rich protein II using solid phase Zn(II) resin in a simple flow-through pipette tip format. *Biomicrofluidics***,** *11* (3), 034115 (**2017**)
5. **Bauer, W. S.**; Kimmel, D. W.; Adams, N. M.; Gibson, L. E.; Scherr, T. F.; Richardson, K. A.; Conrad, J. A.; Matakala, H. K.; Haselton, F. R.; Wright, D. W., Magnetically-enabled biomarker extraction and delivery system: towards integrated ASSURED diagnostic tools. *The Analyst***,** 142 (9), 1569-1580 (**2017**)
6. Scherr, T. F.; Markwalter, C. F.[§]; **Bauer, W.S.**[§]; Gasperino, D.; Wright, D. W.; Haselton, F. R., Application of mass transfer theory to biomarker capture by surface functionalized magnetic beads in microcentrifuge tubes. *Adv Colloid Interface Sci*, 246, 275-288 (**2017**)
7. Davis, K. M., Bitting, A. L., Markwalter, C. F., **Bauer, W. S.**, Wright, D. W. Iridium(III) Luminescent Probe for Detection of the Malarial Protein Biomarker Histidine Rich Protein-II. *J. Vis. Exp.,* http://www.jove.com/video/52856 doi:10.3791/52856 (**2015**)
8. David M. Stevens, Harry A. Watson, Marc-Andre LeBlanc, Ray Y. Wang, Joanne Chou, **Westley S. Bauer**, Eva Harth. Practical polymerization of functionalized lactones and carbonates with $Sn(OTf)_2$ in metal catalysed ring-opening polymerization methods. *Polym. Chem*., 4, 2470 (**2013**)

TECHNICAL SKILLS & EXPERTISE

Expert:

- Enzyme linked immunosorbant assay (ELISA)
- Lateral flow assays (LFAs)
- Chromatography
- Immunomagnetic separation
- Bio-layer interferometry (BLI)
- Flow cytometry
- UV-Vis spectroscopy

Intermediate:

- Chromatography
- Inductively coupled plasma optical emission spectrometry (ICP-OES)

- Bio-conjugation techniques
- Infrared spectroscopy (IR)—Intermediate

Exposure:

- Mass spectrometry (Sample Preparation LC, GC, and MALDI)
- Size-exclusion chromatography (SEC)—Intermediate
- Thermal gravimetric analysis (TGA) and differential scanning calorimetry (DSC)
- High performance liquid chromatography (HPLC)
- Solid phase peptide synthesis (SPPS)
- Dynamic light scattering (DLS)
- Transmission electron microscopy (TEM)
- Nuclear magnetic resonance (NMR)
- Light microscopy

Computer Software

- Proficient in Excel, PowerPoint, and Word
- Proficient in statistical analysis software: Excel, FlowJo, and GraphPad
- Learning python programming software

Training

- Biosafety Level II
- Blood borne pathogen handling
- Chemical waste